



HAL
open science

Density functional theory for Fermi systems with large s-wave scattering length: application to atomic and nuclear physics

Antoine Boulet

► **To cite this version:**

Antoine Boulet. Density functional theory for Fermi systems with large s-wave scattering length: application to atomic and nuclear physics. Nuclear Theory [nucl-th]. Université Paris Saclay (COMUE), 2019. English. NNT: 2019SACLS212 . tel-02355418

HAL Id: tel-02355418

<https://theses.hal.science/tel-02355418>

Submitted on 8 Nov 2019

HAL is a multi-disciplinary open access archive for the deposit and dissemination of scientific research documents, whether they are published or not. The documents may come from teaching and research institutions in France or abroad, or from public or private research centers.

L'archive ouverte pluridisciplinaire **HAL**, est destinée au dépôt et à la diffusion de documents scientifiques de niveau recherche, publiés ou non, émanant des établissements d'enseignement et de recherche français ou étrangers, des laboratoires publics ou privés.

DENSITY FUNCTIONAL THEORY
FOR FERMI SYSTEMS
WITH LARGE S-WAVE SCATTERING LENGTH:
application to atomic and nuclear physics

Thèse de doctorat
de l'UNIVERSITÉ PARIS-SACLAY
préparée à l'UNIVERSITÉ PARIS-SUD
au sein de l'INSTITUT DE PHYSIQUE NUCLÉAIRE d'Orsay

ÉCOLE DOCTORALE N° 576
Particules Hadrons Énergie et Noyau :
Instrumentation, Image, Cosmos et Simulation (PHENICS)

SPÉCIALITÉ : structure et réactions nucléaires

Thèse présentée et soutenue à Orsay, le 19 septembre 2019, par

ANTOINE BOULET

Composition du jury :

| | |
|---|--------------------|
| Marcella GRASSO Directrice de Recherche, IPN Orsay | Présidente |
| Dany DAVESNE Professeur, Université Lyon 1 | Rapporteur |
| Arnau RIOS HUGUET Professeur, University of Surrey | Rapporteur |
| Gianluca COLÒ Professeur, University of Milan | Examineur |
| Dmitry PETROV Directeur de recherche, LPTMS | Examineur |
| Vittorio SOMÀ Ingénieur de recherche, CEA-Saclay | Examineur invité |
| Denis LACROIX Directeur de Recherche, IPN Orsay | Directeur de thèse |

À Kuna, ma tata...

REMERCIEMENTS

La coutume veut qu'après avoir traversé l'ultime épreuve universitaire, à savoir la thèse de doctorat, apparaissent en début du manuscrit, et ce avant toutes choses, la redoutable formulation des *remerciements*. Déjà, l'ambiguïté paradoxale du terme de *remerciements* semble inappropriée au contexte, sans pourtant négliger les pensées qu'ont suscité en nous les autres par des discussions ou des explications, des conseils avisés et inspirés, puisque le travail jugé par de futurs pairs est censé être le fruit de ses propres recherches – en ce sens, il s'agirait plutôt de reconnaissance – ; mais aussi, comment pourrait-on trouver toute la mesure d'un merci, merci à qui, merci pour quoi ?

Doit-on remercier, par écrit ou de vive voix, dans le silence le plus invisible d'un livre spécialisé et accessible aux seuls initiés, ceux qui par persévérance et ténacité ont acquis des connaissances à la limite du savoir, celui qui, ayant agit en répercutant ses actions (la plupart du temps involontaires) sur les conclusions et la qualité du travail présenté, a contribué à l'émergence de nos réflexions aspirant à repousser ces barrières de l'inconnu ? Si la réponse est oui, alors je tiens à remercier l'humanité et même l'univers entier comme le papillon qui, un jour lorsque j'étais encore enfant, virevolta autour de moi, me questionnant sur sa capacité de voler tandis qu'aucun support matériel apparent ne guidait son mouvement, car sans cela, à ce moment précis et dans les configurations introspectives de mon état d'alors, de mon désir de comprendre, peut-être ne me serai-je jamais intéressé à saisir le monde qui m'entoure et les lois qui le régissent. Sinon, le travail présenté ne suppose par essence aucune obligation morale ou éthique de remerciement, mais je ne le crois pas puisque la vérité est toujours ailleurs, non dans les extrêmes mais la mesure, la douceur, en aucun cas dans la brutalité d'une pensée froide, raisonnée et intellectualisée, ou encore divinement cosmologisée, idéalisée dans la bien-pensance insupportable et décadente des lâches. Non, probablement, des remerciements ont lieu et place ici... pour certains tout du moins.

Après tout, comment savoir qui mérite de plus forts et intenses mercis – et comment l'exprimer clairement et justement ? Souvent, on remercie quelqu'un franchement et sincèrement en se disant que ce doit être honnête ; remercier d'autres personnes proches dans notre classification hiérarchique de nos rapports sociaux s'avère peut-être la moindre des choses, une politesse coquette pour soigner l'égo de celui qui n'était là que par hasard. Combien de paragraphes commencent par de prodigieuses éloges sur une personnalité géniale, en effet, ayant eu une importance capitale dans la vie et le travail de l'auteur et se termine par « aussi, je tiens à remercier Charles Swann », agrémenté de compliments faux et forcés (clairs quand on sait lire entre les lignes), uniquement présent pour combler un vide certain, lui laissant croire qu'il eût une réelle importance dans l'aventure. Je pourrais remercier mon directeur de thèse, mes parents et ma sœur, mes amis, mon amour, et ce dans un ordre totalement arbitraire – bien que l'arbitraire reste toutefois soumis à certaines normes – ; et, aussi je pourrais tenir à remercier le jury, des collègues du

laboratoire où j'ai passé le plus clair de mon temps (ou d'autres laboratoires aussi divers que variés), mes collaborateurs plus ou moins directs, certains professeurs qui ont su éveiller ma curiosité, de brillants physiciens disparus dès lors (et même parfois contemporains) qui ont su m'inspirer, etc.

Personnellement, une solution au problème des *remerciements* sera de ne pas en formuler. Cette position pourrait paraître arrogante à bien des égards ; certains y verront de la modestie là où d'autres y verront de l'indifférence et de l'ingratitude ; certains même soulèveront un manque de courage ou une tentative désespérée pour paraître anticonformiste ; les autres seront compréhensifs face à ce qu'ils pensent deviner comme de la pudeur, de la timidité. Quoiqu'il en soit, il y aura toujours quelqu'un pour vous juger avec des *a priori*, en bien ou en mal. Il paraît même que ce nombre d'inquisiteurs sera bien supérieur au nombre de réels lecteurs de ce recueil car, comme souvent, les aspects ludiques et indiscrets sont privilégiés aux aspects, certes moins abordables, visant à améliorer, éclaircir ses propres conceptions. Non pas que ce soit une solution de confort ou juste une supercherie d'introverti mais une réelle volonté s'accordant, sinon parfaitement avec ce que je suis, du moins ce que je crois être, ici et maintenant : on pourrait toujours faire de long discours en inadéquation avec ses actes.

À quoi bon dire merci au vent – car parfois les gens qui rencontrent notre route s'évanouissent de nos vies aussi vite qu'une brise maritime embaumée par un parfum de fleurs (et quelquefois subtilement agrémentée d'une fine touche d'acidité...) – laissant derrière lui un souvenir affûtant seulement l'expérience ? Comme l'eau s'accorde aux sinuosités du parcours qu'elle suit et interagit avec toute sorte d'obstacle, je ne veux pas croire que les actes gouvernant soit motivés par des calculs égoïstes articulés autour du simple profit personnel, mais par l'amour généreux de la vie, de telle sorte que, même si des différences culturelles se laissent parfois entrevoir, la camaraderie reste l'interaction qui lie les individus et ne nécessite pas un émerveillement plus particulier qu'un papillon prenant son envol, poursuivant son voyage en quête de liberté.

Je n'ai ici que la prétention de croire que les personnes ayant toute ma reconnaissance le savent déjà ; soit que je leur ai déjà prouvé par mes actes ; soit par des moments de vie échangés, intenses, tels des égaux ; soit par une future et déjà entamée fidélité. Alors, pour elles, je n'ai qu'un seul mot un peu altéré par le temps : merci !

Dans un train, le 3 octobre 2019

Antoine BOULET

Voici encore des arbres et je connais leur rugueux, de l'eau et j'éprouve sa saveur. Ces parfums d'herbe et d'étoiles, la nuit, certains soirs où le cœur se détend, comment nierais-je ce monde dont j'éprouve la puissance et les forces ? Pourtant toute la science de cette terre ne me donnera rien qui puisse m'assurer que ce monde est à moi. Vous me le décrivez et vous m'apprenez à le classer. Vous énumérez ses lois et dans ma soif de savoir je consens qu'elles soient vraies. Vous démontez son mécanisme et mon espoir s'accroît. Au terme dernier, vous m'apprenez que cet univers prestigieux et bariolé se réduit à l'atome et que l'atome lui-même se réduit à l'électron. Tout ceci est bon et j'attends que vous continuiez. Mais vous me parlez d'un invisible système planétaire où des électrons gravitent autour d'un noyau. Vous m'expliquez ce monde avec une image. Je reconnais alors que vous en êtes venus à la poésie : je ne connaîtrai jamais. Ai-je le temps de m'en indigner ? Vous avez déjà changé de théorie. Ainsi cette science qui devait tout m'apprendre finit dans l'hypothèse, cette lucidité sombre dans la métaphore, cette incertitude se résout en œuvre d'art. Qu'avais-je besoin de tant d'efforts ? Les lignes douces de ces collines et la main du soir sur ce cœur agité m'en apprennent bien plus. Je suis revenu à mon commencement. Je comprends que si je puis par la science saisir les phénomènes et les énumérer, je ne puis pour autant appréhender le monde. Quand j'aurais suivi du doigt son relief tout entier, je n'en saurais pas plus. Et vous me donnez à choisir entre une description qui est certaine, mais qui ne m'apprend rien, et des hypothèses qui prétendent m'enseigner, mais qui ne sont point certaines. Etranger à moi-même et à ce monde, armé pour tout secours d'une pensée qui se nie elle-même dès qu'elle affirme, quelle est cette condition où je ne puis avoir la paix qu'en refusant de savoir et de vivre, où l'appétit de conquête se heurte à des murs qui défient ses assauts ? Vouloir, c'est susciter les paradoxes. Tout est ordonné pour que prenne naissance cette paix empoisonnée que donnent l'insouciance, le sommeil du cœur ou les renoncements mortels.

L'intelligence aussi me dit donc à sa manière que ce monde est absurde. Son contraire qui est la raison aveugle a beau prétendre que tout est clair, j'attendais des preuves et je souhaitais qu'elle eût raison. Mais malgré tant de siècles prétentieux et par-dessus tant d'hommes éloquentes et persuasifs, je sais que cela est faux. Sur ce plan du moins, il n'y a point de bonheur si je ne puis savoir. Cette raison universelle, pratique ou morale, ce déterminisme, ces catégories qui expliquent tout, ont de quoi faire rire l'homme honnête. Ils n'ont rien à voir avec l'esprit. Ils nient sa vérité profonde qui est d'être enchaîné. Dans cet univers indéchiffrable et limité, le destin de l'homme prend désormais son sens. Un peuple d'irrationnels s'est dressé et l'entoure jusqu'à sa fin dernière. Dans sa clairvoyance revenue et maintenant concertée, le sentiment de l'absurde s'éclaire et se précise. Je disais que le monde est absurde et j'allais trop vite. Ce monde en lui-même n'est pas raisonnable, c'est tout ce qu'on en peut dire. Mais ce qui est absurde, c'est la confrontation de cet irrationnel et de ce désir éperdu de clarté dont l'appel résonne au plus profond de l'homme. L'absurde dépend autant de l'homme que du monde. Il est pour le moment leur seul lien. Il les scelle l'un à l'autre comme la haine seule peut river les êtres. C'est tout ce que je puis discerner clairement dans cet univers sans mesure où mon aventure se poursuit. Arrêtons-nous ici. Si je tiens pour vrai cette absurdité qui règle mes rapports avec la vie, si je me pénétre de ce sentiment qui me saisit devant les spectacles du monde, de cette clairvoyance que m'impose la recherche d'une science, je dois tout sacrifier à ces certitudes et je dois les regarder en face pour pouvoir les maintenir. Surtout je dois leur régler ma conduite et les poursuivre dans toutes leurs conséquences. Je parle ici d'honnêteté. Mais je veux savoir auparavant si la pensée peut vivre dans ces déserts.

TABLE OF CONTENTS

| | |
|--|----|
| INTRODUCTION | 1 |
| 1 SELECTED HIGHLIGHTS ON THE AB INITIO AND EDF THEORIES | 5 |
| 1.1 The nucleon-nucleon interaction | 6 |
| 1.1.A Basic aspects of the nucleon-nucleon interaction | 6 |
| 1.1.B Chiral Effective Field Theory | 10 |
| 1.2 Some recent progress in many-body <i>ab initio</i> methods | 15 |
| 1.2.A Nuclear matter | 15 |
| 1.2.B Challenges in atomic nuclei | 20 |
| 1.2.C Discussion on <i>ab initio</i> methods | 22 |
| 1.3 Empirical density functional theories | 24 |
| 1.3.A Basic illustration of how an EDF theory can be introduced from simple arguments | 24 |
| 1.3.B Effective interaction adjusted on mean field | 26 |
| 1.3.C Illustration of predictivity | 33 |
| 1.4 Recent progress in the nuclear EDF | 36 |
| 1.4.A Extension of empirical functionals | 36 |
| 1.4.B Motivation: why <i>ab initio</i> guided EDF? | 39 |
| 1.4.C Towards <i>ab initio</i> nuclear EDF | 41 |
| 2 ENERGY RESUMMATION | 43 |
| 2.1 EFT for dilute Fermi systems | 44 |
| 2.2 Many-body perturbation theory | 45 |
| 2.2.A Green's functions formalism | 45 |
| 2.2.B Energy contribution for dilute Fermi systems | 49 |
| 2.2.C Survey of numerical estimates of the third and fourth order contributions | 54 |
| 2.3 Ladder resummation | 56 |
| 2.3.A Resummation of ladder diagrams: particle-hole propagator | 56 |
| 2.3.B Resummation of ladders diagrams: vacuum-medium propagator | 58 |
| 2.3.C Discussion of the results on energy resummations | 62 |
| 3 DFT INSPIRED FROM EFT RESUMMATION | 65 |
| 3.1 DFT from energy resummation | 66 |
| 3.1.A General strategy | 67 |
| 3.1.B DFT inspired from geometrical series resummation for the ground-state energy | 68 |
| 3.1.C DFT inspired from arctangent resummation for the ground-state energy | 72 |
| 3.1.D Results and comparison of the different functionals | 73 |
| 3.2 Determination of the ground-state thermodynamical properties | 76 |
| 3.3 Generalization of the DFT including effective range | 83 |
| 3.3.A Inclusion of the effective range | 83 |
| 3.3.B Effective range approximation | 85 |
| 3.3.C Discussion and comparison | 87 |

| | | |
|-------|--|-----|
| 3.4 | Application to linear response in Fermi liquids | 93 |
| 3.4.A | Generalities on static response | 94 |
| 3.4.B | Static response in unitary gases | 96 |
| 3.4.C | Static response in neutron matter | 97 |
| 3.4.D | Collective response in the hydrodynamical regime | 99 |
| 3.5 | Summary and critical discussion | 103 |
| 4 | SELF-ENERGY RESUMMATION | 107 |
| 4.1 | Self-energy contribution at different orders | 108 |
| 4.2 | Self-energy resummation: particle-hole propagator | 114 |
| 4.2.A | Discussion on the off-shell ladder diagrams resummation | 115 |
| 4.2.B | Resummation of the on-shell particle-particle self-energy | 116 |
| 4.2.C | Resummation of the on-shell hole-hole self-energy | 117 |
| 4.2.D | Critical discussions | 118 |
| 4.3 | Self-energy resummation: test-particle technique | 124 |
| 4.3.A | Test-particle insertion technique | 124 |
| 4.3.B | Resummed self-energy using the test-particle approach | 127 |
| 4.4 | Summary and discussions | 132 |
| 5 | APPROXIMATE SELF-ENERGY INSPIRED FROM EFT RESUMMATION | 133 |
| 5.1 | Partial phase-space approximation for the resummed self-energy | 140 |
| 5.1.A | Partial phase-space approximation with Hugenholtz-van-Hove constraint | 140 |
| 5.1.B | Approximate GPS self-energy | 142 |
| 5.1.C | Approximate self-energy consistent with the APS functional | 149 |
| 5.2 | Approximate expressions for the self-energy | 152 |
| 5.2.A | Polynomial form of single-particle potential in power of k^{2n} | 153 |
| 5.2.B | Summary and discussions | 156 |
| 5.3 | Link with the empirical Skyrme functionals | 160 |
| 5.3.A | From non-empirical DFT to density-dependent parameters | 160 |
| 5.3.B | Effective Skyrme potential from quasi-particle properties | 161 |
| 5.3.C | Toward finite systems | 163 |
| 5.4 | Conclusion and critical discussions | 165 |
| | CONCLUSION | 167 |

| | | |
|-------|--|-----|
| A | REGULARIZATION OF THE LOOP INTEGRALS | A1 |
| A.1 | Generalities on the scattering theory: scattering amplitude and S -matrix | A2 |
| A.2 | General features of regularized loop integrals | A3 |
| A.3 | Renormalization of the Low Energy Constants | A5 |
| B | EXPLICIT CALCULATIONS OF THE SECOND ORDER CONTRIBUTION | B1 |
| B.1 | MBPT nuclear matter integrals | B2 |
| B.1.A | Preliminary: overlap between two Fermi spheres | B2 |
| B.1.B | Calculation of the integral (B.1a) | B3 |
| B.1.C | Calculation of the integral (B.1b) | B4 |
| B.1.D | Calculation of the integral (B.1e) | B4 |
| B.2 | Calculation of the loop functions | B5 |
| B.2.A | Particle-particle loops function on the accessible phase-space | B6 |
| B.2.B | Hole-hole loops function on the accessible phase-space | B8 |
| B.2.C | Remarks | B9 |
| B.3 | Calculation of the Lee-Yang coefficient | B9 |
| B.3.A | Energy contribution from the effective particle-particle interaction | B9 |
| B.3.B | Energy contribution from the effective hole-hole interaction | B10 |
| B.4 | Calculation of the Galitskii formula | B10 |
| C | EXPLICIT CALCULATIONS OF THE IN-MEDIUM LOOPS | C1 |
| C.1 | Expression in term of the occupation numbers | C2 |
| C.1.A | Bubbles using vacuum-medium Green's functions | C2 |
| C.1.B | On-shell bubble functions | C3 |
| C.1.C | Link between the in-medium loops and the particle-particle loop | C5 |
| C.1.D | Definition of useful notations | C6 |
| C.2 | Calculation of the unperturbed in-medium loops | C7 |
| C.3 | Calculation of the leading order of the perturbed in-medium loops | C8 |
| C.4 | Energy resummation | C10 |
| C.4.A | Full ladder resummation | C11 |
| C.4.B | Restricted particle-particle ladder resummation | C11 |
| C.5 | Self-energy resummation | C12 |
| C.5.A | Full ladder resummation | C12 |
| C.5.B | Restricted particle-particle ladder resummation | C17 |
| D | EXTENSIONS OF THE LADDER RESUMMATION | D1 |
| D.1 | Ladder resummation of the ground-state energy including effective range | D2 |
| D.2 | Ladder resummation of the p -wave ground-state energy | D2 |
| E | PHASE-SPACE AVERAGE OF USED FUNCTIONS | E1 |
| E.1 | Full phase-space average approximation | E1 |
| E.2 | Partial phase-space average approximation | E2 |
| F | PARAMETRIZATION OF THE APPROXIMATE SELF-ENERGY | F1 |
| F.1 | GPS parametrization | F2 |
| F.2 | APS parametrization | F3 |
| G | SUMMARY IN FRENCH – RESUMÉ EN FRANÇAIS | G1 |
| | BIBLIOGRAPHY | I |

INTRODUCTION

*Ô la vie ! Ô moi ! toutes les questions qui reviennent à leur propos,
L'interminable cortège des sans foi, les villes entières d'imbéciles,
Les reproches que je m'adresse à moi-même (y a-t-il plus imbécile que moi,
y a-t-il plus dépourvu de foi ?),
Les yeux qui cherchent en vain la lumière, les objets médiocres,
la lutte qui recommence toujours,
Ce médiocre résultat d'ensemble, les foules sordides et piétinantes
que je vois autour de moi,
Le vide la vanité dans la vie des autres, moi aux autres entremêlé,
Et toujours la triste question qui n'en finit pas de revenir ô moi
– à quoi ça sert d'être au milieu de tout cela, ô la vie, ô moi ?*

*Réponse :
Au fait que tu es sur terre – au fait que la vie existe avec l'identité,
Au fait que la forte pièce théâtrale continue et que tu peux
y apporter ta réplique.*

Walt WHITMAN – Feuilles d'herbe

The low-energy nuclear many-body problem presents an incredible richness and a rare complexity. The question is not so much to know the individual properties of the nucleons but is to understand how they organize themselves to form these complex systems that are the atomic nuclei. Although atomic nuclei can be seen as a standard many-body problem, the specificities of the nuclear problem make it multi-facets and still far from being well understood. The difficulties encountered in the description of the nuclear systems are numerous. Among them, one can mention the understanding of the nuclear interaction structuring the atomic nuclei, its properties, its mutual interaction including its description from the quantum chromodynamics (QCD).

Another difficulty comes from the fact that atomic nuclei are mesoscopic correlated fermionic systems where the finite size effects complicate significantly the many-body methods relying directly or not on the bare nuclear interaction. Despite the apparent complexity of the problem from a fundamental context, simple properties emerge in atomic nuclei such that nuclear properties vary qualitatively smoothly along the nuclear chart. For instance, the binding energy of nuclei can be parametrized with very few parameters (liquid drop formula) for a wide range of nuclei. Their size presents also a very smooth behavior underlying the incompressible property of nuclear systems. This coexistence between complexity and simplicity is illustrated by the fact that the nuclei can be discussed very precisely with relatively simple theories where systems are described only in terms of the one-body density of nucleons. The most versatile and predictive microscopic theory nowadays in nuclear physics is considering the density as the main degree of freedom to obtain a proper description of observations. This theory is often referred as nuclear density functional theory (nuclear DFT), nuclear energy density functional (nuclear EDF) theory, or simply DFT/EDF. Its predictive power illustrates the gap between the intrinsic complexity organizing nuclear systems and the simplicity with which phenomenological properties can be accounted for. Natural questions that are legitimate to ask are then:

- (a) *How can such simplicity emerge?*
- (b) *Can we connect the DFT that are usually adjusted empirically to reproduce global properties of nuclei to the underlying bare nuclear interaction?*

Noticeably, addressing the question (a) might provide some hints to reply to (b) and reciprocally.

Right now, we are experiencing a pivotal period for nuclear physics with a renewal of ideas and concepts. One of the reason of this renewal in the field is the recent progress of effective field theories. These advances have improved our understanding of the nuclear interaction which are now directly related to the low-energy sector of the QCD. Such a new generation of nuclear interactions turns out to simplify many-body methods. This is why in parallel to the progress on the nuclear interaction itself, the *ab initio* methods took advantage of these breakthroughs. Despite the power of *ab initio* methods and the exceptional improvements in the many-body techniques, these approaches in nuclear many-body problem do not offer the possibility to describe globally the richness of phenomena occurring in nuclear systems in a simple way. They are at present indeed restricted to the description of light to medium-mass nuclei, mostly focusing on their static properties.

Even if the DFT approach based on empirical adjustment seems to have reached their limit in term of predictive power and applicability, they remain the only microscopic approaches able to treat in a simple and unified framework the structure, the small and large amplitude dynamics, as well as the thermodynamical properties of nuclear systems. These approaches also allow to apprehend other domains at the frontier with nuclear physics and make connection with astrophysics, atomic physics, condensed matter, etc... Recently, an interesting connection was also made between nuclear physics and atomic physics. More specifically atomic systems close to the unitary limits have received a special and growing interest in nuclear physics. These systems indeed, similarly to neutronic systems, might present an anomalously large *s*-wave scattering length. They have been widely studied both from the theoretical and experimental points of view during the last decades. In particular, contrary to nuclei, they can be manipulated in a laboratory with a tunable interaction. This flexibility offers the possibility to test ideas and approaches in a simplified and controllable framework compared to nuclei.

These advances lead to a surge of interest in connecting the DFT to the underlying bare interaction with the ultimate goal to answer the question (b). The challenge is to start from fundamental aspects of the nuclear interaction and combine them to the versatility of DFT approaches with the aim to render the DFT less empirical and increase its predictive power. In this context, this thesis aims at contributing to this common goal. This work focuses on the description of systems with an anomalously large *s*-wave scattering length as it is the case in neutron matter and/or atomic gas close to unitarity. More precisely the aim is to develop DFT for these systems starting from the interaction. This problem is particularly complex because it is highly non-perturbative. The strategy used in this thesis is to start from standard many-body techniques first in a perturbative regime and extend them to the non-perturbative regime. The developments made from perturbative to non-perturbative approach will serve us as a strong guidance to obtain DFT for these systems where the parameters are directly connected to the low-energy constants of the interaction. The flexibility of the methodology as well as the possibility to obtain important properties like the effective mass will be scrutinized.

The present thesis is organized as follows. We first introduce the context, the recent developments and the main concepts around which is articulated this thesis in chapter 1. A special attention is paid to (i) the nuclear interaction itself and,

in particular, the chiral effective field theory (EFT), (ii) the nuclear *ab initio* methods, and (iii) the empirical nuclear EDF. At each stage, advantages and drawbacks are discussed and some hints towards *ab initio* DFT are given. The possibility to render less empirical the EDF largely motivates the work presented in the present manuscript. In chapter 2, we discuss the possibility to use the dilute Fermi gas limit as a guide to design new generation of non-empirical energy density functionals. We show that, in this limiting case, the interaction provided by the EFT simplify the many-body calculations. This is illustrated within the many-body perturbation theory (MBPT) technique using the Green's functions formalism. In this academic chapter, important technical and physical concepts that will be useful in the present thesis are introduced. We show that the ground state energy of the dilute Fermi system can be written as an explicit function of the density directly connected to the low-energy constants of the interaction. This kind of density functional is a limiting case valid at very low density of the theory we want develop and will be a guide for the present work. Our ultimate goal is to extend the approach, either MBPT or nuclear DFT, to the dense regime or to systems with an anomalously large *s*-wave scattering length. For this, we will propose and develop specific strategies applicable in the non-perturbative regime.

The requirement of non-perturbative approaches to describe properly nuclear systems imposes to go beyond standard MBPT for dilute Fermi gas. A possibility is to introduce the resummation technique allowing to sum up to all orders in MBPT leading to a relatively compact form of the energy. As we will see however, the lack of predictivity of resummed energies in the non-perturbative regime as well as the complexity of the expressions obtained using resummation method in term of density is a motivation to explore other strategies. In chapter 3, we make a survey of recent attempts we made to obtain *non-empirical* DFTs guided by this resummation. A general and well controlled strategy called phase-space average approximation is introduced and extensions of the functional including effective range effect are proposed.

The novel functionals will then be applied both in atomic and nuclear systems showing their predictive power in the non-perturbative regime. In chapter 3, a study of the static linear response of both cold atom and neutron matter as well as collective modes of trapped systems using some of the *non-empirical* functional obtained is discussed. This study reveals that such processes could only be described if quasi-particles properties are properly accounted for. For this reason, an exploratory study is made to describe quasi-particle properties using the concept of self-energy. Similarly to what was done for the energy, we first discuss resummation of diagrams directly in term of the self-energy in chapter 4. This lays the ground toward the design of a functional theory including quasi-particle properties and remains a solid guidance towards *non-empirical* DFT. Then, in chapter 5, we propose a general methodology, guided by the low-density limit and the resummed self-energy in a MBPT context, to extend the phase-space average approximation to the self-energy. This approach leads to a well controlled method and simplified expressions for the energy and more generally for quasi-particle properties paving the way towards applications in finite Fermi systems.

1

SELECTED HIGHLIGHTS ON THE AB INITIO AND ENERGY DENSITY FUNCTIONAL THEORIES

*There is a house built out of stone
Wooden floors, walls and window sills
Tables and chairs worn by all of the dust
This is a place where I don't feel alone
This is a place where I feel at home*

*'Cause, I built a home for you, for me
Until it disappeared from me, from you*

And now, it's time to leave and turn to dust

*Out in the garden where we planted the seeds
There is a tree as old as me
Branches were sewn by the color of green
Ground had arose and passed it's knees*

*By the cracks of the skin I climbed to the top
I climbed the tree to see the world
When the gusts came around to blow me down
I held on as tightly as you held onto me*

*And, I built a home for you, for me
Until it disappeared from me, from you*

And now, it's time to leave and turn to dust

The Cinematic Orchestra – *To Build A Home*

CONTENTS

| | | |
|-------|--|----|
| 1.1 | The nucleon-nucleon interaction | 6 |
| 1.1.A | Basic aspects of the nucleon-nucleon interaction | 6 |
| 1.1.B | Chiral Effective Field Theory | 10 |
| 1.2 | Some recent progress in many-body <i>ab initio</i> methods | 15 |
| 1.2.A | Nuclear matter | 15 |
| 1.2.B | Challenges in atomic nuclei | 20 |
| 1.2.C | Discussion on <i>ab initio</i> methods | 22 |
| 1.3 | Empirical density functional theories | 24 |
| 1.3.A | Basic illustration of how an EDF theory can be introduced from simple arguments | 24 |
| 1.3.B | Effective interaction adjusted on mean field | 26 |
| 1.3.C | Illustration of predictivity | 33 |
| 1.4 | Recent progress in the nuclear EDF | 36 |
| 1.4.A | Extension of empirical functionals | 36 |
| 1.4.B | Motivation: why <i>ab initio</i> guided EDF? | 39 |
| 1.4.C | Towards <i>ab initio</i> nuclear EDF | 41 |

The purpose of this chapter is to introduce the concepts that will be used throughout this thesis, especially on the nucleon-nucleon interaction. Furthermore, an overview is made on the recent advances in *ab initio* methods and also in density functional theories. In particular, this overview will help to better understand and put into perspective the purpose of this thesis as well as the important issues. We present first the nucleon-nucleon interaction and its novel modelization based on the chiral effective field theory that appeared recently. We will then show how these advances have allowed a breakthrough for *ab initio* methods and why it appears more and more timely to make the link with the density functional theory.

1.1

THE NUCLEON-NUCLEON INTERACTION

One important goal of nuclear physics is to understand and describe the emergence of simple and complex phenomena at play in atomic nuclei that reflects the underlying bare nucleon-nucleon (NN) interaction properties. This interaction is denoted V_{NN} hereafter. We can also note the role of multi-body interactions (in particular the three-body interaction [1-4]) playing an important role in nuclear physics and denoted V_{3N}, V_{4N} , etc... hereafter. Theories used in low energy nuclear physics to describe nuclear systems usually make the hypothesis that nucleons (protons and neutrons) are elementary particles. However, nucleons are composite particles and their constituents, namely the u and d quarks, interact through the strong force described in the standard model by the quantum chromodynamics (QCD) theory [5,6].

In recent years, important breakthroughs have been made starting from QCD in the non-perturbative regime, i.e. the low energy sector, especially due to the progress of chiral effective field theory (χ EFT) with or without pions¹ [7-15]. This theory allows *a priori* to obtain a systematic and constructive framework to construct NN interactions from QCD concepts. Thereby, novel generation of NN interactions have been proposed that (i) enable to make direct connection with observation like nucleon-nucleon collisions, (ii) make a clear connection with QCD, and (iii) turn out to simplify greatly the many-body calculations compared to the empirical interactions that were directly adjusted on NN scattering data. Then, three questions are pointed out²: (a) *How to obtain from observations a realistic NN interaction?* (b) *How to relate the NN interaction to the QCD?* (c) *How to describe nuclear systems in term of the bare NN interaction?*

Below we further discuss the recent progress made on questions (a) and (b) and we introduce concepts that will be useful in the present work.

1.1.A Basic aspects of the nucleon-nucleon interaction

The description of the NN interaction from QCD is a very challenging problem for at least two reasons. First, two nucleons system is a very complicated many-body quantum problem due to the complex composition of each nucleon in term

¹ Note that the term *chiral* usually refers to an EFT with pions.

² We will see below that the answers to the questions (a) and (b) are provided by the χ EFT.

of fundamental particles (valence quarks, virtual gluons, pair of virtual quarks-antiquarks...) [16,17]. Then, the strong interaction between quarks described by exchange of gluons is highly non-perturbative at the low energy scale relevant for nuclear physics.

One of the first attempts made by Yukawa [18] to tackle these problems was to consider that the interaction between nucleons, regarded as point like particles, is mediated by meson³ exchange. The concept of meson exchange, that was the subject of tremendous developments during the last decades (see for instance [19, 20] for a review), turns out to be very efficient to give a quantitative description and understanding of the NN interaction.

Essentially, the properties of the NN interaction can be understood from the meson at play at a given relative distance between nucleons. The mesons are shown in figure 1.1. Typical examples of NN interactions are shown in figure 1.2. The hard

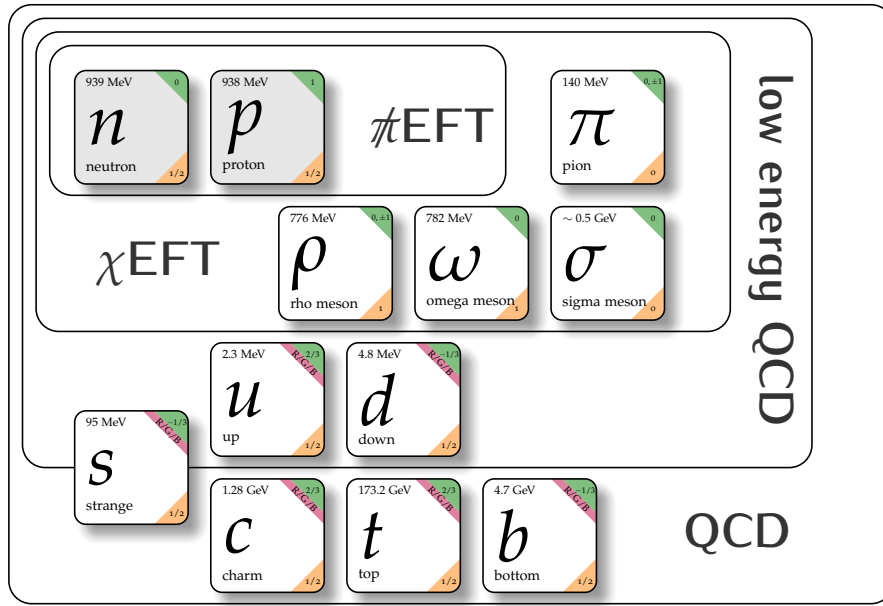


Figure 1.1: Degrees of freedom (dof) of nuclear physics at several energy scales. In each box, the charge, spin and energy are recalled. At high-energy/short-distance, the constituent quarks, described by the QCD theory, are the appropriate dof. Then, for low-energy/long-range process, neutron and proton are the relevant dof of the systems and are described by the pionless effective field theory (π EFT) [see section 1.1.b].

core repulsive short-range part of the nuclear interaction is due to the interaction of the constituent quarks at QCD level while the long range attractive part is mediated by one π -meson exchange between nucleons (see figure 1.1 and 1.2). At intermediate range, two π -meson exchange and heavier meson exchanges, e.g. ρ, ω, σ mesons, are at play. In nuclear systems, the density of interest is $\rho_0 \simeq 0.16 \text{ fm}^{-3}$ corresponding to an inter-particle distance of $L_0 \simeq 2 \text{ fm}$. Consequently, for *standard* nuclear systems, we anticipate that mostly the long-range part of the NN interaction will dictate the physics.

Historically, empirical NN interactions start from a phenomenological parametrization where the parameters are adjusted on experimental NN scattering cross-sections. For instance, some currently used NN interactions are Argonne [22], Bonn [23], Nijmegen [24], Paris [25], or Reid [26] potentials. Some of them are shown in figure 1.2. As a side but important remark, we see that different empirical

³ Particle composed by a valence pair of quark-antiquark.

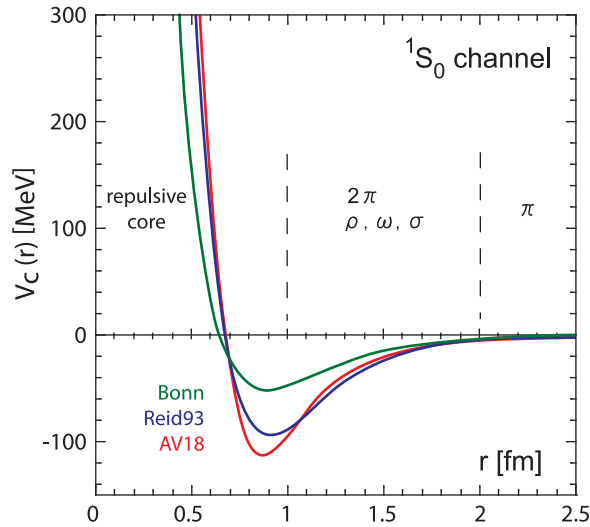


Figure 1.2: Selected examples of realistic NN potentials (central part only) in the 1S_0 channels as a function of the inter-particle distance. Figure taken from [21].

interactions, while adjusted on the same low-energy experimental data, differ from each other. This will be discussed below.

The NN interactions are usually described in term of total angular momentum, spin and isospin channels. These concepts will be regularly used in this document. Therefore we recall here some standard aspects of scattering theory. We focus below on the central part of the interaction.

SCATTERING THEORY AND PHASE-SHIFT

The direct two-body interaction properties can be probed directly by the scattering process of the particles (see appendix A for more details). Considering the situation where an incoming particle of mass m and incident state or momentum \mathbf{k} , i.e. of incident energy $E = k^2/2m$, collides a nucleon at rest in the laboratory frame, the target particle creates a potential $U(\mathbf{r}) = V_{NN}(\mathbf{r})$ on the other particle. For the moment we assume no spin and isospin. The scattering problem can be decomposed onto the different partial waves associated to angular momentum l , that is conserved. For elastic scattering, the cross-section is written as a sum of the different l contributions as:

$$\sigma(k) = \frac{4\pi}{k^2} \sum_l (2l+1) \sin^2 \delta_l(k). \quad (1.1)$$

$\delta_l(k)$ denotes the phase-shift for a given angular momentum⁴ l which fully determines the asymptotic behavior of the eigenstates of the considered two-body problem. Therefore, the phase-shifts encode the information about the NN interaction.

These phase-shifts are determined from experimental analysis of the neutron-neutron, proton-proton and neutron-proton cross-sections (see for example [27–29]). The parameters of the realistic NN interaction are then adjusted to reproduce at best these phase-shifts (with eventually additional constraints on the deuteron

⁴ Due to the spherical symmetry of the nuclear central interaction, we can make the expansion of the angular dependence in spherical harmonics Y_l^m .

properties [20]). Although different parameterizations that have been proposed reproduce the same observables, they present significant differences as displayed in figures 1.2 (see also figure 1.3) for the 1S_0 scattering channel⁵. This underlines that the historical design of empirical NN interactions lacks of a constructive framework to modelize the interactions⁶ More precisely, the empirical NN interactions are globally adjusted on the whole range of relative distance while the scattering datas contain only the long-range physics (low-energy sector). The absence of constraint at short-range leads to these uncertainties. This has been clearly demonstrated by the so-called low momentum interaction [30]. Starting from several empirical interactions (or an interaction obtained from the Chiral Effective Field Theory, see discussion below) and applying renormalization group (RG) techniques, the results lead to the same *universal* low momentum interaction $V_{\text{low}k}$ conserving the phase-shift at low energy as illustrated in figure 1.3. It is also called soft interaction in the

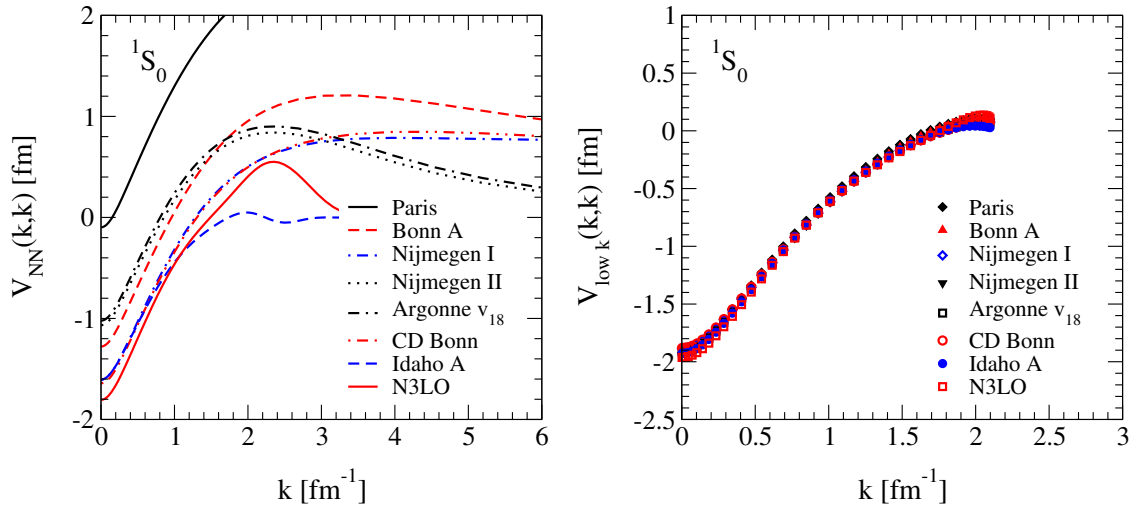


Figure 1.3: The NN interaction in momentum space of the 1S_0 partial wave channel. Left panel: Various realistic NN interactions and a chiral N3LO interaction. Right panel: Renormalization group procedure results deduced from the same potentials and conserving the phase-shift. Figure taken from [13].

sense that the repulsive hard core is smoothed by the RG procedure and only remains the description of the long-range/low-energy physics. The low momentum interaction example is particularly interesting for several reasons:

1. It shows that all empirical interactions were carrying out the same low-energy information although they look differently in figure 1.2.
2. An important byproduct was also to demonstrate that the scattering process at low energy can be described without the hard core. This was a major breakthrough because many approaches like perturbative theory, that were hardly applicable before due to the hard core, can now become useful. This, in 2005, has opened new perspectives for *ab initio* theories (see section 1.2).

⁵ Because of the spherical symmetry of the central part of the interaction, the total orbital angular momentum $L = 0, 1, 2, \dots = S, P, D, \dots$ is coupled to the total spin $S = 0, 1$ of the two-body systems as $J = L + S$ where J is the total angular momentum. Thereby the channel of the interaction of a two-body systems characterized by the (L, S, J) quantum numbers is labeled by the spectroscopic notation $^{2S+1}L_J$.

⁶ Since the potential is not an observable, the fact that they differ from each other is not a problem. The problem is rather that there is no clear connection between different potentials, i.e. there is no systematic approach to model them.

In the last decades, important progress have been made to provide such a systematic construction of NN interactions mainly due to chiral perturbation theory and effective field theory developments (see discussion below).

Remark: In the discussion, the term of “nucleon” is used generically but its state is labeled by the position (in real or momentum space) and by two quantum numbers namely the spin $\sigma = \pm 1/2$ and isospin $\tau = n, p$. Therefore, the problem is much more complex as illustrated in figure 1.4 where a realistic interaction is decomposed on the total spin $S = \sigma_1 + \sigma_2$ and isospin $T = \tau_1 + \tau_2$ channel. As observed, the nuclear force strongly depends on the spin-isospin channels. Moreover, to be complete, the electromagnetic repulsion between protons should be also accounted for in scattering analysis.

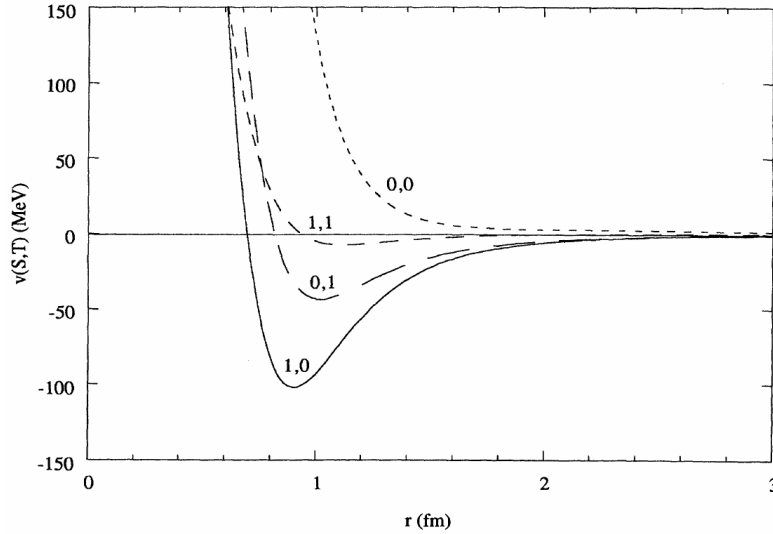


Figure 1.4: Dependence of the realistic Argonne v_{14} NN potential on total spin S and total isospin T as a function of the relative distance between nucleons. Figure taken from [31].

LOW ENERGY CONSTANTS

Before continuing, we introduce some important quantities, namely the low energy constants (LECs) of the two-body interaction. At low energy, $k^{2l+1} \cot \delta_l(k)$ can be expanded in powers of k^2 as [32–36]:

$$k \cot \delta_0 = -\frac{1}{a_s} + \frac{r_s}{2} k^2 + \dots, \quad k \cot \delta_1 = -\frac{3}{k^2 a_p^3} + \dots, \quad (1.2)$$

where the s -wave scattering length a_s , s -wave effective range r_s , and the p -wave scattering volume a_p^3 of the two-body interaction are introduced. The experimental values of a_s, r_s for NN interaction are given in table 1.1 and the p -wave scattering volume a_p^3 for the neutron-proton system obtained using the NijmII and the Reid93 potentials are given in table 1.2. These LECs are key ingredients of the chiral effective field theory (χ EFT) discussed in the following.

1.1.B Chiral Effective Field Theory

The empirical bare NN interactions [20,21,38] present some difficulties in the sense that they strongly depend on the parametrization used to reproduce the phase-shifts of the nucleon-nucleon system. Lots of developments have been made to

| NN | a_s [fm] | r_s [fm] |
|------|-------------------|-----------------|
| nn | -18.9 ± 0.4 | 2.75 ± 0.11 |
| np | -23.74 ± 0.02 | 2.77 ± 0.05 |
| pp | -17.3 ± 0.4 | 2.85 ± 0.04 |

Table 1.1: s -wave scattering length and effective range of NN systems in the 1S_0 scattering channel [20].

| $^{2s+1}P_j$ | a_p^3 (NijmII) [fm ³] | a_p^3 (Reid93) [fm ³] |
|--------------|-------------------------------------|-------------------------------------|
| 3P_0 | -2.468 | -2.469 |
| 3P_1 | 1.529 | 1.530 |
| 3P_2 | -0.2844 | -0.2892 |
| 1P_1 | 2.797 | 2.736 |

Table 1.2: p -wave scattering volume a_p^3 of np systems in the 1P_1 and $^3P_{j=0,1,2}$ scattering channels used in the NijmII and the Reid93 potentials [37].

provide a theoretical framework allowing for a systematic construction of the interaction valid up to a given energy scale. It is the purpose of the χ EFT discussed in this section. This theory relies on the construction of the NN interaction from the QCD Lagrangian denoted by \mathcal{L}_{QCD} hereafter. For a complete review, we can refer to [8–11,38]. Here we make a general and basic overview of the important notions to derive an NN interaction from QCD in an EFT picture.

BREAKING OF MASS SCALE IN QCD

In nuclear physics, the systems of interest are composed essentially of valence quarks (or anti-quarks) u (\bar{u}) and d (\bar{d}), e.g. neutrons (udd), protons (uud) or π -mesons/pions ($\bar{q}q'$) [see figure 1.1]. Their fundamental descriptions are encoded in the QCD Lagrangian:

$$\mathcal{L}_{QCD} = \mathcal{L}_{QCD}^0 - \bar{q}\mathcal{M}q, \quad (1.3)$$

where \mathcal{L}_{QCD}^0 corresponds to the case where quarks masses vanish and the second part corresponds to the mass contribution (q denotes the quark field and \mathcal{M} the mass matrix). Without going into details, the massless part is invariant under chiral symmetry though the mass contribution breaks it explicitly. These properties give to the pions (identified as pseudo-Goldstone bosons of the spontaneous chiral symmetry breaking) a specific role in nuclear physics.

CHIRAL PERTURBATION THEORY

In the chiral limit ($m_\pi \rightarrow 0$), i.e. considering only \mathcal{L}_{QCD}^0 , the pion interaction vanishes. The idea of the χ EFT is to take advantage of the intrinsic small mass of pion compared to other typical hadronic masses, e.g. the mass of the ρ -meson or the mass of nucleon $m_\rho \sim m_N \simeq 1$ GeV, and treat the mass term of the QCD Lagrangian (1.3) in perturbation. In practice, the Lagrangian is expanded in powers of Q/Λ_χ where $\Lambda_\chi \sim 1$ GeV stands for the mass scale between the pion and other hadrons associated to the non-perturbativeness of QCD at high energy. Q denotes a typical energy scale of the process properly described by the EFT. Thereby, the

physical phenomena at energy scale of the order of $Q \leq m_\pi \simeq 140 \text{ MeV} \ll \Lambda_\chi$ remain unchanged compared to a full description in term of the QCD Lagrangian. In other words, the long-range/low-energy process are taken into account explicitly in the EFT whereas the short-range/high-energy physics is effectively encoded in contact interactions.

An effective Lagrangian of the strong interaction for the low-energy sector of QCD is then constructed:

$$\mathcal{L}_{QCD} \rightarrow \mathcal{L}_{\chi EFT} = \mathcal{L}_{\pi\pi} + \mathcal{L}_{\pi N} + \mathcal{L}_{NN} + \dots, \quad (1.4)$$

where $\mathcal{L}_{\pi\pi}$, $\mathcal{L}_{\pi N}$, and \mathcal{L}_{NN} , encoding respectively the pion-pion, pion-nucleon, and nucleon-nucleon interactions, are expanded in powers of Q/Λ_χ . The coupling constants appearing in the NN part are adjusted to reproduce the nucleon-nucleon scattering data and are explicitly related to the LECs of the NN interaction (1.2). This strategy provides a systematic and constructive perturbative scheme deduced directly from QCD to get an approximation of the nuclear interaction at desired scale in energy. The application of χ EFT technique is illustrated in figure 1.5 where the phase-shifts obtained with EFT in several channels converge, order by order, to the experimental one.

The strategy of the χ EFT can be summarized as follow:

1. Write down the most general Lagrangian which respects symmetries of QCD in terms of low-energy degrees of freedom (pions and nucleons).
2. Identify contributions (i.e. Feynman diagrams displayed in figure 1.6) that give contributions at a given order in Q/Λ_χ .
3. Fix the low-energy constants, i.e. determine constants by matching to experimental phase-shift at given order of the expansion.

We can mention that this approach allows to introduce consistently multi-body interactions which are important in the nuclear many-body problem [13]. This point is displayed in figure 1.6 where each contribution at given order in the expansion of the χ EFT Lagrangian is associated to an evaluated Feynman diagrams. For instance a three-body contact interaction appears at next-to-next-leading-order (NNLO).

PIONLESS EFFECTIVE FIELD THEORY

The possibility to obtain interaction optimized for a specific energy scale is at the heart of EFT. In particular, the binding energy of the symmetric nuclear matter is around $E/A \simeq -16 \text{ MeV}$ at saturation density. This typical energy scale of the low energy nuclear physics is small compared to the mass of a pion. A second level of approximation, the pionless EFT ($\not{\pi}$ EFT), consists in making an expansion in term of $Q/\Lambda_\not{\pi}$ of the chiral Lagrangian (1.4):

$$\mathcal{L}_{\chi EFT} \rightarrow \mathcal{L}_{\not{\pi} EFT} = \mathcal{L}_{NN} + \dots \quad (1.5)$$

The new high energy scale is played now by the mass of pion $\Lambda_\not{\pi} \sim m_\pi$ so that the pionless Lagrangian is accounting effectively for meson and nucleon excitations. Ultimately, only remains the nucleon-nucleon part adapted for the low energy nuclear physics [15]. The associated NN interaction is given by a contact interaction of the form:

$$V_{NN}^{\not{\pi}}(\mathbf{k}', \mathbf{k}) = C_0 + \frac{C_2}{2} [\mathbf{k}'^2 + \mathbf{k}^2] + C_2' \mathbf{k}' \cdot \mathbf{k} + \dots, \quad (1.6)$$

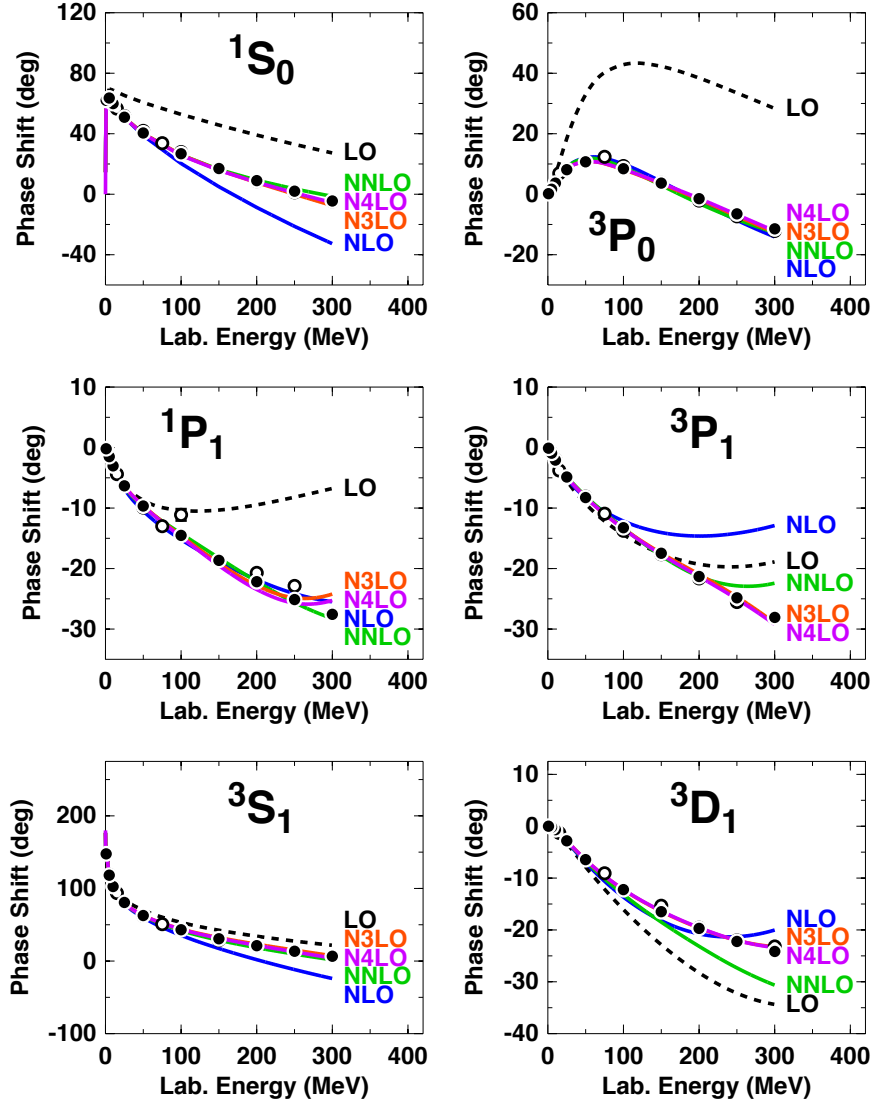


Figure 1.5: Chiral expansion of neutron-proton phase-shifts up to N₄LO for the *S*, *P* and *D* channels with $J \leq 1$. The filled and open circles represent the experimental phase-shift analysis results respectively. Figure taken from [14].

where k' and k denotes the relative momenta of the outgoing and incoming particles respectively.

This interaction has a well-known ultra-violet (UV) divergence that needs to be properly treated. Regularization techniques are rather standard tools in EFT. We mention in particular the standard minimal subtraction (MS) scheme of dimensional regularization [12,39–44] that will be used in the present thesis (see appendix A for more details). In the latter MS case, the coupling constants are linked to the LECs defined in Eq. (1.2) simply by:

$$C_0 = \frac{4\pi a_s}{m}, \quad C_2 = C_0 \frac{a_s r_s}{2}, \quad \text{and} \quad C'_2 = \frac{4\pi a_p^3}{m}, \quad (1.7)$$

where m denotes the mass of nucleons. Note that we have used the convention $\hbar = 1$ and will do it everywhere in the text.

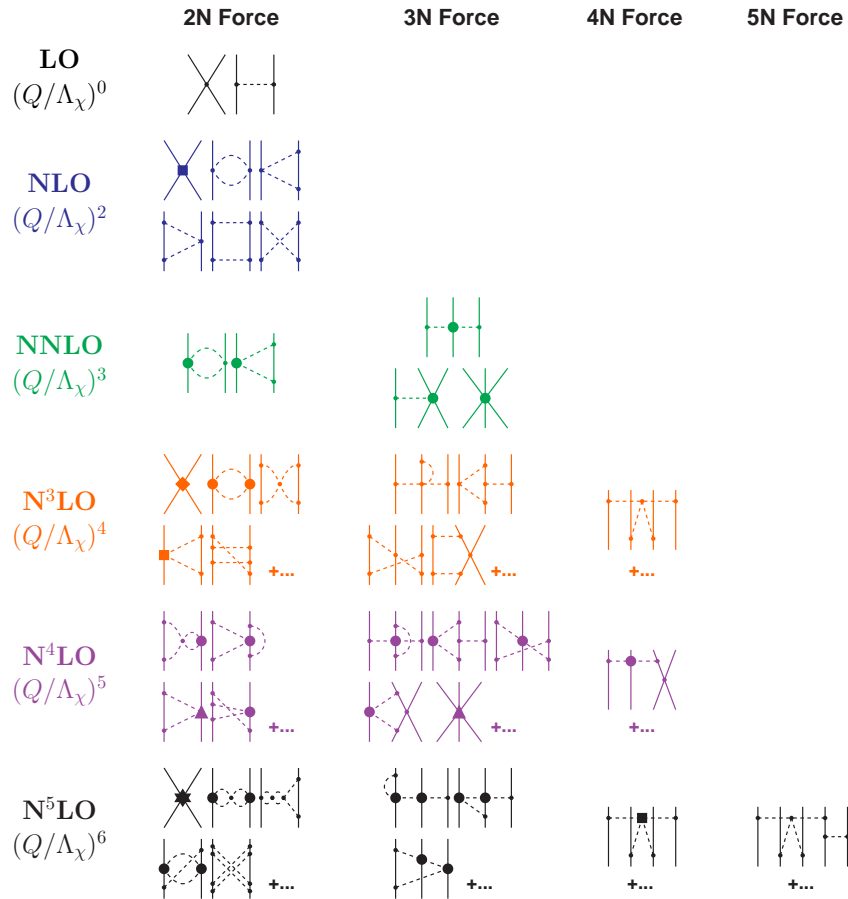


Figure 1.6: Hierarchy of nuclear interactions in Chiral perturbation theory. Nucleon (resp. meson) is represented by solid (resp. dashed) line. Each vertex represented by symbols accounts for different powers in Q/Λ_χ . Figure taken from [11].

1.2

SOME RECENT PROGRESS IN MANY-BODY AB INITIO METHODS

In the previous section, we have introduced basic concepts related to the bare NN interaction highlighting some recent works to construct them from the underlying QCD Lagrangian. Not only recent work has led to a new generation of interactions but also these interactions, with the absence of hard-core, turn out to be easier to use in many-body calculations. We can now focus on the question: *How to describe nuclear systems in term of the bare nuclear interaction?* This is actually the purpose of *ab initio* methods, i.e. solve the few- or many-body Schrödinger equation expressed in terms of nucleonic degrees of freedom subject to the elementary NN interactions introduced in previous section (e.g. empirical, χ EFT interactions with or without pions).

In the present work, the main focus is to describe infinite systems like neutron matter. *Ab initio* methods have been widely used in this context and we give below some illustrations of the results.

1.2.A Nuclear matter

Ideal systems composed by an infinite number of nucleons at finite and homogeneous density, namely infinite matter, are of special interest. For instance, in nuclear astrophysics, the knowledge of the equation of state (EOS) of neutron matter, i.e. the energy per particle (or associated thermodynamic properties, e.g. the pressure) as displayed in figure 1.7, is a central issue. This EOS is for instance used to study the hydrodynamic stability condition in curved space-time, linking the pressure obtained from the EOS to the mass of the neutron star. This stability is analyzed by the resolution of the Tolman-Oppenheimer-Volkov equation [45,46]. This allows to express the mass of the neutron star as a function of its radius as illustrated in figure 1.8 for several parametrizations of the neutron matter EOS. With the recent observation of neutron star merger through gravitational waves by LIGO and Virgo detectors, the interpretation of multi-messenger signals seems a promising way to extract fundamental nuclear physics and constrain some aspects of the EOS.

Below, we discuss the status and limitation of *ab initio* methods for nuclear physics. A special attention will be paid to infinite matter that will be extensively discussed in the present work. The link with ultracold atoms will also be introduced, and finally, we will open the discussion to *ab initio* methods used for the description of atomic nuclei properties.

STATUS OF AB INITIO EQUATION OF STATE

The great simplification in infinite matter compared to finite nuclei stems from the translational Galilean invariance of the systems. The relevant single-particle states for the non-interacting system are identified as plane-waves with energy $e(k) = k^2/2m$. The occupation numbers (at zero temperature), accounting for the Pauli blocking effect, is given by $n(k) = \Theta(k_F - k)$ where k_F is the Fermi momentum and Θ is the Heaviside step function.

Several *ab initio* methods are able to provide, starting from the *bare* NN interaction, controlled EOS that are compatible with each other as showed in figure 1.7 for the pure neutron matter case. To quote some of them, one can mention the self-

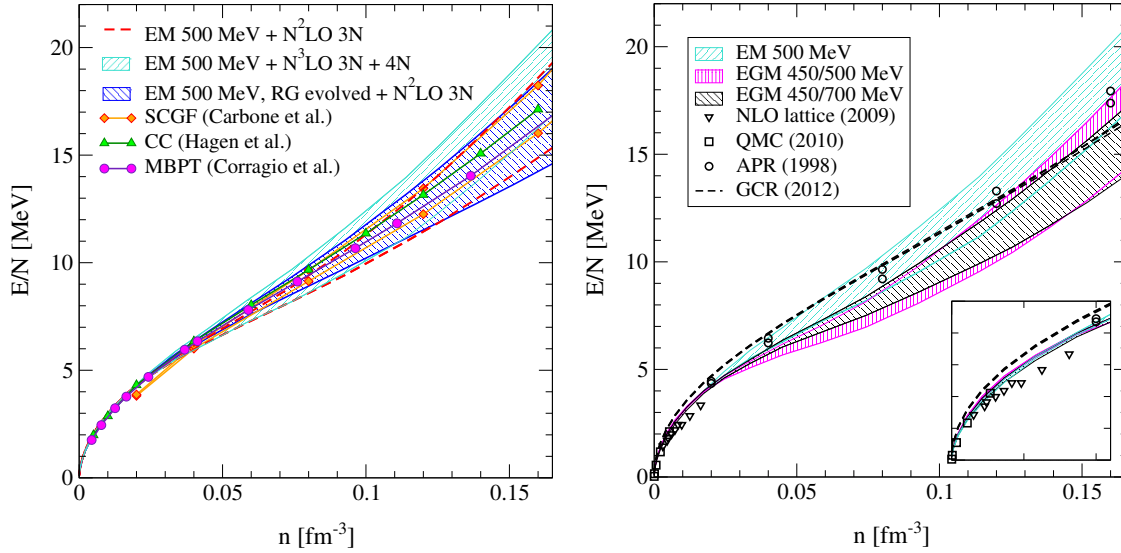


Figure 1.7: Equation of state of pure neutron matter as a function of the density obtained with several *ab initio* methods. Figure taken from [47].

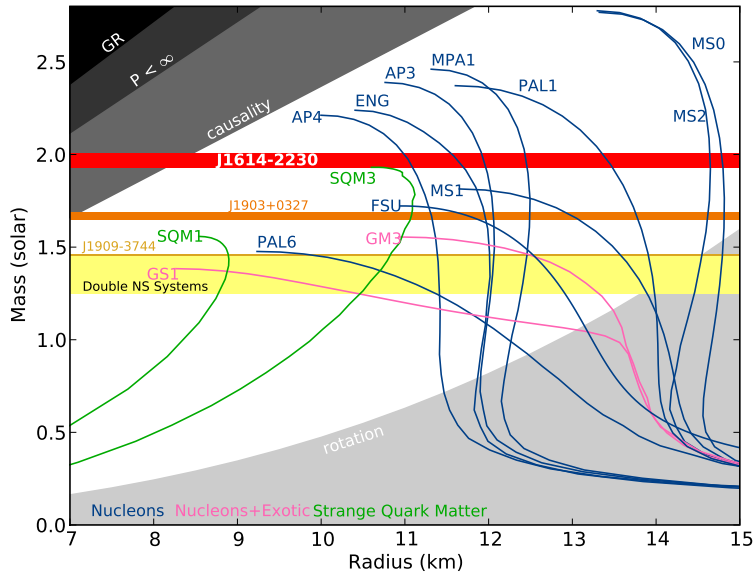


Figure 1.8: Neutron star mass-radius diagram obtained with several typical EOSs. The horizontal bands show the observational constraints. EOS lines that do not fall into the bands should be excluded. Figure taken from [48].

consistent Green's function (SCGF) [49], the Brueckner Hartree-Fock (BHF) [50–52] theories, the QMC [53] and Auxiliary-Field Diffusion Monte-Carlo (AFDMC) [54,55] methods, the many-body perturbation theory (MBPT) calculation [56–60] based on χ EFT interactions, and the coupled-cluster (CC) approach [61].

Note that the two-body interaction is not enough to account for the saturation point of the symmetric matter, i.e. a minimum energy per particle around density $\rho \simeq 0.16 \text{ fm}^{-3}$. The role of the three-body force (see figure 1.6) is an important component to take into account in calculations.

One of the challenges of *ab initio* methods is to get systematic well-controlled reference exact calculations. These calculations can provide important information for energy density functional theory where data are missing. For instance, one important issue is that *ab initio* results can serve as pseudo-data on which an energy density functional (EDF) theory can be adjusted (for example on the Akmal-Friedman-Pandharipande-Ravenhall [62,63] EOSs). This point is discussed in more details in the next section. Another example is the work [64] where the Skyrme energy density functional was constrained with QMC calculations by studying the spin-impurity problem in polarized low-density neutron matter. This work in particular highlights that the *ab initio* calculations can be used to get additional constraints (not available, in practice, from experiment) on the energy density functional (see figure 1.9 where selected energy density functional results on the single-particle energy of the impurity are compared to the QMC calculation).

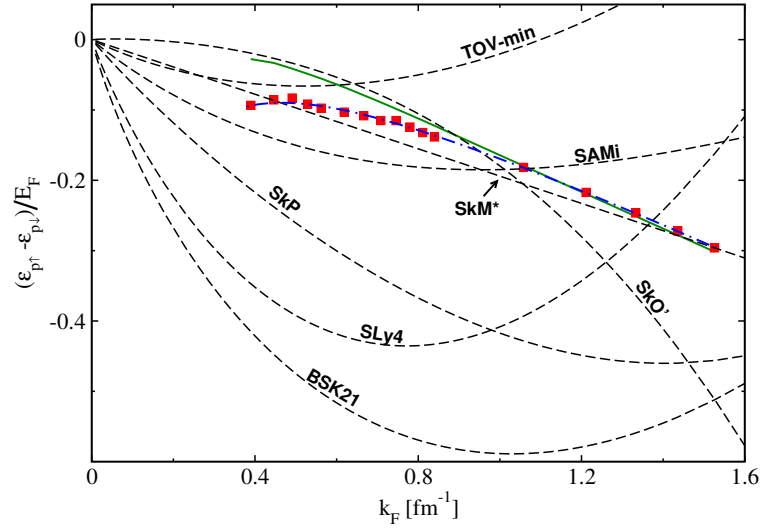


Figure 1.9: Difference between the energies of the (proton) spin-up and spin-down impurities. The red squares are the QMC results of [64]. The black dashed-lines are predictions from various density functionals as a function of the Fermi momentum related to the local density through $k_F = (6\pi^2\rho)^{1/3}$. Figure taken from [64].

LIMITATIONS OF AB INITIO METHODS BASED ON χ EFT INTERACTIONS

As mentioned previously, the χ EFT formalism, used to design the nuclear interaction directly relying on the low-energy sector of the QCD, has strongly impacted the range of application of *ab initio* methods. For symmetric matter, the reproduction of the empirical saturation point $E/A(\rho_0 \simeq 0.16 \text{ fm}^{-3}) \simeq -16 \text{ MeV}$ requires the low-momentum NN interaction together with the three-body interaction interactions [65]. However, the many-body results using EFT parameters fitted only to few-body data have large uncertainty stemming for instance from the cutoff dependence of the two- and three-body interactions. In figure 1.10, the cutoff dependences of the symmetric and neutron matter EOSs are shown and present actually large error bars independently of the accuracy of the *ab initio* method employed. This is also displayed in figure 1.7 where large uncertainties are seen due to the cutoff dependence.

The use of a χ EFT interaction has conceptual interest in the sense that the many-body calculation can be systematically improved. However their uncertainties strongly limit their predictive power in application related to neutron star properties that are of interest in astrophysics as well as for heavy-ion collisions, neutron-

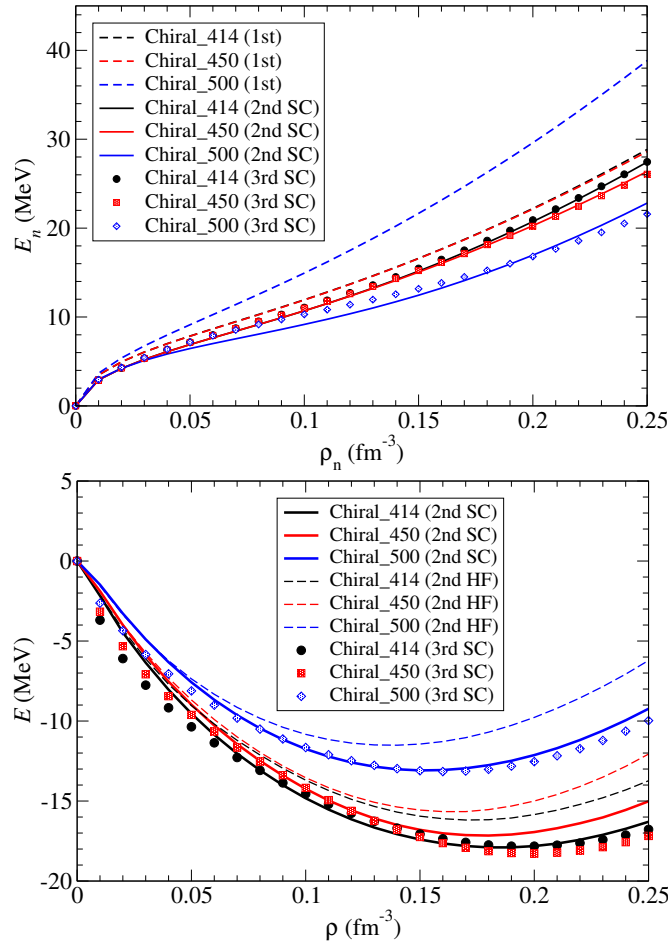


Figure 1.10: EOS for neutron (top) and symmetric matter (bottom) obtained at second and third order in many-body perturbation theory from χ EFT two- and three-body interactions. Results are shown, using χ EFT interaction constructed with different cutoffs ($\Lambda = 414, 450, 500$ MeV), at first, second and third order in many-body perturbation theory, at Hartree-Fock (HF) level or in a self-consistent (SC) calculations. Figure taken from [66].

rich nuclei, or to determine the thicknesses lower limit to the neutron-skin. In particular, important quantities like the symmetry energy $S(\rho)$, encoding the difference in energy between the neutron matter and symmetric matter EOS, and its slope parameter at saturation $L = 3\rho_0 S'(\rho_0)$ (with $\rho_0 \simeq 0.16 \text{ fm}^{-3}$) are strongly impacted. As shown in figure 1.11 (right), the confidence bands between $S(\rho_0)$ and L from the χ EFT interaction are still large even up to N₃LO. For instance, these uncertainties are large in the neutron matter EOS at a density relevant for neutron stars studies. In figure 1.11 (left), QMC calculation are displayed where each set of lines is obtained by adjusting the chosen values of the symmetry energy and its slope at saturation density with the three-body force parameter of the interaction. This leads to a difference at saturation going from $L \simeq 20$ to $L \simeq 60$ MeV per nucleon while being coherent with the constraints provided by the interaction. It is worth mentioning that, at these high densities, the proper treatment of the non-perturbative hard core part of the nuclear interaction (see figure 1.2) becomes necessary.

Another relevant limit is the low density of the nuclear matter. In that case, the $\not{\chi}$ EFT interaction (1.6) is appropriate to describe the relevant scale of the NN interaction (see chapter 2). However, the existence of an unnaturally large s -wave scattering length in nuclear physics (see table 1.1) makes impracticable standard

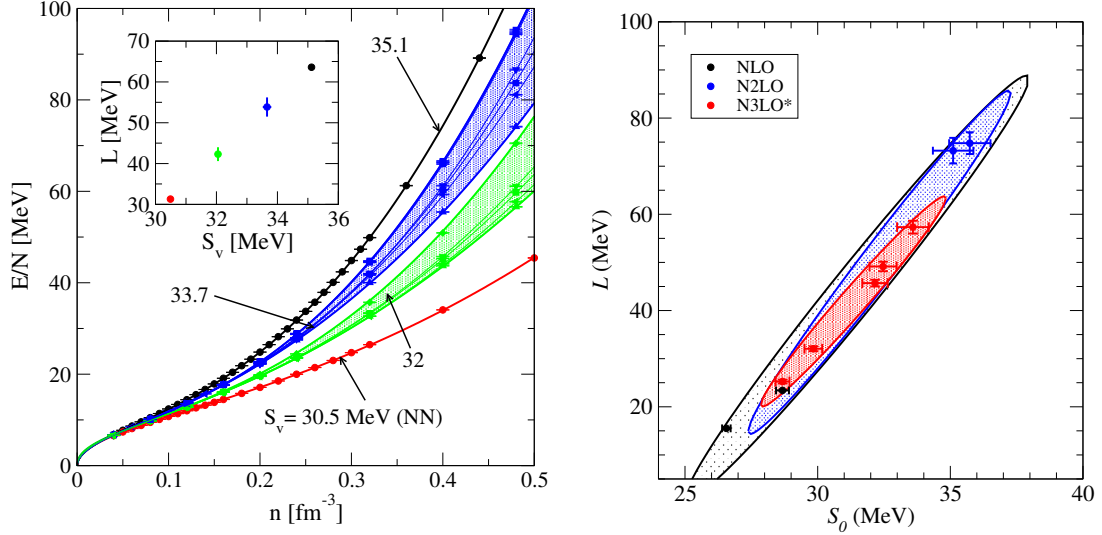


Figure 1.11: Left (taken from [47]): EOS for neutron matter obtained using QMC calculation from phenomenological two- and three-body interactions imposing several values of the symmetry energy at saturation (noted S_v). The inset corresponds to the density dependence of the symmetry energy at saturation characterized by the L parameter.

Right (taken from [66]): The symmetry energy at saturation (noted S_0) as a function of the L parameter. The symbols correspond to the result obtained from *ab initio* calculation using χ EFT two- and three-body interaction at N₃LO, N₂LO and NLO respectively. The confidence bands correlation are also shown.

perturbative approaches to describe this strongly correlated Fermi system. The dilute regime of nuclear matter presents some common aspects with the ultracold Fermi atomic systems discussed below.

UNITARY LIMIT AND ITS LINK WITH NUCLEAR PHYSICS

The low density limit and strong coupling for which the s -wave scattering length a_s is infinite, namely the unitary gas limit, has recently received a special and growing interest in nuclear physics. Such systems have been widely studied both from theoretical and experimental points of view during the last decades [67]. In particular, the recent advances in ultracold atomic Fermi gases experiment, where a_s can be fine tuned from weak to strong coupling by applying an external magnetic field, allowed to determine precisely the equation of state of the unitary Fermi gas [67–69]. The ground state energy of this system is characterized by an infinite s -wave scattering length a_s in the dilute regime. In this regime, C_0 in (1.6) becomes the only relevant LEC. At unitarity, the ground state energy becomes directly proportional to the free Fermi-Gas energy E_{FG} :

$$E = \zeta_0 E_{FG} \quad \text{with} \quad E_{FG} = \frac{3(3\pi^2)^{2/3}}{10m} \rho^{5/3}. \quad (1.8)$$

This energy can be seen as one of the simplest energy density functional one could ever imagine, the energy being only function of the local density ρ (m is the mass of the particle). The constant ζ_0 is the so-called universal Bertsch parameter and its experimentally observed value $\zeta_0 = 0.37$ [70,71] is in good agreement with the *ab initio* calculations of [72,73]. Still, while in a density functional theory framework, unitary gases can be described in a rather simplistic manner (see for instance [74–76]), their treatment, starting from a particle-particle interaction, requires rather

advanced many-body techniques as illustrated in figure 1.12 showing that it took a number of years before the theoretical predictions and experimental observations converge. Among the *ab initio* methods used to describe unitary gas properties, one can mention the Monte-Carlo methods [72,77–82], the SCGF [73,83], the BHF calculation [84], and the Bold Diagrammatic Monte Carlo (BDMC) approach [85, 86] eventually associated to a resummation technique based on a conformal-Borel transformation [87]. Unitary gas turned out to be a remarkable guide to test and design many-body theories. For instance, the unitary limit was used to constrain the nuclear symmetry energy [88].

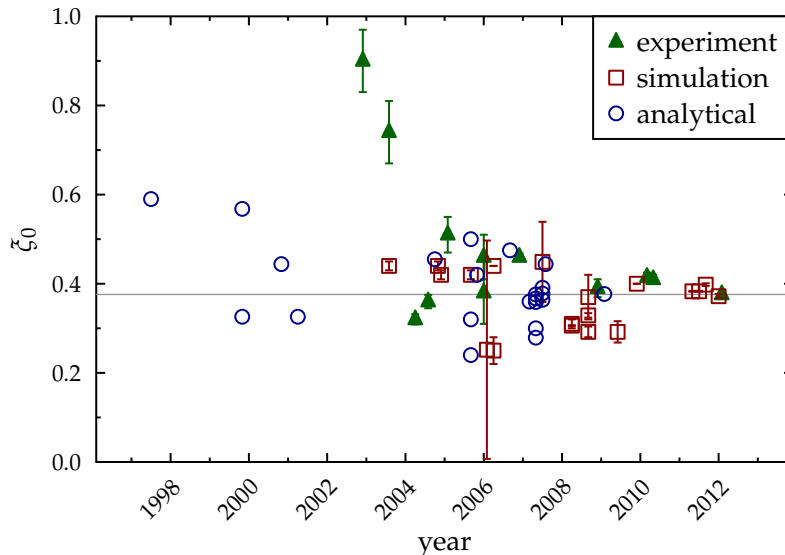


Figure 1.12: Evolution of the Bertsch parameter predictions ζ_0 from experiments, analytical calculations, or numerical simulations (including *ab initio* methods) from 1997 to 2012. Numerical values and references are tabulated in Table VI of [82]. The gray line corresponds to its accepted value $\zeta_0 = 0.37$.

Although in this thesis we will focus on infinite systems, for completeness I give a brief overview of recent results in finite nuclei.

1.2.B Challenges in atomic nuclei

AB INITIO METHODS IN NUCLEAR PHYSICS:

FROM LIGHT- TO MID-MASS CLOSED-SHELL NUCLEI

Although this is slightly out of the scope of this thesis, we slightly discuss some recent progress of *ab initio* methods applied to nuclei for completeness.

Since the seminal works using *ab initio* approaches to describe light-mass nuclei, based on, for instance, quantum Monte Carlo (QMC) [89,90] or no-core shell model (NCSM) [91,92] calculations, extraordinary progress, displayed in figure 1.13, have been made during the last 15 years to extend the reach of *ab initio* calculations to the realm of mid-mass nuclei.

Thanks to the softness of the novel generation of *NN* interaction, several many-body techniques, that were hardly applicable with empirical forces have been developed. In order to grasp crucial dynamical correlations induced by the strong *NN* interactions, non-perturbative approaches resumming perturbative corrections to all orders beyond the mean-field have been developed like the in-medium similarity renormalization group (IMSRG) [93], the coupled-cluster (CC) [94] or the self-consistent Green's function (SCGF) [95] theories.

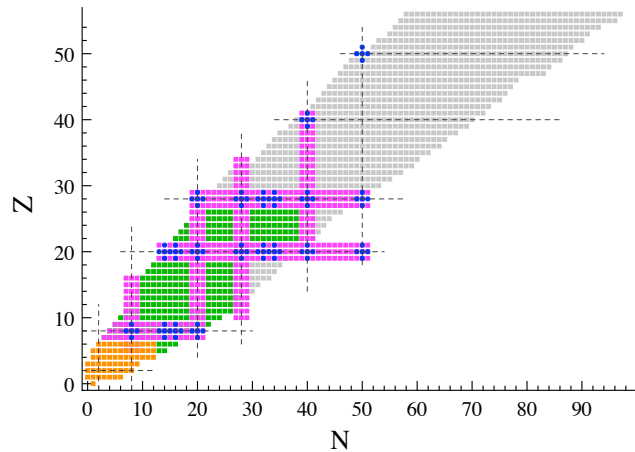


Figure 1.13: State of the art of *ab initio* methods in 2019. Orange: light nuclei (QMC, NCSM, ...); Pink/Blue: medium-mass closed- (SCGF, CC, IMSRG) or singly open-shell nuclei (GoSCGF, MR-IMSRG, ...); Green: open-shell nuclei (CC IMSRG, ...). (V. Somà, private communication.)

SYMMETRY-BREAKING: EXTENSION TO SINGLY OPEN-SHELL NUCLEI

While the breakthrough into the domain of mid-mass nuclei described above was first restricted to so-called doubly closed-(sub)shell nuclei, a current challenge is to extend the different methods to open-shell nuclei. Such description faces the difficulty of an increase of the many-body Hilbert space size due to spontaneous symmetry breaking like pairing. These extensions are needed to grasp so-called static correlations at play in open-shell nuclei. One current option consists in expanding the exact solution around a multi-reference (MR) state described by a linear combination of Slater determinants or quasi-particle vacuum. This was achieved within MR-IMSRG [93] and MR-CC [96] theories. Another option consists in keeping the simplicity of single-reference methods at the price of allowing the reference state to spontaneously break symmetries, e.g. particle number and/or angular momentum, of the Hamiltonian. This was achieved within the frame of Gorkov SCGF (GoSCGF) [97–99] and Bogoliubov CC (BCC) [100] theories.

The breaking of particle number symmetry $U(1)$ (respectively angular momentum $SU(2)$) symmetry⁷ allows to take into account, at the unperturbed level, the dominant part of static, e.g. pairing (respectively deformation), correlations in singly (respectively doubly) open-shell nuclei. Then, dynamical correlations are consistently captured via the systematic expansion of the exact solution around such a symmetry breaking reference state.

RESTORATION OF SYMMETRIES: TOWARDS OPEN-SHELL NUCLEI

While breaking symmetries allows to efficiently grasp most of the static correlations, the symmetry breaking is artificial in finite quantum systems and symmetries need to be eventually restored. In the case of the $U(1)$ group, symmetry breaking results are contaminated by contributions from different particle numbers, i.e. from neighboring nuclei. Restoring the symmetry, i.e. the correct particle number, is needed to properly describe the system of actual interest.

General methodologies have recently been formulated to restore the broken symmetries at any truncation order within (B)MBPT and (B)CC formalisms [102–105]. While recently achieved for (B)CC and (B)MBPT, the particle number (resp. angular momentum) restoration remains to be formulated within the frame of GoSCGF.

⁷ The symmetry breaking concept has a long tradition in the nuclear energy density functional method based on effective interactions [101].

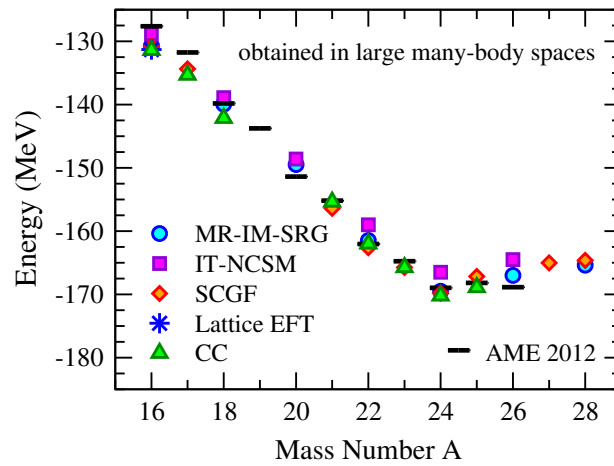


Figure 1.14: Ground state energy of oxygen isotope obtained with several *ab initio* methods and compared to experimental atomic mass evaluation (AME). Figure taken from [47].

1.2.c Discussion on *ab initio* methods

The description of finite systems with *ab initio* using the bare NN interaction is one of the more challenging tasks for the coming decades⁸. In particular, assuming that the many-body techniques do not add uncertainty, the only critical source of uncertainty (increasing with the density still large at saturation density) stems from the interaction itself. Note that important debates exist nowadays on this issue. For instance, it was recently proposed in [106] to develop empirical two- and three-body χ EFT interaction, namely N_2LO_{sat} adjusted on the low-energy NN scattering data, as well as binding energies and radii of few-nucleon systems and selected nuclei. It was shown (see figure 1.15 for an illustration) that the use of this interaction in *ab initio* calculations is able to describe binding energies and radii of light and medium-mass nuclei (up to ^{40}Ca). One of the successes of N_2LO_{sat} is that the *ab initio* EOS of symmetric matter is consistent with the empirical saturation point, still difficult to properly reproduce starting from standard nuclear interaction (see the large uncertainty bands in figure 1.7), as shown in figure 1.16.

We also know that *ab initio* techniques cannot offer right now a quantitative theory for the whole nuclear chart (see figure 1.13) due to the numerical complexity. On the nuclear reaction side, it is also restricted to very specified reaction channels involving rather light nuclei [107]. It is hard now to imagine how the richness of phenomena observed in reactions can be grasped in an *ab initio* framework at present time.

Such limitations are absent in the empirical nuclear energy density functional (EDF) theory that provides a simple and unified framework for nuclear problems with a rather high predictive power. We present below selected aspects of nuclear EDF to illustrate its simplicity, powerfulness as well as its inherent shortcomings.

⁸ One of the difficulties in applying these methods is related to in-medium effects, i.e. the situation when two nucleons interact in the vacuum is different from the situation when the interacting pair of nucleons is surrounded by medium composed of other nucleons. It is mainly due to the Pauli blocking effect which restricts the accessible configuration of the NN interacting systems compared to the free-space situation. One challenge of *ab initio* methods is to take into account the in-medium effect correlations by dressing properly the bare NN interaction. Another difficulty comes from the fact that atomic nuclei are mesoscopic fermionic systems, i.e. finite size of the systems are important and lead to non-trivial effects. Moreover, for a system of A nucleons, the dimension of the Hilbert space is very large of order $\sim A!$. Despite the impressive progress of *ab initio* methods, these techniques are still restricted to a rather small part of the nuclear chart (see figure 1.13).

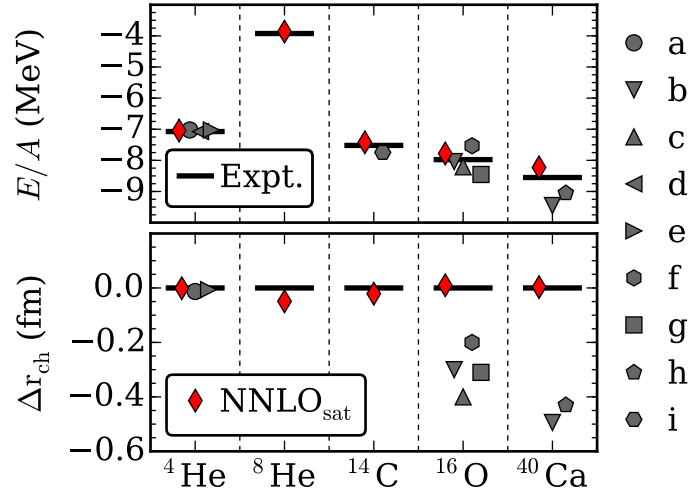


Figure 1.15: Ground-state energy per nucleon (top), and difference between computed and experimental values of charge radii (bottom) for selected nuclei computed with chiral interactions. The red diamonds are $\text{N}^2\text{LO}_{\text{sat}}$ results and other gray symbols are obtained using other χEFT interactions. Figure taken from [106].

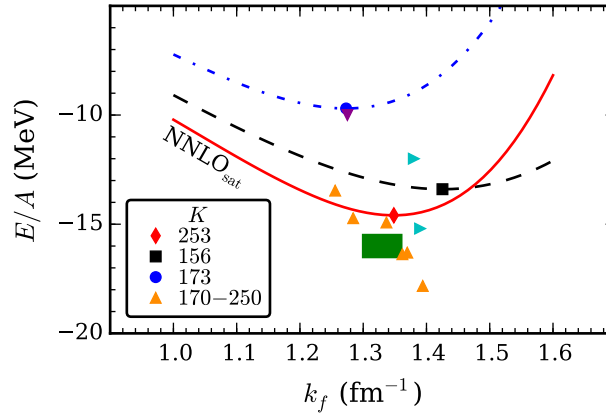


Figure 1.16: EOS for symmetric nuclear matter from chiral interactions. Red solid-line is the $\text{N}^2\text{LO}_{\text{sat}}$ result as function of the Fermi momentum related to the local density through $k_F = (6\pi^2\rho)^{1/3}$. The symbols correspond to other theoretical *ab initio* saturation point predictions associated to their incompressibility in the legend. The green area shows the empirical saturation point. Figure taken from [106].

1.3

EMPIRICAL DENSITY FUNCTIONAL THEORIES

Despite the success of *ab initio* approaches to describe nuclear systems presented in the previous section, their applicabilities are restricted to a rather small part of the nuclear chart and they can hardly attack some important problems of nuclear physics related to dynamics. To overcome the difficulty of the exact resolution of the nuclear many-body problem, simpler approaches have been introduced in nuclear physics like the energy density functional (EDF) theory [101,108–112]. The nuclear EDF is based on the possibility to replace the nuclear many-body problem by a problem of independent particles or quasi-particles if superfluidity is considered. It could be seen as the nuclear physics counterpart of the density functional theory (DFT) approach for electronic systems [113–120], with the important difference that here nuclei are self-bound systems. This difference is crucial because, for the moment, the EDF lacks an existence theorem contrary to the DFT approach [121–123]. Nevertheless this approach turns out to be extremely powerful and aims also at describing exactly the nuclear many-body problem. Even if this framework seems rather simple compared to the high complexity of nuclear physics, many phenomena are very well described in nuclear systems assuming nucleons as independent particles immersed in an effective self-consistent one-body potential. For instance, the single-particle shell effects appearing in atomic nuclei, e.g. the emergence of magic numbers, are important arguments to legitimate the independent-particle character of the in-medium nucleons. The nuclear EDF also provides, in addition to the ground state properties, a unified microscopic framework to the description of lots of phenomena at play in nuclear structure and reactions, as well as in nuclear astrophysics. This approach is able to account for the nuclear spectroscopy, nuclear shapes, small and large amplitude dynamics and thermodynamical properties of finite or infinite systems.

In the following, the concept of nuclear EDF is introduced. A particular attention will be paid to empirical functionals that have been historically introduced in nuclear physics. The important notions that will be useful in the present thesis are discussed.

1.3.A Basic illustration of how an EDF theory can be introduced from simple arguments

In a DFT framework the energy of the system is written in terms of a functional of the density ρ as:

$$E[\rho] = \int \mathcal{E}(\rho(\mathbf{r})) d^3r. \quad (1.9)$$

In the original DFT version, ρ denotes the local density of the system. In a strict DFT framework, at the minimum, the energy matches the exact energy and the local density matches the exact local density [124]. Many extensions exist where the energy becomes a functional not only of $\rho(\mathbf{r})$, but also of its derivatives, i.e. $\mathcal{E} = \mathcal{E}(\rho(\mathbf{r}), \nabla\rho(\mathbf{r}), \dots)$. Also, to treat superfluid systems, the energy is sometimes written as a functional of $\rho(\mathbf{r})$ and of the anomalous density $\kappa(\mathbf{r})$, i.e. $\mathcal{E} = \mathcal{E}(\rho(\mathbf{r}), \kappa(\mathbf{r}))$. The existence of a DFT gives however no guidance on the form of the DFT itself.

Below, we show how the DFT can be empirically introduced for nuclear systems. In this context, although it is absolutely not necessary, the concept of effective interaction that is standardly employed to design the nuclear DFT is discussed.

DFT FOR FINITE NUCLEI IN A NUTSHELL

The experimental observations of the density profile of nuclei, for instance in proton knockout experiments or in electron scattering, show that the density inside the nuclei are almost constant and close to the so-called saturation density $\rho_0 \simeq 0.16 \text{ fm}^{-3}$. This is illustrated in figure 1.17. To a good approximation, the

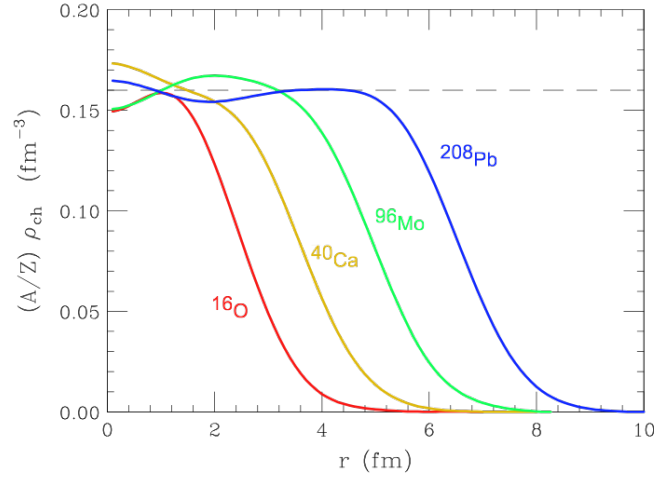


Figure 1.17: Density profile of proton, multiplied by the factor A/Z to get the total density, for several atomic nuclei. Figure taken from [125].

density profile can be parametrized by a Thomas-Fermi shape:

$$\rho(r) = \rho_0 \left[1 + \exp\left(\frac{r - r_0}{a_0}\right) \right]^{-1}. \quad (1.10a)$$

The value of the phenomenological parameters are given by $r_0 \simeq 1.2A^{1/3} \text{ fm}$ and $a_0 \simeq 0.5 \text{ fm}$. In an independent-particle picture, it turns out that an approximate form of the one-body potential felt by nucleons can be parametrized as a Woods-Saxon potential also given by:

$$U(r) = U_0 \left[1 + \exp\left(\frac{r - r_0}{a_0}\right) \right]^{-1}, \quad (1.10b)$$

with $U_0 \simeq -50 \text{ MeV}$. It is then immediate to realize that this potential can be written as a functional of the density with $U(r) = U_0 \rho(r)/\rho_0$.

Starting from this simple argument, we see that the energy of the system can be written as:

$$E = E_{kin} + E_{int}[\rho] \quad (1.11a)$$

with:

$$E_{int}[\rho] = \frac{U_0}{2\rho_0} \int \rho(r)^2 dr, \quad (1.11b)$$

where the single-particle potential can be deduced from:

$$U(\mathbf{r}) = \frac{\delta E_{int}[\rho]}{\delta \rho(\mathbf{r})}. \quad (1.11c)$$

This functional turns out to be too simplistic to describe for instance saturation properties or the internal pressure of the system. However, few additional terms are enough to already give a rather good description of nuclei.

INFINITE NUCLEAR MATTER

In the case of homogeneous infinite matter, the situation is simplified since the local density remains independent of the position. Consequently, the energy becomes a simple functional of the one-body density ρ that is now a number. A natural extension of (1.11b) is to assume a polynomial form of the energy functional:

$$\frac{E_{int}(\rho)}{A} = \alpha_2 \rho^2 + \alpha_3 \rho^3 + \dots \quad (1.12)$$

and fit the parameters $\{\alpha_i\}$ on the equation of state of nuclear matter given for instance by *ab initio* calculations (see figure 1.7). This strategy provides an explicit energy, function of the density, valid up to a certain density according to the order of the polynomial form in ρ .

The interest of these approaches based on the independent-particle picture is that the correlations between particles can be automatically and fully incorporated through the fit of the empirical coefficients on *ab initio* results. These *ab initio* results then serve as pseudo-data in this case. The adjustment of parameters on observables containing all correlations implies that the DFT should *a priori* also be considered as an *ab initio* method (this has been known for a long time in condensed matter but not in nuclear physics). It stands out from other *ab initio* methods by its simplicity.

The two previous illustrations are very schematic. A specific strategy is commonly used in nuclear physics, based on the use of an effective interaction, e.g. Skyrme [108,110,111] or Gogny [126] to quote two of them, and guided by the Hartree-Fock theory. This strategy that is briefly exposed below provides a simple formulation of the nuclear many-body problem accounting for the complexity of the systems, e.g. the spin-isospin dependence of the interaction, inclusion of gradient terms, kinetic density terms, pairing, etc... In the following, we discuss the phenomenological effective two-body interactions largely used in nuclear physics to design the EDF taking as an illustration the case of Skyrme-like effective interactions.

1.3.B Effective interaction adjusted on mean field

The success of Vautherin and Brink [108,110,111] to describe the ground-state properties of nuclei, at mean-field level, starting from a Skyrme-like effective (contact) interaction demonstrated how accurate can be the approach. In the following, we introduce the corresponding functional and discuss the adjustment of the parameters and the link with Landau theory of Fermi liquid. For more details, see [112,127,128] for instance.

SKYRME LIKE EFFECTIVE INTERACTION

The idea of Vautherin and Brink was to propose a Skyrme like two-body and three-body contact interaction able to provide, at the Hartree-Fock level, a simple form of the EDF. Then, the parameters of the interaction are directly adjusted on some properties of finite or infinite systems. In its simplest form, the most commonly used Skyrme effective interaction between two particles, labeled by $(\mathbf{r}_1, \sigma_1, \tau_1)$ and $(\mathbf{r}_2, \sigma_2, \tau_2)$, is written as⁹:

$$\begin{aligned}
 V(\mathbf{r}_1, \sigma_1, \tau_1; \mathbf{r}_2, \sigma_2, \tau_2) = & t_0(1 + x_0 P_\sigma) \delta(\mathbf{r}) \\
 & + \frac{1}{2} t_1(1 + x_1 P_\sigma) \left[\mathbf{k}'^2 \delta(\mathbf{r}) + \delta(\mathbf{r}) \mathbf{k}^2 \right] \\
 & + t_2(1 + x_2 P_\sigma) \mathbf{k}' \cdot \delta(\mathbf{r}) \mathbf{k} \\
 & + \frac{1}{6} t_3(1 + x_3 P_\sigma) [\rho(\mathbf{R})]^\alpha \delta(\mathbf{r}) \\
 & + i W_{so} \sigma \cdot [\mathbf{k}' \times \delta(\mathbf{r}) \mathbf{k}], \tag{1.13}
 \end{aligned}$$

where we recognize a central (t_0, x_0) , non-local (t_1, x_1, t_2, x_2) , density dependent (t_3, x_3, α) and spin-orbit (W_{so}) term. The interaction (1.13) is written using the standard notations:

$$\mathbf{r} = \mathbf{r}_1 - \mathbf{r}_2, \quad \mathbf{R} = \frac{1}{2} [\mathbf{r}_1 + \mathbf{r}_2], \quad \text{and} \quad \mathbf{k} = \frac{1}{2} [\mathbf{k}_1 - \mathbf{k}_2].$$

Note that \mathbf{k}' and \mathbf{k} stand for the outgoing and incoming relative momentum of interacting particles. The spin exchange operator is defined by $P_\sigma = [1 + \boldsymbol{\sigma}_1 \cdot \boldsymbol{\sigma}_2] / 2$ and the total spin by $\mathbf{S} = \boldsymbol{\sigma}_1 + \boldsymbol{\sigma}_2$.

It is worth mentioning that the central (t_0, x_0) and non-local terms (t_1, x_1, t_2, x_2) look like to the $\not\equiv$ EFT interaction (1.6) where the coupling constants are actually expressed, most generally and before projection on the scattering channel, as $C_i = \gamma_i(1 + \kappa_i P_\sigma)$ [15]. More precisely, considering the $L = 0$ partial wave channel with total spin S , the projector P_σ is equivalent to $S^2 + S - 1$. Thus, in the particular case of neutron-neutron scattering, only the state with total spin $S = 0$ is allowed by the Pauli principle because of the use of a contact interaction. By matching (1.13) with (1.6) and using (1.7), one can define an effective s -wave scattering length \tilde{a}_s , an effective s -wave range \tilde{r}_s , and an effective p -wave scattering volume \tilde{a}_p^3 for the Skyrme interaction¹⁰ considering only neutrons:

$$\begin{aligned}
 \frac{4\pi}{m} \tilde{a}_s &= t_0(1 - x_0), & \frac{2\pi}{m} \tilde{r}_s \tilde{a}_s^2 &= t_1(1 - x_1), \\
 \text{and} \quad \frac{4\pi}{m} \tilde{a}_p^3 &= t_2(1 + x_2). \tag{1.14}
 \end{aligned}$$

Finally, the value of the parameters $\{t_0, x_0, t_1, x_1, t_2, x_2, t_3, \alpha, W_{so}\}$ are adjusted to reproduce the properties of nuclear systems. This is quite different from the strat-

⁹ Note that, historically, the three-body contact was written as $t_3 \delta(\mathbf{r}_1 - \mathbf{r}_2) \delta(\mathbf{r}_2 - \mathbf{r}_3)$ [129], but it was at some point replaced by a density-dependent two-body interaction ($t_3 \rho^\alpha$ term with α a whole numbers) to get equilibrium point for asymmetric matter and simplify the calculations. Then, to facilitate the reproduction of the compressibility for instance, α was chosen as rational numbers [101]. This term clearly shows that the effective interaction should not be confused with a true interaction.

¹⁰ For neutron matter, in the p -wave channel, only the total spin $S = 1$ is allowed hence the substitution $P_\sigma \rightarrow +1$.

egy used in *ab initio* theories where the starting point is the bare NN interaction adjusted on the scattering properties of few nucleons in the vacuum. Here the effective interaction is directly adjusted to reproduce the exact properties. Due to this, we see in figure 1.18 that the effective LECs (1.14) obtained from several parametrizations of the Skyrme functional differ strongly from their physical values (see table 1.1). A clear advantage is that the properties of nuclear systems

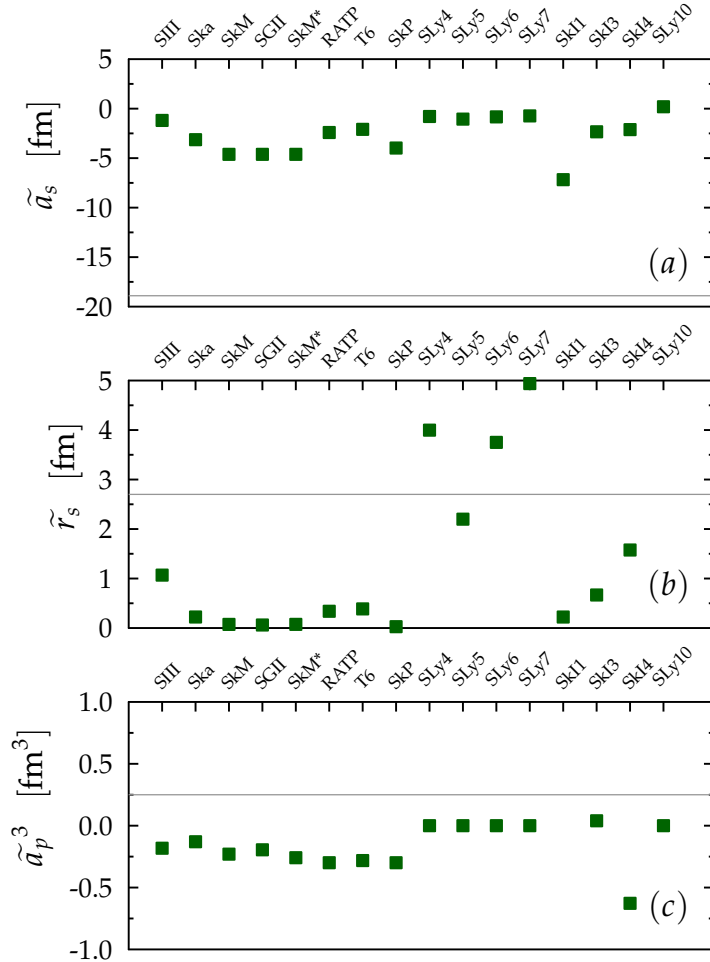


Figure 1.18: Effective LECs (1.14) obtained with various parameterizations of the Skyrme effective interaction (1.13) in the case where only neutron-neutron scattering systems is considered. The gray line corresponds to the bare physical value obtained from experimental scattering data analysis given in table 1.1: $a_s = -18.9$ fm and $r_s = 2.7$ fm. For the value of the p -wave scattering length, we follow [130] using AV4 scattering data: $a_p^3 = 0.25$ fm³.

are then deduced from a mean-field framework and do not require advanced *ab initio* many-body formalism. However, we also see a drawback: the parameters entering in the EDF have lost the connection with the LEC of the interaction.

SKYRME FUNCTIONAL FOR FINITE NUCLEI

The underlying idea of the introduction of effective interactions (1.13) relies on the fact that, in the case of a zero-range interaction, the energy of the system takes a very simple form at the Hartree-Fock level. In the independent particle picture and without superfluidity, the wave function of the systems is a Slater determinant noted by $|\psi\rangle$ and expressed in terms of the independent particle wave functions $\phi_{l,s}^q$ where l,s and $q = p,n$ denote respectively orbital, spin and isospin quantum

numbers. The ground state energy of the system is given by the expectation value of the Hamiltonian, i.e.:

$$E = \langle \psi | H | \psi \rangle = \int \mathcal{H}(\mathbf{r}) d\mathbf{r} = \int [\mathcal{T}(\mathbf{r}) + \mathcal{V}(\mathbf{r}) + \mathcal{V}_c(\mathbf{r})] d\mathbf{r} \quad (1.15)$$

where the Hamiltonian density can be decomposed into a kinetic contribution, a contribution due to the nuclear interaction \mathcal{V} and a Coulomb term \mathcal{V}_c . Eventually, the pairing effect can be included by authorizing the many-body state to break the $U(1)$ symmetry associated with the particle number symmetry. The interaction contribution can also be decomposed as the sum of many terms¹¹:

$$\mathcal{V} = \mathcal{V}_0 + \mathcal{V}_e + \mathcal{V}_\star + \mathcal{V}_3 + \mathcal{V}_j + \mathcal{V}_{so}, \quad (1.16)$$

where \mathcal{V}_0 stands for the zero-range contribution, \mathcal{V}_e for an effective range contribution, \mathcal{V}_\star for an effective mass term, and \mathcal{V}_3 for the contribution of the density dependent term. The contribution \mathcal{V}_j comes from the spin-gradient coupling and \mathcal{V}_{so} from the spin-orbit coupling contribution:

$$\mathcal{V}_0 = \frac{1}{4} t_0 \left[(2 + x_0) \rho^2 - (2x_0 + 1) (\rho_p^2 + \rho_n^2) \right] \quad (1.17a)$$

$$\begin{aligned} \mathcal{V}_e &= \frac{1}{32} [3t_1(2 + x_1) - t_2(2 + x_2)] (\nabla \rho)^2 \\ &\quad - \frac{1}{32} [3t_1(2x_1 + 1) + t_2(2x_2 + 1)] \left[(\nabla \rho_p)^2 + (\nabla \rho_n)^2 \right] \end{aligned} \quad (1.17b)$$

$$\begin{aligned} \mathcal{V}_\star &= \frac{1}{8} [t_1(2 + x_1) + t_2(2 + x_2)] \tau \rho \\ &\quad - \frac{1}{8} [t_1(2x_1 + 1) - t_2(2x_2 + 1)] [\tau_p \rho_p + \tau_n \rho_n] \end{aligned} \quad (1.17c)$$

$$\mathcal{V}_3 = \frac{1}{24} t_3 \rho^\alpha \left[(2 + x_3) \rho^2 - (2x_3 + 1) (\rho_p^2 + \rho_n^2) \right] \quad (1.17d)$$

$$\mathcal{V}_j = -\frac{1}{16} (t_1 x_1 + t_2 x_2) \mathbf{J}^2 + \frac{1}{16} (t_1 - t_2) [\mathbf{J}_p^2 + \mathbf{J}_n^2] \quad (1.17e)$$

$$\mathcal{V}_{so} = \frac{W_{so}}{2} [\mathbf{J} \cdot \nabla \rho + \mathbf{J}_p \cdot \nabla \rho_p + \mathbf{J}_n \cdot \nabla \rho_n], \quad (1.17f)$$

where ρ_p, ρ_n and ρ denote respectively the proton, neutron and total local density with $\rho = \rho_p + \rho_n$. $\tau = \tau_p + \tau_n$ denotes the local kinetic density, and $\mathbf{J} = \mathbf{J}_p + \mathbf{J}_n$ denotes the total spin density. These quantities are defined in term of the particle wave functions as:

$$\rho_q = \sum_{l,s} |\phi_{l,s}^q|^2, \quad \tau_q = \sum_{l,s} |\nabla \phi_{l,s}^q|^2 \quad \text{and} \quad \mathbf{J}_q = \sum_{l,s,s'} \phi_{l,s'}^{q*} \nabla \phi_{l,s}^q \times \langle s' | \boldsymbol{\sigma} | s \rangle. \quad (1.18)$$

In practice, the wave functions $\phi_{l,s}^q$ are obtained by solving the coupled set of self-consistent Schrödinger equations:

$$\left[\frac{k^2}{2m} + U^q(\mathbf{r}) \right] \phi_{l,s}^q(\mathbf{r}) = \varepsilon_{l,s}^q \phi_{l,s}^q(\mathbf{r}), \quad (1.19)$$

¹¹ From now, the space dependence is omitted.

where $\varepsilon_{l,s}^q$ are the single-particle energies. The single-particle potential U^q is obtained using the functional derivative of the energy with respect to $\rho(\mathbf{r})$ similarly to (1.11c). The calculation of U^q , that depends also on the single-particle wave functions, is rather simple for the Skyrme functional [131]. For instance, the contribution of the zero-range part gives:

$$U_0^q = \frac{1}{2}t_0 [(2 + x_0)\rho - (2x_0 + 1)\rho_q]. \quad (1.20)$$

Despite the simplicity of the method, this approach is very powerful and is extremely successful to describe various aspects of nuclei.

SKYRME FUNCTIONAL FOR INFINITE MATTER

In the infinite matter case, the calculation obtained with the Skyrme effective interaction are greatly simplified compared to the case of finite systems. The relevant single-particle wave functions are plane-waves and the local density is constant. The equation of state obtained with the Skyrme functional then reads [112]:

$$\begin{aligned} \frac{E^\beta}{A}(\rho) &= \frac{T^\beta}{A}(\rho) + \frac{1}{8}t_0 [2(2 + x_0) - (1 + 2x_0)I_6(\beta)]\rho \\ &+ \frac{1}{48}t_3 [2(2 + x_3) - (1 + 2x_3)I_6(\beta)]\rho^{\alpha+1} \\ &+ \frac{3}{40} \left(\frac{3\pi^2}{2} \right)^2 \left[\theta_v I_5(\beta) + \frac{1}{2}(\theta_s - 2\theta_v)I_8(\beta) \right] \rho^{5/3}, \end{aligned} \quad (1.21a)$$

where the kinetic part is given by:

$$\frac{T^\beta}{A}(\rho) = \frac{3}{10m} \left[\frac{3\pi^2}{2}\rho \right]^{2/3} I_5(\beta). \quad (1.21b)$$

To shorten the expression, the following notations are standardly used:

$$\theta_s = 3t_1 + t_2(5 + 4x_2), \quad \theta_v = t_1(2 + x_1) + t_2(2 + x_2),$$

and

$$I_n(\beta) = \frac{1}{2} \left[(1 + \beta)^{n/3} + (1 - \beta)^{n/3} \right],$$

where $\beta = (\rho_n - \rho_p)/\rho$ denotes the asymmetry ratio between the proton and neutron densities. The case $\beta = 1$ corresponds to the pure neutron matter whereas $\beta = 0$ corresponds to the symmetric matter.

The crucial advantage of the nuclear EDF is the simplicity of Hartree-Fock like calculations combined with a Skyrme effective contact interaction. This provides rather simple expressions of the physical quantities as a function of the one-body density, e.g. the EOS of nuclear matter (1.21a), that is parametrized by a limited set of parameters. These parameters are usually adjusted on the nuclear systems properties (binding energies and radii of ^{56}Ni , ^{132}Sn , ^{208}Pb , \dots , and nuclear matter properties) such as the experimental nuclear data on spherical nuclei and pseudo-data obtained by *ab initio* calculations (see for instance [132,133] or the UNEDF project). Below, some illustrations of nuclear matter constraints are listed.

NUCLEAR MATTER CONSTRAINTS

From the EOS (1.21a), we can introduce some important physical quantities for the adjustment of the Skyrme parameters $\{t_i, x_i\}$.

- *Saturation of symmetric matter* – The justification of the infinite matter model relies on the fact that the density at the center of heavy nuclei is almost constant (see figure 1.17). This properties signs the incompressible liquid nature of nuclear systems. The infinite symmetric matter can then be seen as the extrapolation of finite systems when the number of nucleons goes to infinity and the Coulomb interaction is switched off. Experimentally, the density in the core of nuclei is almost constant and saturates at around $\rho_0 = 0.16 \pm 0.002 \text{ fm}^{-3}$ for medium mass and heavy nuclei. The simple phenomenological liquid drop model gives an estimation of the energy at saturation¹²:

$$\frac{E}{A}(\rho_0) = -16,0 \pm 0.2 \text{ MeV.} \quad (1.22a)$$

- *Equilibrium condition at saturation* – The saturation properties are due to the equilibrium of the systems and proper saturation requires that the pressure at ρ_0 cancels out, i.e.:

$$P(\rho_0) = \rho_0^2 \left. \frac{dE/A}{d\rho} \right|_{\rho_0} = 0. \quad (1.22b)$$

This property induces a second constraint on the parameters.

- *Incompressibility of symmetric matter at saturation* – Another important quantity defined as:

$$K_\infty = 9\rho_0 \left. \frac{d^2E/A}{d\rho^2} \right|_{\rho_0} = 230 \pm 20 \text{ MeV} \quad (1.22c)$$

stands for the curvature of the symmetric matter EOS at saturation. This quantity gives a measure of the resistance of nuclei against compression. It can be accessed experimentally though the monopole vibration of nuclei (for more details, see for instance [112]).

- *Symmetry energy* – It is also possible to define the symmetry energy:

$$S_0 = \frac{E_{int}^{\beta=1}}{A}(\rho_0) - \frac{E_{int}^{\beta=0}}{A}(\rho_0) = 30.5 \pm 3 \text{ MeV} \quad (1.22d)$$

¹² In the phenomenological liquid drop model, the binding energy per particle is given by the Bethe-Weizsäcker mass formula [134]:

$$\frac{E}{A} = a_v - a_s A^{-1/3} - a_c (A - N + Z)^2 A^{-4/3} + \dots$$

where the volume a_v , surface a_s , and Coulombian a_c contributions are adjusted to reproduce the binding energy of nuclei composed by $A = N + Z$ nucleons. For infinite symmetric matter, only remains the volume contribution $a_v \simeq -16 \text{ MeV}$.

corresponding to the difference of energy between pure neutron and symmetric nuclear matter at ρ_0 in the so-called parabolic approximation¹³. Its value can be obtained from *ab initio* calculation for instance or using phenomenological liquid drop model arguments.

The set of equations (1.22) gives strong constraints on the accessible value of parameters defining the Skyrme functional. On top of these constraints in infinite systems, additional constraints can be imposed such as binding energies or radii of specific, typically closed-shell, nuclei (see [132,133] for instance).

LINK WITH LANDAU THEORY OF FERMI LIQUID

To finish the discussion on empirical functionals, we discuss here its link with the Landau theory of Fermi liquid [135–137] that will be discussed later on in this thesis. The Skyrme functional establishes a clear connection to the Fermi liquid theory (FLT). In infinite matter, the FLT assumes that the physical properties of the systems can be expressed as a function of the effective two-body interaction matrix elements, written as:

$$V(\mathbf{k}_1, \sigma_1, \tau_1; \mathbf{k}_2, \sigma_2, \tau_2) \xrightarrow[k_i=k_F]{} N(0)^{-1} \left[F^s(\theta) + F^a(\theta)\sigma_1 \cdot \sigma_2 + (G^s(\theta) + G^a(\theta)\sigma_1 \cdot \sigma_2)\tau_1 \cdot \tau_2 \right] \quad (1.23)$$

where $F^{s,a}$ and $G^{s,a}$ are functions of the angle θ between \mathbf{k}_1 and \mathbf{k}_2 , and $N(0) = 2k_F m^* / \pi^2$. Then, a multipole expansion on a spherical harmonics basis of these quantities defines the so-called Landau parameters $F_l^{s,a}$ and $G_l^{s,a}$ [138–143]. Note that, for Skyrme-like contact interactions (1.13), the Landau parameters vanish for $l \geq 2$. Finally, the physical properties of nuclear matter can be written in terms of the Landau parameters. For instance, in symmetric matter, the incompressibility (1.22c) is given by:

$$K_\infty = \frac{3k_F^2}{m} \frac{1 + F_0^s}{1 + F_1^s/3}. \quad (1.24)$$

Another important quantity is the effective mass. For interacting systems treated as independent quasi-particles, the momentum dependence of the single-particle potential is linked to the effective mass m^* that differs from the bare mass. In the Skyrme functional case and at the mean-field level, the effective mass is given by the term in $\tau\rho$ (1.17c) and leads to:

$$\frac{m}{m_q^*} = 1 + \frac{m}{4}\theta_v\rho + \frac{m}{4}[\theta_s - 2\theta_v]\rho_q. \quad (1.25)$$

For instance, in symmetric matter, the effective mass (1.25) are given in terms of the Landau parameters as:

$$\frac{m^*}{m} = 1 + \frac{F_1^s}{3}. \quad (1.26)$$

¹³ More precisely, the symmetry energy is defined as:

$$S(\rho) = \frac{1}{2} \frac{\partial^2 E^\beta}{\partial \beta^2} \bigg|_{\beta=0}(\rho) \quad \text{and} \quad S_0 = S(\rho_0).$$

1.3.c Illustration of predictivity

Many parametrizations of the Skyrme functional have been proposed. Such proliferation reveals the simplicity of the approach. Many of the parameter sets are able to describe fairly well the experimental observations in atomic nuclei. The high predictive power of Skyrme EDF is illustrated in figures 1.19, 1.20, 1.21 and 1.22 showing comparisons between theoretical and experimental density profiles, single-particle shell effect, total binding energy, and separation energies respectively.

The phenomenological density functional framework can also be used to describe the dynamical properties as illustrated in figure 1.23 where the time evolution of a collision between two ^{238}U atomic nuclei using SLy4d Skyrme interaction in the Time-Dependent Hartree-Fock (TDFH) formalism is shown [144–147].

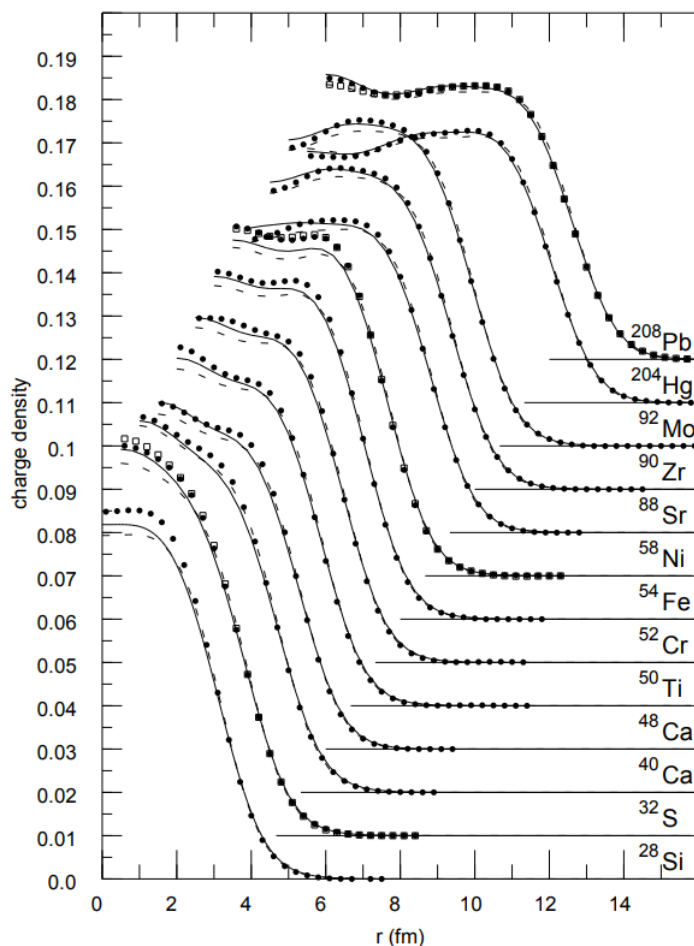


Figure 1.19: Experimental charge density distributions (filled circles) compared with the SKX (dashed lines) and SKM* (solid lines) Skyrme interaction of selected atomic nuclei. The charge density units are $e \text{ fm}^{-3}$. For clarity, the data have been progressively offset by 1 fm and 0.01 in the charge density. Figure taken from Lecture Notes in Nuclear Structure Physics by Alex Brown at Michigan State University in 2005.

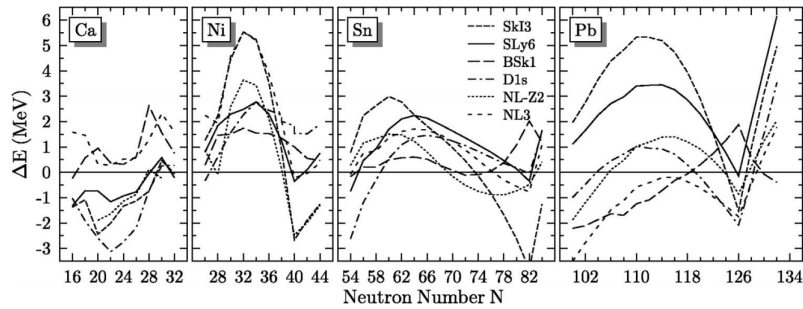


Figure 1.20: Error on the total binding energy ΔE , with respect to experimental data, for selected isotopic chains and Skyrme functionals. Figure taken from [101].

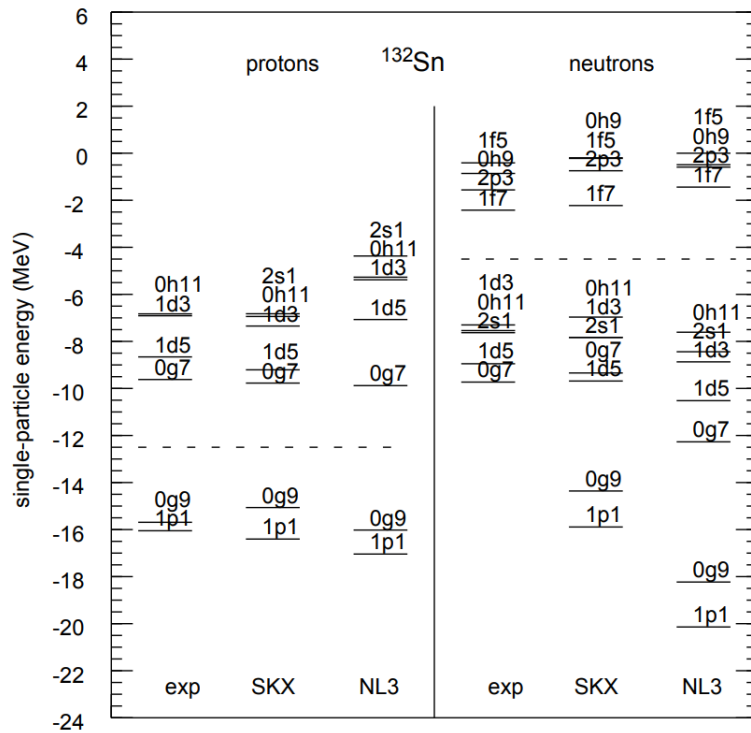


Figure 1.21: Experimental and theoretical (obtained with the SKX Skyrme interaction and NL3 Dirac Hartree calculations) proton and neutron single-particle energies for ^{132}Sn . The orbits are labeled by $(n, l, 2j)$, and the dashed line is the Fermi energy. Figure taken from Lecture Notes in Nuclear Structure Physics by Alex Brown at Michigan State University in 2005.

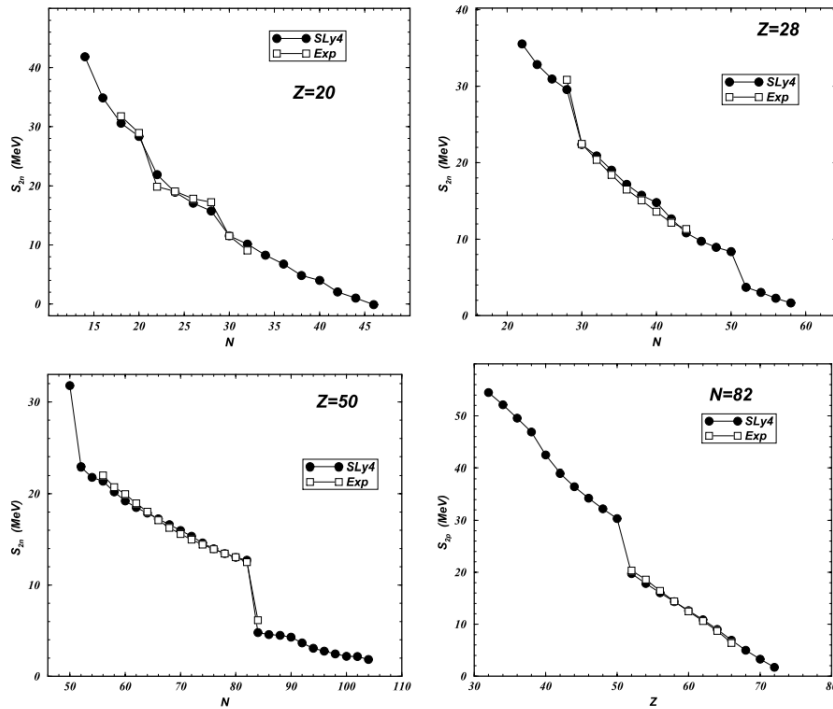


Figure 1.22: Two neutron separation energies S_{2n} of calcium, nickel and tin isotopes, and two proton separation energies S_{2p} of $N = 82$ isotones obtained with SLy4 Skyrme functional and compared to experimental data. Figure taken from [133].

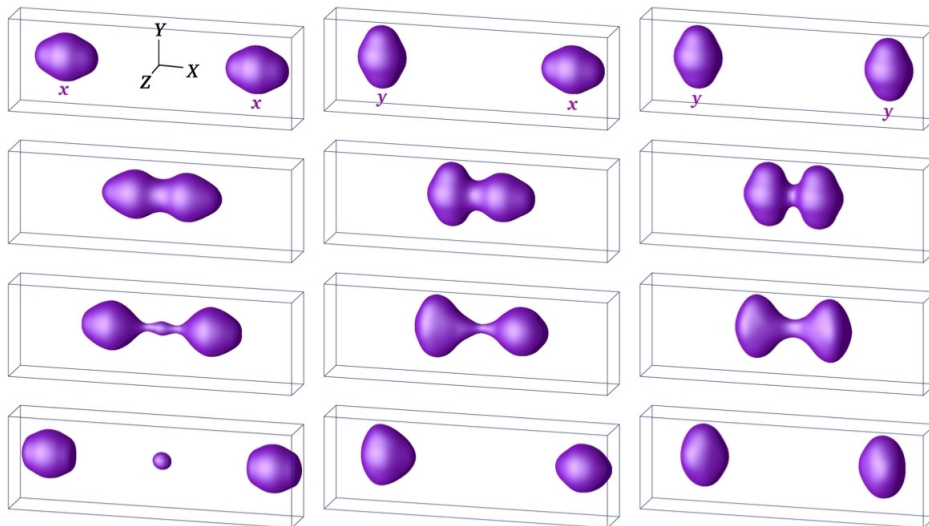


Figure 1.23: Evolutions in time (from top to bottom at $t = 0, 15, 27, 42 \times 10^{-22}$ s) associated to three different initial configurations (discriminated by the column considered) of the collision (at energy 900 MeV in the center of mass) between two ^{238}U nuclei using SLy4d Skyrme interaction in the Time-Dependent Hartree-Fock (TDFH) formalism. Figure taken from [144].

1.4

RECENT PROGRESS IN THE NUCLEAR EDF

Although the Skyrme interaction in its simple form (1.13) can reproduce many properties of nuclear systems, very recently, large efforts were devoted to obtain alternative functionals. They were several motivations for this renewal of interest. Among them, we note:

1. The functionals are usually predictive in the vicinity of nuclear chart where they have been adjusted. Large differences usually appear between different parametrizations away from where they are adjusted.
2. Some components of the functional, e.g. time-odd terms, are not or are poorly constrained by experiments [64]. One motivation to render less empirical these functionals is to add new constraints to these components.
3. The strong analogy between the Skyrme effective interaction and the π interaction used in EFT and the search for a constructive framework behind the EDF theory. More generally the exploration of richer functional. A general overview of these aspects can be found in [148].

We will discuss here two types of strategies that were used in the last few years. These strategies are illustrated in figure 1.24.

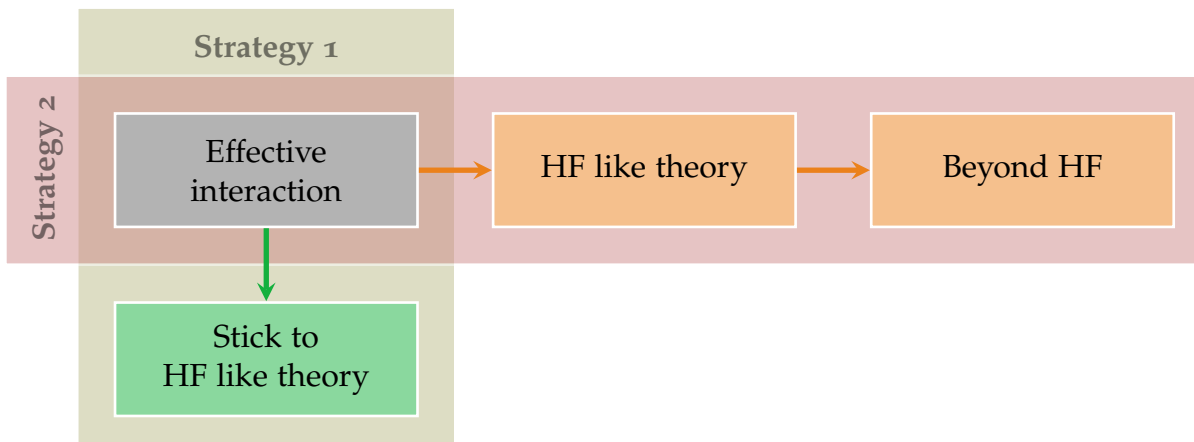


Figure 1.24: Schematic representation of the recent strategies employed to develop the EDF theory. See text for more details.

1.4.A Extension of empirical functionals

EXTENSION OF THE FUNCTIONAL AT THE MEAN-FIELD LEVEL

The use of contact interactions was justified by Negele and Vautherin [109,149] starting from a microscopic point of view. The approach they used is the density matrix expansion (DME) directly in a many-body calculation. This leads to a functional justifying all the terms of the Skyrme-like contact interaction $\mathcal{H}(\rho(\mathbf{r}), \nabla\rho(\mathbf{r}), \tau(\mathbf{r}))$ (1.17). Even more, it suggests a systematic generalization of functionals $\mathcal{H}(\rho, \nabla\rho, \tau)$ in terms of higher derivatives of the density. For instance the next-to-leading order (NLO), i.e. the DME up to second order in derivative of the density, reveals the

same structure as the standard Skyrme effective interaction (1.13). Note that the leading order (LO) corresponds to the term in (t_0, x_0) only [150,151]. Nevertheless, Negele itself in [152] discussed the limitation of the approach and concluded that the density-dependent Skyrme-like effective interaction is not efficient because of the lack of generality compared to the DME results. One can mention that the recent progress in *ab initio* methods have provided a renewed interest on the DME and have reached now a certain level of maturity [150,153–163].

Another way to enrich the functional while keeping the historical strategy (strategy 1 in figure 1.24) is to stick to the Hartree-Fock theory but with alternative effective interactions (the Gogny force [126] for example). This was recently explored in particular to get rid of the density-dependent term. For instance, three-body semi-contact interactions [164] or non-local interactions [165–168] have been proposed.

Another attempt that was made recently is to use a systematic improvement of contact interactions that turns out to be similar to the one used in EFT. In [169–171], it was proposed to introduce N^lLO Skyrme functional by including higher order derivatives of the density in the standard form (1.13). When only two-body interactions are used at the Hartree-Fock level, one difficulty that is observed is that the effective mass of symmetric matter obtained with this approach (also using Gogny functional) is shown to systematically give $m^*/m \simeq 0.4$ at saturation that is below the expected value $m^*/m \simeq 0.7$.

One can also mention for instance other approaches as the development of the Fayans functional [172,173] based on a local EDF containing volume and surface contributions, the SeaLL1 functional based on a generalization of the liquid drop model [174], the Barcelona–Catania–Paris–Madrid (BCPM) functional [175–180] based on BHF calculation, or the work of [181] where it was suggested a general strategy to design *ab initio* DFT.

BEYOND MEAN FIELD USING STANDARD EFFECTIVE INTERACTION

All the EDF theories exposed above are designed to provide a correct description of nuclear properties using Hartree-Fock like calculations. Often, some correlations that are not properly accounted for in these approaches are necessary to well describe the physical properties of the systems and beyond-mean-field (BMF) technique should be used. To quote some of them, this includes the generator coordinate method (GCM) [182] used in a symmetry restoration framework to include short-range correlations, the extensions of the random phase approximation (RPA) models [183–188]. On some of these extensions, single-particle states are coupled to multiparticle-multihole configurations resulting in the fragmentation of collective excitations. There are however a number of formal and/or technical difficulties:

1. The first one is that most EDF at the BMF level are based on a MF reference framework. Fundamentally, these approaches are beyond the scope of standard DFT theorems. They also aim at describing observables that are not *a priori* accessible in DFT and that are linked to two-body effects.
2. These approaches are strongly guided by the Hamiltonian framework while an effective interaction or a functional is not *a priori* related to a true Hamiltonian (density-dependent term). The direct application of techniques designed for Hamiltonian to EDF might lead to serious pathologies. These difficulties can be eventually corrected using advanced techniques (see for instance [189–191] in a GCM framework). The drawback is then that the simplicity of standard EDF approach is lost by the requirement to use complicated procedures to remove the double-counting and/or pathologies.

3. Another issue is that the set of parameters of the functionals are usually adjusted at the mean field level on data or pseudo data containing all physical correlations. Consequently, the BMF methods, starting from standard EDF, without specific attention has the risk of double counting the correlations (already present in EDF at the MF level).

These difficulties in BMF frameworks suggest the requirement of EDF directly constructed at BMF level. The functionals should be coherently introduced at the same level of approximation as the BMF model employed. In the following, some recent exploratory studies going in that direction are presented.

BEYOND MEAN-FIELD FUNCTIONAL

The general conclusion of the first strategy displayed in figure 1.24 and discussed above is that two-body effective interactions adjusted at Hartree-Fock level seem to have difficulty to replace the density dependent term as in (1.13). The resemblance between the Skyrme like effective interaction (1.13) and the \not{r} EFT two-body interaction (1.6) is one of the motivation of the second strategy shown in figure 1.24. A second motivation is due to the recent developments in renormalization group methods [13] that allow to describe nuclear systems with perturbative approaches (see for instance [66]), provided by the so-called Dyson equation [192–194].

In [195,196], a first attempt was made to adjust a Skyrme-like interaction at second order of many-body perturbation theory to reproduce the EOS of nuclear matter. The EOS takes then the form:

$$\frac{E_{int}}{A}(\rho, \Lambda) = \frac{E_{int}^{(1)}}{A}(\rho) + \frac{E_{int}^{(2)}}{A}(\rho, \Lambda). \quad (1.27)$$

The first term corresponds to the standard (Hartree-Fock) contribution (1.21a) and $E_{int}^{(2)}$ stands for the second order results. This part contains terms proportional to $t_0^2, t_3^2, t_0 t_3, t_0 t_1, t_1 t_3, t_2^2$. Due to the use of contact interaction, the energy contribution has an ultra-violet (UV) divergence and a cutoff regularization scheme was used. Note that a dimensional regularization scheme can also be chosen to remove the UV divergence of the results. Finally a fitting procedure (for every value of Λ) is performed to adjust the Skyrme parameters $\{t_0, t_1, t_2, t_3, \alpha\}$ to reproduce the desired EOS with (1.27). In figure 1.25, the obtained second order EOS is shown for various values of the cutoff Λ . The reference data is provided by the SLy5 parametrization of the standard Skyrme effective interaction adjusted at the mean field level. The readjustment of parameters at the BMF level in particular avoids the double counting problem.

This approach can be systematically generalized including higher orders in perturbation but the many-body perturbation theory becomes rapidly a tedious task due to the increasing number of terms to consider. Eventually, resummation technique can be employed by summing up all orders in many-body perturbation theory of a certain class of correlation. This was the starting point of further developments to design a new generation of energy density functionals like the YGLO functional [197], EYLO functional [198], or the functional using unitarity limit constraints [76,130,199,200]. For the moment, we do not develop further details on resummation since it is precisely the topic of this work and since it will be extensively studied in this thesis.

Renormalizability of the approach, i.e. the possibility to obtain a theory independent of the regularization scheme which is chosen, and required by a power-counting analysis as done in EFT to obtain a systematic improvement of the inter-

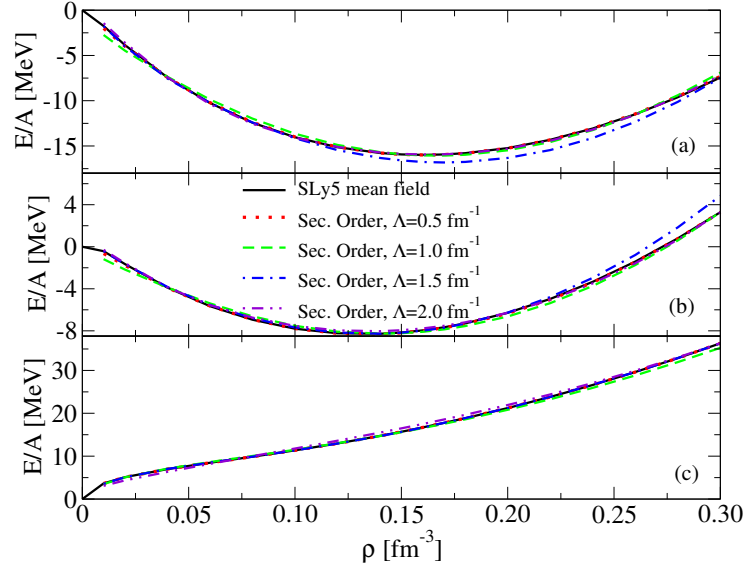


Figure 1.25: EOS for symmetric (a), asymmetric matter $\beta = 0.5$ (b), and neutron matter (c) obtained by the second order of MBPT based EDF using Skyrme like effective interaction after proper adjustment to the SLy5 EOS for various cutoff Λ . Figure taken from [196].

action (see section 1.1.b), was discussed in [201]. The conclusion is that restricted conditions are required and only some specific density-dependent terms can be allowed. Guided by this study, a first step toward a power-counting in an EDF framework was explored in [202] where a methodology to avoid the restrictions based on the inclusion of counter terms is proposed. These works clearly illustrate how the EDF and EFT can cross-fertilize each other.

1.4.B Motivation: why *ab initio* guided EDF?

The energy density functional approaches based on mean-field (see discussion 1.3.c) or BMF are remarkable in terms of predictivity. Still, it is often observed that they work well close or in the domain where the functionals were adjusted empirically, e.g. symmetric nuclear matter EOS, binding energy and radii of nuclei close to the stability, etc. Nevertheless, a number of properties are not accounted for in the standard empirical functionals. For instance, in figure 1.9, we have seen that the Skyrme functionals suffer for a lack of constraint on its time-odd components [64]. Two examples of shortcomings are given below.

1. In figure 1.26, the neutron matter equation of state are displayed for an extended set of Skyrme functionals. We remark that all functionals cross each other slightly below saturation density ρ_0 . Notably, this is due to the fact that the parameters entering in functional are typically adjusted close to ρ_0 . Besides, we also notice that large discrepancies exist at low density as well as beyond the saturation. The slope of the symmetry energy, which is an important quantity to describe astrophysical phenomena (see section 1.2.a), presents also large differences around ρ_0 .
2. The figure 1.27 illustrates that the empirical Skyrme functionals suffer from the adjustment procedure near ρ_0 . Consequently, it is not surprising that these functionals do not provide a proper description of the low-density regime. Again, this dilute regime influences the description of several nuclear systems and phenomena (neutron skin, nuclear reactions, neutron star crust, etc...).

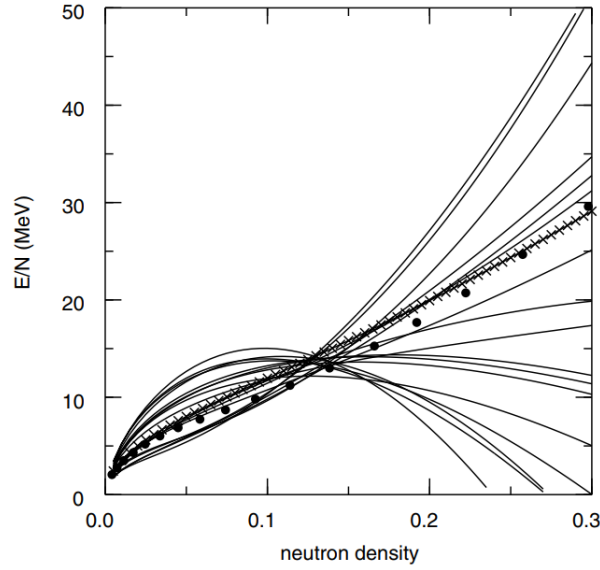


Figure 1.26: Neutron matter EOS obtained using several parametrizations of the Skyrme functional. The circles are the Friedman-Pandharipande reference *ab initio* results [62]. The neutron density is in units of fm^{-3} . Figure taken from [203].

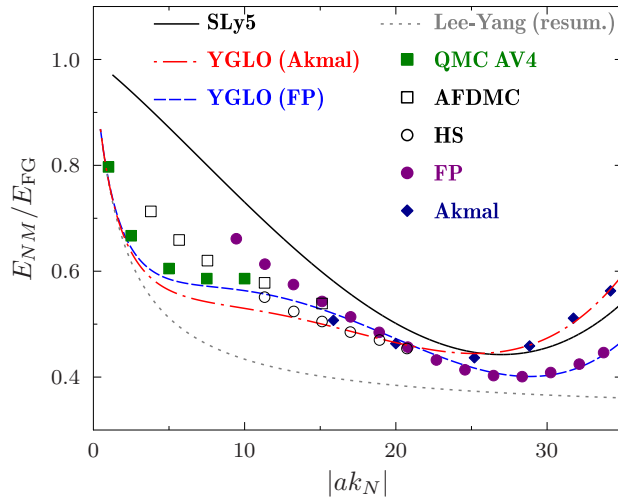


Figure 1.27: Neutron matter EOS as function of $a_s k_F$ (noted ak_N here). The symbols are *ab initio* calculations results. The black solid-line corresponds to a typical result obtained using Skyrme functional (SLy5 parametrization in this case). Figure taken from [197].

These two typical examples illustrate the limitations of the standard EDF. They show the fact that these functionals reached their limits in terms of predictivity and proper description of nuclear systems. New ideas and new ways to constrain the functionals are therefore desirable to increase the predictive power of the EDF approaches. In that sense, exact calculations could provide decisive hints to design new functionals driven by *ab initio* methods.

1.4.c Towards *ab initio* nuclear EDF

The approaches based on the resolution of the many-body Schrödinger equation, namely the *ab initio* methods presented in section 1.2, do not lead in general to clear guidance for the functional form. Even if these approaches are directly connected to the bare nuclear interaction, they are numerical and they do not lead to analytical formulas in term of the one-body density. On the other hand, despite the complexity of the strong multi-body interaction between in-medium nucleons, the DFT framework illustrates the fact that nuclear systems can be rather well described by adopting a single-particle picture. Contrary to the *ab initio* theories, the EDF theory provides directly such description in a much simpler framework which usually does not require advanced numerical calculations. A natural way that the *ab initio* theory can impact the EDF is, as we have seen, to provide pseudo-data that are not reachable by experiments. This was systematically done in the past. However, EDF approaches remains still rather empirical. Indeed, if we restrict the discussion to the case of infinite matter, the methodology can be summarized as follows:

1. Start from an effective interaction, e.g. Skyrme like contact interaction (1.13), parametrized by a set of parameters $\{x\}$.
2. Compute the EOS of nuclear matter $E_{\{x\}}(\rho)/A$, parametrized by $\{x\}$, as function of the one-body density ρ at a given order in the many-body perturbation theory. Typically, the Hartree-Fock calculation leads to (1.21a) and the second order to (1.27). Eventually, other properties can be calculated as illustrated in (1.22).
3. Choose a set of experimental data or pseudo data from *ab initio* calculations, and perform a fit such that the data are properly reproduced.

The functionals obtained this way are able to describe the properties of nuclear matter in a very simple framework. The *NN* interaction as well as the many-body correlations (due principally to the in-medium dressing of the bare interaction) are encoded in the $\{x\}$.

The drawback of this procedure is that there is no explicit link between the set of parameters $\{x\}$ and the nuclear bare interaction [204], represented for instance by the low energy constants (LECs) (1.2) (see figure 1.18). To render the functional less empirical, we can try to answer the following question: *Can we connect the parameters of the EDFs used in nuclear physics with the LECs of the bare interaction?* It is a challenging problem since the goal is to obtain non-empirical functionals, depending only of the LECs and one-body density without other parameters. The strong renormalization of the bare nuclear interaction by the nuclear medium is a key issue.

An illustrative example where it is possible is the case of dilute interacting fermions. An EFT approach shows that the relevant two-body interaction to consider is here the low-momentum expansion (1.6). Then, starting from this effective interaction, one can perform the standard many-body perturbation theory (MBPT) up to second order [192]. This leads to the so-called Lee-Yang formula [205–207]:

$$\begin{aligned} \frac{E}{A}(\rho, a_s) = & \frac{(9\sqrt{3}\pi^2\rho)^{2/3}}{10m} \left[1 + \frac{10a_s}{9\pi} (3\pi^2\rho)^{1/3} \right. \\ & \left. + \frac{4a_s^2}{21\pi^2} (11 - 2\ln 2) (3\pi^2\rho)^{2/3} + \dots \right]. \end{aligned} \quad (1.28)$$

For this illustrative example, the simplification $C_2 = C'_2 = 0$ has been made and a degenerate two-components spin system was considered. The expansion obtained by MBPT at low density gives directly the energy as a function of the density and the low-energy constant a_s . However, this expansion is not applicable in nuclear systems due to the unnatural large value of the scattering length $|a_s| \simeq 20$ fm (see table 1.1). This low-density expansion is valid if $|a_s|\rho^{1/3} \ll 1$ where $|a_s|\rho^{1/3}$ plays the role of a perturbative parameter. For neutron matter, the range of applicability is $\rho \ll 10^{-6} \text{ fm}^{-3}$. It is very small compared to the density of interest in nuclear physics $\rho_0 \simeq 0.16 \text{ fm}^{-3}$.

Nevertheless, the Lee-Yang formula has very interesting features:

- The MBPT for dilute Fermi systems leads to an EDF expressed explicitly in terms of the local density.
- The EDF is directly linked to the bare interaction and depends directly on the low energy constant a_s .
- BMF effects are properly incorporated in the functional.

Besides, the functional can be exported from infinite matter to finite systems, in principle, in a second step. A standard technique to do this is to use a local density approximation (LDA) where the EOS, written in term of the local density, is first transformed into an integral over space (1.15). This procedure, connected to the so-called Thomas-Fermi approximation [127,182], leads to functionals of the local density consistent with the Hohenberg-Kohn theorem [113]. The single particle wave functions derive then from (1.19). This strategy was used recently at several occasions in nuclear physics [197,198,208] and a similar strategy is currently used in order to incorporate quantum corrections that might stabilize quantum droplets [209,210].

The functional (1.28) is only valid in the perturbative regime. The aim of the present thesis is to introduce a non-empirical EDF for strongly interacting systems inspired by the recent progress of the EFTs associated with resummation techniques. One advantage of these resummations of many-body contributions is that they account for BMF effects to all orders in the LECs. A second advantage is that these resummation schemes are mostly analytical in terms of the density. Here we will concentrate on a two-component spin degenerate infinite system, e.g. neutron matter. The dimer bound state appearing in the case of symmetric matter needs a specific treatment which is out of the scope of the present thesis.

2

ENERGY RESUMMATION

Dans l'horizon de l'infini. — Nous avons quitté la terre et sommes montés à bord ! Nous avons brisé le pont qui était derrière nous, — mieux encore, nous avons brisé la terre qui était derrière nous ! Eh bien ! petit navire, prends garde ! À tes côtés il y a l'océan : il est vrai qu'il ne mugit pas toujours, et parfois sa nappe s'étend comme de la soie et de l'or, une rêverie de bonté. Mais il viendra des heures où tu reconnaîtras qu'il est infini et qu'il n'y a rien de plus terrible que l'infini. Hélas ! pauvre oiseau, toi qui t'es senti libre, tu te heurtes maintenant aux barreaux de cette cage ! Malheur à toi, si tu es saisi du mal du pays de la terre, comme s'il y avait eu là plus de liberté, — et maintenant il n'y a plus de « terre » !

Friedrich NIETZSCHE – *Le Gai Savoir*

CONTENTS

| | | |
|-------|---|----|
| 2.1 | EFT for dilute Fermi systems | 44 |
| 2.2 | Many-body perturbation theory | 45 |
| 2.2.A | Green's functions formalism | 45 |
| 2.2.B | Energy contribution for dilute Fermi systems | 49 |
| 2.2.C | Survey of numerical estimates of the third and fourth order contributions | 54 |
| 2.3 | Ladder resummation | 56 |
| 2.3.A | Resummation of ladder diagrams: particle-hole propagator | 56 |
| 2.3.B | Resummation of ladders diagrams: vacuum-medium propagator | 58 |
| 2.3.C | Discussion of the results on energy resummations | 62 |

The purpose of this chapter is to introduce and summarize recent progress made in effective field theory to describe interacting Fermi systems that will be useful in the rest of the thesis. We introduce in a didactic/academic manner the many-body perturbation theory in the Green's functions formalism for dilute Fermi gas. For instance, the Lee-Yang formula (1.28) will be rederived in the EFT framework. Later on we will use this work as a guide to obtain non-empirical functionals for the ground-state energy, as explicit functions of the density and s -wave scattering length only. We will then perform a resummation of some classes of correlations to go beyond the perturbative low-density regime and introduce what we call here the phase-space average approximation to simplify the functional. A special focus is then put on the unitarity gas limit where $|a_s k_F| \rightarrow \infty$. Below, we first give general remarks on the Green's functions theory approach. One of the main goal of this chapter is to present different compact forms of the energy obtained by resummation.

2.1

EFT FOR DILUTE FERMI SYSTEMS

A justification of the use of $\not\equiv$ EFT, i.e. considering the contact two-body interaction (1.6) to describe dilute system, was given for instance in [35,211,212]. The main argument relies on the fact that, for dilute Fermi systems, the inter-particle distance¹ $d \sim \rho^{-1/3}$ is large compared to the short-range part of the interaction, i.e. the hard core part (see figure 1.2). In that case, only the long-range/low-energy part of the interaction is relevant. The EFT states that any observable can be described at desired accuracy by making an expansion in a small parameter Q such that $Q/\Lambda_{EFT} \ll 1$, i.e. that there exists a separation of energy scales. In that case, the EFT framework will be valid. In the low-density limit, $\Lambda_{EFT} \sim 1/R$ is given by the typical range of the hard core potential. For nuclear systems, $R \simeq 0.5$ fm (see figure 1.2) while the typical energy scale probed is $Q \sim 1/d \sim \rho^{1/3} \simeq 0.5$ fm⁻¹.

The long-range/low-energy part of the interaction is governed by the low-energy constants (LECs) given by (1.2) and two cases can be distinguished:

1. The *natural* case corresponds to $|a_s| \sim R$. Typically, the effective range stands for the range of the potential, i.e. $r_s \sim R$. In this case, the standard minimal subtraction (MS) scheme of dimensional regularization [12,39–44] is usually used to properly treat the ultra-violet (UV) divergences induced by contact interactions (see appendix A for more details). The naturalness of the systems implies a perturbative expansion in powers of $Q/\Lambda_{EFT} \sim k_F R$ such that the expansion parameters of observables are:

$$\rho^{1/3} a_s, \rho^{1/3} r_s, \rho^{2/3} a_s^2, \dots$$

This expansion is actually the one appearing in the Lee-Yang formula (1.28). An illustration is the hard-sphere model [204,213,214] for which $a_s = a_p = R$ and $r_s = 2R/3$ commonly discussed as *natural* systems.

2. The so-called *unnatural* case corresponds to $|a_s| \gg R$. It is particularly interesting for nuclear physics where the *s*-wave scattering lengths are large (see table 1.1). This case also takes place in the ultracold atomic physics context where the scattering length can be tuned continuously up to the unitary limit ($a_s \rightarrow \pm\infty$) via the Feshbach resonance [67–69]. The proper treatment of UV divergences requires specific regularization techniques, e.g. the power divergence subtraction (PDS) scheme of dimensional regularization [12,39–44] or cutoff regularization [215,216] (see appendix A for more details).

Just to mention it, the extension of the EFT formalism including pairing is introduced in [217] but is not discussed in this thesis. See also [204] for a complete discussion.

The goal of the present work is to build from the interaction provided by the EFT for dilute Fermi systems an explicit non-empirical functional of the local density which captures the infinite neutron matter properties. As mentioned in chapter 1, the low-density standard many-body perturbation theory (MBPT) fails for such systems because of the *unnatural* *s*-wave scattering length. To overcome this difficulty, we first study a simplified problem that will serve us as a guide. We consider here a homogeneous infinite Fermi system degenerate in spin, at zero temperature,

¹ The inter-particle distance is defined by $4\pi d^3 \rho / 3 = 1$ leading to $d = (4\pi\rho/3)^{-1/3}$.

and interacting via the leading order of the two-body spin independent interaction (1.6) (C_0 term). In that case, the calculation of the physical properties and the discussions are simplified and the standard minimal subtraction (MS) scheme of dimensional regularization can be employed without restriction to avoid properly the UV divergences. Note that the inclusion of the effective range (C_2 term), and eventually the p -wave scattering length (C_2' term), should also be discussed because of their importance in nuclear systems (see chapter 3). In the following, before discussing the low-density MBPT for dilute Fermi gas in a EFT picture, we introduce some important aspects of the Green's functions approach as well as the associated diagrammatic representation.

2.2

MANY-BODY PERTURBATION THEORY

2.2.A Green's functions formalism

The Green's functions formalism in the framework of many-body calculations is an extensive subject by itself. Advanced introductions to Green's functions and associated diagrammatic representation are presented in details in many textbooks [192–194, 218–223]. We introduce here only the important concepts for the present study.

We consider an infinite system (with the Fermi momentum k_F) composed of non-relativistic fermions (of mass m and spin degeneracy g) interacting through a two-body spin-independent contact interaction:

$$\widehat{V}_0 = C_0 \sum_{1,2,3,4} a_1^\dagger a_2^\dagger a_3 a_4 \bar{\delta}(1+2-3-4), \quad (2.1)$$

where (a_i^\dagger, a_i) are the creation and annihilation operators of a particle $i \equiv \{\mathbf{k}_i, \omega_i, \sigma_i\}$ with a momentum \mathbf{k}_i , an energy ω_i and a spin σ_i . $\bar{\delta}$ contains the conservation laws. In the present case (continuous limit) we have:

$$\bar{\delta}(1+2-3-4) = \begin{cases} [\delta_{\sigma_1\sigma_3}\delta_{\sigma_2\sigma_4} - \delta_{\sigma_1\sigma_4}\delta_{\sigma_2\sigma_3}] & \text{– spin} \\ \times (2\pi)^3 \delta(\mathbf{k}_1 + \mathbf{k}_2 - \mathbf{k}_3 - \mathbf{k}_4) & \text{– center of mass} \\ \times (2i\pi) \delta(\omega_1 + \omega_2 - \omega_3 - \omega_4) & \text{– energy} \end{cases}$$

Note that, due to the spin independence of the interaction \widehat{V}_0 , the treatment of the direct and exchange terms is included in the linear combination of $\delta_{\sigma_i\sigma_j}$ and will lead to factors proportional to the spin-degeneracy g . The C_0 -coupling constant is related to the s -wave scattering length a_s through the relation (1.7):

$$C_0 = \frac{4\pi a_s}{m}. \quad (2.2)$$

This model is commonly called the *zero-range two-body scattering model* of dilute Fermi systems and was largely studied in the past [192, 205–207, 224, 225].

ONE-BODY GREEN'S FUNCTION AND CONTACT INTERACTION

The one-body Green's function, or propagator, of the non-interacting particle i is denoted by $G_{\sigma\sigma_i}(\mathbf{k}_i, \omega_i)$ where σ and σ_i are the indices of the incoming and outgoing spins respectively. In a diagrammatic representation, it can be represented as an arrowed line and it is given by:

$$\begin{aligned} \sigma \xrightarrow{\substack{\longrightarrow \\ (\mathbf{k}_i, \omega_i)}} \sigma_i &= G_{\sigma\sigma_i}(\mathbf{k}_i, \omega_i) = G(\mathbf{k}_i, \omega_i) \delta_{\sigma\sigma_i} \\ &= \left[\frac{n(\mathbf{k}_i)}{\omega_i - e(\mathbf{k}_i) - i\tau} + \frac{1 - n(\mathbf{k}_i)}{\omega_i - e(\mathbf{k}_i) + i\tau} \right] \delta_{\sigma\sigma_i}, \end{aligned} \quad (2.3)$$

where we have factorized $\delta_{\sigma\sigma_i}$ due to the fact that we consider here a spin-independent interaction. The $e(\mathbf{k})$ are the single-particle energies of the free particles and $n(\mathbf{k})$ the occupation numbers at zero-temperature given by:

$$e(\mathbf{k}) = \frac{\mathbf{k}^2}{2m} \quad \text{and} \quad n(\mathbf{k}) = \Theta(k_F - |\mathbf{k}|). \quad (2.4)$$

The first part of the Green's function (2.3) proportional to $n(\mathbf{k})$ corresponds to the propagation of a hole inside the Fermi sea and the second term in $[1 - n(\mathbf{k})]$ corresponds to a particle propagation above the Fermi surface. Note that $\tau \rightarrow 0^+$ at the end of the calculation insures that the time integral converges.

The density ρ of the system is obtained by summing up on all occupied states, i.e. all particles with a momentum below k_F :

$$\rho = g \int \frac{d^3k}{(2\pi)^3} n(\mathbf{k}) = \frac{gk_F^3}{6\pi^2}. \quad (2.5)$$

For homogeneous infinite systems, this relation between the density ρ and the Fermi momentum k_F remains unchanged even if the particles interact with each other² [192].

The C_0 -contact interaction, or C_0 -vertex, is represented diagrammatically as a dot:

$$\begin{array}{ccc} 2 & & 4 \\ & \searrow & \nearrow \\ & \bullet & \\ & \nearrow & \searrow \\ 1 & & 3 \end{array} = \langle 3, 4 | \widehat{V}_0 | 1, 2 \rangle = C_0 \bar{\delta}(1 + 2 - 3 - 4). \quad (2.6)$$

This diagrammatic representation of vertex is called two-body Hugenholtz diagrams [35,226]. Another widespread convention, the two-body Goldstone diagrams, represents a vertex by a (wiggly or dashed) line as used in [192] for instance.

SELF-ENERGY CONCEPT

For a Galilean invariant interaction, the exact one-body Green's function $\mathcal{G}_{\sigma\sigma_i}(\mathbf{k}_i, \omega_i)$ in a homogeneous medium verifies the so-called Dyson equation:

$$\mathcal{G}_{\sigma\sigma_i}(\mathbf{k}_i, \omega_i) = G_{\sigma\sigma_i}(\mathbf{k}_i, \omega_i) + G_{\sigma\mu}(\mathbf{k}_i, \omega_i) \Sigma_{\mu\nu}^*(\mathbf{k}_i, \omega_i) \mathcal{G}_{\nu\sigma_i}(\mathbf{k}_i, \omega_i), \quad (2.7)$$

² More precisely, this relation holds even if the occupation numbers are renormalized due to the interaction as observed in Fermi liquid [128,135–137,225].

where Σ^* is the proper self-energy which corresponds to the sum of all irreducible diagrams insertion connected to the rest of the diagram by a two-particles line and which cannot be separated into two pieces by cutting a single-particle line (for more details, see [192]). We will come to this notion in more details in chapter 4.

For a spin-independent interaction, \mathcal{G} , G and Σ^* are diagonal in spin-space and the Dyson equation can be formally solved as:

$$[\mathcal{G}(\mathbf{k}_i, \omega_i)]^{-1} = [G(\mathbf{k}_i, \omega_i)]^{-1} - \Sigma^*(\mathbf{k}_i, \omega_i). \quad (2.8)$$

The corresponding contribution to the energy is then given by:

$$E = \frac{g}{2} \int \frac{d^3k}{(2\pi)^3} \frac{d\omega}{2i\pi} [\Sigma^*(\mathbf{k}, \omega) + 2e(\mathbf{k})] \mathcal{G}(\mathbf{k}, \omega), \quad (2.9)$$

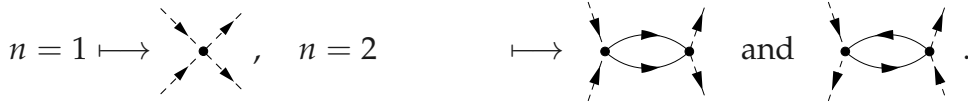
where we have used the Dyson equation and the fact that:

$$\lim_{\tau \rightarrow 0^+} \left[\int_{-\infty}^{\infty} d\omega e^{i\omega\tau} \right] = 0.$$

We see that the knowledge of the Green's functions and self-energy gives access to the energy. As we will see in chapter 4, the self-energy gives direct connection to the quasi-particle properties. Many approaches are dedicated to the determination of Σ^* and/or \mathcal{G} . Below we present how the MBPT can be developed with this formalism.

FEYNMAN RULES

We start by drawing all topologically distinct connected Feynman diagrams composed by n vertices joined by arrowed lines (2.3) and having two incoming and two outgoing arrowed lines. The two leading orders read for instance:



Then, the energy contribution of each diagram is obtained following the systematic rules:

1. Close the diagrams with two hole propagators and draw all topologically distinct energy diagrams (see table 2.1).
2. For each vertex, include the corresponding interaction given by (2.6).
3. For each internal line, include a propagator $G(\mathbf{k}_i, \omega_i)$ given by (2.3). Multiply by $\exp(i\omega_i\tau)$ for each line ending and originating at the same vertex³ (see (2.13) for instance).
4. Perform the integration over the $2n$ independent internal momenta and the energy:

$$\prod_{i=1}^{2n} \int \frac{d^3k_i}{(2\pi)^3} \int \frac{d\omega_i}{2i\pi'}$$

³ It is equivalent to close the energy integration contour in the upper complex plane. This procedure takes into account the fact that such lines must be hole lines.

and take the limit $\tau \rightarrow 0^+$ after the contour integration on ω_i . For simplicity and compactness of equations, the limit $\tau \rightarrow 0^+$ is implicit in the following.

5. Multiply every diagram by the appropriate symmetry factor⁴ $(-1)^{n-1}\sigma(S,l)$ and by the degeneracy factor D_g , depending on the considered diagram, obtained by summing up over all independent spins.

The rules to calculate a given order contribution to the self-energy are the same except that the diagrams are composed of $2n - 1$ lines with arrows (Green's function), *i.e.* with one line broken compared to the associated energy diagram. The Feynman rules for the energy (respectively the self-energy) contribution up to third order are illustrated in table 2.1 (respectively table 4.1). In particular, the degeneracy and symmetry factors of each diagram that does contribute to the energy are given.

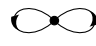



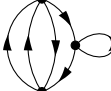
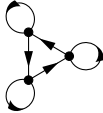


| Diagram (nz) | D_g | $\sigma(S,l) = (2^l S)^{-1}$ | Integrand on (s,t) |
|--|---------------|------------------------------|---|
| (1a)  | $g(g-1)$ | $\sigma(0!,1) = 1/2$ | θ^- |
| (2a)  | — | — | — |
| (2b)  | $2g(g-1)$ | $\sigma(1!,2) = 1/4$ | $\theta^- \Pi_{pp}$ |
| (3a)  | — | — | — |
| (3b)  | — | — | — |
| (3c)  | — | — | — |
| (3d)  | $4g(g-1)$ | $\sigma(1!,3) = 1/8$ | $\theta^- \Pi_{pp}^2 + \theta^+ \Pi_{hh}^2$ |
| (3e)  | $g(g-1)(g-3)$ | $\sigma(2!,0) = 1/2$ | $\theta^\pm \Pi_{ph}^2 + \theta^\mp \Pi_{ph}^2$ |

Table 2.1: Diagrams obtained using the Feynman rules for the energy contribution up to third order. The symbols Π_{xy} and θ are functions of (s,t) defined in the text (see also appendix B). The first order contribution corresponds to diagram (1a), the second order to (2a) and (2b), and the third order to (3a – 3e). If “—” is indicated, it means that the specific diagrams do not contribute at zero-temperature. The contribution of the diagram (nz), applying the Feynman rules, is simply $E_{(nz)} = 2^3 m^{n-1} C_0^n k_F^{6+n} \times D_g(nZ) \times \sigma(nZ) \times \int_{s,t} [\text{integrand}]$.

⁴ The symmetry factor of a diagram is given by: $\sigma(S,l) = (2^l S)^{-1}$ where S is the number of vertex permutations which transform the diagram into itself and l the number of equivalent couples of lines. Equivalent lines are lines that begin and end at the same vertices with the same direction of arrows.

COMPACT NOTATIONS

We introduce some useful notations to write in a compact form the contribution of each diagram:

- $e_{i\pm j} = e(\mathbf{k}_i \pm \mathbf{k}_j)$, $n_{i\pm j} = n(\mathbf{k}_i \pm \mathbf{k}_j)$, and $\omega_{i\pm j} = \omega_i \pm \omega_j$.
- $G_i = G(\mathbf{k}_i, \omega_i)$ and $G_{i\pm j} = G(\mathbf{k}_i \pm \mathbf{k}_j, \omega_i \pm \omega_j)$.
- $G_i^\pm = G_i e^{\pm i\tau\omega_i}$ to discriminate hole (+) and particle (−) propagators.
- $\bar{\delta}(i \pm j) = (2\pi)^3 \delta(\mathbf{k}_i \pm \mathbf{k}_j) \times (2i\pi) \delta(\omega_i \pm \omega_j)$.
- We denote the integration schematically as:

$$\int \frac{d\omega_i}{2i\pi} = \int_{\omega_i}', \quad \int \frac{d^3k_i}{(2\pi)^3} = \int_{k_i}', \quad \int \frac{d^3k_i}{(2\pi)^3} \int \frac{d\omega_i}{2i\pi} = \int_i'$$

$$\int_{a,b,\dots} = \int_a \int_b \dots, \quad \text{and} \quad \int_{x,y}^{\bar{\delta}} = \int_{x,y} \bar{\delta}(1 + 2 - x - y).$$

These notations are used in the following to give an illustration of the explicit contribution to the ground-state energy up to third order in perturbation.

2.2.B Energy contribution for dilute Fermi systems

We give here more details on the MBPT applied to the case of dilute Fermi systems.

FREE FERMI GAS

The energy of a non-interacting Fermi gas is given by the sum of all single-particle (kinetic) energies⁵:

$$E_{FG} = g \int \frac{d^3k}{(2\pi)^3} e(\mathbf{k}) n(\mathbf{k}) = \frac{3}{5} \frac{k_F^2}{2m} \rho. \quad (2.10)$$

Then, plugging the interaction, the EFT yields a ground state energy given by the sum of contributions:

$$\frac{E}{E_{FG}} = 1 + \frac{E_{(1)}}{E_{FG}} + \frac{E_{(2)}}{E_{FG}} + \dots \quad (2.11)$$

where $E_{(1)}/E_{FG}$ denotes the linear contribution in $(a_s k_F)$, $E_{(2)}/E_{FG}$ the quadratic contribution (1.28) in $(a_s k_F)$, etc. Below, we discuss step by step the calculation of each contribution in the EFT framework.

⁵ Here, we consider N particles in a unit volume $V = 1$. In that case, the density $\rho = N/V$ can be identified with the number of particles N .

FIRST ORDER: HARTREE-FOCK CONTRIBUTION

At first order, there is only one connected diagram (1a). Applying the Feynman rules for the energy, we can write:

$$\begin{aligned}
 \text{Diagram (1a)} &= E_{(1a)} = (-1)^{1-1} \times D_g(1a) \times \sigma(1a) \times C_0 \times \int_{1,2} G_1^+ G_2^+, \\
 &= g(g-1) \times \frac{1}{2} \times C_0 \times \left[\int_1 G_1^+ \right]^2, \\
 &= \frac{g}{2}(g-1)C_0 \left[\int_1 n_1 \right]^2 = \frac{g}{2}(g-1)C_0 \left[\frac{k_F}{6\pi^2} \right]^2, \\
 &= E_{\text{FG}}(g-1) \frac{10}{9\pi} (a_s k_F), \tag{2.12}
 \end{aligned}$$

where we have used (2.2) that gives the relation between the C_0 -coupling constant and the s -wave scattering length a_s . The degeneracy and symmetry factors D_g and σ for the diagram (1a) are given in table 2.1.

SECOND ORDER: LEE-YANG FORMULA

At second order in perturbation or in C_0^2 , there are two connected diagrams (see table 2.1). Let us estimate their energy contributions. The first contribution is given by the diagram (2a):

$$E_{(2a)} = \text{Diagram (2a)}$$

It is composed by a piece represented by:

$$\begin{array}{c}
 \uparrow 2(h) \\
 \bullet \\
 \text{---} \circlearrowleft 3(h) \\
 \bullet \\
 \uparrow 1(p)
 \end{array} \tag{2.13}$$

which requires a particle-hole configuration at the Fermi surface. This configuration is not allowed due to the Pauli blocking effect at zero temperature and all diagrams composed by this piece will not contribute to the energy. More precisely, this configuration corresponds to the case where the particle 1 (above the Fermi surface) interacts with the Fermi sea (represented by the *tadpole* labeled by 3(h)) to become a hole state inside the Fermi sea. This process is allowed only at the Fermi surface because of the momentum-energy conservation and of the Pauli blocking factor $[1 - n(\mathbf{k})]n(\mathbf{k})$ that appears in the calculation after the contour integration. Finally, the diagram (2a), and more generally diagrams where (2.13) appear, do not contribute to the energy.

The second diagram is given by the diagram (2b):

$$E_{(2b)} = \text{Diagram (2b)} \tag{2.14}$$

To obtain the expression of the second-order contribution to the energy, it is interesting to first express the particle-particle loop represented as:

$$\begin{array}{c}
2 \\
\swarrow \\
\bullet \\
\searrow \\
1
\end{array}
\begin{array}{c}
3(p) \\
\rightarrow \\
\bullet \\
\leftarrow \\
4(p)
\end{array}
= L_{pp}(\mathbf{k}_1, \omega_1; \mathbf{k}_2, \omega_2), \quad (2.15)$$

where $3(p)$ and $4(p)$ means that 3 and 4 are particle propagators. A more systematic discussion on the hole-hole L_{hh} , particle-hole L_{ph} and hole-particle L_{hp} loops, displayed in figure 2.1, is given in appendix C. The connection of one of these functions to the energy can be understood easily from the fact that L_{pp} , L_{hh} , L_{ph} and L_{hp} are obtained by breaking two lines in (2.14).

$$\begin{array}{cc}
\begin{array}{c} 2 \\ \swarrow \\ \bullet \\ \searrow \\ 1 \end{array} \begin{array}{c} 3(p) \\ \rightarrow \\ \bullet \\ \leftarrow \\ 4(p) \end{array} = L_{pp}(1;2) & \begin{array}{c} 2 \\ \swarrow \\ \bullet \\ \searrow \\ 1 \end{array} \begin{array}{c} 3(h) \\ \rightarrow \\ \bullet \\ \leftarrow \\ 4(h) \end{array} = L_{hh}(1;2) \\
\begin{array}{c} 2 \\ \swarrow \\ \bullet \\ \searrow \\ 1 \end{array} \begin{array}{c} 3(h) \\ \rightarrow \\ \bullet \\ \leftarrow \\ 4(p) \end{array} = L_{ph}(1;2) & \begin{array}{c} 2 \\ \swarrow \\ \bullet \\ \searrow \\ 1 \end{array} \begin{array}{c} 3(p) \\ \rightarrow \\ \bullet \\ \leftarrow \\ 4(h) \end{array} = L_{hp}(1;2)
\end{array}$$

Figure 2.1: Diagrammatic representation of the particle-particle, hole-hole, particle-hole and hole-particle loops.

We start by evaluating the integrals over the internal momenta and energies (\mathbf{k}_3, ω_3) and (\mathbf{k}_4, ω_4) assuming the conservation of energy and momentum at each vertex. This gives for L_{pp} :

$$\begin{aligned}
L_{pp}(1,2) &= \int_{3,4}^{\bar{\delta}} G_3^- G_4^- = \int_3 G_{1-3}^- G_{2+3}^- \\
&= \int_3 \frac{(1 - n_{1-3})(1 - n_{2+3})}{(\omega_{1-3} - e_{1-3} + i\tau)(\omega_{2+3} - e_{2+3} + i\tau)}, \\
&= - \int_{k_3} \frac{(1 - n_{1-3})(1 - n_{2+3})}{\omega_{1+2} - e_{1-3} - e_{2+3} + i\tau}, \quad (2.16)
\end{aligned}$$

where the contour integral has been carried out on the lower/upper complex plane.

We now return to the energy contribution (2.14). It can be obtained by closing the particle-particle loop integral L_{pp} (2.15) by two holes. Using the compact notations discussed previously, we have:

$$E_{(2b)} = (-1)^{2-1} D_g(2b) \sigma(2b) C_0^2 \int_{1,2} L_{pp}(1;2) G_1^+ G_2^+. \quad (2.17)$$

Note that another possibility would be to close the hole-hole loops by two other hole lines h_1 and h_2 . It means that, before closing the diagrams using the rule 1, the situation would be translated diagrammatically as:

$$\begin{array}{c}
2(h) \\
\swarrow \\
\bullet \\
\searrow \\
1(h)
\end{array}
\begin{array}{c}
3(h) \\
\rightarrow \\
\bullet \\
\leftarrow \\
4(h)
\end{array}
,$$

i.e. the two (real) holes 1 and 2 scatter as two (virtual) hole configurations. Due to the Pauli blocking, this process is not allowed since all hole-hole configurations are already occupied. The same reasoning can be made with the particle-hole and hole-particle loops and only remains the contribution due to the particle-particle loop. Note that the contour integration on ω_i insures automatically this property. Thus, the particle-particle loop plays the role of virtual excitation above the Fermi surface, at second order, and can be interpreted as an effective interaction inside the Fermi sea. The ground-state energy is then given by the sum of all virtual excitations (or effective interaction) between two holes.

After the integration on ω_1 and ω_2 in (2.17), we obtain:

$$E_{(2b)} = \frac{g}{2}(g-1)C_0^2 \int_{k_1, k_2, k_3} \frac{n_1 n_2 (1 - n_{1-3})(1 - n_{2+3})}{e_1 + e_2 - e_{1-3} - e_{2+3}}. \quad (2.18)$$

Note that we recover here the standard perturbation theory starting from a Slater determinant wave function. Then, the energy contribution of the second order comes from the coupling between the Hartree-Fock ground state and the $2p - 2h$ configurations with a factor $n_{p_1} n_{p_2} [1 - n_{h_1}] [1 - n_{h_2}]$.

To perform explicitly the integration, we introduce the dimensionless variables:

$$\mathbf{s} = \frac{\mathbf{k}_1 + \mathbf{k}_2}{2k_F}, \quad \mathbf{t} = \frac{\mathbf{k}_1 - \mathbf{k}_2}{2k_F}, \quad \mathbf{u} = \frac{\mathbf{k}_1 - \mathbf{k}_2 - 2\mathbf{k}_3}{2k_F}. \quad (2.19)$$

We can rewrite⁶ (2.18) using (2.4) as:

$$E_{(2b)} = 4mg(g-1)k_F^7 C_0^2 \int_{s,t} \int_u \frac{\theta_s^-(\mathbf{t})\theta_s^+(\mathbf{u})}{t^2 - u^2}, \quad (2.20)$$

where, following [227], we have defined:

$$\begin{cases} \theta_s^-(\boldsymbol{\kappa}) = \Theta(k_F - |\mathbf{s} + \boldsymbol{\kappa}|)\Theta(k_F - |\mathbf{s} - \boldsymbol{\kappa}|) = n_1 n_2, \\ \theta_s^+(\boldsymbol{\kappa}) = \Theta(|\mathbf{s} + \boldsymbol{\kappa}| - k_F)\Theta(|\mathbf{s} - \boldsymbol{\kappa}| - k_F) = (1 - n_1)(1 - n_2). \end{cases}$$

We can now define the effective particle-particle interactions:

$$B_{pp}(\mathbf{s}, \mathbf{t}) = mC_0 k_F \int_u \frac{\theta_s^+(\mathbf{u})}{t^2 - u^2} \equiv mC_0 k_F \Pi_{pp}(\mathbf{s}, \mathbf{t}). \quad (2.21)$$

A similar effective interaction can also be defined for the hole-hole, particle-hole and/or hole-particle. In appendix B, the effective hole-hole interactions B_{hh} (or equivalently the dimensionless function Π_{hh}), effective particle-hole interactions B_{ph} (or Π_{ph}) and effective hole-particle interactions B_{hp} (or Π_{hp}) are introduced following the same strategy as for B_{pp} . It is worth mentioning that, for a C_0 -contact interaction, the integrals appearing in the effective interaction like in (2.21) diverge and should be properly regularized. A complete discussion on regularization techniques as well as illustrations are given in appendix A and B. In the following, we will implicitly assumed that the effective interactions are properly regularized.

⁶ The Jacobian of this transformation is 2^3 .

Using B_{pp} , the energy contribution of diagram (2b) can be rewritten in a more compact form:

$$E_{(2b)} = 4g(g-1)k_F^6 C_0 \int_{s,t} \theta_s^-(t) B_{pp}(s,t). \quad (2.22)$$

After proper regularization of divergences, we obtain (see appendix B for explicit calculation):

$$\int_{s,t} \theta_s^-(t) \Pi_{pp}(s,t) = \frac{1}{(2\pi)^6} \frac{11 - 2 \ln 2}{105}, \quad (2.23)$$

leading to the well know second-order contribution to the Lee-Yang formula (1.28):

$$E_{(2b)} = (g-1)E_{FG} \frac{4}{21\pi^2} (11 - 2 \ln 2) (a_s k_F)^2. \quad (2.24)$$

THIRD AND FOURTH ORDERS

At third order, there are five diagrams that are shown in table 2.1. Their contributions are discussed below one after the other. The contribution to the energy of diagrams (3a, 3b, 3c):

$$E_{(3a)} = \text{diagram 3a}, \quad E_{(3b)} = \text{diagram 3b}, \quad \text{and} \quad E_{(3c)} = \text{diagram 3c},$$

vanish. As discussed previously, these diagrams are composed of a part represented by (2.13) and therefore do not contribute to the energy.

It only remains to estimate the diagrams (3d, 3e). These diagrams can also be written in terms of the loops displayed in figure 2.1. To do so, we first decompose each diagram as:

$$E_{(3d)} = hh \text{diagram 3d} + hh \text{diagram 3d} = E_{(3d)}^{1hh-2pp} + E_{(3d)}^{2hh-1pp},$$

$$E_{(3e)} = ph \text{diagram 3e} + hp \text{diagram 3e} = E_{(3e)}^{1ph-2hp} + E_{(3e)}^{1hp-2ph}.$$

For instance, the energy contribution of the third order term $2pp - 1hh$, namely the particle-particle ladder diagram contribution, using the Feynman rules and the functions introduced before, can be written as:

$$\begin{aligned} E_{(3d)}^{1hh-2pp} &= (-1)^{3-1} D_g(3d) \sigma(3d) C_0^3 \int_{1,2} L_{pp}(1,2)^2 G_1^+ G_2^+, \\ &= 4g(g-1) C_0 k_F^6 \int_{s,t} \theta_s^-(t) B_{pp}(s,t)^2. \end{aligned} \quad (2.25)$$

Other contributions take similar forms that are easily obtained using the same rules (see [227]). Finally, the third order contribution to the ground state energy is given by:

$$E_{(3)} = E_{(3d)}^{1hh-2pp} + E_{(3d)}^{2hh-1pp} + E_{(3e)}^{1ph-2hp} + E_{(3e)}^{1hp-2ph}. \quad (2.26)$$

Note that the diagrams $1ph - 2hp$ and $2ph - 1hp$ contribute equivalently⁷ but the contribution of diagrams $1pp - 2hh$ and $2pp - 1hh$ are not equivalent [227].

2.2.C Survey of numerical estimates of the third and fourth order contributions

The discussion on the first, second and third-order MBPT is here an illustration of the application of the EFT technique within the MBPT framework. Our scope is not to give further details on the third order. However it is useful for the discussion below to make a short summary of previous numerical/analytical estimates of the third and fourth-order energy contributions at low density. The energy per particle at third order has been historically obtained by Efimov and Amusia using correlation functions methods [228,229], Baker using an expansion of Goldstone diagrams [230] and Bishop using an expansion of Feynman diagrams [231] in term of the s -wave scattering length a_s :

$$\frac{E_{(3)}}{E_{FG}} = (g - 1) [0.126 + 0.096(g - 3)] (a_s k_F)^3 \quad (2.27)$$

In 2000, Hammer and Furnstahl [35] as well as Steele [227] have calculated the ground-state energy of an infinite Fermi system at low density up to third-order in perturbation. In these works, they use the EFT framework together with the Green's functions formalism described in previous section. The energy per particle obtained with EFT coincides with the historical result given by (2.27). Platter, Hammer and Meißner [232] have also obtained the third order contribution evaluating first the self-energy.

We mention also the recent work [233], where the energy contributions up to fourth order using the EFT framework for dilute Fermi systems including the effective range, and leading order of the p -wave (and also the leading order of the three-body force) have been obtained in the form:

$$\frac{E}{E_{FG}} = 1 + (g - 1) \sum_{n=1}^4 C_n(k_F) + \mathcal{O}(k_F^5) \quad (2.28a)$$

with:

$$C_1(k_F) = \frac{10}{9\pi} (a_s k_F), \quad C_2(k_F) = \frac{4}{21\pi^2} (11 - 2 \ln 2) (a_s k_F)^2, \quad (2.28b)$$

$$C_3(k_F) = [0.126 + 0.096(g - 3)] (a_s k_F)^3 + \frac{1}{6\pi} (a_s k_F)^2 (r_s k_F) + \frac{1}{3\pi} \frac{g + 1}{g - 1} (a_p k_F)^3, \quad (2.28c)$$

⁷ This could actually be seen from their expression by a simple change of variables.

$$\begin{aligned} \mathcal{C}_4(k_F) = & -0.071(a_s k_F)^4 + 0.107(a_s k_F)^3(r_s k_F) \\ & + \gamma_4(k_F)(g-2)(a_s k_F)^4, \end{aligned} \quad (2.28d)$$

where:

$$\gamma_4(k_F) = 0.451 - 0.014(g-2) + \frac{80}{81\pi^3}(4\pi - 3\sqrt{3}) \ln |a_s k_F|. \quad (2.28e)$$

The last term contains the logarithmic divergent term at fourth order [35,230,231] that cancels out for $g = 2$. The contributing diagrams considering only the C_0 -contact interaction up to fourth order are displayed in figure 2.2. We observe an increasing complexity in terms of the number of diagrams to take into account. In that case, the diagrammatic representation is simplified since, for instance, the ladder diagram at fourth order represented in figure 2.2 contains only three channels: $3pp - 1hh$, $2pp - 2hh$ and $1pp - 3hh$.

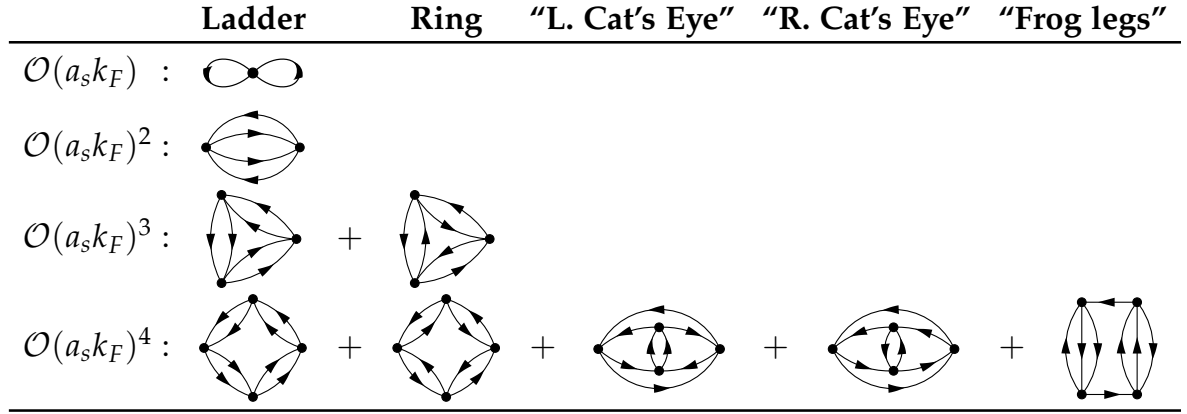


Figure 2.2: Class of non-vanishing Hugenholtz energy diagrams contributing from second to fourth order in $(a_s k_F)$. In [230], Baker gave the explicit contributions of each diagram to the energy. The same calculations in the context of EFT have been done in [233]. The class *Ladder*, *Ring*, *L. Cat's Eye*, *R. Cat's Eye* and *Frog legs* are named class I, IA, II, IIA and III respectively in [230,233].

The MBPT approach for dilute systems can be applied when $|a_s k_F|$ is small. When the s -wave scattering length is large, the perturbative expansion at low density discussed above breaks down and leads to a range of validity in density:

$$\rho \lesssim 10^{-6} \text{ fm}^{-3} \ll \rho_0 \simeq 0.16 \text{ fm}^{-3},$$

for nuclear matter (see table 1.1). Non-perturbative treatments are then mandatory. A common strategy used in nuclear physics is the so-called Brueckner theory [192, 234–236]. It consists in summing all or a restricted class of diagrams, like the ladder diagrams (see figure 2.2).

In the next section, we give an overview of recent attempts to make the resummation of diagrams in a compact and explicit form in terms of the density (or equivalently the Fermi momentum) and of the low-energy constants using the two-body contact interaction (2.6). The theories exposed here, based on resummation of perturbative diagrams, lead to a finite value of physical quantities at unitarity.

2.3

LADDER RESUMMATION

2.3.A Resummation of ladder diagrams: particle-hole propagator

The work of Steele [227] is particularly highlighting on the resummation techniques in the sense that it gives the energy contribution of each ladder and ring diagrams displayed in figure 2.2 separately as an integral over the phase-space of combinations of the effective particle-particle, effective hole-hole, effective particle-hole and effective hole-particle interactions. For instance (2.27) can be decomposed as a sum of four contributions [227], see (2.26), and numerically gives:

$$\begin{aligned}\frac{E_{FG}^{ladder(3)}}{E_{FG}} &= (g-1) \left[\frac{0.107}{2pp-1hh} + \frac{0.019}{1pp-2hh} \right] (a_s k_F)^3, \\ \frac{E_{FG}^{ring(3)}}{E_{FG}} &= (g-1)(g-3) \left[\frac{0.048}{2ph-1hp} + \frac{0.048}{1ph-2hp} \right] (a_s k_F)^3.\end{aligned}$$

Once we sum the two contributions it is also in fairly good agreement with the result (2.27). Similarly, at fourth order, the numerical estimations of ladder and ring diagrams give [227,233]:

$$\begin{aligned}\frac{E_{FG}^{ladder(4)}}{E_{FG}} &= (g-1) \left[\frac{0.064}{3pp-1hh} + \frac{0.025}{2pp-2hh} - \frac{0.001}{1pp-3hh} \right] (a_s k_F)^4, \\ \frac{E_{FG}^{ring(4)}}{E_{FG}} &= -(g-1)^2(g-3) \left[\frac{0.006}{3ph-1hp} + \frac{0.003}{2ph-2hp} + \frac{0.006}{1ph-3hp} \right] (a_s k_F)^4.\end{aligned}$$

Here we concentrate on the ladder diagrams. We remark that the energy diagrams composed by $(n-1)pp$ and $1hh$ loops are the dominant contributions in $E_{(n)}^{ladder}$ at each order in perturbation. Retaining only these contributions (namely particle-particle ladder diagrams as (2b) and (3d) shown in table 2.1) and using the Feynman rules, the contribution at each order n of the retained diagrams can be written as the factorization of $n-1$ effective particle-particle vertices closed by two hole lines:

$$E_{(n)}^{pp-ladder} = 4g(g-1)C_0 k_F^6 \int_{s,t} \theta_s^-(t) B_{pp}(s,t)^{n-1}. \quad (2.29)$$

It is worth mentioning that this expression is exact for $n=1$ [see (2.12)] and for $n=2$ [see (2.22)]. Therefore, the approximation starts at third order. By summing up all orders, we recognize a geometric series leading to the compact form of the ground-state energy [192,227,237]:

$$E = E_{FG} + \sum_{n=1}^{\infty} E_{(n)}^{pp-ladder} = E_{FG} + 4g(g-1)k_F^6 \int_{s,t} \theta_s^-(t) \Gamma_{pp}(s,t). \quad (2.30)$$

Note that here, we have added the kinetic energy contribution E_{FG} . We also introduced the resummed effective interaction given by:

$$\Gamma_{pp}(s, t) = C_0 \sum_{n=1}^{\infty} B_{pp}(s, t)^{n-1} = \frac{C_0}{1 - B_{pp}(s, t)}. \quad (2.31)$$

The diagrammatic representation of this resummation is shown in figure 2.3. Note

$$\sum_{n=1}^{\infty} E_{(n)}^{pp-ladder} = \text{Hartree-Fock} + \text{1-ladder} + \text{2-ladder} + \dots + \text{n-ladder} + \dots$$

Figure 2.3: Diagrammatic energy resummation of particle-particle ladder diagrams. Except for the Hartree-Fock diagram, a line from left to right represents a particle and from right to left a hole.

that the particle-particle effective interaction $\Gamma_{(2)}^{pp}$ is independent of the angle between s and t (see appendix C) and the integration on the solid angle can be performed using the relation valid for any function $f(s, t)$:

$$\int_{s,t} \theta_s^-(t) f(s, t) = \frac{1}{4\pi^4} \int_0^1 s^2 ds \int_0^{\sqrt{1-s^2}} t dt I_*(s, t) f(s, t), \quad (2.32)$$

with:

$$I_*(s, t) = \frac{1}{2s} \min \left\{ 2st; |1 - s^2 - t^2| \right\} \Theta(1 - s^2 - t^2). \quad (2.33)$$

This function encodes the angle integration of the overlap between two Fermi spheres. Finally, using (2.2), (2.5), (2.10), (2.21), (2.32) and (2.30), the ground state energy can be recast as [238]:

$$\frac{E}{E_{FG}} = 1 + (g - 1) \frac{80}{\pi} \int_0^1 s^2 ds \int_0^{\sqrt{1-s^2}} t dt \frac{(a_s k_F) \pi I_*(s, t)}{\pi - (a_s k_F) F(s, t)}, \quad (2.34)$$

where $F(s, t) = (2\pi)^2 \Pi_{pp}(s, t)$ is a dimensionless function of (s, t) given in appendix B and C after regularization [see (C.15c)]. Note that the imaginary part of Π_{pp} vanishes in the region defined by $s^2 + t^2 \leq 1$, i.e. the ground state energy (2.34), as expected, is a real quantity.

$$\sum_{n=1}^{\infty} E_{(n)}^{ladder} = \text{Hartree-Fock} + \text{1-ladder} + \text{2-ladder} + \dots + \text{n-ladder} + \dots$$

Figure 2.4: Diagrammatic energy resummation of combined particle-particle and hole-hole ladder diagrams. Except for one equivalent pair of lines (necessary hole lines), each pair of equivalent lines represents indistinguishable particles pair or holes pair excitations.

2.3.B Resummation of ladders diagrams: vacuum-medium propagator

An alternative technique employed in [238–240] leads to a resummation of a larger class of ladder diagrams considering simultaneously indistinguishable particle-particle and hole-hole pair excitations represented in figure 2.4. This technique, employing in-medium formalism, is discussed in this section.

VACUUM MEDIUM DECOMPOSITION OF PROPAGATOR

To introduce the in-medium Green's functions formalism, we first write the Green's functions (2.3) (particle-hole propagators) distinguishing explicitly the vacuum and medium pieces⁸:

$$\begin{aligned} G_i &= \frac{n_i}{\omega_i - e_i - i\tau} + \frac{1 - n_i}{\omega_i - e_i + i\tau}, \\ &= \frac{1}{\omega_i - e_i + i\tau} + \frac{n_i}{\omega_i - e_i - i\tau} - \frac{n_i}{\omega_i - e_i + i\tau}, \end{aligned} \quad (2.35)$$

$$= \underbrace{\frac{1}{\omega_i - e_i + i\tau}}_{\bar{G}_i} + \underbrace{2i\pi\delta(\omega_i - e_i)n_i}_{H_i}. \quad (2.36)$$

Here, we have used the identity:

$$\frac{1}{X \pm i\tau} = \mathcal{P} \frac{1}{X} \mp i\pi\delta(X), \quad (2.37)$$

where \mathcal{P} denotes the Cauchy principal value. The first term in (2.36), noted \bar{G}_i , is the vacuum particle propagator and the second term, noted H_i , corresponds to an in-medium insertion that puts in the Fermi sea an on-shell particle (an on-shell hole strictly speaking), i.e. a particle with $\omega_i = e_i$. We follow [238] and introduce the diagrammatic representation of vacuum and medium propagator:

$$\bar{G}_i = \text{---}\blacktriangleright\text{---} \quad \text{and} \quad H_i = \text{---}\#\text{---},$$

such that (2.36) can be represented diagrammatically as:

$$\text{---}\blacktriangleright\text{---} + \text{---}\blacktriangleleft\text{---} = \text{---}\blacktriangleright\text{---} + \text{---}\#\text{---}.$$

$G_i^+ \quad G_i^- \quad \bar{G}_i \quad H_i$

This decomposition of the propagator reorganizes the many-body calculation compared to the MBPT presented previously. In particular, combinatorial occurrence of each diagram should be properly incorporated and the Feynman diagrams are closed by medium propagator, i.e. the Feynman rules 1 and 5 presented previously are modified. Below, we illustrate the new rules for ladder diagrams from first to third orders.

⁸ Note that the Green's functions (2.36) can be also written as the sum of the vacuum hole propagator and its associated in-medium insertion:

$$\begin{aligned} G_i &= \frac{n_i}{\omega_i - e_i - i\tau} + \frac{1 - n_i}{\omega_i - e_i + i\tau} = \frac{1}{\omega_i - e_i - i\tau} - \frac{1 - n_i}{\omega_i - e_i - i\tau} + \frac{1 - n_i}{\omega_i - e_i + i\tau}, \\ &= \frac{1}{\omega_i - e_i - i\tau} - 2i\pi\delta(\omega_i - e_i)(1 - n_i). \end{aligned}$$

PERTURBATIVE IN-MEDIUM FORMALISM

The energy contribution at first order in $(a_s k_F)$ is given by the C_0 -vertex interaction closed by two medium propagators:

$$\begin{aligned} E_{(1a)} &= \text{diagram} = D_g(1a) \times \sigma(1a) \times C_0 \int_{1,2} H_1 H_2, \\ &= \frac{g}{2}(g-1) \times C_0 \left[\int_{k_1} n_1 \right]^2 = E_{\text{FG}}(g-1) \frac{10}{9\pi} (a_s k_F), \end{aligned} \quad (2.38)$$

and rest unchanged according to (2.12).

The second order is given by the diagram (2b) showed in table 2.1. In the in-medium formalism, it is decomposed into four contributions:

$$E_{(2b)} = \text{diagram} + \left[\text{diagram} + \text{diagram} \right] + \frac{1}{2} \times \text{diagram}, \quad (2.39)$$

where the vacuum propagator is diagrammatically represented by a white arrowed line. The extra factor 1/2 is due to the fact that there are two equivalent pairs of double in-medium insertion. Then, we can define the vacuum-medium loops, at second order in perturbation, as:

$$\begin{aligned} L_{(2)}(1;2) &= \text{diagram} + \left[\text{diagram} + \text{diagram} \right] + \frac{1}{2} \times \text{diagram}, \\ &= L_0 + L_1 + \frac{1}{2} L_2. \end{aligned} \quad (2.40)$$

The loops L_0, L_1 and L_2 are displayed in figure 2.5.

$$L_0 = \text{diagram} \quad L_1 = \text{diagram} + \text{diagram} \quad L_2 = \text{diagram}$$

Figure 2.5: Diagrammatic representation of the functions L_0, L_1, L_2 . The lines with an empty arrow represent the free propagator \bar{G}_i and the lines with double bar (“=”) represent the in-medium insertion H_i .

The procedure described above consists in treating the symmetry factor directly in the definition of the vacuum-medium loops (which plays the role of the particle-particle loops L_{pp} defined by (2.16) in the particle-hole formalism) such that the energy contribution is given by:

$$E_{(2b)} = D_g(2b) \times \sigma(2b) \times C_0^2 \int_{1,2} [-L_{(2)}(1;2)] H_1 H_2. \quad (2.41)$$

Then, taking advantage of the definition of the medium propagator H_i , the contour integration on ω_i is straightforward and we obtain:

$$E_{(2b)} = \frac{g}{2}(g-1) \times C_0^2 \int_{k_1, k_2} [-L_{(2)}(\mathbf{k}_1, e_1; \mathbf{k}_2, e_2)] n_1 n_2. \quad (2.42)$$

Following the particle-hole formalism, we then define the effective interaction at second order as:

$$\Gamma_{(2)}(s, t) = -C_0 L_{(2)}(\mathbf{k}_1, e_1; \mathbf{k}_2, e_2) = B_0(s, t) + B_1(s, t) + \frac{1}{2}B_2(s, t), \quad (2.43)$$

where $B_j(s, t) = -C_0 L_j(\mathbf{k}_1, e_1; \mathbf{k}_2, e_2)$ are explicit functions of the dimensionless momentum (2.19) given in appendix C. For instance:

$$\frac{B_0(s, t)}{mC_0k_F} = \int_u \frac{1}{t^2 - u^2 + i\tau} = -\frac{it}{4\pi'}, \quad (2.44)$$

is obtained using the standard minimal subtraction (MS) scheme of dimensional regularization [12,39–44] to treat properly the ultra-violet divergence (see appendix A). Finally, (2.42) leads to:

$$\begin{aligned} E_{(2b)} &= 4g(g-1)k_F^6 C_0 \int_{s,t} \theta_s^-(t) \Gamma_{(2)}(s, t), \\ &= (g-1)E_{FG} \frac{4}{21\pi^2} (11 - 2 \ln 2) (a_s k_F)^2, \end{aligned} \quad (2.45)$$

and the Lee-Yang contribution (2.24) is recovered.

Using the same argument on the symmetry factor for the third order ladder diagrams contribution (3d), we have:

$$\begin{aligned} E_{(3d)} &= \begin{array}{c} \text{Diagram 1} + \text{Diagram 2} + \text{Diagram 3} + \text{Diagram 4} + \frac{1}{3} \times \text{Diagram 5} \\ + \frac{1}{2} \times \left[\text{Diagram 6} + \text{Diagram 7} + \text{Diagram 8} + \text{Diagram 9} \right] \end{array} \quad (2.46) \end{aligned}$$

Here, for simplicity and compactness, we have not drawn the second reflected term of the L_1 contribution (see definition of L_1 in figure 2.5). In other words, when a bubble composed by one free propagator (empty arrowed line) and one in-medium insertion appears, we have to considered the total L_1 bubble. Taking into account these symmetry factors (1, 1/2, 1/3), we get the third order effective interaction by breaking a double in-medium insertion:

$$\begin{aligned} \Gamma_{(3d)} &= \left[B_0^2 + 2B_0B_1 + B_1^2 \right] + \frac{1}{2} \times (2B_0B_2 + 2B_1B_2) + \frac{1}{3} \times B_2^2, \\ &= (B_0 + B_1)^2 + (B_0 + B_1)B_2 + \frac{1}{3}B_2^3, \end{aligned} \quad (2.47)$$

such that the energy contribution of the third order is given by:

$$E_{(3d)} = 4g(g-1)k_F^6 C_0 \int_{s,t} \theta_s^-(t) \Gamma_{(3)}(s, t). \quad (2.48)$$

Similarly, in figure 4 of [238], Kaiser gave an illustration of the fourth order ladder diagram term leading to:

$$\Gamma_{(4)}^{ladder} = (B_0 + B_1)^3 + \frac{3}{2}(B_0 + B_1)^2 B_2 + (B_0 + B_1)B_2^2 + \frac{1}{4}B_2^3. \quad (2.49)$$

RESUMMED GROUND STATE ENERGY

The in-medium formalism allows one to write the contribution of the n^{th} order ladder diagrams to the ground-state energy including indistinguishable particle-particle and hole-hole pair excitations as in the particle-hole formalism (2.29) where the effective particle-particle interaction is replaced by the effective interaction $\Gamma_{(n)}$. More precisely, the ground-state energy at n^{th} order now reads:

$$E_{(n)}^{\text{ladder}} = 4g(g-1)k_F^6 C_0 \oint_{s,t} \theta_s^-(\mathbf{t}) \Gamma_{(n)}(\mathbf{s}, \mathbf{t}). \quad (2.50)$$

Studies of the topological symmetry of the diagrams lead to the effective interaction at n^{th} order given in terms of the analytical function B_j given in appendix C by:

$$\Gamma_{(n)} = \sum_{j=0}^{n-1} \binom{n-1}{j} \frac{1}{j+1} (B_0 + B_1)^{n-1-j} B_2^j. \quad (2.51)$$

Here, the j index corresponds to the number of double in-medium insertions B_2 composing the effective interaction. Now, summing up all orders, we obtain the resummed effective interaction:

$$\begin{aligned} \Gamma &= C_0 \sum_{n=1}^{\infty} \Gamma_{(n)} = C_0 \sum_{n=1}^{\infty} \sum_{j=0}^{n-1} \binom{n-1}{j} \frac{1}{j+1} (B_0 + B_1)^{n-1-j} B_2^j, \\ &= C_0 \sum_{n=1}^{\infty} \frac{1}{nB_2} \left[(B_0 + B_1)^n - (B_0 + B_1 + B_2)^n \right], \\ &= C_0 B_2^{-1} \text{Ln} \left[\frac{1 - B_0 - B_1 - B_2}{1 - B_0 - B_1} \right]. \end{aligned} \quad (2.52)$$

The resummed energy is given by:

$$E = E_{FG} + 4g(g-1)k_F^6 \oint_{s,t} \theta_s^-(\mathbf{t}) \Gamma(\mathbf{s}, \mathbf{t}). \quad (2.53)$$

Note that the logarithm function is here the complex logarithm [$\text{Ln}(z) = \ln|z| + i \arg z$]. This means that the effective interaction is now complex. However the ground state energy is real order by order by construction, and consequently the resummed ground state energy is also real [238]. Finally, using (2.2), (2.5), (2.10), (2.32), (2.53), and the definition of function B_j given in appendix C, the resummed ground state energy obtained by summing up the larger class of ladder diagrams displayed in figure 2.4 reads:

$$\frac{E}{E_{FG}} = 1 + (g-1) \frac{80}{\pi} \int_0^1 s^2 ds \int_0^{\sqrt{1-s^2}} dt \arctan \left[\frac{(a_s k_F) \pi I_*(s, t)}{\pi - (a_s k_F) R(s, t)} \right]. \quad (2.54)$$

where $R(s, t) = F(s, t) + F(-s, t)$ is given in appendix C [see (C.14d)].

2.3.c Discussion of the results on energy resummations

In the following, results of the numerical integrations of (2.34) and (2.54) will be referred as *Geometric series Exact Integration* (GEI) and *Arctangent series Exact Integration* (AEI) respectively. The resummations of the energy discussed in this chapter are depicted in figure 2.6. In both cases, the effective interaction Γ_{pp} (2.31) and Γ (2.52) are solutions of the so-called Bethe-Salpeter equation [192,241] (more rigorously, its on-shell version, i.e. $\omega_i = e_i$, in the ladder approximation). The ground state energy is then given by closing this effective interaction similarly to the case of the Hartree-Fock diagrams (1a) except that the C_0 vertex is replaced by Γ_{pp} (respectively Γ) and is closed by two hole (respectively two medium) propagators for the GEI (respectively AEI) case.

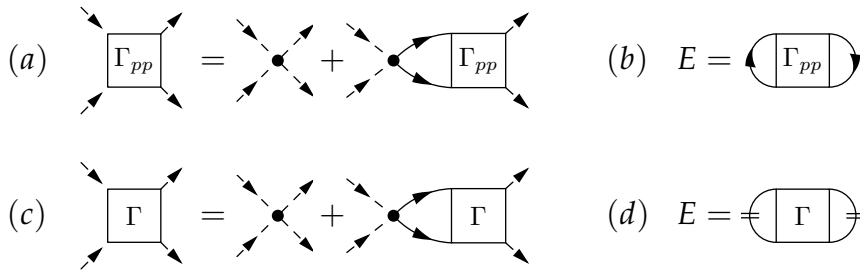


Figure 2.6: Schematic representation of the ladder resummation for the ground state energy discussed in this chapter. (a) Bethe-Salpeter equation [192,241] for the diagrammatic particle-particle ladder resummation. The solution of this equation is given by (2.30). Here, solid arrowed lines from left to right correspond to particle lines. (b) Ground state energy from particle-particle ladder resummation in term of Γ_{pp} closed by two hole lines. (c) Bethe-Salpeter equation [192,241] for the diagrammatic ladder resummation. Here, solid arrowed lines from left to right correspond to indistinguishable pair of particle or pair of hole lines. (d) Ground state energy from ladder resummation in term of Γ closed by two in-medium propagators. Note that the energy is given by a diagram similar to the diagram (1a) where the C_0 -vertex is replaced by the effective interaction Γ_{pp} or Γ .

We can remark that both resummed energies have the same structure after the use of (2.32) consisting in an integral over the accessible phase-space (s, t) :

$$\frac{E}{E_{FG}} = 1 + (g - 1) \int_0^1 s^2 ds \int_0^{\sqrt{1-s^2}} t dt \mathcal{E}(s, t; a_s k_F), \quad (2.55a)$$

with:

$$[\text{GEI}] \mapsto \mathcal{E}(s, t; a_s k_F) = \frac{80}{\pi} \frac{(a_s k_F) \pi I_*(s, t)}{\pi - (a_s k_F) F(s, t)}, \quad (2.55b)$$

$$[\text{AEI}] \mapsto \mathcal{E}(s, t; a_s k_F) = \frac{80}{\pi} \arctan \left[\frac{(a_s k_F) \pi I_*(s, t)}{\pi - (a_s k_F) R(s, t)} \right]. \quad (2.55c)$$

These expressions present several interesting features compared to a perturbative expansion. Firstly, they could be expanded in powers of $(a_s k_F)$ and, noteworthy, their second order contributions match, in both case the Lee-Yang formula (1.28).

Note that (2.54) is slightly more predictive in the sense that it is valid up to third order⁹ in $(a_s k_F)$.

We show in panel (a) of figure 2.7 a comparison of the energy obtained by integrating numerically¹⁰ the two resummed expressions as a function of $(a_s k_F)$. One of the motivations for the use of resummation is that, contrary to any truncation, the energy is not diverging as $|a_s k_F| \rightarrow \infty$, i.e. in the unitary gas regime (see panel (b) of figure 2.7). This was firstly discussed in [237] for the GEI case and latter in [238] for the AEI case. As noted in these works, the ratio:

$$\zeta_0 = \lim_{|a_s k_F| \rightarrow \infty} \frac{E}{E_{FG}}, \quad (2.56)$$

generally referred to as the universal Bertsch parameter, significantly depends on the class of diagrams selected for resummation. This is clearly illustrated in the inset of figure 2.7(b). In the two cases considered here, we have:

$$\zeta_{\text{GEI}} \simeq 0.24 \quad \text{and} \quad \zeta_{\text{AEI}} \simeq 0.51. \quad (2.57)$$

These values in both cases significantly differ from the experimentally observed value of the Bertsch parameter $\zeta_0 = 0.37$ [70–73]. It should however be kept in mind that the value of ζ_0 corresponds to the one of a superfluid unitary gas while superfluidity is not accounted for in the present resummation. Therefore, to be consistent, one should a priori compare with the value of the Bertsch parameter in normal systems. In [84], using Brueckner Hartree-Fock (BHF) approach, a value $\zeta_0 = 0.507$ was found for normal systems, which is compatible with the experimental result of [71] giving $\zeta_0 = 0.45$. This value is actually consistent with the AEI case given by (2.54). Nevertheless, one obvious conclusion is that the choice of certain diagrams significantly affects the energy behavior as $(a_s k_F)$ increases.

Despite the fact that the selection of diagrams influences the results of a resummation approach, the resulting expressions of the energy in terms of $(a_s k_F)$ is an interesting step towards a non-empirical functional for interacting systems beyond the Lee-Yang formula. Still, the deduced expressions (2.55) are rather complicated especially due to the necessity to perform explicit integrations on phase-space for all values of k_F . This complexity can however be partially reduced using an approximation discussed in the next chapter.

⁹ Only the ladder diagram contribution term at third order is accounted for since the ring diagrams composed by particle-hole loops (the non-vanishing diagram (3e) of table 2.1) are not taken into account in the resummation.

¹⁰ For the multidimensional numerical integration of the equations, we used the Vegas method implemented in the Cuba library [242]. We have cross-checked the results with Wolfram Mathematica using the “LocalAdaptive” method.

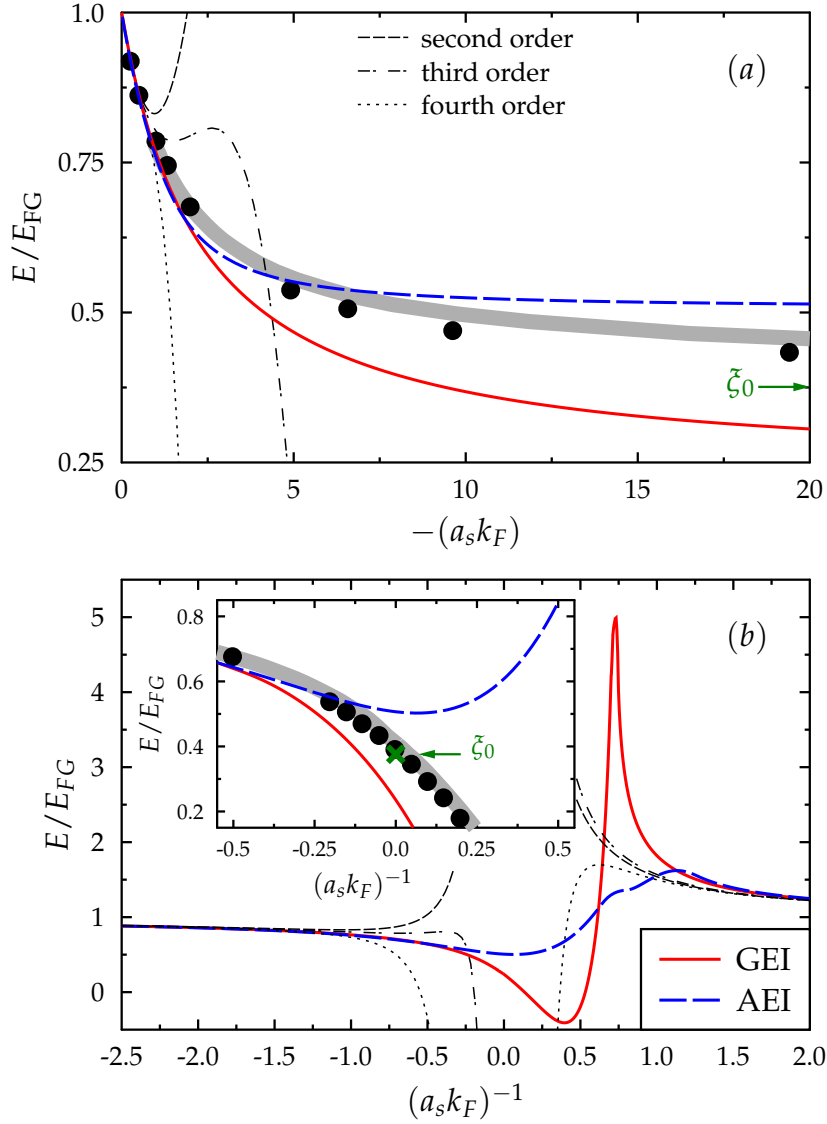


Figure 2.7: Energy in unit of the free Fermi gas energy as a function of (a) $-(a_s k_F)$ and (b) $(a_s k_F)^{-1}$. The red solid and blue dashed lines are respectively obtained by direct numerical integration of (2.34) and (2.54). For reference, the thin black short-dashed line, thin black dash-dotted line and thin black dotted line correspond respectively to (2.28) truncated at second order (Lee-Yang formula), at third and fourth order in $(a_s k_F)$ for $g = 2$ and $r_s = a_p = 0$. In both panels, the grey area indicates the result obtained by fitting the experiment [70] with a Padé approximation while the black circles are the Diffusion Monte-Carlo (DMC) results of [72]. In the inset of panel (b), a focus is made near unitarity. In all panels, the arrow indicates the value of the Bertsch parameter $\zeta_0 = 0.376$.

3

DFT INSPIRED FROM EFT RESUMMATION

Jean-Claude

On n'est pas bien là ?

Pierrot

Si.

Jean-Claude

Paisible ? À la fraîche ? Décontracté du gland ? Et on bandera quand on aura envie de bander ?

G erard DEPARDIEU et Patrick DEWAERE – *Les Valseuses*

CONTENTS

| | | |
|-------|---|-----|
| 3.1 | DFT from energy resummation | 66 |
| 3.1.A | General strategy | 67 |
| 3.1.B | DFT inspired from geometrical series resummation for the ground-state energy | 68 |
| 3.1.C | DFT inspired from arctangent resummation for the ground-state energy | 72 |
| 3.1.D | Results and comparison of the different functionals | 73 |
| 3.2 | Determination of the ground-state thermodynamical properties | 76 |
| 3.3 | Generalization of the DFT including effective range | 83 |
| 3.3.A | Inclusion of the effective range | 83 |
| 3.3.B | Effective range approximation | 85 |
| 3.3.C | Discussion and comparison | 87 |
| 3.4 | Application to linear response in Fermi liquids | 93 |
| 3.4.A | Generalities on static response | 94 |
| 3.4.B | Static response in unitary gases | 96 |
| 3.4.C | Static response in neutron matter | 97 |
| 3.4.D | Collective response in the hydrodynamical regime | 99 |
| 3.5 | Summary and critical discussion | 103 |

In this chapter, we explore the possibility to start from the resummed expressions of the energy obtained in chapter 2 and obtain an explicit DFT to describe the Fermi gas in the low-density and large scattering-length limits. It is shown that the different resummations give strong guidance for obtaining simple DFT where the energy is written directly as a function of $(a_s k_F)$ in a compact form. Then, interpreting k_F as a functional of the density ρ leads to a DFT. Such a DFT reformulation is motivated by the fact that (i) MBPT calculation rapidly becomes highly involved as the order of perturbation increases and that (ii) the compact resummed expressions found in chapter 2 are complex to implement in finite systems because of the integrals on the phase-space. Once simpler functionals are found, we will see how this could serve as a guidance to obtain DFT for systems with large s -wave scattering length. We will then illustrate the predictive power of the functional we recently proposed along this line.

3.1

DFT FROM ENERGY RESUMMATION

When the s -wave scattering length at play in a system becomes large, the perturbation theory at low density discussed in chapter 2 is not valid anymore. The summation of diagrams to all orders becomes then necessary to describe such case. Typical examples in nature are unitary Fermi gases or nuclear neutron matter. In this section, I summarize some of the results obtained previously from diagrammatic resummation and make an extended overview of recent attempts to obtain simpler DFT from it in order to reproduce the ground state energy of systems with strong s -wave interaction.

We now introduce some notations that will be useful in this chapter. Guided by the low-density expansion, we will generally introduce the set of coefficients¹ $\gamma = \{\gamma_n\}$ such that, the energy can be written order by order as a series:

$$\frac{E}{E_{\text{FG}}} = \sum_{n=0}^{\infty} \gamma_n (a_s k_F)^n. \quad (3.1)$$

Note that, in the absence of truncation, such expression can be valid at all values of $(a_s k_F)$. We see that, in the limit of small $(a_s k_F)$, by comparing with expression (2.28), we have:

$$\gamma_0 = 1, \quad \gamma_1 = \frac{10}{9\pi}, \quad \text{and} \quad \gamma_2 = \frac{4}{21\pi^2}(11 - 2 \ln 2).$$

Alternatively, one might use a different expansion guided by a Taylor expansion in $(a_s k_F)^{-1}$ around unitarity. We then introduce a set of parameters² $\xi = \{\xi_n\}$ such that:

$$\frac{E}{E_{\text{FG}}} = \sum_{n=0}^{\infty} \xi_n (a_s k_F)^{-n}. \quad (3.2)$$

Note that, from *ab initio* calculations, it was found that:

$$\frac{E}{E_{\text{FG}}} = \xi_0 - \zeta_0 (a_s k_F)^{-1} - \frac{5}{3} \nu_0 (a_s k_F)^{-2} + \mathcal{O}(a_s k_F)^{-3} \quad (3.3)$$

where ξ_0 is the usual Bertsch parameter and (ζ_0, ν_0) have been found to be close to 1 [77,243–245].

This section is organized as follow. First, we focus on the Geometrical series resummation obtained by summing up all orders of the particle-particle ladder diagrams presented in section 2.3.a. We recall the main results and present three types of approximations that we can do to obtain an explicit functional of the density for the energy: (i) the Phase-Space average method [237], (ii) the Large Dimension limit [227], or (iii) the Unitary Limit constraint [76]. These techniques are then applied starting from expressions obtained in section 2.3.b by summing up combined particle-particle and hole-hole ladder diagrams.

¹ Note that these coefficients depend implicitly on the degeneracy g .

² We restrict this expansion to the case $g = 2$.

3.1.A General strategy

The study of MBPT and the resummation of the energy diagrams in chapter 2 have highlighted that the ground state energy given by (3.1) or (3.2) can be written as an integral on the phase-space:

$$\frac{E}{E_{FG}} = 1 + (g - 1) \int_0^1 s^2 ds \int_0^{\sqrt{1-s^2}} t dt \mathcal{E}(s, t; a_s k_F). \quad (3.4)$$

Here \mathcal{E} , that depends of the parameter $(a_s k_F)$, has a finite limit at strict unitarity, and is strongly dependent on the class of diagrams selected for the resummation. Its expression obtained from ladders resummation is given by (2.55). The energy, under this form, is a density functional in the sense that it depends explicitly on the Fermi momentum k_F linked to the density ρ through the relationship (2.5). There are however two difficulties:

- The functional given by (3.4) is a rather complex function of k_F . In particular, it seems hard to export it in finite systems. For comparison, Skyrme functionals [108,110,111], that are widely used, are simple polynomial functions of ρ without the need of integration on the phase-space. Let us take for instance the t_0 -term (equivalent to the s -wave leading order term of neutron matter energy). This term is simply written as:

$$\frac{E}{E_{FG}} = 1 + \frac{5m}{6} \frac{\rho^{1/3}}{(3\pi^2)^{2/3}} t_0 (1 - x_0), \quad (3.5)$$

where, as we have seen in section 1.3, the parameters (t_0, x_0) are fitted on nuclear data or pseudo-data. This form is particularly useful and practical for finite systems due to its simplicity. However, one drawback compared to (3.4) is that the connection with the LEC like a_s is lost (see figure 1.18).

- This functional lacks predictivity for systems with a large scattering length (see figure 2.7).

The goal here is to propose a density functional inspired by (3.4) that (i) simplifies its application both in infinite and finite systems, (ii) has a better predictive power, and (iii) is still connected to the LEC, here a_s . To this end, we used the following strategy:

1. Start from a resummed expression of the energy in a given scheme (ladder resummation or its restriction to the particle-particle channel for instance).
2. Use simplified expressions, for example obtained by phase-space average of dimensionless functions appearing in \mathcal{E} .
3. Replace eventually the constants by parameters depending on the quality of the DFT obtained in step 2.
4. Impose well defined limits as the low-density or unitary limits to fix the value of these parameters.

Although the aim of the authors was not to obtain a DFT, some attempts have been made previously to obtain a simplified expression of the energy (for instance the GPS and GLD approximation discussed below) [227,237]. In the present work,

we complete these attempts by simplifying the expressions following the strategy discussed above. In the following, we make a survey on the approximations done in the past or in the present study to combine and take advantage of the effectiveness of the functional theory and the richness of the resummation.

Altogether, based on the different approximation techniques introduced in chapter 2, we explore eight types of DFT. Acronyms associated to these functionals are listed in table 3.1.

| Type of resummation | Name of functionals | | Equations |
|---------------------|---------------------|-----|-----------|
| Geometrical series | Exact Integration | GEI | (3.6) |
| | Phase-Space | GPS | (3.10) |
| | Large Dimension | GLD | (3.11) |
| | Unitary Limit | GUL | (3.12) |
| Arctangent function | Exact Integration | AEI | (3.13) |
| | Phase-Space | APS | (3.14) |
| | Large Dimension | ALD | (3.15) |
| | Unitary Limit | AUL | (3.16) |

Table 3.1: Names and acronyms of the resummation inspired functionals discussed in the text. We also give the corresponding equations in the text.

3.1.B DFT inspired from geometrical series resummation for the ground-state energy

Here, we recall the result obtained in section 2.3.a. By summing up the particle-particle ladder diagrams, we have shown that the ground-state energy can be written as an integral over the accessible phase-space [see (2.55) and figure 2.7]:

$$\frac{E}{E_{FG}} = 1 + \frac{80}{\pi} \int_0^1 s^2 ds \int_0^{\sqrt{1-s^2}} t dt \frac{(a_s k_F) \pi I_*(s, t)}{\pi - (a_s k_F) F(s, t)}, \quad (3.6)$$

where the functions F and I_* are given by (C.15c) and (C.14e) in appendix C. We have called this approximation GEI for *Geometric series Exact Integration*. In particular, the numerical integration at unitarity gives a Bertsch parameter $\xi_{GEI} \simeq 0.24$ and the Taylor expansion at low density in terms of $(a_s k_F)$ is valid up to second order. The energy obtained in the GEI approximation is shown in figure 3.1 (see also figure 2.7).

(I) PHASE-SPACE (PS) AVERAGE

Despite the sensitivity of the resummation approach to the selection of the diagrams, the resulting expressions of the energy in terms of $(a_s k_F)$ are an interesting step towards a DFT for interacting systems beyond the Lee-Yang formula. The complexity of the expressions can be partially reduced using what we call below a Phase-Space (PS) average approximation.

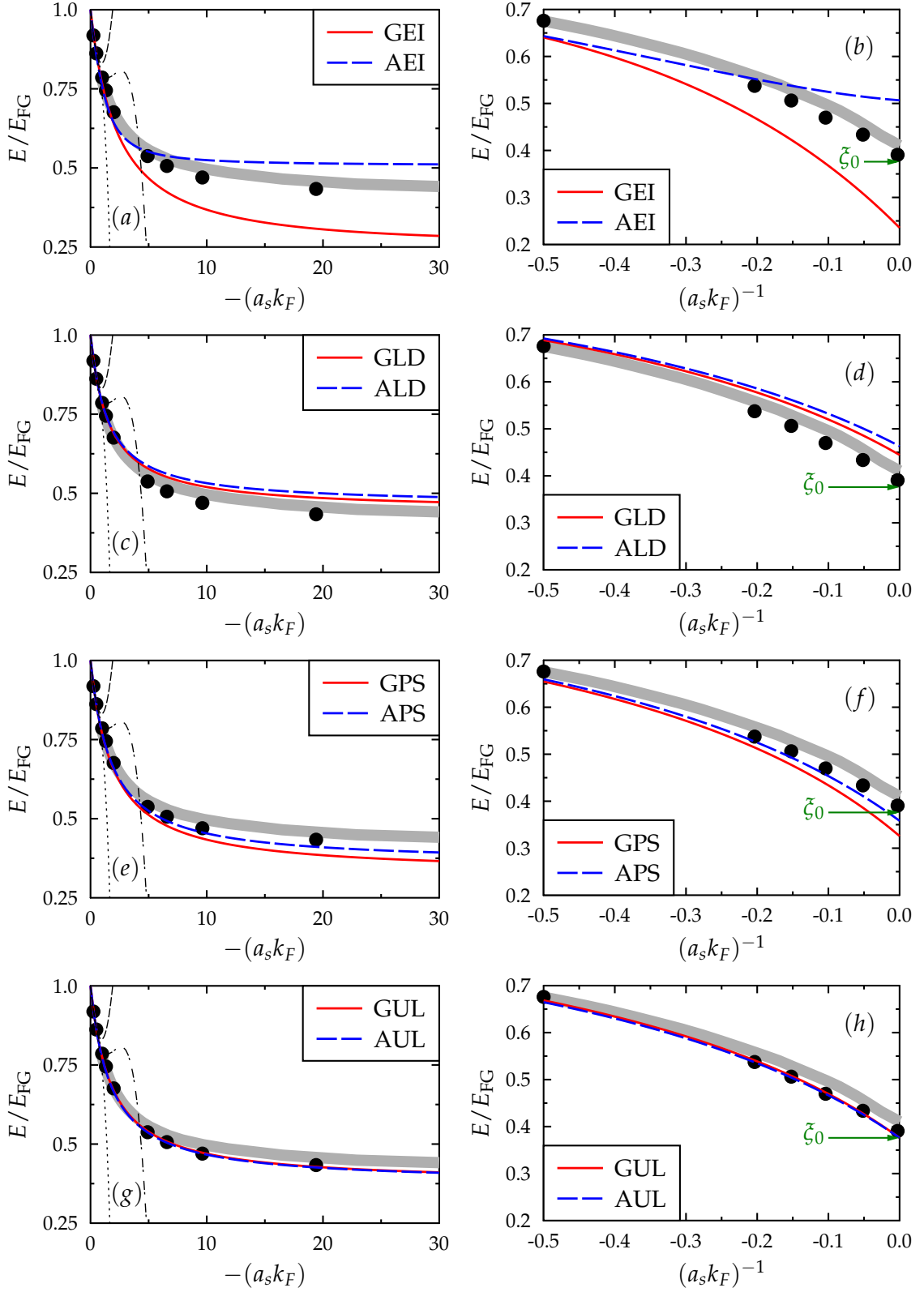


Figure 3.1: Ground-state energy as a function of $-(a_s k_F)$ (left) and $(a_s k_F)^{-1}$ (right) obtained with the different functionals introduced in the text. From top to bottom, we compare for each approximation discussed [EI (a – b), LD (c – d), PS (e – f), UL (g – h)], the Geometric series (red solid line) and Arctangent function (blue dashed line) energy density functionals. For reference, the green arrow in right panels indicates the Bertsch parameter at strict unitarity ($\zeta_0 = 0.376$). As in figure 2.7, the second, third and fourth orders of MBPT calculations [see (2.28)], experimental data of [70] (grey area) and *ab initio* results of [72] (black circle) are displayed.

The PS approximation was discussed for the Geometric series case in [237]. It consists simply in replacing the numerator and denominator entering in the integral respectively by their average values integrated over the phase-space, leading in this way to a much simpler approximation. Let us introduce the notation $\langle\langle X \rangle\rangle$ defined as:

$$\langle\langle X \rangle\rangle \equiv \int_0^1 s^2 ds \int_0^{\sqrt{1-s^2}} t dt X(s, t). \quad (3.7)$$

We see for instance that the GEI functional can be written as:

$$\begin{aligned} \frac{E}{E_{\text{FG}}} &= 1 + \frac{80}{\pi} \left\langle\left\langle \frac{(a_s k_F) I_*}{1 - (a_s k_F / \pi) F} \right\rangle\right\rangle \\ &= 1 + \frac{80}{\pi} (a_s k_F) \langle\langle I_* \rangle\rangle \left\{ 1 + \frac{(a_s k_F)}{\pi} \frac{\langle\langle I_* F \rangle\rangle}{\langle\langle I_* \rangle\rangle} + \frac{(a_s k_F)^2}{\pi^2} \frac{\langle\langle I_* F^2 \rangle\rangle}{\langle\langle I_* \rangle\rangle^2} + \dots \right\}. \end{aligned} \quad (3.8)$$

The PS approximation consists in replacing this expression in the following way:

$$\begin{aligned} \frac{E}{E_{\text{FG}}} &\simeq 1 + \frac{80}{\pi} (a_s k_F) \langle\langle I_* \rangle\rangle \left\{ 1 + \frac{(a_s k_F)}{\pi} \frac{\langle\langle I_* F \rangle\rangle}{\langle\langle I_* \rangle\rangle} + \frac{(a_s k_F)^2}{\pi^2} \frac{\langle\langle I_* F \rangle\rangle^2}{\langle\langle I_* \rangle\rangle^2} + \dots \right\} \\ &= 1 + \frac{80}{\pi} \frac{(a_s k_F) \langle\langle I_* \rangle\rangle}{1 - (a_s k_F / \pi) \langle\langle I_* F \rangle\rangle / \langle\langle I_* \rangle\rangle}. \end{aligned} \quad (3.9)$$

This approximation still insures that the Lee-Yang expression is recovered up to second order in $(a_s k_F)$ as it was the case for (3.6). Using the integrals given in appendix E, we obtain:

$$\frac{E}{E_{\text{FG}}} = 1 + \frac{\frac{10}{9\pi} (a_s k_F)}{1 - \frac{6}{35\pi} (11 - 2 \ln 2) (a_s k_F)}. \quad (3.10)$$

This compact form, called hereafter Geometric series Phase-Space (GPS), was introduced at several occasions in the nuclear physics and/or cold atom context³ [233,237,246,247]. The energy obtained in the GPS approximation is shown in figure 3.1.

One important conclusion is that the energy obtained from (3.10) largely extend the domain of density over which it reproduces the exact Monte-Carlo results compared to the Lee-Yang formula, i.e. compared to the second order perturbation theory at low density. Essentially, above $-(a_s k_F) = 1$ in figure 3.1.e, the Lee-Yang expression deviates significantly from the exact calculation. Note that the inclusion of third and fourth orders perturbation theory only slightly extends the domain of validity. On contrary, we see in figure 3.1.e and 3.1.f that the resummed formula follows closely the exact results and therefore it could be useful to obtain a compact form for a DFT beyond the perturbative regime. The GPS approximation has

³ The GPS functional (3.10) could be interpreted as a minimal Padé approximation in $(a_s k_F)$ at low density, the Padé[1/1] recently shown for instance in figure 2 of [233]. We mention that higher orders Padé approximations $[k/k]$ can be obtained (see for instance [246]) that could reproduce the development (3.8) to a given desired order in $(a_s k_F)$ for any k .

indeed been recently used in [197] to obtain a nuclear EDF where some of the parameters are directly connected to the physical s -wave scattering length, contrary to the widely used Skyrme EDF [108,110,111].

Although the main goal of the present work is to obtain DFTs suitable beyond the perturbative regime, we would like to mention that the approximated form (3.10) leads to a Bertsch parameter $\zeta_{GPS} = 0.32$ [197,237], that is closer to the one obtained at unitarity for superfluid systems $\zeta_0 = 0.37$ [70–73] compared to the one obtained with direct integration. It should be noted however that a relatively small difference in the value of ζ_0 leads to large deviations in the energy due to the fact that the energy is multiplied by the Free-Gas energy.

(II) LARGE DIMENSION (LD) LIMIT

Motivated by the first experimental estimate of ζ_0 (at that time, $\zeta_0 \gtrsim 0.4$, see figure 1.12), the author of [227] proposed an alternative explanation for the emergence of such a value from (3.6). He also ended up with a compact DFT that slightly differs from the GPS one.

In [227], Steele started his work by considering the large d -expansion limit (d being the dimension of the space) of the particle-particle loop integral (2.21) and has suggested to simplify the resummed energy per particle as:

$$\frac{E}{E_{FG}} = 1 + \frac{\frac{10}{9\pi}(a_s k_F)}{1 - \frac{2}{\pi}(a_s k_F)}. \quad (3.11)$$

Here, the function F appearing in (3.6) is replaced by its asymptotic value in large dimension of space ($F \rightarrow 2$). We immediately see that the expansion at low density is now valid only at first order in $(a_s k_F)$. The functional (3.11), called GLD (*Geometric series Large Dimension limit*) hereafter, leads to a Bertsch parameter $\zeta_{GLD} = 4/9 \simeq 0.44$ which is not too far from $\zeta_0 = 0.37$ and matches the first historical attempt to extract ζ_0 from *ab initio* calculations [82]. The predictive power of the GLD functional is illustrated in figure 3.1. We see that, while the result differs from the GPS at large $(a_s k_F)$, at low density [small $(a_s k_F)$], the energy of GPS and GLD are very close from each other. This suggests that, replacing the function F in the denominator of (2.30) by a constant value to obtain a simpler functional without explicit integration on the phase-space, offers some flexibility to reproduce the energy at low density or/and close to unitarity.

(III) UNITARY LIMIT (UL) CONSTRAINT

Both phase-space average and large dimension limits lead to simpler DFTs that take a geometric series form. However both give a rough approximation at unitarity. Based on the argument given above, it was proposed to adjust directly the numerator such that the unitary gas limit is reproduced [76,248], i.e.:

$$\frac{E}{E_{FG}} = 1 + \frac{(a_s k_F)A}{1 - (a_s k_F)B'} \quad (3.12a)$$

where the coefficient A is constrained on the leading order at low density in $(a_s k_F)$ of the energy (2.28) and B directly at unitarity limit. This leads to:

$$A = \frac{10}{9\pi} \quad \text{and} \quad B = \frac{10}{9\pi}(1 - \zeta_0)^{-1}. \quad (3.12b)$$

The unitarity is exactly reproduced by the functional (within experimental error bars) with the price to pay that the second-order expansion in $(a_s k_F)$ is again not anymore properly accounted for. This approximation is called GUL (*Geometric series Unitary Limit constraint*) hereafter.

Illustration of the GUL functional is given in figure 3.1. As can be seen on this figure, the GUL functional reproduces perfectly the results for all values of $(a_s k_F)$. As we will see in section 3.2, this functional turns out to be extremely predictive for atomic systems.

3.1.c DFT inspired from arctangent resummation for the ground-state energy

For the sake of completeness, we introduce below the functionals obtained starting from the resummation of the full ladder diagrams (AEI functional) and using the same three approximations discussed previously.

The technique employed in [238] based on vacuum/medium propagator (see section 2.3.b) to sum a certain class of diagrams consists in discriminating the number of *medium-insertions* combining particle-particle and hole-hole ladder diagrams. The resummed energy takes the form of a phase-space integral of an arctangent function [see (2.55) and figure 2.7]:

$$\frac{E}{E_{FG}} = 1 + \frac{80}{\pi} \int_0^1 s^2 ds \int_0^{\sqrt{1-s^2}} t dt \arctan \left[\frac{(a_s k_F) \pi I_*(s, t)}{\pi - (a_s k_F) R(s, t)} \right], \quad (3.13)$$

where R and I_* are given by (C.14d) and (C.14e) in appendix C. We call this energy density functional AEI for *Arctangent function Exact Integration*. The exact integration leads to a Bertsch parameter $\zeta_{AEI} \simeq 0.51$ which is larger compared to the expected value. Nevertheless, the Taylor expansion in $(a_s k_F)$ of the energy is valid up to third order. While simplified expressions have already been explored for the geometric series case, up to now, no attempt has been made to get a simpler DFT from expression (3.13). Such a study is made below, and discussed in detail in [200], leading to rather interesting results. As before, we explore the possibility to make approximations to obtain simple functional: (i) Phase-Space average, (ii) Large Dimension limit, and (iii) Unitary Limit constraint.

(i) PHASE-SPACE (PS) AVERAGE

Using the same approximation as above, a phase-space approximation of (3.13) leads to the functional:

$$\frac{E}{E_{FG}} = 1 + \frac{16}{3\pi} \arctan \frac{\frac{5}{24}(a_s k_F)}{1 - \frac{6}{35\pi}(11 - 2 \ln 2)(a_s k_F)}. \quad (3.14)$$

Illustrations of the energy obtained in the APS (*Arctangent function Phase-Space average*) approximation are given in figure 3.1. We note that the APS closely follows the GPS case at low density. This is indeed expected since both are constructed to match the same Lee-Yang expansion for low-density Fermi gas. More surprisingly, the APS turns out to be very satisfactory up to unitarity. It indeed gives a Bertsch parameter equal to $\zeta_{APS} \simeq 0.36$ that is very close to $\zeta_0 = 0.37$. This is an interesting finding since, contrary to the GPS case where the unitary limit can only be repro-

duced at the price of degrading the description of the low-density regime, in the APS case, both low density [second-order expansion in $(a_s k_F)$] and unitary limit can be very reasonably accounted for without adjusting any parameter.

For the sake of completeness and although we do not expect to gain so much in terms of predictive power compared to the APS, we present similarly to the GLD and GUL cases, an ALD (*Arctangent function Large Dimension limit*) and AUL (*Arctangent function Unitary Limit*) approximations.

(II) LARGE DIMENSION (LD) LIMIT

The asymptotic value of the function R in large dimension is the same as for F , i.e. $R \rightarrow 2$. Then, replacing the function R simply by 2 in the functional gives:

$$\frac{E}{E_{FG}} = 1 + \frac{16}{3\pi} \arctan \frac{\frac{5}{24}(a_s k_F)}{1 - \frac{2}{\pi}(a_s k_F)}. \quad (3.15)$$

Note that the function I_* is replaced by its Phase-Space average value to reproduce the leading order of the energy in $(a_s k_F)$. Again, the second order in $(a_s k_F)$ at low density is not correct and we found a Bertsch parameter $\xi_{ALD} \simeq 0.46$. This is closer to 0.37 compared to the original value of 0.51 and it turns out to be very similar to the geometric series case when doing the same approximation, i.e. 0.44. This approximation is called ALD (*Arctangent Large Dimension limit*) hereafter and is illustrated in figure 3.1.

(III) UNITARY LIMIT (UL) CONSTRAINT

Finally, we can directly constrain the functional with the exact Bertsch parameter as a physical input:

$$\frac{E}{E_{FG}} = 1 + \frac{16}{3\pi} \arctan \frac{(a_s k_F)\mathcal{A}}{1 - (a_s k_F)\mathcal{B}'}, \quad (3.16a)$$

where \mathcal{A} is constrained on the leading order in $(a_s k_F)$ of the energy and \mathcal{B} on unitarity. This leads to:

$$\mathcal{A} = \frac{5}{24} \quad \text{and} \quad \mathcal{B} = \frac{5}{24} \tan^{-1} \left[\frac{3\pi}{16}(1 - \xi_0) \right]. \quad (3.16b)$$

Here the unitary gas is exactly reproduced at the price of not reproducing anymore the second order in $(a_s k_F)$ at low density. This approximation is called AUL (*Arctangent Unitarity Limit constraint*) hereafter. The functional is illustrated in figure 3.1 and leads to results very similar to the APS case.

3.1.D Results and comparison of the different functionals

In figure 3.1, we show the energy obtained with the six functionals introduced⁴ above both at low density and close to unitarity. We also summarize the value of the parameters $\{\gamma_2, \gamma_3\}$ and $\{\xi_0, \zeta_0, \nu_0\}$ respectively defined by (3.1) and (3.2) for all functionals and represented in figure 3.2 and 3.3 (and table 3.2). We can make some remarks:

⁴ Their name, acronym and definition are summarized in table 3.1.

| | Unitarity | | | Low density | |
|-----|-------------------|-----------|----------|-------------|------------|
| | $\tilde{\zeta}_0$ | ζ_0 | ν_0 | γ_2 | γ_3 |
| | 0.376 | ~ 1 | ~ 1 | 0.186 | 0.127 |
| GEI | 0.24 | 1.48 | 0.95 | 0.19 | 0.11 |
| GLD | 0.44 | 0.87 | 0.82 | 0.23 | 0.14 |
| GPS | 0.32 | 1.29 | 1.47 | γ_2 | 0.10 |
| GUL | $\tilde{\zeta}_0$ | 1.10 | 1.17 | 0.20 | 0.11 |
| AEI | 0.51 | 1.89 | 1.47 | γ_2 | γ_3 |
| ALD | 0.46 | 0.79 | 0.67 | 0.23 | 0.14 |
| APS | 0.36 | 1.11 | 1.10 | γ_2 | 0.09 |
| AUL | $\tilde{\zeta}_0$ | 1.05 | 1.02 | 0.19 | 0.10 |

Table 3.2: Coefficients of the Taylor expansion around unitarity $\{\tilde{\zeta}_0, \zeta_0, \nu_0\}$ as defined in (3.2) and at low density $\{\gamma_2, \gamma_3\}$ as defined in (3.1) of the different functionals discussed in the text. Note the accepted/exact value of coefficient are: $\tilde{\zeta}_0 = 0.376(5)$, $\zeta_0 \sim \nu_0 \sim 1$, $\gamma_2 \simeq 0.186$ and $\gamma_3 \simeq 0.127$. Note also that we consider only the third order coming from the ladder diagram since the resummation do not consider ring diagrams associated to the additional contribution $\gamma'_3 \simeq (g-1)(g-3)0.095$.

1. The direct integration (GEI and AEI) leads to very different results [panels (a) and (b)] that are both far away from the expected result at unitarity.
2. Once an approximation scheme is chosen, geometric series or arctangent resummation lead to results very close to each other whatever the approximation.
3. The Large Dimension limit (respectively Phase-Space average) leads to an overestimation (respectively underestimation) of the energy.
4. In general, we see that all approximation schemes, not only simplify the functionals but also result in better reproduction of exact results compared to the AEI/GEI cases.
5. The GUL and AUL cannot be distinguished. The APS is also very close from the AUL. These three functionals reproduce very well the exact results for all $(a_s k_F)$.

Surprisingly, the APS functional reproduces at the same time the second order at low density and the coefficients $\{\tilde{\zeta}_0, \zeta_0, \nu_0\}$ of a unitary gas. This functional reproduces rather well the ground state energy from low density to unitary limits and we expect that the ground state thermodynamical properties are also in good agreement with the observations. Below, we make an extensive survey of the thermodynamical properties of dilute Fermi gas described by the use of the functionals introduced here.

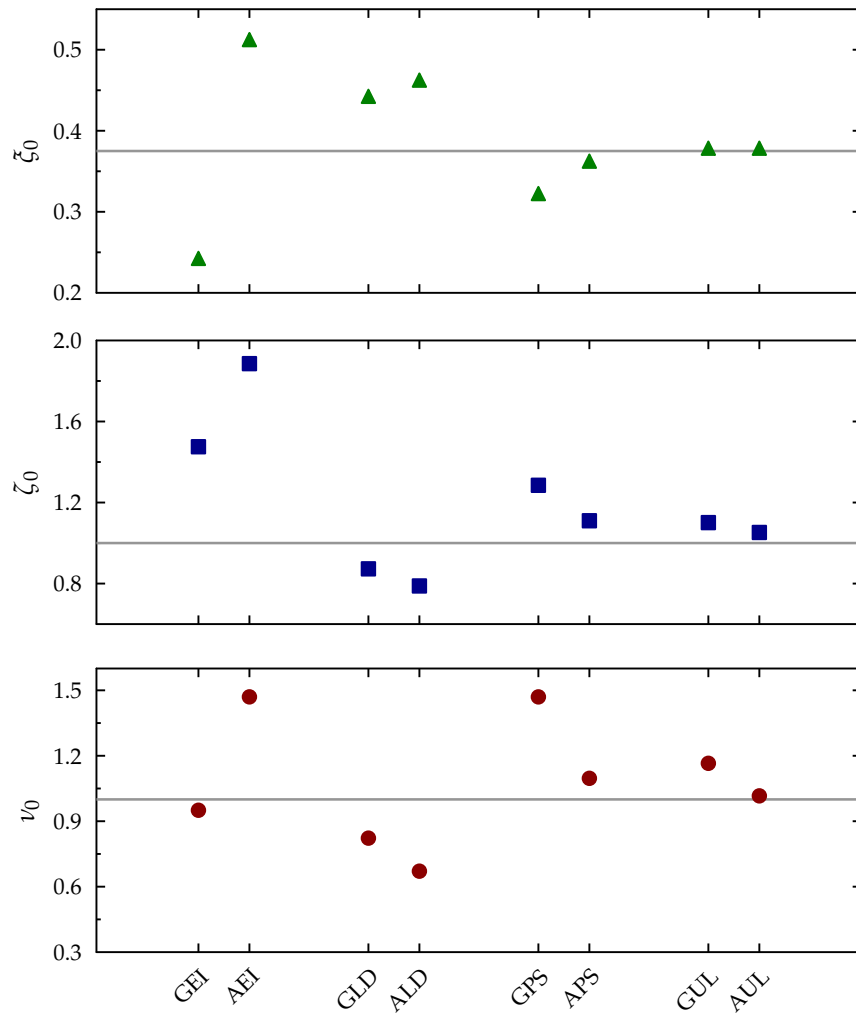


Figure 3.2: Coefficients of the Taylor expansion around unitarity $\{\xi_0, \zeta_0, \nu_0\}$ defined in (3.2) obtained for the different functionals and tabulated in table 3.2. The gray lines correspond to the accepted values: $\xi_0 = 0.376(4)$ and $\zeta_0 \sim \nu_0 \sim 1$ [77,243–245].

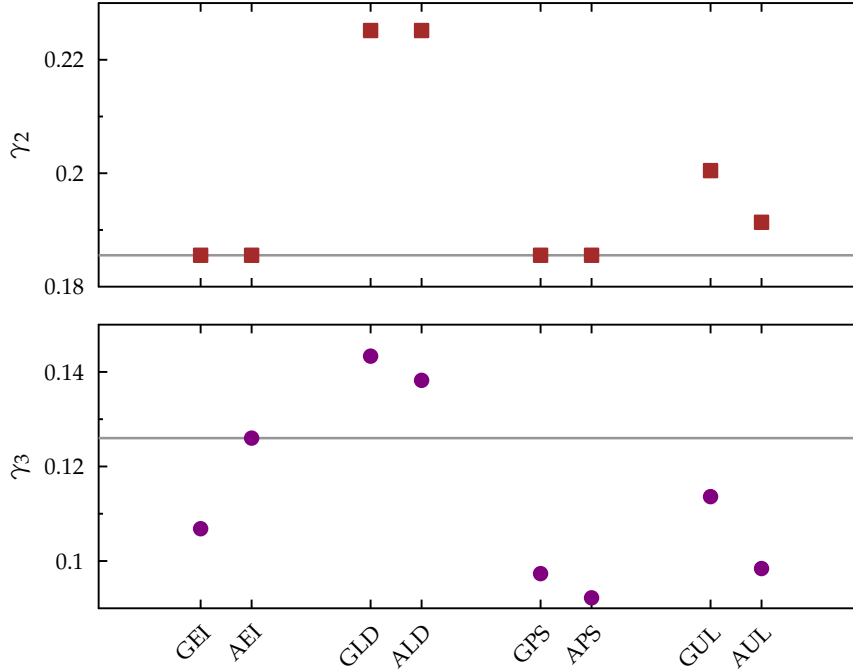


Figure 3.3: Coefficients of the Taylor expansion at low density (γ_2, γ_3) defined in (3.1) obtained for the different functionals and tabulated in table 3.2. The gray lines correspond to the exact values: $\gamma_2 \simeq 0.186$ and $\gamma_3 \simeq 0.127$.

3.2

DETERMINATION OF THE GROUND-STATE THERMODYNAMICAL PROPERTIES

In this section, we illustrate some applications of the GPS/APS and GUL/AUL functionals and calculate some thermodynamical quantities like the pressure P , the compressibility κ , the sound velocity c_s , the non-adiabatic index Γ and the chemical potential μ . These quantities are of interest because they have been extensively studied both experimentally and theoretically. Below, we first give generic expressions that will be useful in this section.

USEFUL EXPRESSION FOR THERMODYNAMICAL QUANTITIES

Starting from an EDF that depends on the density ρ , the different quantities of interest are given by the relationships listed below.

- The pressure is obtained from:

$$P = \rho^2 \left. \frac{\partial E/N}{\partial \rho} \right|_N. \quad (3.17a)$$

- The compressibility is given by:

$$\kappa = \frac{1}{\rho} \left(\left. \frac{\partial P}{\partial \rho} \right|_N \right)^{-1}, \quad (3.17b)$$

leading to:

$$\frac{1}{\rho\kappa} = \frac{2P}{\rho} + \rho^2 \left. \frac{\partial^2 E/N}{\partial \rho^2} \right|_N. \quad (3.17c)$$

- The chemical potential is defined as:

$$\begin{aligned} \mu &= \left. \frac{\partial E}{\partial N} \right|_V = \left. \frac{\partial \rho E/N}{\partial \rho} \right|_V, \\ &= \frac{E}{N} + \rho \left. \frac{\partial E/N}{\partial \rho} \right|_V = \frac{E}{N} + \frac{P}{\rho}. \end{aligned} \quad (3.17d)$$

- The sound velocity $c_s = (m\rho\kappa)^{-1/2}$ and the non-adiabatic index Γ are defined from previous quantities using (note that here, c_s is already in units of the speed of light c):

$$\Gamma = \left. \frac{\rho}{P} \frac{\partial P}{\partial \rho} \right|_N = \frac{1}{\kappa P} = \frac{5}{3} \frac{\kappa_{FG} P_{FG}}{\kappa P}. \quad (3.17e)$$

USEFUL EQUATIONS AND GENERIC FUNCTIONAL

In the following, we will normalize these thermodynamical quantities to their corresponding values for the free Fermi gas denoted by the subscript FG ; we have:

$$\begin{aligned} P_{FG} &\equiv \frac{2}{3} \rho \mathcal{E}_{FG}, & \frac{1}{\kappa_{FG}} &\equiv \frac{10}{9} \rho \mathcal{E}_{FG}, & c_{FG}^2 &\equiv \frac{10}{9m} \mathcal{E}_{FG}, \\ \text{and } \mu_{FG} &\equiv \frac{5}{3} \mathcal{E}_{FG} = \frac{k_F^2}{2m}, \end{aligned} \quad (3.18)$$

where $\mathcal{E}_{FG} = E_{FG}/N$. These quantities are equal to the values that would be obtained if we imposed $a_s = 0$ in the functionals.

Note that in general, the functionals are given in terms of k_F and not ρ and it might be useful to express the thermodynamical quantities directly as partial derivatives with respect to k_F . Assuming a generic functional written as:

$$\frac{E}{E_{FG}} \equiv \zeta(k_F), \quad (3.19)$$

we can obtain the following expressions for our different quantities⁵

$$\left\{ \begin{array}{l} \frac{P}{P_{FG}} = \zeta + \frac{k_F}{2} \frac{\partial \zeta}{\partial k_F}, \\ \frac{\mu}{\mu_{FG}} = \zeta + \frac{k_F}{5} \frac{\partial \zeta}{\partial k_F}, \\ \frac{\kappa_{FG}}{\kappa} = \zeta + \frac{4k_F}{5} \frac{\partial \zeta}{\partial k_F} + \frac{k_F^2}{10} \frac{\partial^2 \zeta}{\partial k_F^2}. \end{array} \right. \quad (3.20)$$

⁵ We can use the relation between the density and the Fermi momentum $3\pi^2\rho = k_F^3$ to write:

$$\frac{\partial}{\partial \rho} = \frac{dk_F}{d\rho} \frac{\partial}{\partial k_F} = \frac{\pi^2}{k_F^2} \frac{\partial}{\partial k_F}$$

All these relations, and the results obtained using the limiting situations (3.1) and (3.2), are summarized in table 3.3.

SURVEY ON THERMODYNAMICAL PROPERTIES OF ULTRACOLD ATOMIC FERMI GAS

Thermodynamical quantities obtained using the APS/GPS (respectively AUL/GUL) functionals are compared in figure 3.4 (respectively in figure 3.5) with various experimental observations and/or theoretical estimates. Not surprisingly, the AUL/GUL functionals (since they have explicitly been adjusted to reproduce the Bertsch parameter ξ_0) as well as the APS functional reproduce the unitary limit. We see that, despite their simplicity and the fact that the AUL/GUL functionals only depend on ξ_0 , they are able to reproduce rather well the thermodynamics of a Fermi gas away from unitarity. It should be noted that none of the Taylor expansions in $(a_s k_F)$ or $(a_s k_F)^{-1}$ would be able to reproduce these quantities from very low to very high densities, as illustrated in figure 3.6 for the pressure. A similar behavior is obtained for the other quantities shown in figures 3.4 and 3.5.

In [76], the study of the Tan's contact parameter C defined by the adiabatic relation [254–256]:

$$\frac{dE}{da_s^{-1}} = -\frac{C}{4\pi m} \quad (3.21)$$

was made using the GPS/GUL functional. This is a central property of the system that has been extensively studied experimentally and theoretically (see for instance [67]). The contact parameters obtained with the GPS and GUL functionals are shown as a function of $(a_s k_F)^{-1}$ in figure 3.7. The contact C deduced from the new functional is in good agreement with experimental data and within the errorbars of theoretical calculations. It is interesting to note that the GPS and GUL results are very close from each other. In particular, different curves cannot be distinguished in the perturbative regime for $(a_s k_F)^{-1} < -1$. However, at strict unitarity, the contact is simply given by:

$$\frac{C(a_s k_F \rightarrow \infty)}{Nk_F} = \frac{27\pi^2}{25}(1 - \xi_0)^2 \quad (3.22)$$

and differences are noticeable around unitarity due to the difference of predicted Bertsch parameter by the GPS and GUL functionals (see table 3.2).

CONCLUSION ON THE GROUND STATE PROPERTIES OF DILUTE FERMI GAS

The extensive study of the functionals made above shows that the ground-state energy, as well as the ground-state thermodynamical properties, obtained from the APS and AUL/GUL functionals, reproduce rather well *ab initio* results and/or experimental observations from the low-density to the unitary limits.

Such functionals can however only be applied to systems where other LECs besides a_s have no effects. This is unfortunately not the case in nuclear physics where the s -wave effective range, r_s , and the p -wave scattering volume, a_p^3 , can play a role, although there exist a hierarchy $|a_s| \gg |r_s| \gg |a_p|$ (see tables 1.1 and 1.2). As a first step towards non-empirical DFT for neutron matter, we explored the possibility to include effective-range effects in the functionals.

| X/X_{FG} | E/E_{FG} | $\mu/\mu_{FG} = \mu \left(\frac{5}{3} \mathcal{E}_{FG} \right)^{-1}$ | $\kappa_{FG}/\kappa = \frac{1}{\kappa} \left(\frac{10}{9} \rho \mathcal{E}_{FG} \right)^{-1}$ | $P/P_{FG} = P \left(\frac{2}{3} \rho \mathcal{E}_{FG} \right)^{-1}$ |
|---|--|---|--|--|
| Definition | $\frac{E}{N}$ | $\frac{E}{N} + \rho \frac{\partial E/N}{\partial \rho} \Big _N$ | $2\rho^2 \frac{\partial E/N}{\partial \rho} \Big _N + \rho^3 \frac{\partial^2 E/N}{\partial \rho^2} \Big _N$ | $\rho^2 \frac{\partial E/N}{\partial \rho} \Big _N$ |
| As function of ξ | ξ | $\xi + \frac{k_F}{5} \frac{\partial \xi}{\partial k_F}$ | $\xi + \frac{4}{5} k_F \frac{\partial \xi}{\partial k_F} + \frac{k_F^2}{10} \frac{\partial^2 \xi}{\partial k_F^2}$ | $\xi + \frac{k_F}{2} \frac{\partial \xi}{\partial k_F}$ |
| Low density $(a_s k_F, r_e k_F) \rightarrow (0, 0)$ | $1 + \frac{10}{9\pi} (a_s k_F) + \frac{1}{6\pi} (r_e k_F) (a_s k_F)^2$ | $1 + \frac{4}{3\pi} (a_s k_F) + \frac{4}{15\pi} (r_e k_F) (a_s k_F)^2$ | $1 + \frac{2}{\pi} (a_s k_F) + \frac{2}{3\pi} (r_e k_F) (a_s k_F)^2$ | $1 + \frac{5}{3\pi} (a_s k_F) + \frac{5}{12\pi} (r_e k_F) (a_s k_F)^2$ |
| Unitary limits $-(a_s k_F)^{-1} \rightarrow 0$ $r_e k_F = 0$ | $\xi_0 - (a_s k_F)^{-1} \xi_0 - \frac{5}{3} (a_s k_F)^{-2} \nu_0$ | $\xi_0 - \frac{4\xi_0}{5} (a_s k_F)^{-1} - (a_s k_F)^{-2} \nu_0$ | $\xi_0 - \frac{2\xi_0}{5} (a_s k_F)^{-1} + \frac{2\nu_0}{3} (a_s k_F)^{-2}$ | $\xi_0 - \frac{\xi_0}{2} (a_s k_F)^{-1}$ |
| Unitary limits $-(a_s k_F)^{-1} = 0$ $r_e k_F \rightarrow 0$ | $\xi_0 + (r_e k_F) \eta_e + (r_e k_F)^2 \delta_e$ | $\xi_0 + \frac{6}{5} (r_e k_F) \eta_e + \frac{7}{5} (r_e k_F)^2 \delta_e$ | $\xi_0 + \frac{9}{5} (r_e k_F) \eta_e + \frac{14}{5} (r_e k_F)^2 \delta_e$ | $\xi_0 + \frac{3}{2} (r_e k_F) \eta_e + 2 (r_e k_F)^2 \delta_e$ |

Table 3.3: Summary of the different thermodynamical quantities obtained in different limiting situations.

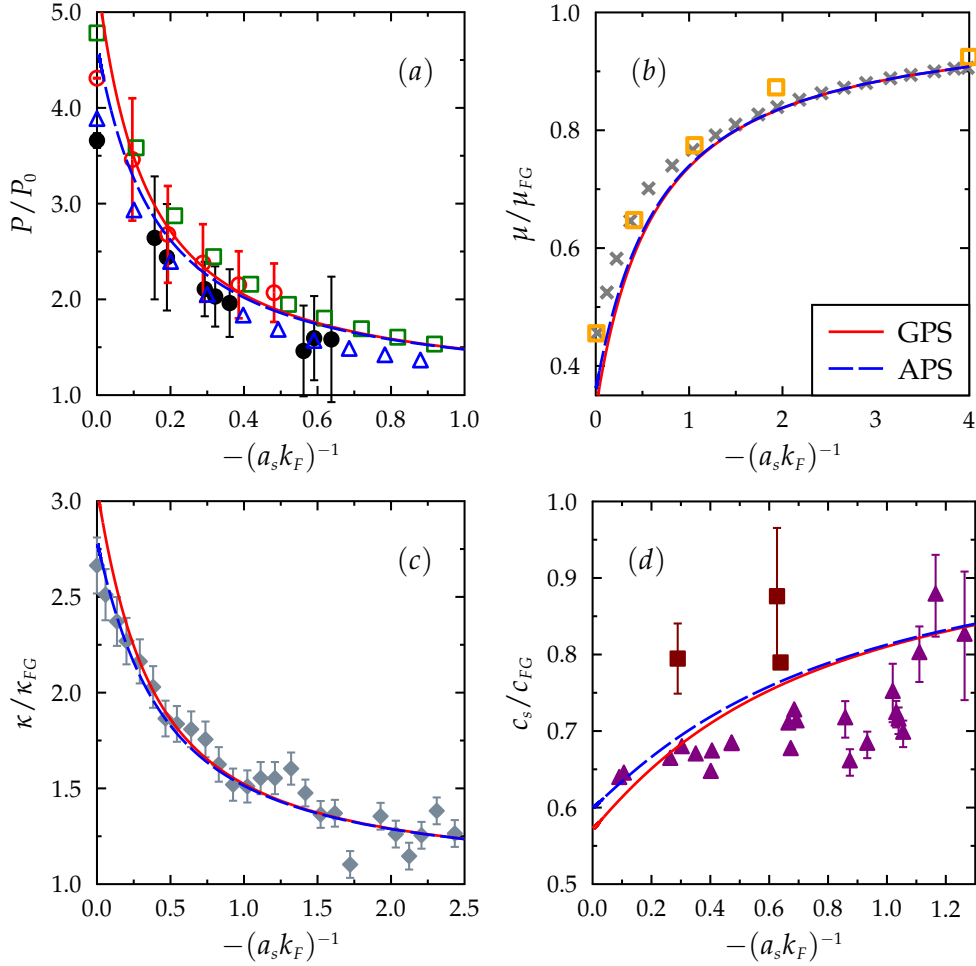


Figure 3.4: The pressure (a) [normalized by $P_0 = 2 (2m)^{3/2} \mu^{5/2} / (15\pi^2)$], the inverse of the compressibility (b), the chemical potential (c) and the sound velocity (d) as a function of $-(a_s k_F)^{-1}$ obtained from the GPS (red solid line) and APS (blue dashed line) functionals. For comparison, different experimental data are shown: black circles from [70], brown squares from [249], purple triangles from [250] and gray diamonds from [251]. The open dots are the results from different many-body theories: a quantum Monte-Carlo calculation (red open circles [78]), a Nozière-Schmitt-Rink approximation (blue open triangles [252]), results obtained with a Green's functions method [De Dominicis Martin formalism] (green open squares [83]), calculation from [253] [t-matrix-II] (open orange squares) and the gray dotted line is calculated from the best fit to the QMC energy [245] (data from figure 3 of [252]).

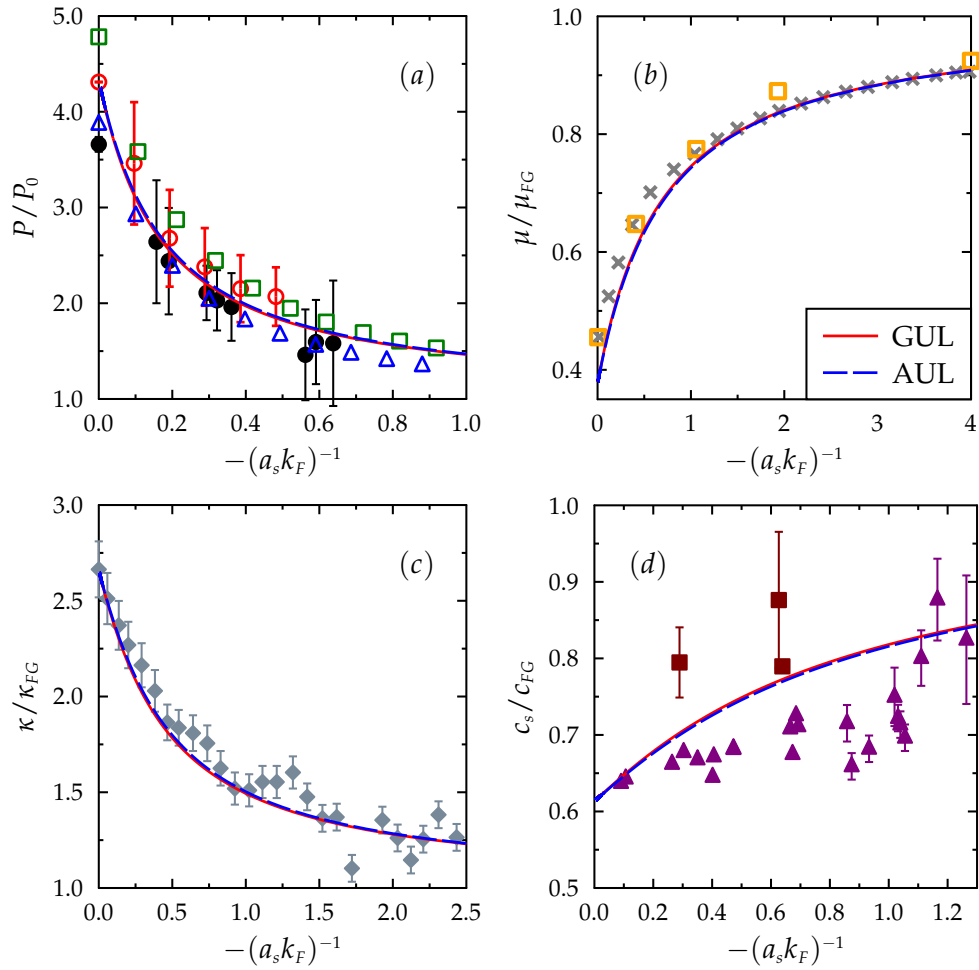


Figure 3.5: Same as figure 3.4 for the GUL functional (red solid line) and AUL (blue dashed line) functionals.

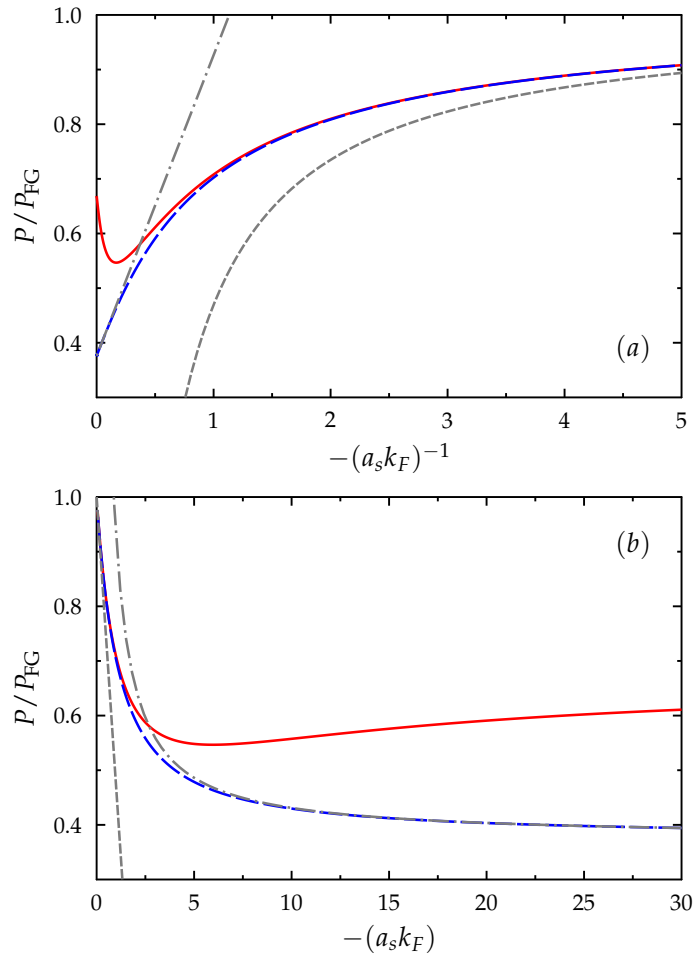


Figure 3.6: Pressure as a function of $-(a_s k_F)^{-1}$ (a) or as a function of $-(a_s k_F)$ (b) obtained from the GUL functional (blue dashed line). For comparison, the gray short dashed and gray short dot-dashed lines correspond to the Taylor expansion to first order in $(a_s k_F)$ or to first order in $(a_s k_F)^{-1}$ respectively. The red solid line corresponds to the neutron matter case using the $gGUL_2$ functional assuming $r_s = 2.716$ fm and $a_s = -18.9$ fm so that $-(a_s k_F) = 10, 20$ and 30 correspond respectively to $\rho = 0.005, 0.040$ and 0.135 fm $^{-3}$.

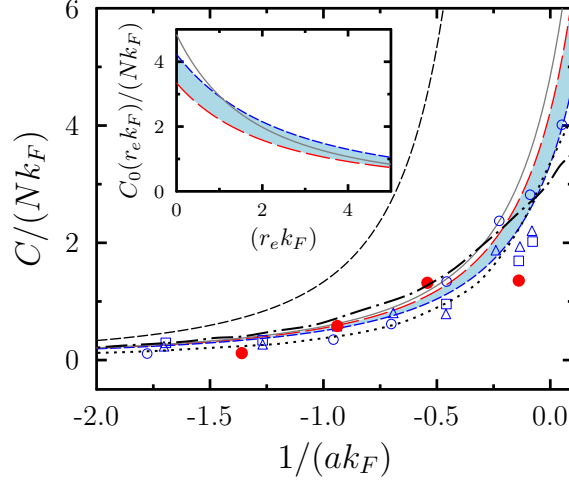


Figure 3.7: Contact parameter as a function of $(a_s k_F)^{-1}$. The light blue area is the region between the two GUL functional results obtained either with $\zeta_0 = 0.37$ and $\zeta_0 = 0.44$. The gray solid line corresponds to the contact parameter obtained using the GPS functional. The black dashed line is the BCS result given by $4(a_s k_F)^2/3$. The black dotted and dot-dashed lines are the theoretical results of [257] and [73] respectively. The blue open circles, triangles and squares are the moment, PES and rf measurements of [258]. The red filled circles is the measure of [259]. With the same conventions for the lines, the inset correspond to the effective range dependance of the contact parameter at stric unitarity (notted C_0) as a function of $r_s k_F$ obtained using the gGUL/gGPS functionals. Figure taken from [76].

3.3

GENERALIZATION OF THE DFT INCLUDING EFFECTIVE RANGE

In this section, we discuss the generalization of the functionals including effective-range effects based on MPBT resummation in the EFT framework for dilute Fermi gases introduced in the previous section. The description of Fermi gases with non-zero effective range and unnatural large a_s is largely motivated by the fact that neutron systems enter into such a class of interacting fermions.

3.3.A Inclusion of the effective range

In [239], the author has generalized the GEI (3.6) and the AEI (3.13) functionals by including the effective range. These generalized functionals will be call gGEI and gAEI respectively (for *generalized GEI* and *generalized AEI*) in the following.

In this section we consider a two-body s -wave contact (low-momentum) interaction including an effective-range term C_2 [see (1.6)]:

$$V(\mathbf{k}, \mathbf{k}') = C_0 + \frac{C_2}{2} [\mathbf{k}'^2 + \mathbf{k}^2], \quad (3.23)$$

where the coupling constants are related to the s -wave scattering length a_s and the effective range r_s though (1.7). Then, we can construct the resummed effective interaction and energy as illustrated in chapter 2 for a simplified interaction includ-

ing now the effective range. Here we present the results obtained in [239] without going into technical details and discussing only the key points.

When the effective range is included, the resummed energy still has the same structure as in (2.55) and can be written again as an integral over the accessible phase-space (s, t) :

$$\frac{E}{E_{FG}} = 1 + (g - 1) \int_0^1 s^2 ds \int_0^{\sqrt{1-s^2}} t dt \mathcal{E}(s, t; a_s k_F, r_s k_F), \quad (3.24a)$$

with respectively:

$$[\text{gGEI}] \mapsto \mathcal{E}(s, t; a_s k_F, r_s k_F) = \frac{80}{\pi} \frac{(a_s k_F) \pi I_*(s, t)}{\pi \psi^{-1} - (a_s k_F) F(s, t)}, \quad (3.24b)$$

$$[\text{gAEI}] \mapsto \mathcal{E}(s, t; a_s k_F, r_s k_F) = \frac{80}{\pi} \arctan \left[\frac{(a_s k_F) \pi I_*(s, t)}{\pi \phi^{-1} - (a_s k_F) R(s, t)} \right]. \quad (3.24c)$$

The difference compared to (2.55) is the appearance of the functions ψ and ϕ that account for the effective range. The dependence of these two functions, given by (D.1b) and (D.2b) in appendix D, are highly non-trivial in terms of $(a_s k_F, r_s k_F)$ and in terms of the center-of-mass and relative dimensionless momenta (s, t) . The expressions (3.24) present several interesting features compared to a perturbative expansion (2.28). Firstly, they could be expanded in powers of $(a_s k_F)$ and, noteworthy, their second order contributions in $(a_s k_F)$ match, in both cases, the generalized Lee-Yang formula (2.28). Note that, similarly to the AEI case, the gAEI functional is slightly more predictive than gGEI in the sense that it is valid up to third order in $(a_s k_F)$.

In the limit $r_s \rightarrow 0$, the two functions ψ and ϕ go to 1 so that we recover the AEI and GEI functionals. However, we also observe the non-commutativity of the limits $|a_s| \rightarrow \infty$ and $r_s \rightarrow 0$, i.e. :

$$\lim_{|a_s| \rightarrow \infty} \left\{ \lim_{r_s \rightarrow 0} \mathcal{E} \right\} \neq \lim_{r_s \rightarrow 0} \left\{ \lim_{|a_s| \rightarrow \infty} \mathcal{E} \right\}. \quad (3.25)$$

This is due to the specific structure of the functions ψ and ϕ . In particular, the Bertsch parameter defined by (2.56) in the case $r_s \neq 0$ is independent of the value of the effective range and we find:

$$\begin{aligned} \zeta_{gAEI}(r_s = 0) &= \zeta_{AEI} = 0.51, & \zeta_{gAEI}(r_s \neq 0) &= 0.88, \\ \zeta_{gGEI}(r_s = 0) &= \zeta_{GEI} = 0.24, & \zeta_{gGEI}(r_s \neq 0) &= 0.43. \end{aligned}$$

The Bertsch parameter value $\zeta_0(r_s \neq 0)$ is independent of r_s whatever small is the value of r_s leading to a sharp transition from $r_s = 0$ to $r_s \neq 0$. This is in contradiction with the *ab initio* predictions [79,81]. We then conclude that the direct integration of (3.24) is bound to fail at large $(a_s k_F)$.

We now explore the possibility to use (3.24) as a starting point to obtain a well behaved evolution of the energy as function of the effective range.

3.3.B Effective range approximation

GENERALIZED APS/GPS FUNCTIONALS

As just mentioned, the sharp transition of ξ_0 when going from $r_s \neq 0$ to $r_s = 0$ is in contradiction with the observation [79,81]. To obtain an effective-range dependence, one possibility is to start from (3.24) and make the so-called *Effective Range Approximation* (ERA) [237,260]: we treat the effective range in perturbation keeping all orders in $(a_s k_F)$. As a matter of fact, we follow the prescription proposed in [260] considering the leading order in $(r_s k_F)$ of the functions ϕ and ψ as suggested by the effective range expansion in free space. First, we rewrite the gAEI and gGEI functionals by replacing the functions ϕ and ψ by their effective-range expansion:

$$\phi^{-1} \rightarrow \phi_{ERA}^{-1} = 1 - \frac{a_s r_s}{2} k_F^2 t^2 \quad \text{and} \quad \psi^{-1} \rightarrow \psi_{ERA}^{-1} = 1 - \frac{a_s r_s}{2} k_F^2 t^2, \quad (3.26)$$

where ϕ_{ERA}^{-1} and ψ_{ERA}^{-1} denote the effective range expansions, i.e. the leading order in $(r_s k_F)$, of the original functions ϕ^{-1} and ψ^{-1} respectively. Note that, at leading order, these two functions are identical.

Then, the strategy is the same as discussed in section 3.1.a: once the functions ϕ and ψ in (3.24) are replaced by their ERA, a phase-space approximation is made in the numerator and in the denominator leading to:

$$\frac{E}{E_{FG}} = 1 + \frac{16}{3\pi} \arctan \left[\frac{(a_s k_F) B_*}{1 - (a_s k_F) [B_{LY} + (r_s k_F) B_{t^2}]} \right]. \quad (3.27)$$

This DFT is called gAPS hereafter. Similarly we define the gGPS functional as:

$$\frac{E}{E_{FG}} = 1 + \frac{16}{3\pi} \frac{(a_s k_F) B_*}{1 - (a_s k_F) [B_{LY} + (r_s k_F) B_{t^2}]}. \quad (3.28)$$

To shorten the equations, we have introduced the following notations (using the notations introduced in (3.7) and integrals given in appendix E):

$$B_{LY} = \frac{6}{35\pi} (11 - 2 \ln 2) = \frac{1}{\pi} \frac{\langle\langle I_* R \rangle\rangle}{\langle\langle I_* \rangle\rangle} = \frac{1}{\pi} \frac{\langle\langle I_* F \rangle\rangle}{\langle\langle I_* \rangle\rangle},$$

$$B_* = \frac{5}{24} = \frac{\langle\langle I_* \rangle\rangle}{\langle\langle 1 \rangle\rangle}, \quad \text{and} \quad B_{t^2} = \frac{3}{20} = \frac{1}{2} \frac{\langle\langle I_* t^2 \rangle\rangle}{\langle\langle I_* \rangle\rangle}.$$

Note that the Taylor expansion of the above functionals (gAPS/gGPS) up to second order in $(a_s k_F)$ and first order in $(r_s k_F)$ matches the generalized Lee-Yang expansion including effective range (2.28).

The GPS and APS functionals are recovered simply by setting r_s to zero in the gGPS and gAPS expressions. Therefore, at unitarity we recover in that case the same Bertsch parameter, i.e. :

$$\xi_{gAPS} = \xi_{APS} = 0.36 \quad \text{and} \quad \xi_{gGPS} = \xi_{GPS} = 0.24.$$

For $r_s \neq 0$, one can obtain a generalization of the Bertsch parameter with explicit effective range dependence. For $|a_s k_F| \rightarrow \infty$, we obtain respectively:

$$\frac{E}{E_{FG}} = 1 - \frac{16}{3\pi} \arctan \left[\frac{B_*}{B_{LY} + (r_s k_F) B_{t^2}} \right] \equiv \tilde{\zeta}_{gAPS}(r_s k_F), \quad (3.29a)$$

and

$$\frac{E}{E_{FG}} = 1 - \frac{16}{3\pi} \frac{B_*}{B_{LY} + (r_s k_F) B_{t^2}} \equiv \tilde{\zeta}_{gGPS}(r_s k_F). \quad (3.29b)$$

For small values of r_s , the effective range dependence of $\tilde{\zeta}$ has been studied in [79,81] leading to:

$$\tilde{\zeta}(r_s k_F) = \tilde{\zeta}_0 + (r_s k_F) \eta_e + \mathcal{O}(r_s k_F)^2. \quad (3.30)$$

Although η_e was found to depend slightly on the two-body potential, an average value $\eta_e \simeq 0.127$ has been obtained [79,81]. Using (3.29), we obtain $\eta_{gAPS} = 0.17$ and $\eta_{gGPS} = 0.19$ which differ from the *ab initio* results. To improve these results we also introduce below functionals generalizing the AUL and GUL functionals by including an effective-range dependence that directly reproduces the unitary limit parameters (3.30).

GENERALIZED AUL/GUL FUNCTIONALS

Inspired by the section 3.1, we now propose to constrain the parameters directly on the unitary limit keeping the same parametrization as for the gAPS functional introduced in the ERA. The low-density constants B_* , B_{LY} and B_{t^2} appearing in the gAPS functional are now considered as adjustable parameters, noted respectively \mathcal{A}_0 , \mathcal{A}_1 and \mathcal{A}_2 , and chosen to reproduce the effective-range expansion (3.30) at low-density and unitary limits [76]. This constraint generates the gAUL functional:

$$\frac{E}{E_{FG}} = 1 + \frac{16}{3\pi} \arctan \left[\frac{(a_s k_F) \mathcal{A}_0}{1 - (a_s k_F) [\mathcal{A}_1 + (r_s k_F) \mathcal{A}_2]} \right], \quad (3.31a)$$

leading at strict unitarity to:

$$\tilde{\zeta}_{gAUL}(r_s k_F) = 1 - \frac{16}{3\pi} \arctan \left[\frac{\mathcal{A}_0}{\mathcal{A}_1 + (r_s k_F) \mathcal{A}_2} \right]. \quad (3.31b)$$

Then, the parameters $\{\mathcal{A}_i\}$ are chosen by:

1. making the Taylor expansion in $(r_s k_F)$ of (3.31b) and imposing the constraint (3.30),
2. conserving the low-density expansion given by (2.28) up to first order in $(a_s k_F)$ of (3.31a).

This gives three independent equalities that uniquely determine the three parameters $\{\mathcal{A}_i\}$ as functions of $\tilde{\zeta}_0$ and η_e :

$$\mathcal{A}_0 = \frac{5}{24}, \quad \mathcal{A}_1 = \frac{5}{24} \mathcal{T}_{\tilde{\zeta}_0}^{-1} \quad \text{and} \quad \mathcal{A}_2 = \frac{5}{24} \frac{3\pi}{16} \eta_e \left[1 + \mathcal{T}_{\tilde{\zeta}_0}^{-2} \right], \quad (3.31c)$$

where we have defined:

$$\mathcal{T}_{\xi_0} = \tan \left[\frac{3\pi}{16} (1 - \xi_0) \right]. \quad (3.31d)$$

Similarly, starting from the gGPS functional, we introduce the gGUL functional given by:

$$\frac{E}{E_{FG}} = 1 + \frac{(a_s k_F) A_0}{1 - (a_s k_F) [A_1 + (r_s k_F) A_2]} \quad (3.32a)$$

leading at strict unitarity to:

$$\xi_{gGUL}(r_s k_F) = 1 - \frac{A_0}{A_1 + (r_s k_F) A_2}, \quad (3.32b)$$

with:

$$A_0 = \frac{10}{9\pi}, \quad A_1 = \frac{10}{9\pi} (1 - \xi_0)^{-1} \quad \text{and} \quad A_2 = \frac{10}{9\pi} \frac{\eta_e}{(1 - \xi_0)^2}. \quad (3.32c)$$

3.3.c Discussion and comparison

The effective-range energy dependence at unitarity for each functional is shown in figure 3.8 and compared to other calculations. We remark two things:

1. The gAUL and gGUL functionals lead to indistinguishable results as well as the gAPS and gGPS functionals in the limit of large effective range. As for the functionals introduced above without effective range (AUL/GUL functionals), the approximation consisting in imposing the unitary limit leads to equivalent functionals independently of the fact that we consider the geometric series resummation or the arctangent resummation.
2. The gAPS, gAUL, and gGUL functionals are relatively close to each other and in good agreement with the prediction [79,81,260]. The gGPS functional suffers from the fact that the Bertsch parameter is already rather different from its accepted value at $r_s = 0$.

GENERALIZED AUL/GUL FUNCTIONALS WITH RELAXED CONSTRAINTS

Following the strategy proposed in [130], we rewrite the gAUL functionals as⁶:

$$\frac{E}{E_{FG}} = 1 + \frac{16}{3\pi} \arctan \left[\frac{\mathcal{U}_0}{1 - (a_s k_F)^{-1} \mathcal{U}_1} + \frac{(r_s k_F) \mathcal{R}_0 [1 - (a_s k_F)^{-1} \mathcal{R}_1]^{-1}}{1 - (a_s k_F)^{-1} \mathcal{R}_1 + (r_s k_F) \mathcal{R}_2} \right]. \quad (3.33a)$$

These parameters are *a priori* linked to the original $\{\mathcal{A}_i\}$ coefficients entering in (3.31b). Here we assume directly that the $\{\mathcal{U}_i, \mathcal{R}_i\}$ are adjustable parameters. Five

⁶ We can show that functional (3.31) and (3.33a) are equivalent with the relationships: $\mathcal{U}_1 = \mathcal{R}_1$ and $\mathcal{R}_0 = -\mathcal{U}_0 \mathcal{R}_2$.

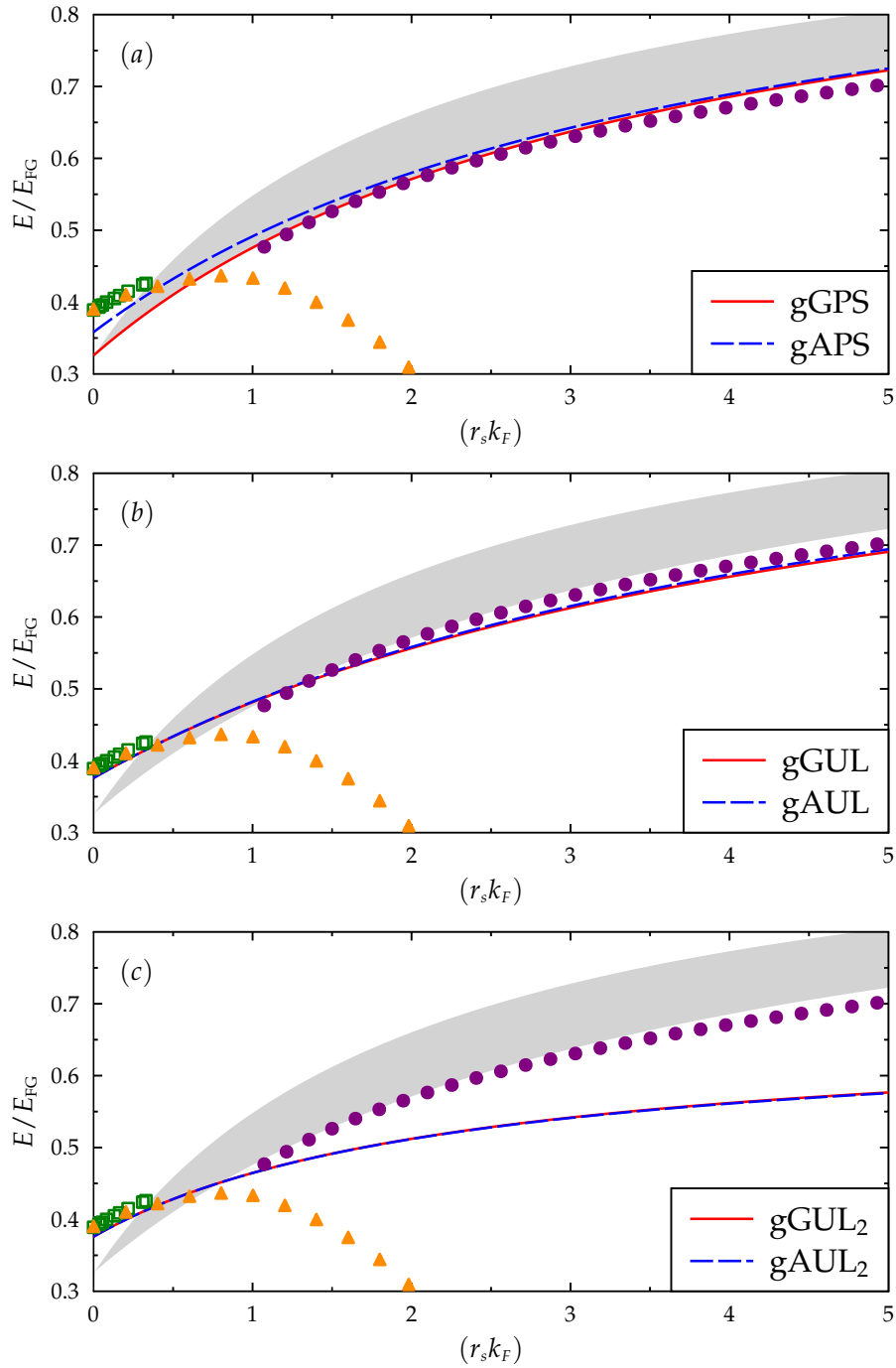


Figure 3.8: Energy as function of $(r_s k_F)$ at strict unitarity obtained with the gAPS/gGPS (a), gAUL/gGUL (b) and gAUL₂/gGUL₂ functionals (blue dashed line / red solid line). The results are compared with the ones of [260] (purple points) and with the low-density results of [79,81] (green open squares). Note that in [260], results are given for the Hartree-Fock energy only. The orange triangles correspond to QMC results (equivalent to use a Poschl-Teller potential) [261]. The gray area corresponds to the results given in [237] and reflects the renormalization scale dependence in EFT calculations.

independent relations are needed to fix their values. For this, we impose that the second-order expansion in the effective range at strict unitarity:

$$\zeta(r_s k_F) = \zeta_0 + (r_s k_F)\eta_e + (r_s k_F)^2 \delta_e + \mathcal{O}(r_s k_F)^3,$$

is reproduced as well as the leading order in $(a_s k_F)$ and in $(a_s k_F)^2 (r_s k_F)$ of the generalized Lee-Yang formula (2.28). This gives five independent relations that fix the parameters to:

$$\begin{aligned} \mathcal{U}_0 &= -\mathcal{T}_{\zeta_0}, \quad \mathcal{U}_1 = \frac{24}{5}\mathcal{T}_{\zeta_0}, \quad \mathcal{R}_0 = \frac{3\pi}{16}\eta_e \left[1 + \mathcal{T}_{\zeta_0}^2\right], \\ \mathcal{R}_1 &= \sqrt{6\pi\eta_e \left[1 + \mathcal{T}_{\zeta_0}^2\right]} \quad \text{and} \quad \mathcal{R}_2 = -\frac{\delta_e}{\eta_e} + \frac{3\pi}{16}\eta_e \mathcal{T}_{\zeta_0}, \end{aligned} \quad (3.33b)$$

where \mathcal{T}_{ζ_0} is given by (3.31d). This parametrization is called gAUL₂.

Similarly, starting from the gGUL functional, we call this functional the gGUL₂ [130]:

$$\frac{E}{E_{FG}} = 1 + \frac{U_0}{1 - (a_s k_F)^{-1} U_1} + \frac{(r_s k_F) R_0 [1 - (a_s k_F)^{-1} R_1]^{-1}}{1 - (a_s k_F)^{-1} R_1 + (r_s k_F) R_2}, \quad (3.34a)$$

with:

$$\begin{aligned} U_0 &= -(1 - \zeta_0), \quad U_1 = \frac{9\pi}{10}(1 - \zeta_0), \quad R_0 = \eta_e, \\ R_1 &= \sqrt{6\pi\eta_e} \quad \text{and} \quad R_2 = -\frac{\delta_e}{\eta_e}. \end{aligned} \quad (3.34b)$$

In practice, the different coefficients are obtained using the values: $\zeta_0 = 0.376$, $\eta_e = 0.127$, and $\delta_e = -0.055$ [81].

The effective-range dependence of the energy at unitarity for the gAUL₂ and gGUL₂ functionals are shown in figure 3.8. We remark that:

1. The gAUL₂ and gGUL₂ functionals with relaxed constraints have indistinguishable effective-range dependence at unitarity.
2. The gAUL₂ and gGUL₂ functionals give energy lower than the original gAUL or gGUL functionals and much closer to the recent *ab initio* results of [261] although they deviate from these results rather rapidly. This could explain why the functionals with relaxed constraints improve slightly the description of neutron matter compared to the original gAUL/gGUL functional (see figure 3.9).

In figure 3.9, we show the EOS of neutron matter ($r_s = 2.7$ fm) energy in the *s*-wave channel predicted by each functional proposed in the present work. We compare with the cold atoms case ($r_s = 0$) to illustrate the effective-range effect. In the left panels, we see that the functionals reproduce very well the low-density regime both for the neutron and cold atom matter. For neutron matter it is interesting that the functionals predict the EOS much beyond the perturbative regime. Indeed $|a_s k_F| < 12$ correspond to $\rho = 0.01 \text{ fm}^{-3} \gg 10^{-6} \text{ fm}^{-3}$. This is already quite remarkable. We also note that the effective-range effects fully explain the difference between cold atoms and nuclear systems.

Let us now focus more on the difference between different functionals. We see that the gAPS/gGPS and gAUL/gGUL are quite similar at low density and only start to differ from each other around $|a_s k_F| \sim 7$. The gAUL₂/gGUL₂ functionals with relaxed constraints slightly improve the agreement with QMC results [72]. Actually, at unitarity (see figure 3.8), the gAUL₂/gGUL₂ functionals give lower energies for large ($r_s k_F$) compared to other functionals as suggested by the QMC calculation showed in figure 3.9 (left) as well as the many-body calculation [filled black squares in figure 3.9 (right)]. This seems to be an indirect evidence that the unitary gas constraint help to understand the neutron matter EOS for intermediate density regime $10^{-6} \text{ fm}^{-3} < \rho < 10^{-1} \text{ fm}^{-3}$. Below, we illustrate further how these functionals can be used to describe the thermodynamical properties of strongly correlated Fermi systems, as neutron matter, and see the impact of the effective range effect.

THERMODYNAMICAL PROPERTIES WITH EFFECTIVE RANGE EFFECT

Unitary gases with effective range have been rarely discussed in atomic physics. Below we show how thermodynamical properties are affected by the effective range. Most often, no experimental data exist. Then, the results we obtain can be seen as predictions.

In figure 3.6, we show an example of the evolution of thermodynamical quantities for a non-zero effective range. In the present functional, the effect of r_s is mainly visible at large ($a_s k_F$) values, i.e. close to unitarity. To illustrate the dependence with r_s , we consider the strict unitary limit of the gGUL₂ functional. In that case, the ξ function depends only on ($r_s k_F$) and we deduce:

$$\tilde{\xi}(r_s k_F) = \xi_0 + \frac{\eta_e^2(r_s k_F)}{\eta_e - \delta_e(r_s k_F)}, \quad (3.35)$$

from which all thermodynamical quantities can be calculated (see table 3.3 for instance). The effective-range effect is predicted to increase the apparent Bertsch parameter leading also to an increase of the thermodynamical quantities at unitarity. This is illustrated in figure 3.10 for the pressure, the chemical potential, and the inverse of the compressibility. We see in particular that the maximum value of ξ at unitarity is $\xi_0 - \eta_e^2/\delta_e = 0.66$ which is almost twice the value of ξ_0 and therefore might be significant.

We have extended the above study to the case of neutron matter for which we anticipate an important influence of the effective range r_s as well as, possibly, of higher-order channels contributions when the density increases. The different thermodynamical quantities obtained using the gGUL₂ functional with realistic values of the low-energy constants a_s and r_s are shown in figure 3.11. While at very low density the different quantities are only slightly affected by effective range, we indeed observe at densities of interest in the nuclear context, i.e. $\rho \simeq 0.05 - 0.15 \text{ fm}^{-3}$, differences with the cold atom case ($r_s = 0$).

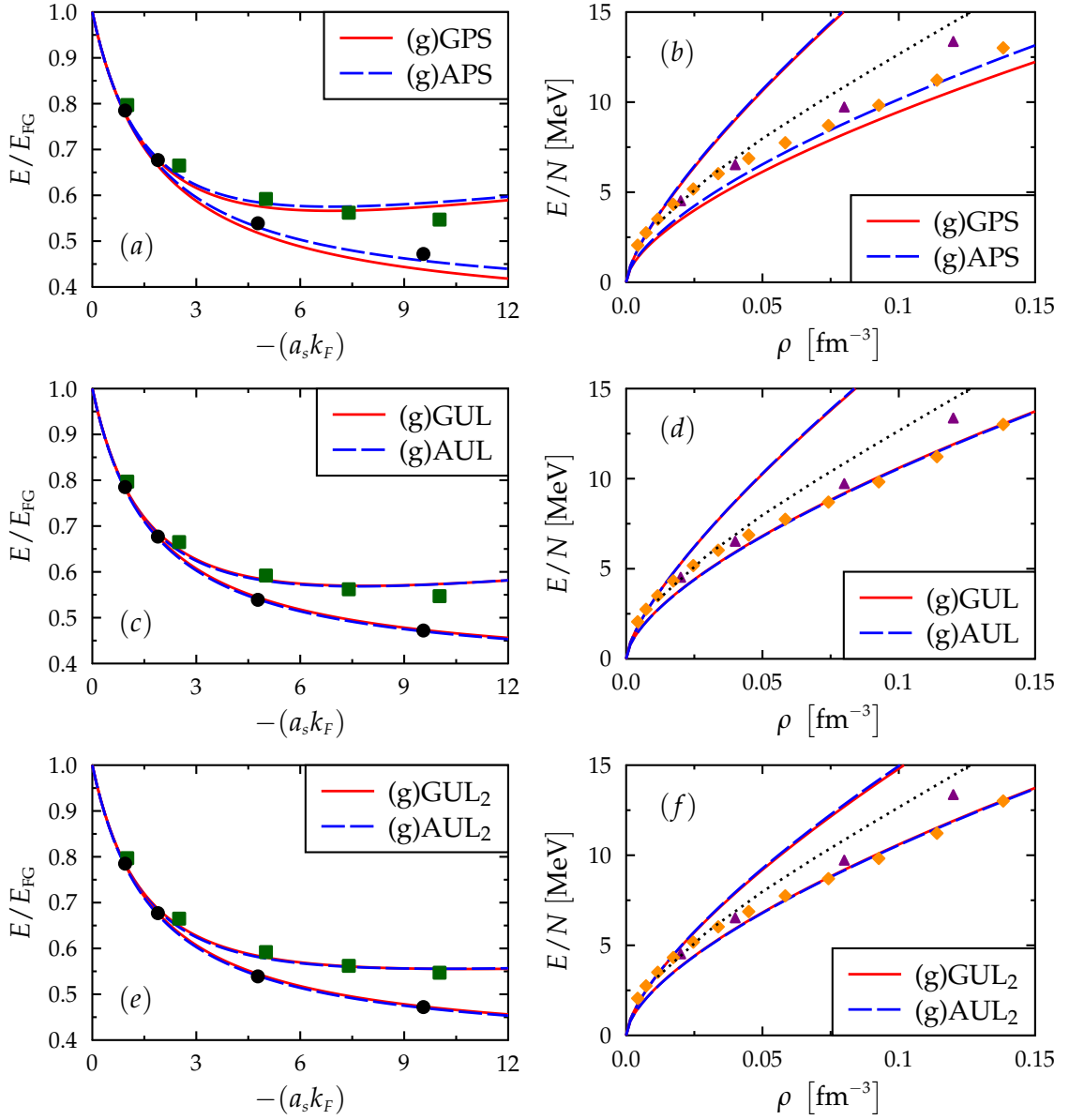


Figure 3.9: Neutron matter energy as a function of $-(a_s k_F)$ (left) or as a function of the density ρ (right). In each panel, the lower set of lines corresponds to the cold atom case ($r_s = 0$), i.e. using the APS/GPS ($a - b$) and AUL/GUL ($c - d - e - f$) functionals (blue dashed line / red solid line); and the upper set to the results obtained using the generalized functional including effective range effect (gAPS/gGPS ($a - b$), gAUL/gGUL ($c - d$), and gAUL₂/gGUL₂ ($e - f$) [blue dashed line / red solid line]) with the AV₄ interaction LEC parameters: $a_s = -19.295$ fm and $r_s = 2.716$ fm. The black circles and green squares in the left panels represent the QMC results of [53,72] respectively for cold atom case and AV₄ (s -wave only). The orange diamonds and purple triangles in the right panel stand for respectively the *ab initio* results of [62,63]. Note finally that the highest density shown in the left panels corresponds to $\rho \simeq 0.01$ fm^{-3} and accounts for a very narrow region of the right panels.

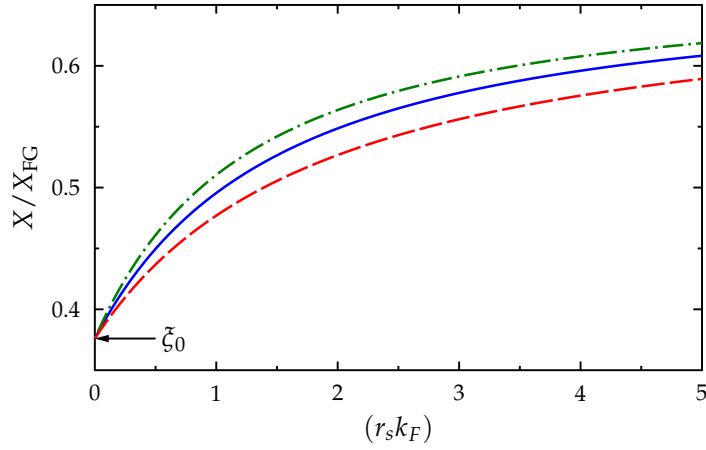


Figure 3.10: The pressure [$X = P$] (blue solid line), chemical potential [$X = \mu$] (red dashed line) and inverse compressibility [$X = 1/\kappa$] (green dot-dashed line) obtained at unitarity using the functional (3.35) as a function of $(r_s k_F)$. The arrow indicates the unitary limit for $r_s = 0$ (with $\xi_0 = 0.37$).

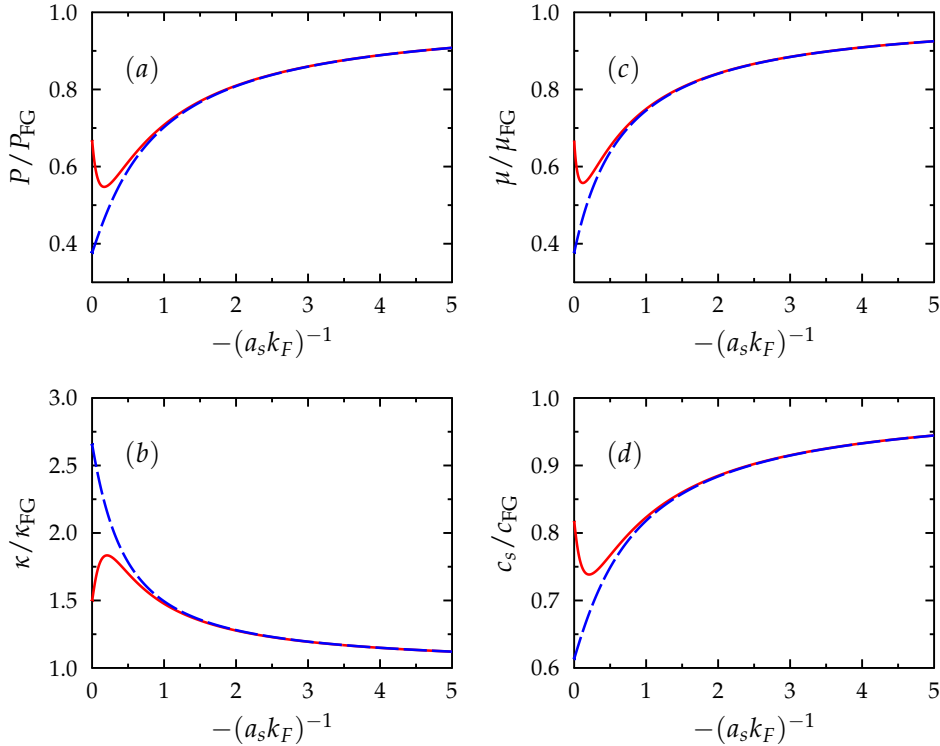


Figure 3.11: The pressure (a), the inverse of the compressibility (b), the chemical potential (c) and the sound velocity (d) obtained in neutron matter as a function of $-(a_s k_F)^{-1}$ using the gGUL_2 functional (red solid line). The case with $r_s = 0$ (cold atom reference) is displayed with a blue dashed line. In this figure, we used $a_s = 18.9$ fm and $r_s = 2.716$ fm.

LINK WITH THE HYBRID YGLO FUNCTIONAL OF [197]

In the above strategy, well defined limits are imposed to fix parameters of the functional. Alternatively, the resummed expression can serve as starting point to design new functionals and/or fix some of their parameters. This is for instance what was done in [197] for the YGLO functional. In this case, guided by the gGPS functional, the EOS was parametrized as:

$$\frac{E}{E_{FG}} = 1 + \frac{(a_s k_F)B}{1 - (a_s k_F)R + C\rho^{2/3}} + D\rho + F\rho^\alpha, \quad (3.36a)$$

where some of the coefficients $\{B, R\}$ are obtained by imposing the Lee-Yang expansion (2.28):

$$B = \frac{10}{9\pi} \quad \text{and} \quad R = \frac{6}{35\pi}(11 - 2\ln 2) \quad (3.36b)$$

Other parameters $\{C, D, F, \alpha\}$ are then adjusted by a direct fit to reproduce *ab initio* EOS of neutron matter and encode higher correlations (as the effective range, the p -wave, the three-body force, etc...). The results are shown in figure 1.27 where, contrary to the empirical Skyrme functional that does not reproduce the low-density regime, the new hybrid YGLO functional encodes the proper low-density behavior of the neutron matter EOS⁷. Recently this functional has been employed to describe successfully (that is to say in good agreement with *ab initio* calculations) the structure properties of finite neutron droplets [208]. These works are proofs of principle that such functionals based on resummation are of practical interest for both infinite and finite systems.

Below we introduce a new strategy we have proposed recently in [130] to obtain an alternative DFT forms that treats the effective-range dependence.

3.4

APPLICATION TO LINEAR RESPONSE IN FERMI LIQUIDS

Some of the ground-state quantities discussed above are directly connected to the static response of the Fermi system to an external field. In general, the static response provides interesting insight about the complex internal reorganization in strongly interacting Fermi liquids [264,265]. The static or dynamical responses have been the subject of extensive studies in the context of nuclear density functional theory [266–270] especially those based on the Skyrme EDF. As we will see, in the latter case, the static response strongly depends on the set of parameters used in the Skyrme EDF. Recently, the *ab-initio* static response of neutron matter has been obtained using AFDMC for the first time in [262,263] giving strong constraints on nuclear EDF. One surprising result is that the static response is very close to the free Fermi gas response. Below we make a detailed discussion on the static response obtained using the gGUL₂ functional. Since the methodology to obtain the static response is already well documented [264,265], we only give the important equations and summarize our published work [199].

⁷ This strategy was also extended to the symmetric matter EOS (and to the asymmetric matter EOS using the so called parabolic approximation) [197].

3.4.A Generalities on static response

Let us consider a system described by a many-body Hamiltonian \hat{H} . A static external one-body field, denoted by V_{ext} is applied to the system leading to a change of its properties. The static response, denoted by χ contains the information on how the one-body density and the total energy vary with the external field. χ is defined through:

$$\delta\rho(\mathbf{r}) = \int d^3\mathbf{r}' \chi(\mathbf{r} - \mathbf{r}') V_{\text{ext}}(\mathbf{r}'), \quad (3.37)$$

where $\delta\rho(\mathbf{r}) = \rho(\mathbf{r}) - \rho_0$, $\rho(\mathbf{r})$ and ρ_0 being respectively the local one-body density and the equilibrium density of the uniform system in its ground state. From this, one can express the static response formally as:

$$\chi(\mathbf{r} - \mathbf{r}') = \frac{\delta\rho(\mathbf{r})}{\delta V_{\text{ext}}(\mathbf{r}')}. \quad (3.38)$$

Performing the Fourier transform of (3.37), we simply have:

$$\delta\rho(\mathbf{q}) = \chi(\mathbf{q}) V_{\text{ext}}(\mathbf{q}). \quad (3.39)$$

Following [262,263], we assume $V_{\text{ext}}(\mathbf{q}) = \sum_q 2v_q \cos(\mathbf{q}\cdot\mathbf{r})$. The Fourier transform of V_{ext} at \mathbf{q} is then simply a constant and we have for the energy:

$$E(\mathbf{q}) = E_0 + \frac{\chi(q)}{\rho_0} v_q^2 + \dots \quad (3.40)$$

The static response function is directly linked to the compressibility κ discussed above (see table 3.3 for instance) due to the asymptotic relationship (compressibility sum rule) [270]:

$$\lim_{q \rightarrow 0} \chi(q) = -\rho^2 \kappa. \quad (3.41)$$

The function $\chi(q)$ or its dynamical equivalent has been extensively studied for the Skyrme EDF [270]. In figure 3.12, we give examples of results obtained using different sets of Skyrme parameters and compare them with the AFDMC results of [262,263]. It is clear from this figure that there is a large dispersion in the Skyrme EDF response depending on the parameter sets. Such a dispersion is not surprising since it is well known that the neutron equation of state is weakly constrained in Skyrme EDF (see for instance [203]). In all cases, even if the Skyrme EDF gives reasonable neutron matter EOS, significant differences are observed with the exact AFDMC result for all ranges of q/k_F . This figure also illustrates the fact that the exact result is very close to the free Fermi gas response (black dashed line).

An important ingredient of the response in Skyrme EDF is the evolution of the effective mass as a function of the density. Such evolution is shown in figure 3.13.a. Again, large differences are observed between the different sets of Skyrme EDF. We also show for comparison, the effective mass obtained in neutron matter using alternative many-body techniques. In these cases, the deduced effective mass are closer to the bare mass but still significantly differ with each other.

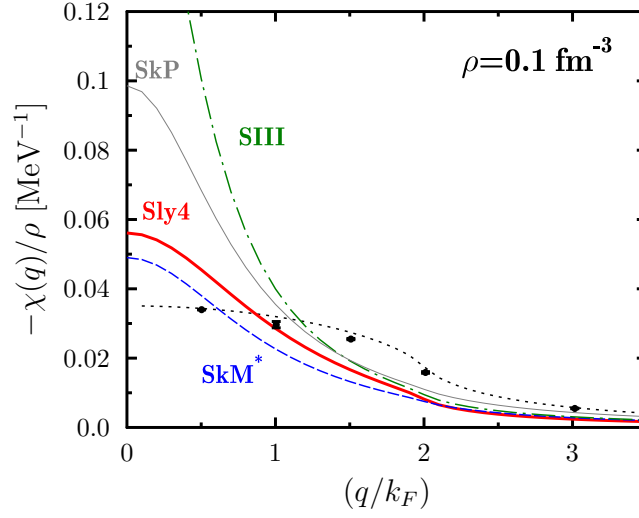


Figure 3.12: Static response of neutron matter at density $\rho = 0.1 \text{ fm}^{-3}$ obtained with the Skyrme EDF using the Sly4 (red thick solid line), SkM* (blue dashed line), SkP (gray thin solid line) and SIII (green dot-dashed line) sets of Skyrme parameters (see [112] for their values). Note that the EDF results are obtained by neglecting the spin-orbit term in the functional. Adding the spin-orbit contribution does not change significantly the result. The black circles (with errorbars) are those of [263] while the black dotted line is the free Fermi-gas static response. Figure taken from [199].

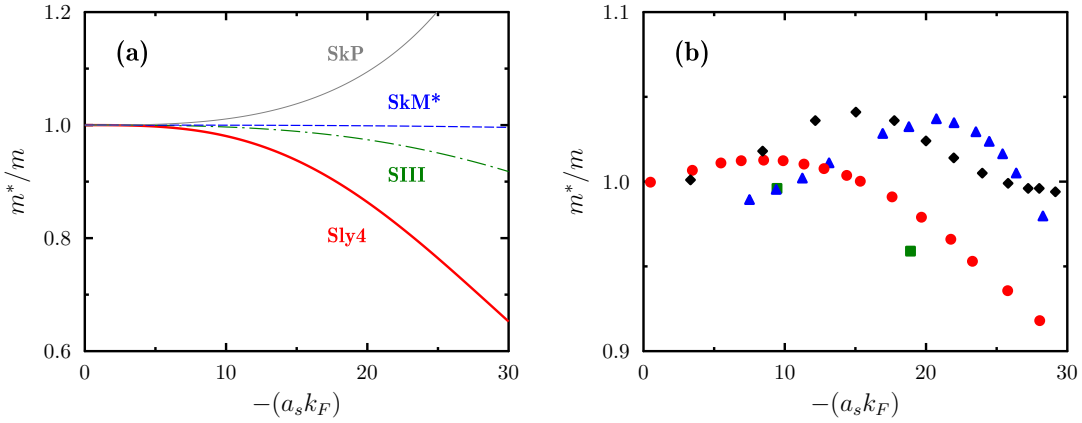


Figure 3.13: (a) Evolution of the effective mass m^*/m in neutron matter as a function of $-(a_s k_F)$ (with $a_s = -18.9 \text{ fm}$) using Skyrme EDF for the set of parameters used in figure 3.12 with the same lines convention. (b) Evolution of the effective mass in neutron matter deduced from selected many-body calculations: blue triangles [271], red circles [272], green squares [62], black diamonds [273]. Figure taken from [199].

In the absence of clear guidance for the effective masses behavior, we simply assume below that $m^*/m = 1$. Then, the calculation of the static response within the density functional approach reduces to:

$$\chi(q) = \frac{\chi_0(q)}{1 - J(\rho)\chi_0(q)}, \quad (3.42)$$

where $\chi_0(q)$ is the response of the free gas given in terms of the so-called Lindhard function (dashed line in figure 3.12) [192,265]:

$$\chi_0(q) = -\frac{mk_F}{2\pi^2\hbar^2} \left\{ 1 + \frac{k_F}{q} \left[1 - \left(\frac{q}{2k_F} \right)^2 \right] \ln \left| \frac{q + 2k_F}{q - 2k_F} \right| \right\} \equiv -\frac{mk_F}{\pi^2\hbar^2} f(q/k_F). \quad (3.43)$$

The density-dependent coefficient $J(\rho)$ in (3.42) is obtained from the second derivative of the energy density after subtraction of the kinetic contribution. Explicitly, the energy can be rewritten as an integral over the energy density through:

$$E = \int [\mathcal{K}(\mathbf{r}) + \mathcal{V}(\mathbf{r})] d^3r,$$

where \mathcal{K} is the kinetic energy density and \mathcal{V} is the potential energy density. For uniform system, $J(\rho)$ is given by:

$$J(\rho) = \frac{\partial^2 \mathcal{V}}{\partial \rho^2}, \quad (3.44)$$

that could again eventually be transformed as partial derivatives with respect to k_F .

3.4.B Static response in unitary gases

We consider first the strict unitary-gas limit with $r_s = 0$. In this case, we have:

$$\mathcal{V}(\rho) = \frac{3}{5} \frac{\hbar^2}{2m} (3\pi)^{2/3} \rho^{5/3} (\xi_0 - 1). \quad (3.45)$$

Using this expression, we obtain:

$$\chi(q) = -\frac{mk_F}{\pi^2\hbar^2} \frac{f(q/k_F)}{[1 + (\xi_0 - 1)f(q/k_F)]} \quad (3.46)$$

where $f(q/k_F)$ is defined through (3.43). In particular, we see immediately that $\chi(0) = \chi_0(0)/\xi_0$, with $\chi_0(0) = -mk_F/\pi^2$ that is a direct consequence of the property (3.41) and of the fact that $\kappa_{FG}/\kappa = \xi_0$ in unitary gas (see table 3.3).

The full static response is shown in figure 3.14 and compared to the result obtained in [274] using the Superfluid Local Density Approximation (SLDA) proposed in [75,275]. The static response calculated with the functional (3.43) perfectly matches the SLDA result when the Bertsch parameter is artificially increased to match the one used in the SLDA. Note that, the SLDA assumes a significant contribution from the effective mass and accounts also for superfluid effects, which is not

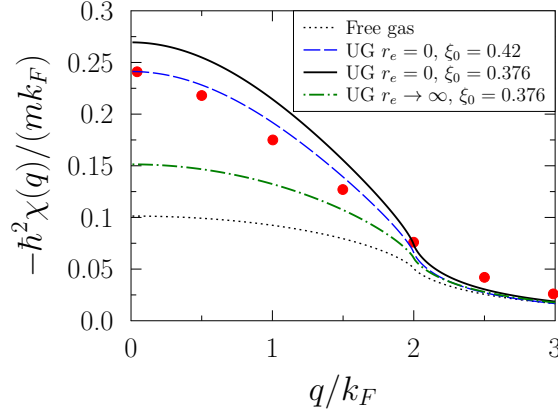


Figure 3.14: Static response of unitary gas (UG) obtained with the gGUL₂ functional assuming $r_s = 0$ (black solid line) or $r_s \rightarrow +\infty$ (green dot-dashed line). The latter case corresponds to the maximum effect induced by r_s and corresponds to an effective Bertsch parameter equal to 0.66. The free Fermi-gas response (black dotted line) is also shown as a reference. For comparison, the red filled circles corresponds to the static response at unitarity obtained in [274] using the SLDA where a slightly different value of the Bertsch parameter $\xi_0 = 0.42$ was assumed. For completeness, we also show (blue dashed line) the UG result obtained with (3.35) for $\xi_0 = 0.42$. Figure taken from [199].

the case in the present work. Therefore, an indirect conclusion is that the static response for unitary gas does not seem to be significantly influenced in particular by superfluidity. We would like to insist on the fact that this is most probably specific to the response to a static field (see section 3.5).

Note finally that the matching of the static response obtained with the two functional approaches observed in figure 3.14 is an interesting information but does not mean that the static response is the correct one at unitarity. A comparison with an exact calculation would be desirable (see also discussion in section 3.5).

The effect of r_s at unitarity on the response can be studied using the generalization of (3.45):

$$\mathcal{V}(\rho) = E_{FG}(\rho)[\tilde{\xi}(r_s k_F) - 1],$$

where $\tilde{\xi}(r_s k_F)$ is given by (3.35). The predicted influence of r_s is illustrated in figure 3.14. The effective range induces a global reduction of $\chi(q)$. The maximum effect is achieved by considering the limit $r_s \rightarrow +\infty$ (green dot dashed curve).

3.4.c Static response in neutron matter

Neutron matter differs from a unitary gas by the finite value of the scattering length as well as by a significant effect of the effective range even at rather low density [130]. When the density increases, it is also anticipated that higher partial waves of the interaction contribute. Since our aim is to compare with the recent result of [263] where the AV8 interaction has been used, we use the gGUL₂ functional adopting the AV8 values for the different parameters: $a_s = -19.295$ fm and $r_s = 2.716$ fm. We note that, the gGUL₂ functional reproduces well the energy for rather low densities $\rho < 0.02 - 0.03$ fm⁻³ [130] (see figure 3.9) while the static responses of [263] have been obtained for $\rho = 0.04$ and 0.1 fm⁻³ which is not optimal for the comparison.

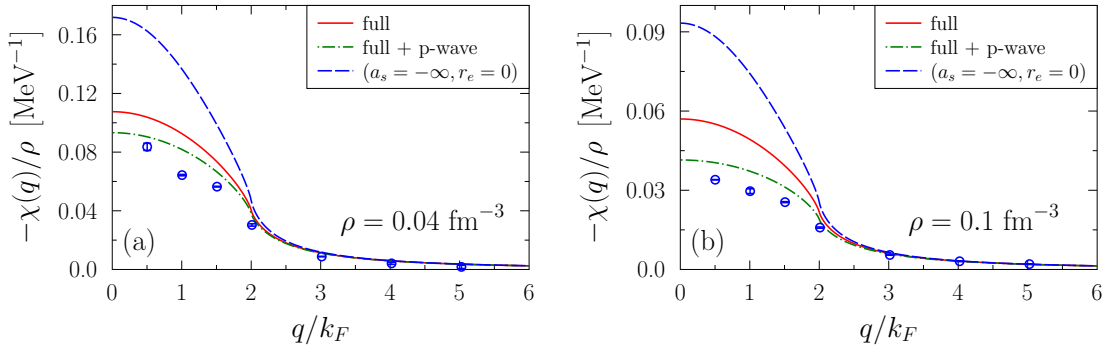


Figure 3.15: Static response function obtained with the $g\text{GUL}_2$ functional as a function of q/k_F for (a) $\rho = 0.04 \text{ fm}^{-3}$ and (b) $\rho = 0.1 \text{ fm}^{-3}$. The blue dashed line and red solid line correspond respectively to the UG case (cold atom reference) and $r_s = 2.716 \text{ fm}$ (neutron matter case). Note that, at the density considered, the UG case cannot be distinguished from the neutron matter assuming $r_s = 0$. At both densities, the AFDMC results of [262,263] are shown with blue open circles. The green dot-dashed line finally displays the result obtained by adding the p -wave contribution to the $g\text{GUL}_2$ functional. Consistently with the use of the AV8 interaction in the AFDMC calculation, we use a value $a_p^3 = 0.0916 \text{ fm}$ for the p -wave scattering volume. Figure taken from [199].

We show in figure 3.15 the static response obtained from the $g\text{GUL}_2$ functional and compare it to the AFDMC results of [262,263]. While slightly overestimated, especially in the highest density considered, we first observe that the new functional is in much better agreement than the empirical functional considered in figure 3.12. For the considered densities, as underlined in [130], the $g\text{GUL}_2$ functional can be accurately replaced by its unitary gas limit, i.e. taking $-(a_s k_F)^{-1} = 0$. Indeed, replacing the full $g\text{GUL}_2$ functional by ζ given by (3.35) leads almost to the same total energy and static response (not shown). Still, the static response obtained by neglecting the r_s effect is rather far from the static response obtained with the physical r_s , underlying the key role played by the effective range.

Following [130], we also study the possible influence of the p -wave contribution by adding simply its leading-order contribution to the energy, that is [see (2.28)]:

$$\frac{E_p}{E_{FG}} = \frac{1}{\pi} (a_p k_F)^3 \quad (3.47)$$

The results are displayed in figure 3.15. We see that the p -wave term, treated simply by its leading-order contribution does contribute to the static response and, most importantly, the result is very close to the *ab initio* one. For the sake of completeness, we also report in figure 3.11 the different thermodynamical quantities obtained by including the p -wave term. However the contribution should only be taken here as indicative. As noted already in [130], the inclusion of the leading term of the p -wave, produces a rather large, most probably unphysical, contribution to the different quantities and, when the density increases, one should a priori properly account for the p -wave contribution accounting for the resummation of the s -wave effect as illustrated in [237]. This resummation is however out of the scope of the present application.

Finally, to systematically quantify the effects of finite a_s , influence of r_s and p -wave, we have reproduced the figure 15 of [263] where the normalized response function is shown for different densities (figure 3.16). In this figure, we can clearly

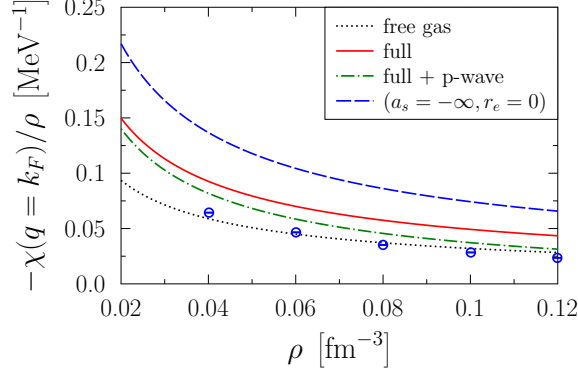


Figure 3.16: Evolution of the normalized static response as a function of density for $q = k_F$ (same as figure 15 of [263]). The AFDMC results of [263] is shown by blue open circles. The result of the gGUL₂ functional with $r_s = 2.176$ fm and $r_s = 0$ fm are shown by red solid and blue dashed line respectively. The result obtained by adding the p -wave contribution (with $a_p^3 = 0.0916$ fm³) to the functional is shown by green dot-dashed line. The black dotted line corresponds to the free Fermi gas limit. Figure taken from [199].

see the importance of the effective range and, to a lesser extent, the slightly smaller effect of the p -wave. Still the free Fermi–gas case is the one that best reproduces the AFDMC result. However, this is most probably accidental in view of the strong interaction at play in nuclear systems.

We finally would like to mention that we are unable with the present density functional to reproduce the strong increase of the response function as $q \rightarrow 0$ that is observed in the AFDMC. This limit is directly connected to the compressibility [see (3.41)]. The compressibilities predicted by our EDF are $\rho\kappa = 0.108$ MeV and $\rho\kappa = 0.057$ MeV at $\rho = 0.04$ fm⁻³ and $\rho = 0.1$ fm⁻³ respectively. These values are lower than those reported in [263] which are respectively $\rho\kappa = 0.19$ MeV and $\rho\kappa = 0.089$ MeV at $\rho = 0.04$ fm⁻³ and $\rho = 0.1$ fm⁻³.

3.4.D Collective response in the hydrodynamical regime

We conclude this application of the gGUL₂ functional by using previous results to study the collective excitations in cold atoms and neutron matter in the hydrodynamical regime. For boson systems, the hydrodynamical regime is well documented [127,276]. Similar techniques can be applied to fermionic superfluid systems. Note that here, we do not include explicitly the pairing correlations through the anomalous density. However, the fact that we properly describe the total energy of cold atoms, is an indication that pairing effect is accounted for in some way. For a superfluid Fermi system, the hydrodynamical regime is justified when the collective frequency is below the energy necessary to break a Cooper pair (see for instance [243]). Our aim is to study the dynamical response of a system confined in a trap, described by an external potential $U(\mathbf{r})$. At equilibrium, the external field is counterbalanced by the internal pressure leading to the equilibrium equation:

$$\nabla^2 P(\mathbf{r}) = -\frac{1}{m} \nabla [\rho_0(\mathbf{r}) \cdot \nabla U(\mathbf{r})], \quad (3.48)$$

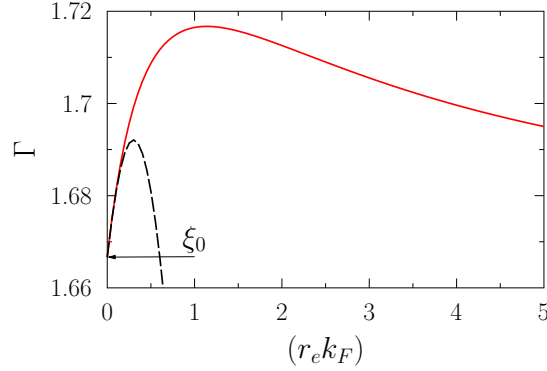


Figure 3.17: Evolution of the non-adiabatic index Γ at unitarity (red solid line) deduced from the functional (3.35) as a function of $(r_s k_F)$. The arrow indicates the unitary limit for $r_s = 0$. For comparison, the black short-dashed line corresponds to the Taylor expansion of ξ to second order in $(r_s k_F)$. Figure taken from [199].

where ρ_0 denotes the equilibrium density while P is the pressure at equilibrium given by (3.17a). We now consider small-amplitude oscillations around equilibrium such that $\rho(\mathbf{r}, t) = \rho_0(\mathbf{r}) + \delta\rho(\mathbf{r}, t)$ with $\delta\rho(\mathbf{r}, t) = \rho_1(\mathbf{r})e^{i\omega t} + \text{h.c.}$ The linearization of the hydrodynamical equation leads to the equation:

$$\omega^2 \rho_1(\mathbf{r}) = -\frac{1}{m} \nabla \cdot [\rho_1(\mathbf{r}) \nabla U(\mathbf{r})] - \nabla^2 [c_0^2(\mathbf{r}) \rho_1(\mathbf{r})], \quad (3.49)$$

where $c_0^2(\mathbf{r})$ is the local sound velocity defined through: $mc_0^2(\mathbf{r}) \equiv dP(\mathbf{r})/d\rho_0(\mathbf{r})$. This equation has been used in several works to study collective oscillations in Fermi gas around unitarity [243,248,276,277]. Below we extend these studies by considering the possible effect of non-zero r_s and by going from cold atoms to neutron matter.

ADIABATIC INDEX IN COLD ATOMS AND NEUTRON MATTER

For the sake of simplicity, we assume that the system has a polytropic equation of state, i.e. that we simply have [277]:

$$P(\mathbf{r}) \propto \rho_0^\Gamma(\mathbf{r}), \quad (3.50)$$

where Γ is the adiabatic index in the center of the trapping potential. As in infinite systems, we have the relation $\Gamma = (\kappa_c P_c)^{-1}$ where P_c and κ_c denote the pressure and the compressibility in the center of the trapping potential at equilibrium given by (3.17a) and (3.17c). The quantity Γ has been studied in cold atoms varying $-(a_s k_F)$ in [77]. For vanishing r_s , it is known that Γ tends toward $5/3$ both in the unitary limit and in the low-density regime. For a unitary gas, when r_s cannot be neglected anymore, using the functional (3.35), we predict that Γ deviate from $5/3$. The dependence of Γ on the effective range is shown in figure 3.17. We see that Γ first increases and then decreases. In the extreme limit $r_s \rightarrow +\infty$, it is possible to show that we again obtain $\Gamma \rightarrow 5/3$.

More generally, we illustrate in figure 3.18 the dependence of Γ (obtained with or without effective range effects) on low-energy constants taken from neutron matter. For $r_s = 0$, we qualitatively and quantitatively reproduce the result of [77] with the presence of a minimum in Γ for $-2.5 < (a_s k_F) < 0$. While the minimum persists

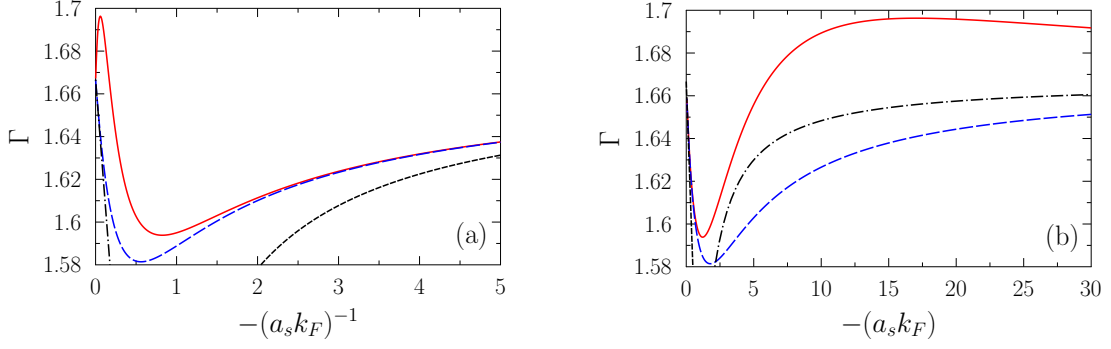


Figure 3.18: Adiabatic index as a function of $-(a_s k_F)^{-1}$ (a) or as a function of $-(a_s k_F)$ (b) obtained from the gGUL₂ functional assuming $r_s = 0$ fm (blue long dashed line). For comparison, the black short-dashed and the black short dot-dashed lines correspond to the Taylor expansion to first order in $(a_s k_F)$ or to first order in $(a_s k_F)^{-1}$ respectively. The red solid line corresponds to the neutron matter case assuming $r_s = 2.716$ fm. In both cases, $a_s = -18.9$ fm. Figure taken from [199].

for non-vanishing r_s , we observe that it is slightly shifted to lower values of $|a_s k_F|$. Overall, we see that r_s significantly affects the evolution of Γ that now presents a maximum and approaches $\Gamma = 5/3$ from above as $-(a_s k_F) \rightarrow +\infty$.

COLLECTIVE FREQUENCIES IN AN ANISOTROPIC TRAP

As shown in [277], assuming a polytropic EOS leads to a rather simple expression of the collective oscillations of a deformed system. More precisely, we consider here a system confined in an anisotropic trap

$$U(\mathbf{r}) = \frac{m}{2} \omega_0^2 (x^2 + y^2 + \lambda^2 z^2), \quad (3.51)$$

where λ gives a measure of the anisotropy, with $\lambda < 1$ and $\lambda > 1$ for prolate or oblate deformations respectively. Then the author of [277] has obtained analytical expressions for the collective frequencies along the elongation axis or perpendicular to the elongation axis. These collective frequencies are called below axial or radial collective frequencies and are denoted by ω_{ax} and ω_{rad} respectively.

For prolate deformations with $\lambda \ll 1$, the two frequencies are given by:

$$\frac{\omega_{\text{ax}}^p}{\omega_0} = \lambda \sqrt{3 - \Gamma^{-1}} \quad \text{and} \quad \frac{\omega_{\text{rad}}^p}{\omega_0} = \sqrt{2\Gamma}, \quad (3.52)$$

while in the oblate limit $\lambda \gg 1$, we have:

$$\frac{\omega_{\text{ax}}^o}{\omega_0} = \lambda \sqrt{\Gamma + 1} \quad \text{and} \quad \frac{\omega_{\text{rad}}^o}{\omega_0} = \sqrt{\frac{6\Gamma - 2}{\Gamma + 1}}. \quad (3.53)$$

Note that, for $\lambda = 1$, we recover the results obtained for an isotropic trap [277,278]. We then see that a change in Γ will be reflected by a change in the axial and radial collective frequencies.

The collective response of cold atoms with a possible anisotropy in the trapping potential has attracted much attention in the last decades. The experimental axial and radial frequencies are shown at or around unitarity for prolate shapes in figure 3.19. At unitarity ($\Gamma = 5/3$), we expect to have $\omega_{\text{ax}}^p / (\lambda \omega_0) = \sqrt{12/5} \simeq 1.549$ and

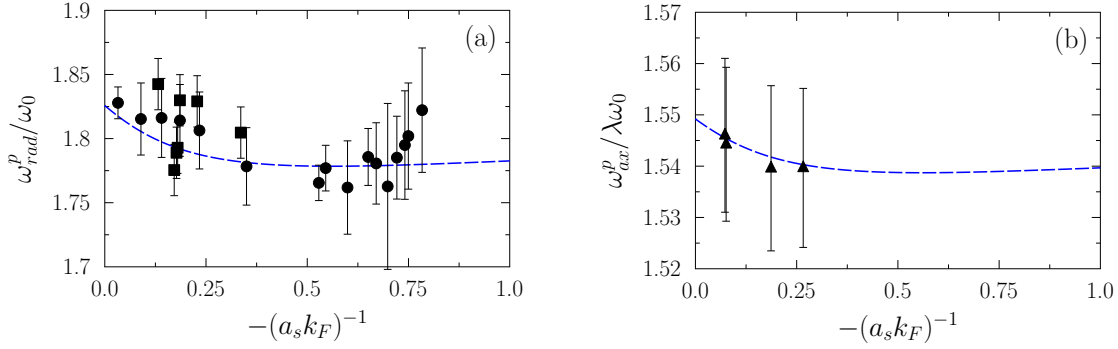


Figure 3.19: ω_{rad}^p/ω_0 (a) and $\omega_{ax}^p/(\lambda\omega_0)$ (b) as a function of $-(a_s k_F)^{-1}$ obtained with the gGUL₂ functional with $r_s = 0$ (blue dashed line). The symbols are experimental data: triangles from [279], circles from [280] and squares from [281]. (All data sets are taken from figure 3 of [282]). Figure taken from [199].

$\omega_{rad}^p/\omega_0 = \sqrt{10/3} \simeq 1.826$ that seems coherent with the observations. In figure 3.19, we also display the results of (3.52) using the adiabatic index obtained from the gGUL₂ functional on $r_s = 0$. We see that the estimated collective frequencies are consistent with the observation in cold atoms. We then investigate the possible effect of r_s in the strict unitary regime in figure 3.20. In this case, the Γ that is used in (3.52) is displayed in figure 3.17. We see a rather weak dependence of the collective frequencies with r_s .

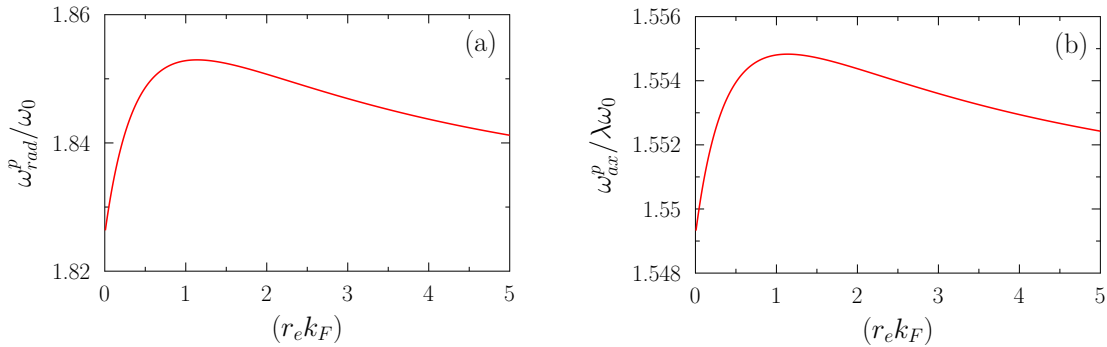


Figure 3.20: ω_{rad}^p/ω_0 (a) and $\omega_{ax}^p/(\lambda\omega_0)$ (b) as a function of $(r_s k_F)$ obtained with the gGUL₂ functional at unitarity $(a_s k_F)^{-1} = 0$. Figure taken from [199].

We finally display in figure 3.21 the collective frequencies obtained for confined neutron systems in an anisotropic trap. As far as we know, the present application is the first attempt to determine this particular quantity in neutronic systems. Collective frequencies obtained with the functional are compared with the case of cold atoms and with the result of the empirical Skyrme EDF with the SLy5 set of parameters. It is first noted that collective frequencies are strongly dependent on the used functional and therefore the dynamical collective frequencies of trapped neutrons are a stringent test of the functional used. We finally would like to mention that collective frequencies are calculated here assuming that the local density approximation is valid. However, the collective frequencies might be affected by the introduction of gradients of the densities as is usually done in more empirical functionals like Skyrme ones. In addition, we predict rather large differences between neutron matter and cold atoms that are due to effective range effects as well as higher-order channels like p -wave when the density increases.

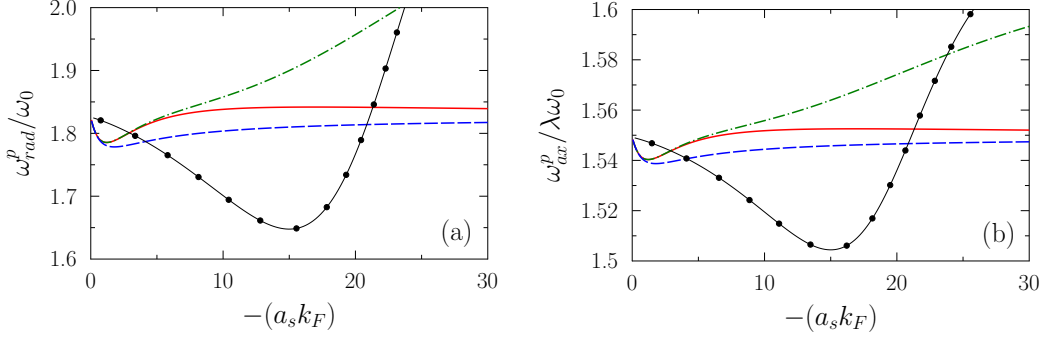


Figure 3.21: $\omega_{\text{rad}}^p/\omega_0$ (resp. $\omega_{\text{ax}}^p/\omega_0$) as a function of $-(a_s k_F)$ (a) (resp. (b)) obtained in neutron matter using $a_s = -18.9$ fm and $r_s = 2.716$ fm (red solid line) in the gGUL₂ functional while the blue long-dashed line corresponds to the result obtained with $r_s = 0$. For comparison, we also show the result of the Skyrme SLy5 parameter sets (black filled circles) and the result obtained by adding to the functional the leading order p -wave contribution (green dot-dashed line). Figure taken from [199].

3.5

SUMMARY AND CRITICAL DISCUSSION

The goals of the present chapter were twofold. First starting from the resummation technique presented in chapter 2, we have shown how the phase-space average method can be used to simplify the expression in terms of $(a_s k_F)$ and henceforth provide a compact form of DFT applicable from low density to strong coupling regime. Then, based on these expressions, we have relaxed some of the parameters to properly reproduce the unitary gas limit and eventually extend the DFT to include effective-range effects. The latter development was indeed necessary to go from atomic gases to neutron matter. In a second step, we have illustrated how these functionals can be applied with some success to both atomic and neutron matter by studying various aspects including the EOS, thermodynamical quantities, static response, and collective dynamics. This study was also very useful to uncover some difficulties. These difficulties are discussed below and some of them will be the motivation for the developments presented in next sections.

ROLE OF THE EFFECTIVE RANGE

As we have seen, the strategy employed here to design a functional in some cases strongly relies on *ab initio* pseudo-data. Therefore their properties depend on the quality and robustness of these pseudo-data. One critical aspect of the present study is that the reference pseudo-data from [260] (purple dots) and [237] (gray area) in figure 3.8 are empirical in the sense that the effective-range approximation was used starting from the gGEI functional (particle-particle ladder resummation). This dependence at unitarity and large $(r_s k_F)$ is actually scarcely known. However, the authors of [261] (results shown by orange triangles in figure 3.8) made recently calculations [in agreement with the QMC results [79,81] for small values of $(r_s k_F)$] that seem to be more robust and can serve as a guidance. This work tends to indicate a completely different behaviour of $\zeta(r_s k_F)$ compared to the one used here to design the functional. Another guidance could be neutron matter EOS with only the 1S_0 channel contribution (see the filled squares in figure 3.9). We have made some attempts to improve the technique but one of our conclusions is that extensive *ab initio* studies of unitarity gases with large effective range are desirable to further progress.

ROLE OF PAIRING

In the present application, we focused our attention on the static response of a spin degenerate Fermi liquid with anomalously large s -wave scattering length. We have seen that, assuming that the effective mass is approximately equal to the bare mass and neglecting possible effects of superfluidity, our functional can describe reasonably well the ground-state thermodynamical quantities close or at unitarity in cold atoms and can give interesting insight for the static response of neutron matter. The comparison is less favorable when performing the full dynamical response. Using the same assumptions as for the static response, we also calculated the dynamical response of the system to a small oscillating external perturbation $V_{\text{ext}}(\mathbf{r}, t)$ with varying frequency ω . The dynamical response function $\chi(q, \omega)$ then generalizes the static response [266,270] that is obtained as the specific case $\omega = 0$.

One then defines the dynamical structure function $S(q, \omega)$ through:

$$S(q, \omega) = -\frac{1}{\pi} \text{Im} [\chi(q, \omega)]. \quad (3.54)$$

While the static response function has not been directly measured in unitary gases, its dynamical structure function has been studied both experimentally and theoretically in [283] and [284] respectively. The experimental structure function obtained

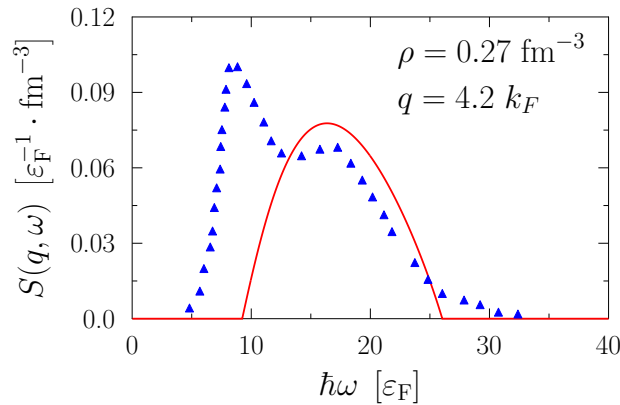


Figure 3.22: Dynamical structure function at unitarity obtained from the $g\text{GUL}_2$ functional (red solid line) compared to the experimental results of [283] (blue triangles). $\varepsilon_F = \hbar^2 k_F^2 / 2m$ is the Fermi energy. Figure taken from [199].

in [283] is compared to the response obtained with the $g\text{GUL}_2$ functional in figure 3.22. The experimental response presents two separated peaks. Indeed, due to superfluidity, the dynamical response will present a low-energy mode, the so-called Bogoliubov-Anderson mode that has been studied for instance in [284]. The superfluid nature of Fermi gases at unitarity has been unambiguously directly probed by the presence of a lattice of quantized vortices in [285]. We obviously see that the dynamical response obtained with our functional is able to approximately reproduce the second peak but completely misses the collective mode at low energy. This mode seems difficult to be described without explicitly using a quasi-particle picture. As shown in [286] using the RPA approach with the SLDA, accounting for superfluidity, leads back to the proper low-energy collective modes and reproduces qualitatively the observation. As shown above, many aspects can be properly reproduced in cold atoms without explicitly introducing superfluidity. However, the

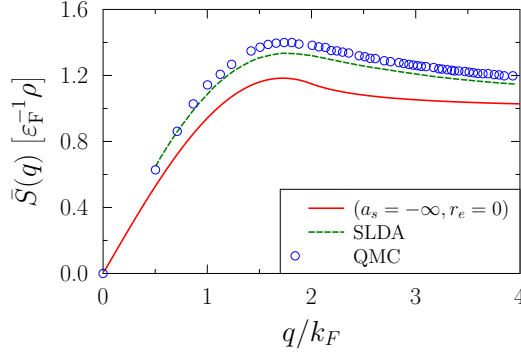


Figure 3.23: Static structure function obtained with the functional (with $r_s = 0$) (red solid line) as a function of q/k_F compared to the Diffusion Monte-Carlo result of [288] (blue circles). For comparison, we also show the result obtained in [286] with the SLDA (green dashed line). Figure taken from [199].

dynamical response clearly points out the necessity in the near future to explicitly include the anomalous density in the description.

One can also obtain the static structure function $\bar{S}(q)$, defined through

$$\bar{S}(q) = \int d\omega S(q, \omega),$$

that has been studied for unitary gases in [287] where it is compared to QMC results (see also [288]). We show in figure 3.23 a comparison of the static structure factor obtained with the functional and with the Monte-Carlo result of [288]. Not surprisingly, due to the missing peak at low energy, $\bar{S}(q)$ is underestimated compared to the exact results. Our conclusion, is that for specific aspects like the dynamical response, it will be necessary to improve the functional by allowing $U(1)$ symmetry breaking. The same situation will also happen for neutron matter at very low density. However, in this case, when the density increases the pairing gap exponentially decreases. In particular, at densities considered in the DFMC results of [262,263], pairing is expected not to affect the static response.

ROLE OF QUASI-PARTICLE PROPERTIES

A second source of difficulty is the absence of a clear prescription for the effective mass in the large a_s limit. Such effective mass and more generally quasi-particle properties are rather standard quantities helping to understand Fermi liquids (see section 1.3.b). Its knowledge is of particular importance for instance to understand certain properties like the static response of neutron matter recently calculated with an *ab initio* theory in [262,263]. In the case of neutron matter, it turns out that the effective mass is scarcely known (see figure 3.13) and has only been very recently estimated using AFDMC in [289] and BHF calculation [51,52]. For this reason, it is highly desirable to explore the possibility to obtain self-energies also using resummation techniques, for which a direct link with the Fermi liquid theory can be made, as functionals of $(a_s k_F)$ in the non-perturbative regime.

In order to achieve this goal, we start from resummation techniques presented in the following chapter and extend the phase-space average technique to the self-energy in chapter 5. We will concentrate on the generalization of the functionals without effective range and without pairing effects introducing quasi-particle properties (in particular the effective mass) consistently with the APS/GPS and AUL/GUL approximations.

4

SELF-ENERGY RESUMMATION

*“C’est pas l’homme qui prend la mer
C’est la mer qui prend l’homme”
Moi la mer elle m’a pris
Au dépourou, tans pis...*

*J’ai eu si mal au cœur
Sur la mer en furie
Qu’j’ai vomi mon quatre-heures
Et mon minuit aussi*

*J’m suis cogné partout
J’ai dormi dans des draps mouillés
Ça m’a coûté des sous
C’est d’la plaisance, c’est le pied !*

*Dès que le vent soufflera je repartira
Dès que les vents tourneront nous nous en allons...*

Renaud – *Dès que le vent soufflera*

CONTENTS

| | | |
|-------|---|------------|
| 4.1 | Self-energy contribution at different orders | 108 |
| 4.2 | Self-energy resummation: particle-hole propagator | 114 |
| 4.2.A | Discussion on the off-shell ladder diagrams resummation | 115 |
| 4.2.B | Resummation of the on-shell particle-particle self-energy . | 116 |
| 4.2.C | Resummation of the on-shell hole-hole self-energy | 117 |
| 4.2.D | Critical discussions | 118 |
| 4.3 | Self-energy resummation: test-particle technique | 124 |
| 4.3.A | Test-particle insertion technique | 124 |
| 4.3.B | Resummed self-energy using the test-particle approach . . | 127 |
| 4.4 | Summary and discussions | 132 |

In chapter 2, we have discussed the resummation technique for the energy leading to a compact form where selected diagrams, namely ladder diagrams, have been retained. As we have seen, the resummation of particle-particle ladder diagrams leads to a geometrical series form while the combined particle-particle and hole-hole ladder diagrams lead to an arctangent form [see (2.55)]. The goal of this chapter is to perform an equivalent resummation directly for the self-energy. This will provide microscopic information on the system such as the effective mass and/or the lifetime of quasi-particles. It will also make a direct link with the Landau Fermi liquid theory. We have already emphasized in chapter 3 the importance of these quantities to describe non-equilibrium properties like linear response or collective modes. Here, we first illustrate the calculation of the self-energy diagrams from first to third order in $(a_s k_F)$ and discuss the relation with the MBPT calculation for the ground state energy presented in section 2.2.b. We then explain how to obtain some compact expressions for the self-energy, similarly to what was done for the energy, by including either only particle-particle ladder or combined particle-particle and hole-hole ladder diagrams. Advantages and drawbacks of the two selected classes of diagrams will be discussed.

4.1

SELF-ENERGY CONTRIBUTION AT DIFFERENT ORDERS

In this section, instead of estimating the energy contributions order by order, we work directly on the proper self-energy and estimate it with a perturbation theory in powers of $(a_s k_F)$. Using the Feynman rules enunciated in section 2.2.a, diagrams contributing to the self-energy at first, second and third order are shown in table 4.1. Their analytical/numerical estimates are discussed below but we first discuss here the correspondence between the energy diagrams (table 2.1) and the proper self-energy (table 4.1). For each energy diagram, by breaking a leg, i.e. a propagator, we obtain the associated self-energy diagram. Reciprocally, closing the broken dashed line of a self-energy diagram, we obtain the corresponding energy diagram. This will be illustrated below for the first, second and third orders in $(a_s k_F)$ by applying in more details the MBPT for dilute Fermi systems and using the notation introduced in chapter 2. We already introduced some aspects related to the self-energy in section 2.2.a and more details are available in different textbooks [192–194, 218–223]. Here we will stick with principal aspects of the on-shell self-energy using a contact interaction (2.1) that is properly regularized (more details on the regularization are given in appendices A and B).

FIRST ORDER

At first order, there is only one connected diagram (1α). Applying the Feynman rules for the self-energy and the notations introduced in chapter 2, we can write¹:

$$\begin{aligned} \text{---}\circ\text{---} &= \Sigma_{(1\alpha)}^* = (g-1)C_0 \int_2 G^+(2) \\ &= (g-1)C_0 \frac{k_F^3}{6\pi^2} = \varepsilon_F (g-1) \frac{4}{3\pi} (a_s k_F), \end{aligned} \quad (4.1)$$

where $\varepsilon_F = k_F^2/2m$ is the single-particle energy at the Fermi surface (the chemical potential μ_{FG}) of the free Fermi gas.

Knowing the self-energy contribution of a given diagram, we can deduce its energy contribution closing the open dashed lines (see table 4.1) with a Green's function²:

$$\Sigma_{(1)}^* = \text{---}\circ\text{---} \longrightarrow \text{---}\circ\text{---} = E_{(1)} = \frac{g}{2} \int_1 G^+(1) \Sigma_{(1)}^*,$$

where the integral comes from the fact that we have closed the diagram by a single line leading to integrate $G^+(1)\Sigma_{(1)}^*$ over (\mathbf{k}_1, ω_1) . The factor g stems from the extra spin summation induced by the closure relation while the factor $1/2$ stems from the number of equivalent lines which is zero for the self-energy diagram (1α) and one for the energy diagram ($1a$). Note that, at first order, the self-energy does not depend on the open line and is just a constant. As we will see below, the self-energy is generally a function of the energy and momentum (\mathbf{k}_1, ω_1) of the dressed propagator.

-
- ¹ The integration on ω_2 is done in the upper complex plane because G^+ is the hole propagator.
 - ² This line is named a dressed propagator (by the self-energy). This dressing of propagator is also called in-medium insertion since the self-energy can be interpreted as an induced correction to the single-particle energy due to the medium effect.



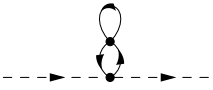

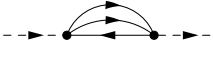
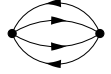
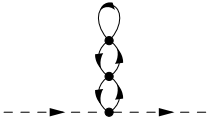



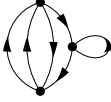

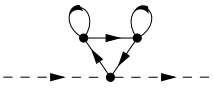
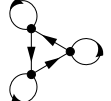
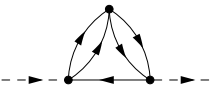
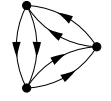
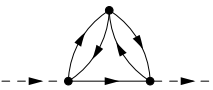
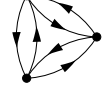
| Self-energy diagram ($n\zeta$) | D_g | $\sigma(S, l) = (2^l S)^{-1}$ | Energy diagram (nz) |
|---|------------------|-------------------------------|--|
| (1 α)  | $(g - 1)$ | $\sigma(0!, 0) = 1$ | (1a)  |
| (2 α)  | — | — | (2a)  |
| (2 β)  | $2(g - 1)$ | $\sigma(1!, 1) = 1/2$ | (2b)  |
| (3 α)  | — | — | (3a)  |
| (3 β)  | — | — | |
| (3 β')  | | | (3b)  |
| (3 β'')  | $4(g - 1)^2$ | $\sigma(2!, 1) = 1/4$ | |
| (3 γ)  | — | — | (3c)  |
| (3 δ)  | $4(g - 1)$ | $\sigma(2!, 2) = 1/4$ | (3d)  |
| (3 ϵ)  | $(g - 1)(g - 3)$ | $\sigma(2!, 0) = 1$ | (3e)  |

Table 4.1: Diagrams obtained using the Feynman rules for the self-energy contribution up to third order. If “—” is indicated, it means that diagrams do not contribute. The last column corresponds to the associated energy diagram obtained by closing the dashed legs (see figure 2.1). In this table, D_g corresponds to the degeneracy and $\sigma(S, l)$ to the spin angular momentum symmetry factor.

SECOND ORDER

Before performing the explicit calculation of the second-order contribution, we discuss how these diagrams can be evaluated. Due to the same arguments as for the second-order energy [see discussion in sections 2.2.b and (2.13)], the diagram (2 α) shown in table 4.1 does not contribute [see (2.13)]. The second diagram (2 β) can be evaluated considering two cases: it can be composed by 2-particle and 1-hole (2 $p1h$) or 1 $p2h$. This gives two different contributions denoted respectively as $\Sigma_{(2)}^{pp}$ and $\Sigma_{(2)}^{hh}$. Using the Feynman rules, we have³:

$$\begin{aligned} \Sigma_{(2\beta)}^*(\mathbf{k}_1, \omega_1) &= \text{---} \text{---} \text{---} \text{---} \text{---} \text{---} \\ &= -(g-1)C_0^2 \int_{2,3} \left[G_2^+ G_{1-3}^- G_{2+3}^- + G_2^- G_{1-3}^+ G_{2+3}^+ \right]. \end{aligned} \quad (4.2)$$

Now, evaluating this expression on-shell (that is to say: $\omega_1 = \omega_{\mathbf{k}_1} \equiv \mathbf{k}_1^2/2m$) using the appropriate substitution to dimensionless variables given by (2.19), we obtain:

$$\Sigma_{(2\beta)}^*(\mathbf{k}_1, \omega_{\mathbf{k}_1}) = \Sigma_{(2)}^{pp}(\mathbf{k}_1, \omega_{\mathbf{k}_1}) + \Sigma_{(2)}^{hh}(\mathbf{k}_1, \omega_{\mathbf{k}_1}), \quad (4.3a)$$

with

$$\Sigma_{(2)}^{pp}(\mathbf{k}_1, \omega_{\mathbf{k}_1}) = (g-1)C_0 \int_{k_2} n_2 B_{pp}(s, t), \quad (4.3b)$$

$$\Sigma_{(2)}^{hh}(\mathbf{k}_1, \omega_{\mathbf{k}_1}) = (g-1)C_0 \int_{k_2} (1-n_2) B_{hh}(s, t). \quad (4.3c)$$

Here, we have decomposed the self-energy into two components, $\Sigma_{(2)}^{pp}$ and $\Sigma_{(2)}^{hh}$, coming from the contributions of the diagrams composed by 2 $p1h$ and 1 $p2h$ lines respectively. These contributions depend of the pp and hh effective interaction B_{pp} and B_{hh} introduced in chapter 2 [see (2.21)] and are given in appendices B and C.

We can also decompose the self-energy in terms of its real and imaginary parts:

$$\Sigma_{(2\beta)}^*(\mathbf{k}, \omega_{\mathbf{k}}) \equiv \varepsilon_F(g-1) \left[\Phi_2(k/k_F) + i\Omega_2(k/k_F) \right] (a_s k_F)^2, \quad (4.4)$$

which are respectively directly related to the energy and to the damping of the quasi-particles. The quasi-particles are elementary excitations of the system which, in first approximation, can be considered as a gas of elementary excitations with an effective mass and a lifetime (linked to the damping) [135]. Galitskii [225] provided the analytical expressions of the real functions $\Phi_2(p)$ and $\Omega_2(p)$. These functions are recalled in (B.22) of appendix B and we give below only the Taylor expansion around $k = k_F$ (or $p = 1$) up to second order that will be useful in the following discussions:

$$\Phi_2(p) \underset{p \rightarrow 1}{\sim} \frac{4}{15\pi^2} (11 - 2 \ln 2) - \frac{16}{15\pi^2} (7 \ln 2 - 1)(p-1), \quad (4.5a)$$

$$\Omega_2(p) \underset{p \rightarrow 1}{\sim} \text{sgn}(1-p) \frac{2}{\pi} (1-p)^2. \quad (4.5b)$$

³ Here, we have chosen to integrate the diagram to exhibit the function B_{pp} and B_{hh} as intermediate steps of the calculation. By the same way, the second order self-energy could be estimated using the sum of the ph and hp contributions only.

Under these polynomial forms, we can directly link the coefficients to the chemical potential and to the effective mass at low density [192].

- The chemical potential is defined through the so-called Hugenholtz-van-Hove theorem [290]:

$$\mu \equiv \mu_{FG} + \text{Re}[\Sigma^*(\mathbf{k}, \omega_{\mathbf{k}})] \Big|_{k=k_F}. \quad (4.6a)$$

We will discuss more precisely this theorem in the following chapter. Using this property, we obtain at second order in $(a_s k_F)$:

$$\frac{\mu}{\mu_{FG}} = 1 + (g-1) \left[\frac{4}{3\pi} (a_s k_F) + \frac{4}{15\pi^2} (11 - 2 \ln 2) (a_s k_F)^2 + \dots \right]. \quad (4.6b)$$

Then, using the relation (3.17d) between the ground-state energy and the chemical potential given in (4.6b), we recover⁴ the Lee-Yang formula (1.28):

$$\frac{E}{E_{FG}} = \frac{1}{E_{FG}} \frac{g}{2\pi^2} \int_0^{k_F} k_F'^2 dk_F' \mu(k_F'), \quad (4.6c)$$

$$= 1 + (g-1) \left[\frac{10}{9\pi} (a_s k_F) + \frac{4}{21\pi^2} (11 - 2 \ln 2) (a_s k_F)^2 + \dots \right]. \quad (4.6d)$$

- The effective mass is defined as:

$$\frac{m}{m^*} \equiv 1 + \frac{m}{k_F} \frac{\partial \text{Re}[\Sigma^*(\mathbf{k}, \omega_{\mathbf{k}})]}{\partial k} \Big|_{k=k_F}, \quad (4.6e)$$

leading to:

$$\frac{m}{m^*} = 1 - (g-1) \frac{8}{15\pi^2} (7 \ln 2 - 1) (a_s k_F)^2 + \dots \quad (4.6f)$$

The real and imaginary parts of the second-order self-energy calculated numerically by integrating (4.3) are shown in figure 4.1. They are also compared to the analytical expression (B.22) given in appendix B. The agreement is a proof that we used the correct expressions for these functions once the regularization of divergences is properly treated (see appendix B). In panels (c) and (d), we have displayed the real and imaginary parts and their decomposition in terms of the pp and hh channels, i.e. the sum of the two is the total self-energy at second order in $(a_s k_F)$. We see that the proper description of quasi-particle properties requires the inclusion of both contributions to get the correct second-order behavior in $(a_s k_F)$. Then, above the Fermi surface, the lifetime of quasi-particles is determined only by the hh contributions whereas below it is given by the pp part of the self-energy. The imaginary part of each component does not change its sign. In particular, the hh contribution is positive⁵ as required by the stability of the hole state in the Fermi

⁴ Useful integral:

$$\frac{g}{2\pi^2} \int_0^{k_F} dk_F' k_F'^2 \varepsilon_F(a_s k_F')^n = \frac{5}{3} \frac{3}{n+5} E_{FG} (a_s k_F)^n.$$

⁵ Note that at first order in $(a_s k_F)$, the imaginary part of the self-energy is zero.

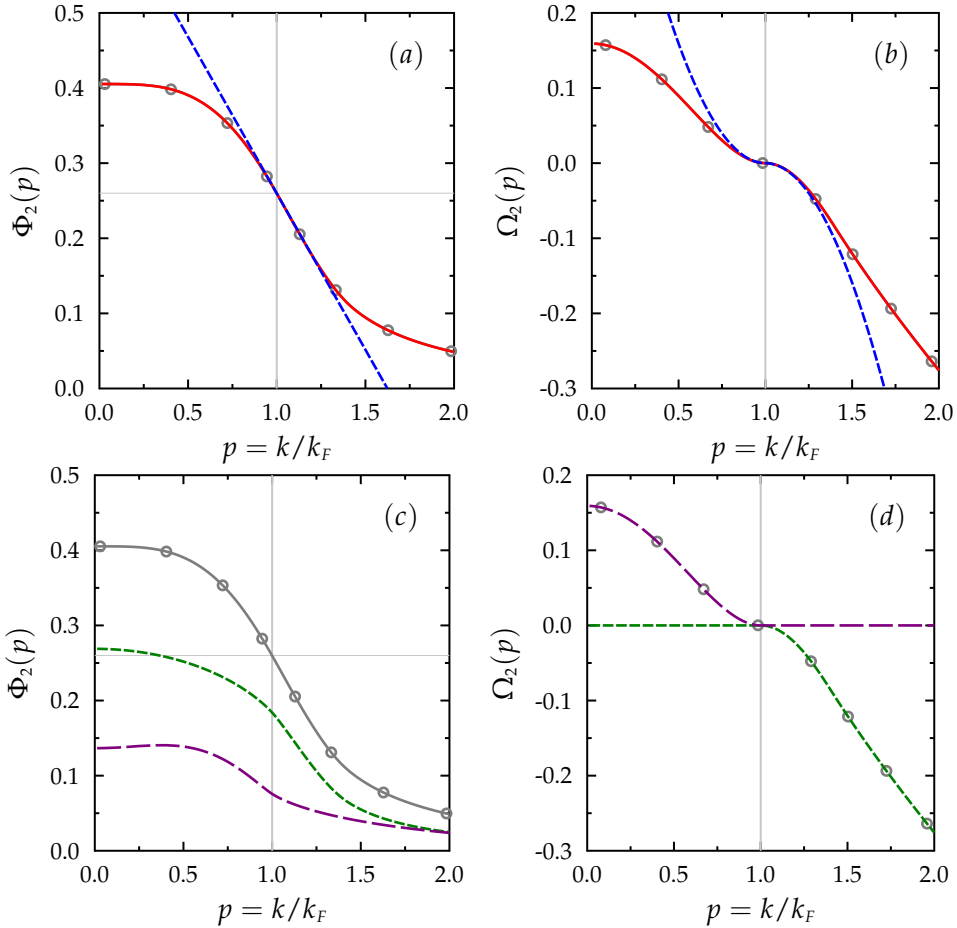


Figure 4.1: Real (left) and imaginary (right) parts of the second-order self-energy on-shell as a function of k/k_F obtained by numerical integration of (4.3) (red line). For comparison, the exact result obtained using analytical expressions given by (B.22) in appendix B are shown (gray circled line). Top: The blue dashed line corresponds to the Taylor expansion up to leading order around the Fermi momentum $k = k_F$ given by (4.5). Bottom: The green short dashed line corresponds to the particle-particle contribution and the purple long dashed line to the hole-hole contribution. Panels (c) and (d) illustrate that both pp and hh contributions are necessary to recover Φ_2 and Ω_2 .

sea. The negative contribution of the pp channel induces an exponential decay of the particle states.

Finally, by closing the dressed propagator, we properly recovered the energy contribution at second order:

$$\begin{aligned}
 \Sigma_{(2\beta)}^*(\mathbf{k}_1, \omega_{\mathbf{k}_1}) &\longrightarrow E_{(2b)} = \frac{g}{2} \int_{k_1} n_1 \Sigma_{(2)}^{pp}(\mathbf{k}_1, \omega_{\mathbf{k}_1}) \\
 &= \frac{g}{2} \int_{k_1} (1 - n_1) \Sigma_{(2)}^{hh}(\mathbf{k}_1, \omega_{\mathbf{k}_1}),
 \end{aligned}$$

where we have paid attention to close the diagram with a hole line for the configuration $2p1h$ and to close these with a particle line for $1p2h$ imposed by the directions of the arrow. As we have seen in chapter 2 the energy diagram (2b) is composed by $2p2h$. As mentioned before, the two energy contributions are identical (see appendix B) and must not be double counted.

THIRD ORDER

The third order contributions to the self-energy have been discussed in [232] and here we give a brief overview of this work. Diagrams (3 α), (3 β) and (3 γ) represented in table 4.1 vanish when evaluated on-shell. Diagrams (3 β') and (3 β'') can be related to the self-energy at lowest order through:

$$\Sigma_{(3\beta')}^*(\mathbf{k}, \omega) + \Sigma_{(3\beta'')}^*(\mathbf{k}, \omega) = -\Sigma_{(1)}^* \frac{\partial \Sigma_{(2)}^*}{\partial \omega} \Big|_{\omega=\omega_{\mathbf{k}}}, \quad (4.7)$$

and do not contribute to the quasi-particle properties at third order [232]. Finally, the contribution of the (on-shell) self-energy diagrams (3 δ) and (3 ϵ) were given as a numerical expansion in $(1-p)$ in [232]. Again, by closing the dressed propagator, we recover the different energy contributions at third order as depicted in table 4.1.

In [232], the authors have started directly from the self-energy and have obtained an energy per particle in good agreement with (2.27). The third order of the on-shell self-energy, i.e. without any dependence on energy, is given for each third-order diagram presented in table 4.1. Quasi-particle properties deduced by their calculations are also discussed. In particular they give the excitation energy, the damping rate, the renormalization constant of the Green's function, the effective mass, the heat capacity and the chemical potential, as well as numerical estimates of the self-energy related to the diagrams (3 δ) and (3 ϵ) of table 4.1. The self-energy is given as a polynomial in $(1-p)$, where $p = k/k_F$. The coefficients of this polynomial form are fitted on the numerical results. As was noted at second order, this polynomial expansion of the real part of $\Sigma_{(3)}^*$ to first order in $(1-p)$ is sufficient to calculate the chemical potential and henceforth the energy as well as the effective mass. Summing up the different contributions to $\Sigma_{(3)}^*$, we have [232]:

$$\begin{aligned} \frac{\text{Re}[\Sigma_{(3)}^*(\mathbf{k}, \omega_{\mathbf{k}})]}{(g-1)(a_s k_F)^3 \varepsilon_F} &\simeq \left[0.202 + 0.273(1-p) + \mathcal{O}(1-p)^2 \right] \\ &+ (g-3) \left[0.152 - 0.228(1-p) + \mathcal{O}(1-p)^2 \right]. \end{aligned} \quad (4.8a)$$

Starting from this polynomial form, we can link the coefficients to the chemical potential and effective mass (see (4.6) for an illustration with the second order):

$$\frac{\mu_{(3)}}{\mu_{FG}} = (g-1)(a_s k_F)^3 [0.202 + 0.152(g-3)], \quad (4.8b)$$

$$\frac{m_{(3)}^*}{m} = (g-1)(a_s k_F)^3 [0.137 - 0.114(g-3)]. \quad (4.8c)$$

The chemical potential and the effective mass up to third order are shown in figures 4.2 and 4.3. We see that, as for the MBPT result of the ground state energy (2.28), these quantities diverge when $(a_s k_F)$ becomes larger. The goal of the self-energy resummation is to obtain these quasi-particle properties for systems close to unitarity, i.e. obtain finite limits of them at unitary limit. In the following, we explore different strategies to make the resummation of the self-energy and obtain resummed expressions for the chemical potential and the effective mass.

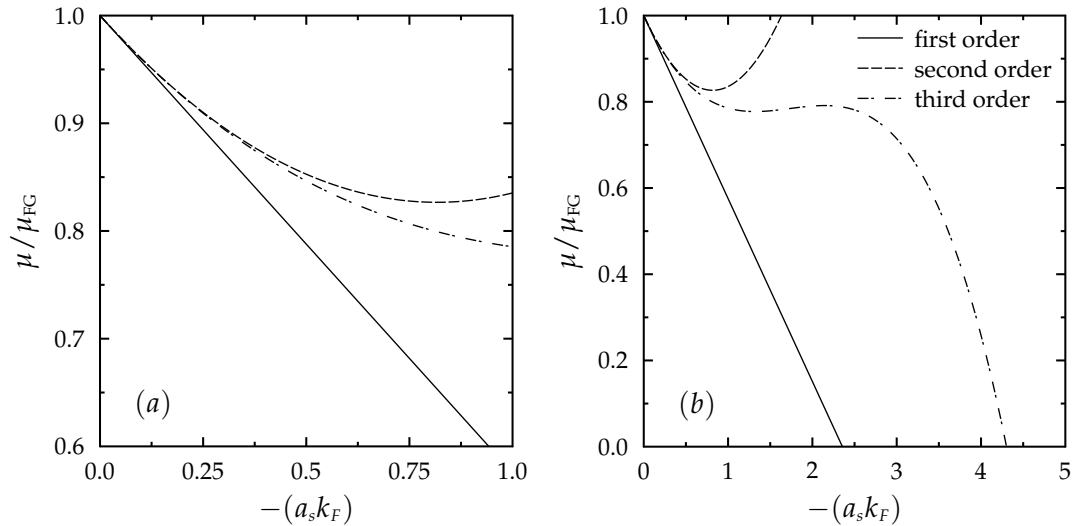


Figure 4.2: Chemical potential as a function of $-(a_s k_F)$. The panel (a) is a zoom of (b) for $(a_s k_F) < 1$. The solid, dashed, and dot-dashed line correspond respectively to the MBPT results [232] truncated at first, second, and third order in $(a_s k_F)$.

4.2

SELF-ENERGY RESUMMATION: PARTICLE-HOLE PROPAGATOR

The resummation of (on-shell) ladder ground-state energy diagrams under a geometric series was developed in [227] and completed in [237] (see chapter 2 for a detailed discussion). In this section, following the methodology employed in [227,237] to get a compact expression of the energy by resumming the particle-particle ladder energy diagrams, we explore the possibility to make the resummation directly at the level of the self-energy.

The goals are two:

1. provide a resummed expression consistent with the work [237] starting from the proper self-energy. This means recovering the analytical/numerical results obtained for the energy (Bertsch parameter and low-density limits obtained in section 2.3.a). This is a stringent test of the method and of the proper treatment of divergences;
2. find the quasi-particle properties of the systems described by the resummed proper self-energy: chemical potential, effective mass, etc...

This section is organized as follows. We first discuss the summation of all ladder diagrams and the difficulties appearing when considering off-shell effects, i.e. the energy dependence of the self-energy. Due to these difficulties, we concentrate after this preliminary discussion on the on-shell self-energy. Then, we discuss the possibility to make the resummation of particle-particle ladder self-energy diagrams under a geometric series form.

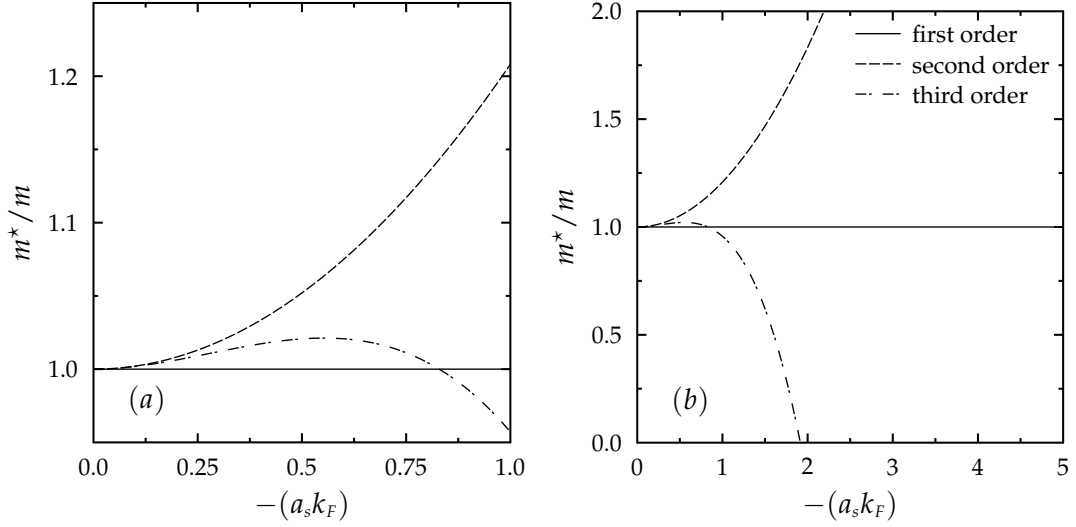


Figure 4.3: Same as figure 4.2 for the effective mass. Note that up to first order, $m^* = m$ since the self-energy at first order in $(a_s k_F)$ is constant.

4.2.A Discussion on the off-shell ladder diagrams resummation

We discuss here how the off-shell self-energy can eventually be resummed. We consider ladder diagrams composed by $(n - 1)pp$ loops and $1h$ line, i.e. a pp energy ladder diagram for which we have a broken $1h$ line. For instance, the diagrams (2 β) and (3 δ) shown in table 4.1 correspond respectively to the second and third order ladder diagrams for Σ_{pp}^* (considering only pp loops). The Feynman rules give for the third-order self-energy $\Sigma_{(3)}^{pp}$ (only ladder contribution with $2pp$ loops and $1h$ line):

$$\Sigma_{(3)}^{pp}(\mathbf{k}_1, \omega_1) = (-1)^{3-1} (g - 1) C_0^3 \int_2 G_2^+ \int_{3,4}^{\bar{\delta}} G_3^- G_4^- \int_{5,6}^{\bar{\delta}} G_5^- G_6^-. \quad (4.9)$$

We see that the integrations over each pp loop, $(3 + 4)$ and $(5 + 6)$ appearing in the $\bar{\delta}$ functions, are independent from each other and can be factorized under the hole integration of a particle (labeled by 2) by two equal terms. After factorization, we obtain:

$$\Sigma_{(3)}^{pp}(\mathbf{k}_1, \omega_1) = (g - 1) C_0 \int_2 G_2^+ \left[-C_0 L_{pp}(1; 2) \right]^2, \quad (4.10)$$

where the off-shell pp loop integral⁶ L_{pp} was introduced in (2.16). Similarly, at any order in perturbation, the n^{th} order ladder pp diagram (composed by $(n - 1)pp$ loops and $1h$ line) contribution to the pp self-energy can be recast as:

$$\Sigma_{(n)}^{pp}(\mathbf{k}_1, \omega_1) = (g - 1) C_0 \int_2 G_2^+ \left[-C_0 L_{pp}(1; 2) \right]^{n-1}. \quad (4.11)$$

⁶ By definition, this loop corresponds to the second-order pp contribution in the self-energy:

$$\Sigma_{(2)}^{pp}(\mathbf{k}_1, \omega_1) = (g - 1) C_0 \int_2 G_2^+ \left[-C_0 L_{pp}(1; 2) \right].$$

Note that, to estimate the n^{th} order pp self-energy contribution, as done in chapter 2 for the ground-state energy, we have made the approximation of non self-consistency where the Green's functions G appearing in the integrals is approximated by the one of the non-interacting system⁷. Summing up all orders under a geometric series, we can write the resummed pp self-energy as:

$$\begin{aligned}\Sigma_{pp}^*(\mathbf{k}_1, \omega_1) &= \sum_{n=1}^{\infty} \Sigma_{(n)}^{pp}(\mathbf{k}_1, \omega_1) \\ &= (g-1)C_0 \int_2 \frac{G_2^+}{1 + C_0 L_{pp}(1; 2)}.\end{aligned}\quad (4.12)$$

The estimation of this self-energy requires to know the off-shell pp loop integrals L_{pp} . This function is rather complex [291–293] and it seems tricky to find its poles (analytically) in order to proceed with the contour integration on ω_2 . Following the works [227,237], we can first make one further approximation by treating the self-energy on-shell, that is to say imposing $\omega_1 = \omega_{\mathbf{k}_1} = \mathbf{k}_1^2/(2m)$. Doing this approximation, we loose the energy dependence of the self-energy which could have an important role in nuclear matter [294]. In the following, we focus on the on-shell resummation of the self-energy.

4.2.B Resummation of the on-shell particle-particle self-energy

The n^{th} order of the pp contribution to the on-shell self-energy is given by contour integration on ω_2 and considering $\omega_1 = \omega_{\mathbf{k}_1}$ in (4.11). Using the dimensionless variables defined by (2.19), we obtain:

$$\Sigma_{(n)}^{pp}(\mathbf{k}_1, \omega_{\mathbf{k}_1}) = (g-1)C_0 \int_{k_2} n_2 B_{pp}(s, t)^{n-1}, \quad (4.13)$$

where we have introduced the on-shell pp loops integral B_{pp} defined by (2.21) and explicitly calculated in appendices B and C treating properly the divergences. Again, summing up to all orders under a geometric series, we can write the on-shell resummed pp self-energy as:

$$\begin{aligned}\Sigma_{pp}^*(\mathbf{k}_1, \omega_{\mathbf{k}_1}) &= \sum_{n=1}^{\infty} \Sigma_{(n)}^{pp}(\mathbf{k}_1, \omega_{\mathbf{k}_1}) \\ &= (g-1)C_0 \int_{k_2} \frac{n_2}{1 - B_{pp}(s, t)}.\end{aligned}\quad (4.14)$$

By construction, the expansion in perturbation at second order gives:

$$\Sigma_{pp}^*(\mathbf{k}, \omega_{\mathbf{k}}) = \Sigma_{(1)}^* + \Sigma_{(2)}^{pp}(\mathbf{k}, \omega_{\mathbf{k}}) + \mathcal{O}(a_s k_F)^3, \quad (4.15)$$

where $\Sigma_{(2)}^{pp}$ is the second-order contribution of the pp component to the (on-shell) self-energy (4.3) (see figure 4.1.c and 4.1.d). In the following, we refer to this re-

⁷ See discussion in [192] (pp. 149-150) and in [225] for more details about this approximation which is valid for dilute systems.

summation scheme as GR_{pp} for *Geometric series Resummation* of the pp part of the self-energy.

Before continuing the discussion, a critical analysis of the on-shell GR_{pp} self-energy can be made. The following points deserve to be underlined:

- It is interesting to mention that, taking the off-shell resummed pp self-energy given by (4.12) on-shell and doing the contour integration on ω_2 , we obtain the same results given by (4.14) where the only pole is given by G_2^+ .
- The unitary limit leads to a finite resummed pp self-energy:

$$\Sigma_{pp}^*(\mathbf{k}_1, \omega_{\mathbf{k}_1}) \xrightarrow{|a_s k_F| \rightarrow \infty} -2(g-1)\varepsilon_F \int_{p_2} \frac{n_2}{\Pi_{pp}(\mathbf{s}, \mathbf{t})}, \quad (4.16)$$

where we have used the function Π_{pp} defined as $B_{pp} = mC_0 k_F \Pi_{pp}$ and where Π_{pp} is given in appendix B.

- We recover the resummed ground-state energy (2.30) from the pp ladder diagrams resummation by closing the on-shell self-energy (4.14) by a hole line, i.e. multiplying (4.14) by G_1^+ and performing the integration on (\mathbf{k}_1, ω_1) . We will discuss this particular point in more details below.
- By construction, the perturbation expansion gives the correct second-order contribution to the energy without considering the hh component of the self-energy:

$$E_{pp} = E_{(1)} + E_{(2)} + \mathcal{O}(a_s k_F)^3. \quad (4.17)$$

However, one drawback of considering only this resummed pp self-energy is that we have no information on the quasi-particle properties at low density since the resummed pp self-energy does not reproduce by itself the second-order contribution of the total self-energy (see figure 4.1.c and 4.1.d). The hh self-energy is therefore also required to describe the correct quasi-particles properties. Below, we discuss the resummation of the hh ladder diagrams to reproduce the correct (on-shell) self-energy up to second order at low density.

4.2.c Resummation of the on-shell hole-hole self-energy

Here, we follow the same strategy as the one we used to obtain the GR_{pp} self-energy except that we consider now the n^{th} order of the (on-shell) hh self-energy ladder diagrams (composed by $(n-1)hh$ loppes and $1p$ line). Following (4.13), we write this self-energy as:

$$\Sigma_{(n)}^{hh}(\mathbf{k}_1, \omega_{\mathbf{k}_1}) = (g-1)C_0 \int_{k_2} (1-n_2) B_{hh}(\mathbf{s}, \mathbf{t})^{n-1}, \quad (4.18)$$

where we have introduced the on-shell hh loops integral B_{hh} (see chapter 2) explicitly calculated in appendix B. Again, summing up all orders under a geometric series, we can write the on-shell resummed hh self-energy as:

$$\begin{aligned}\Sigma_{hh}^*(\mathbf{k}_1, \omega_{\mathbf{k}_1}) &= \sum_{n=2}^{\infty} \Sigma_{(n)}^{hh}(\mathbf{k}_1, \omega_{\mathbf{k}_1}) \\ &= (g-1)C_0 \int_{k_2} (1-n_2) \left[\frac{1}{1-B_{hh}(\mathbf{s}, \mathbf{t})} - 1 \right].\end{aligned}\quad (4.19)$$

Note that the sum starts from $n = 2$ because the first-order self-energy is defined by considering only the integration on the hole-states⁸ (or Hartree-Fock contribution). The second term in (4.19) compensates the fact that the first term is obtained by summing up from $n = 1$ to write the result as a geometric series form.

By construction, the expansion in perturbation at second order in $(a_s k_F)$ of Σ_{hh}^* gives:

$$\Sigma_{hh}^*(\mathbf{k}, \omega_{\mathbf{k}}) = \Sigma_{(2)}^{hh}(\mathbf{k}, \omega_{\mathbf{k}}) + \mathcal{O}(a_s k_F)^3, \quad (4.20)$$

where $\Sigma_{(2)}^{hh}$ is the second-order contribution of the hh component to the (on-shell) self-energy that is entering in (4.3). As a result, in the low-density limit, the sum of the resummed pp and hh self-energy given respectively by (4.14) and (4.19) leads to the correct self-energy up to second order, i.e. :

$$\Sigma_{pp}^*(\mathbf{k}, \omega_{\mathbf{k}}) + \Sigma_{hh}^*(\mathbf{k}, \omega_{\mathbf{k}}) = \Sigma_{(1)}^* + \Sigma_{(2)}^*(\mathbf{k}, \omega_{\mathbf{k}}) + \mathcal{O}(a_s k_F)^3. \quad (4.21)$$

Note that at unitarity, the hh self-energy diverges due to the second term of (4.19):

$$\Sigma_{hh}^*(\mathbf{k}_1, \omega_{\mathbf{k}_1}) \Big|_{|a_s k_F| \rightarrow \infty} \sim -(g-1)C_0 \int_{k_2} (1-n_2). \quad (4.22)$$

This problem suggests that the chosen resummation scheme is unphysical. This will be also discussed later on. Note that in [237], when working directly on the energy, the authors proposed to remove the first and second orders in the hh resummed ground-state energy because it is already accounted for in the pp part [see (4.17)]. This has also the advantage to remove the divergence (see the critical analysis below).

4.2.D Critical discussions

Before discussing the combination of the resummed pp and hh self-energy and the associated quasi-particle properties in the next subsection, we can make some remarks. To estimate the energy, the self-energy should be multiplied either by the particle (G^+) or hole (G^-) propagator and then integrated on the available phase-space. It is important in particular to note that Σ_{pp}^* and Σ_{hh}^* should be integrated

⁸ More precisely, the first order energy diagram (1a), for which $n = 1$, is composed by two hole lines (see the Feynman rules for the self-energy introduced in chapter 2) and consequently, the associated self-energy contribution from the hh channel (consisting here to break 1p line) does not exist.

on different contours. For instance, the second-order energy contribution can be written, keeping the ω dependence of the self-energy discussed before, as:

$$\begin{aligned} E_{(2)} &= \frac{g}{2}(g-1)C_0k_F^6 \oint_1 G^\eta(1)\Sigma_{(2)}^*(\mathbf{k}_1, \omega_1), \\ &= \frac{g}{2}(g-1)C_0k_F^6 \oint_{k_1} \begin{cases} n_1 \Sigma_{(2)}^{pp}(\mathbf{k}_1, \omega_{k_1}) & \text{if } \eta = +, \\ (1-n_1)\Sigma_{(2)}^{hh}(\mathbf{k}_1, \omega_{k_1}) & \text{if } \eta = -. \end{cases} \end{aligned} \quad (4.23)$$

The contour integration on ω_1 from the first to the second line of this equation is straightforward since the off-shell pp (contour integration on the hole states: upper complex plane) and hh (contour integration on the particle states: lower complex plane) self-energy has no pole. This point is discussed at the end of section 4.2.a. This is a crucial property. Indeed, we see that in order to estimate the energy up to second order, we only need one of the self-energy components. However, at second order, the quasi-particle properties can only be properly deduced if both $\Sigma_{(2)}^{pp}$ and $\Sigma_{(2)}^{hh}$ are simultaneously taken into account (see for instance figures 4.1.c and 4.1.d). This is also the case in the ladder approximation and we should combine the pp and hh contributions of the resummed self-energy to get the quasi-particle properties. This point is discussed in the next section and, as we will see, this complexifies the resummed form of the on-shell self-energy.

QUASI-PARTICLE PROPERTIES FROM

NAIVE SEPARATE RESUMMATION OF Σ_{pp}^* AND Σ_{hh}^*

We now construct the total resummed self-energy Σ_{pp+hh}^* , referred as the GR_{pp+hh} self-energy, simply by adding the pp and hh self-energies given respectively by (4.14) and (4.19):

$$\Sigma_{pp+hh}^*(\mathbf{k}, \omega_{\mathbf{k}}) = \Sigma_{pp}^*(\mathbf{k}, \omega_{\mathbf{k}}) + \Sigma_{hh}^*(\mathbf{k}, \omega_{\mathbf{k}}). \quad (4.24)$$

This brute strategy reproduces by construction the first and second-order self-energy at low density as shown by (4.21). Of course, this naive summation of the two contributions, as we mentioned above, will also diverge at unitarity due to the divergence of the Σ_{hh}^* term. Nevertheless, this strategy can eventually be used away from unitarity and has the correct low-density limit. We also have performed the direct numerical integration of (4.24) using (4.14) and (4.19). The result is compared to the analytical expression for different values of $(a_s k_F)$ in figures 4.4 and 4.5. We observe that, as we expect at very low density, the resummed self-energy is close to the result obtained with (4.21), i.e. keeping only the first two terms (figures 4.4.a and 4.5.a). This figure illustrates again that the proper self-energy is obtained at low density only if both pp and hh contributions are treated simultaneously.

GROUND STATE ENERGY FROM THE SELF-ENERGY Σ_{pp+hh}^*

As mentioned above, the resummed ground-state energy (given by ladder diagrams only, without cross-terms between the pp and hh components) can be obtained by integrating $G^+\Sigma_{pp}^*$ (or $G^-\Sigma_{hh}^*$). More precisely, the resummed pp ground-state energy can be written as (see (4.23) for an illustration with the second order):

$$E = \frac{g}{2}(g-1)C_0k_F^6 \oint_1 G_1^+\Sigma_{pp+hh}^*(\mathbf{k}_1, \omega_{k_1}) = \frac{g}{2}(g-1)C_0k_F^6 \oint_{k_1} n_1 \Sigma_{pp}^*(\mathbf{k}_1, \omega_{k_1}). \quad (4.25)$$

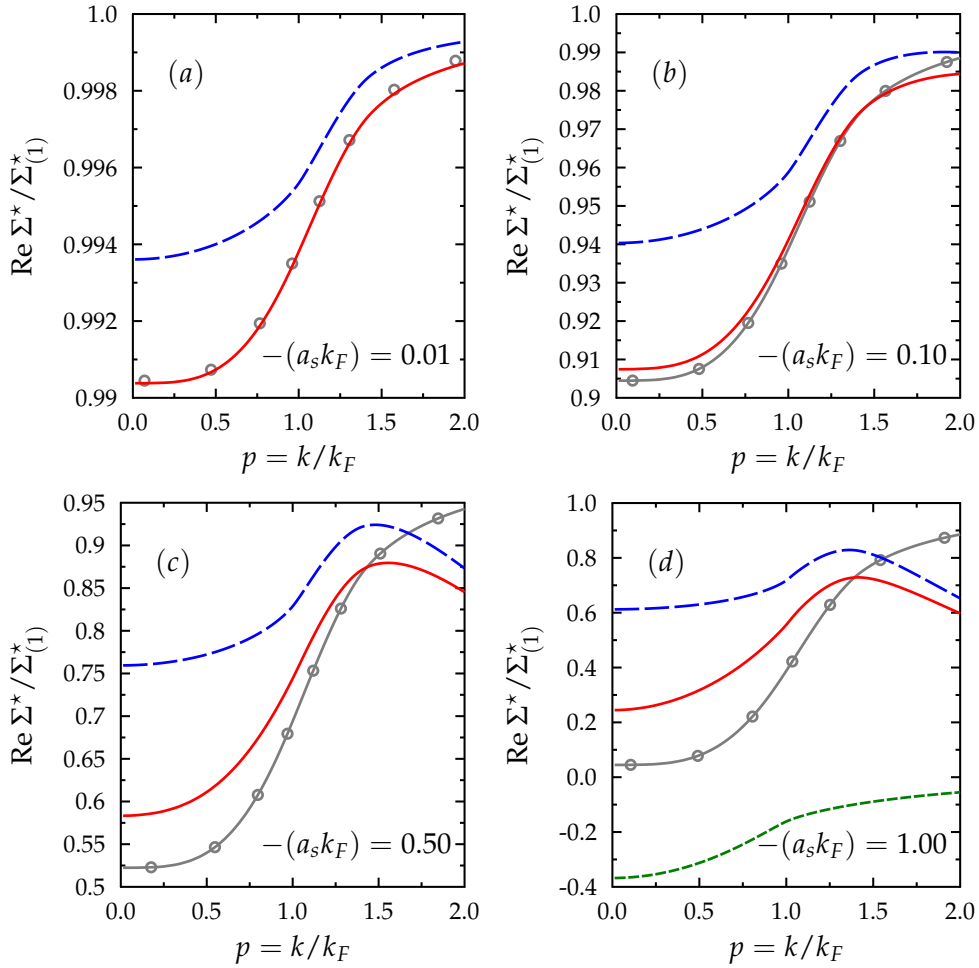


Figure 4.4: Real part of the resummed self-energy given by (4.24) in unit of $\Sigma_{(1)}^*$ as a function of $p = k/k_F$ (red solid line) at $-(a_s k_F) = \{0.01; 0.1; 0.5; 1.00\}$. The blue long-dashed line corresponds to its pp component and the green short-dashed line to its hh component (shown only at $-(a_s k_F) = 1.00$ because for other $(a_s k_F)$, the green short-dashed line is out of the limit of the plot). Note that the contribution of the hh component is very small at low density (corresponding to the difference between the blue long-dashed line and the red solid line) and increases as the density increases. As a consequence, it only appears in panel (d). For reference, we show the sum of the first and second order self-energy (gray open circles line).

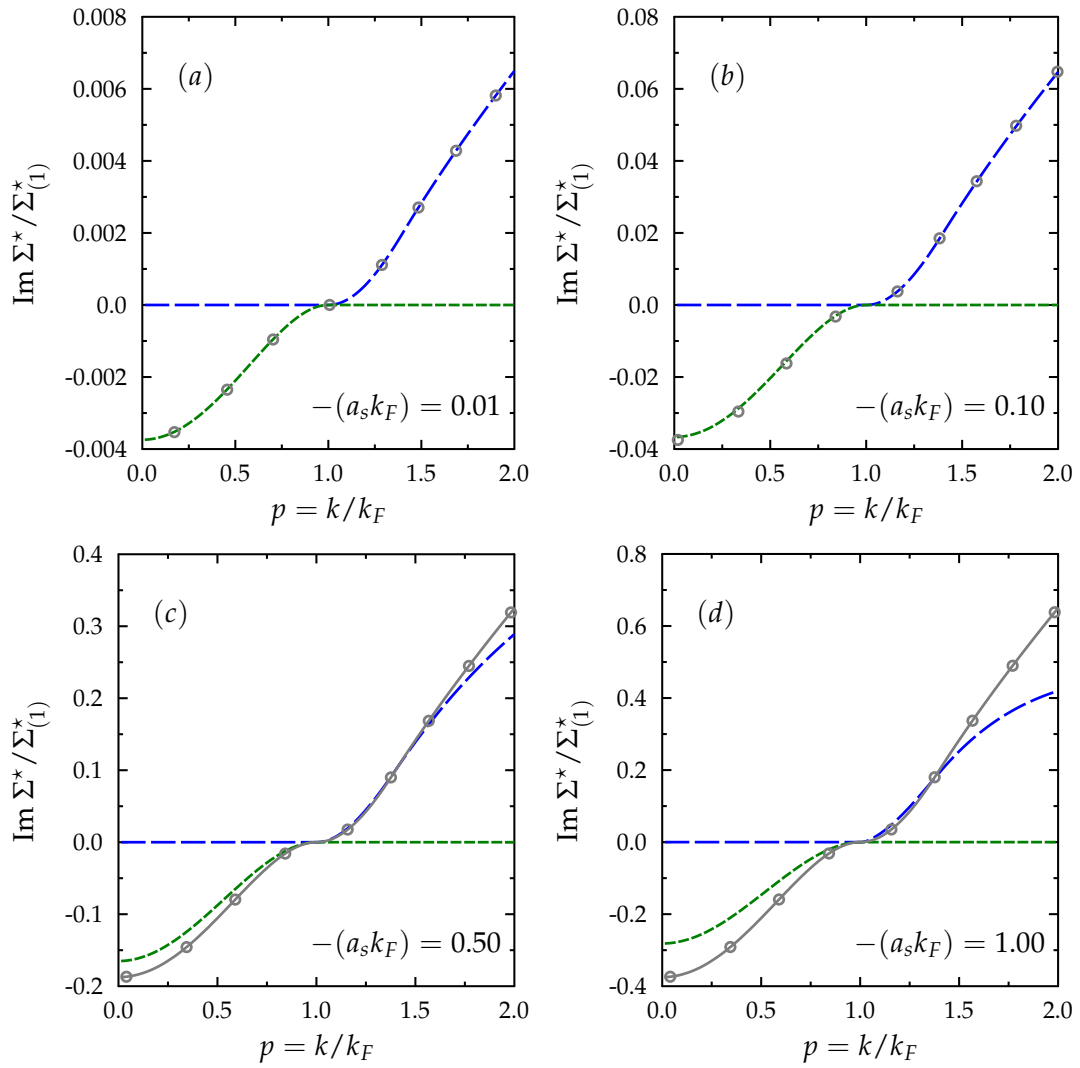


Figure 4.5: Same as figure 4.4 for the imaginary part of the self-energy. For representation issues, the imaginary part of the resummed self-energy given by (4.24) is not shown because it is exactly equal to the hh (respectively pp) contribution for $p < 1$ (respectively $p > 1$).

Taking the integral form of the resummed self-energy given by (4.14) for the pp part we properly recover (2.30). This proves that the self-energy resummation is consistent with the pp ladder resummation for the energy described in section 2.3.a.

Note that, making the Taylor expansion in $(a_s k_F)$, this expression is valid up to second order, i.e. $E = E_{(1)} + E_{(2)} + \mathcal{O}(a_s k_F)^3$ without resorting to the hh component of the resummed self-energy. Thus, as mentioned in [237], the hh resummed ground state energy starts to contribute only at third order in $(a_s k_F)$. This justifies the subtraction of the first and second order terms made in [237] of E_{hh} to avoid double counting. For the self-energy however, the second-order term should be kept to get the proper quasi-particle properties and here we have to subtract only the first term [see (4.19)].

GROUND STATE ENERGY FROM QUASI-PARTICLE PROPERTIES

The information on quasi-particles (chemical potential, effective mass, etc...) is encoded in the self-energy. Following the decomposition in terms of pp and hh components of the self-energy given by (4.24) with (4.14) and (4.19), we introduce the pp and hh contributions to the chemical potential and effective mass:

$$\mu_{xx} = \Sigma_{xx}^*(\mathbf{k}, \omega_{\mathbf{k}}) \Big|_{k=k_F}, \quad (4.26)$$

$$\frac{m_{xx}^*}{m} = \frac{k_F}{m} \left[\frac{d\text{Re} [\Sigma_{xx}^*(\mathbf{k}, \omega_{\mathbf{k}})]}{dk} \Big|_{k=k_F} \right]^{-1}, \quad (4.27)$$

where $xx = pp$ or hh . By construction, the total chemical potential and the effective mass obtained with the resummed self-energy (4.24) are $\mu = \mu_{FG} + \mu_{pp} + \mu_{hh}$ and $m/m^* = 1 + m/m_{pp}^* + m/m_{hh}^*$. These quantities are respectively shown in figures 4.6 and 4.7 as a function of $(a_s k_F)$. We remark that:

1. the proper low-density limit is only obtained again if the pp and hh contributions are simultaneously treated;
2. keeping solely the pp contribution does not give the proper low-density limit for μ or m^*
3. the resummed expression starts to deviate rather fast from low density around $|a_s k_F| \sim 0.5$.

Using the relation between the chemical potential and the ground-state energy, we can decompose the contribution of the pp and hh components such that $E = E_{FG} + E_{pp} + E_{hh}$ with:

$$E_{xx} = \frac{g}{2\pi^2} \int_0^{k_F} dk'_F k'_F \mu_{xx}(k'_F). \quad (4.28)$$

In figure 4.7.b, the ground-state energy obtained using this method is shown for various $(a_s k_F)$. We can check that, at low density, both E_{pp+hh} or E_{pp} match the low-density results given by (4.6). This is a further verification of the numerical treatment of integrals considered to estimate the resummed quantities from the proper self-energy with the proper regularization of divergences. Note that only the pp part of these quantities have a finite limit when $|a_s k_F| \rightarrow \infty$. This is the

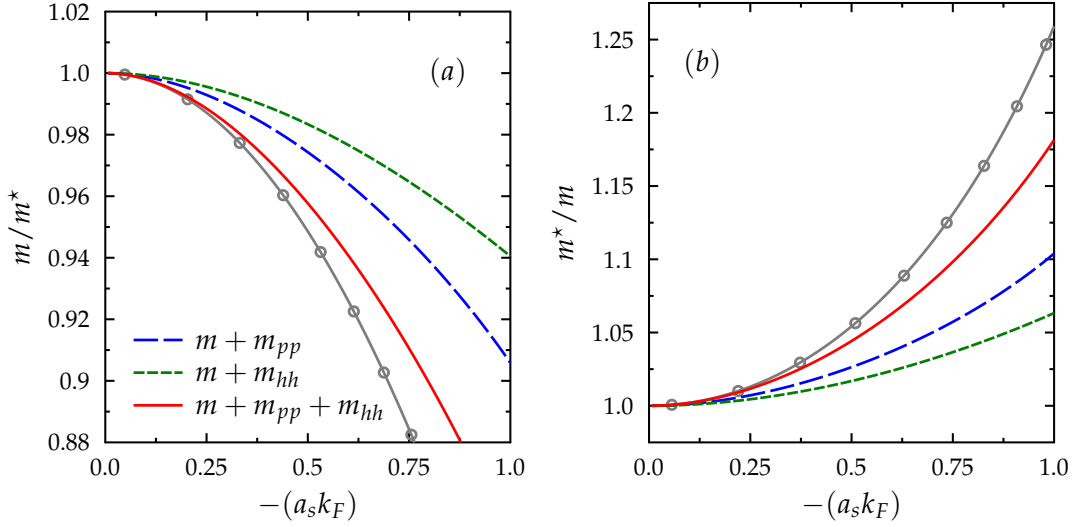


Figure 4.6: The effective mass m^* and its inverse in unit of the bare mass m obtained from the resummed self-energy (4.24) as a function of $(a_s k_F)$. The pp and hh contributions are also shown using the same convention for the lines as in figure 4.4. The gray circles correspond to the second order expansion (4.6).

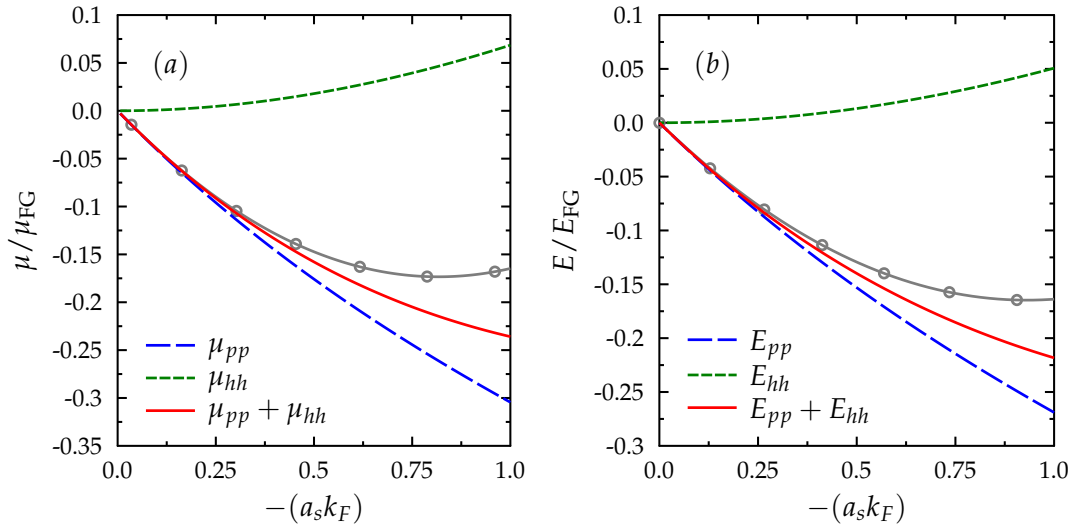


Figure 4.7: (a) The chemical potential μ (without the free gas part) and (b) the energy (without the free gas part) obtained from the resummed self-energy (4.24) as a function of $(a_s k_F)$. The convention for the lines are the same as in figure 4.6.

reason why we have only displayed in figures 4.6 and 4.7 μ , E and m^* obtained with Σ_{pp+hh}^* at finite values of $(a_s k_F)$.

In the present section, we have used a simple strategy that consists in directly adding two independent contributions obtained by simple geometric resummation of the pp or hh diagrams. This approach has the advantage to properly lead to the correct low-density limit. As we have seen, this strategy leads to divergences of physical quantities as $(a_s k_F)$ increases. It also has a second disadvantage that has not yet been mentioned. Starting from Σ_{pp+hh}^* we can deduce the chemical potential μ and eventually use the Hugenholtz-van-Hove (HvH) theorem to obtain the corresponding energy. This gives an energy that differs in particular from any of the energies obtained in section 2.3.a, and in particular it differs from the GEI approx-

imation. We show below that an alternative strategy can be employed to account simultaneously for the pp and hh contributions, while, using the HvH theorem, the GEI energy can be recovered. Note that, the recovery of one of the resummed expressions given in chapter 2 or 3 is not an absolute necessity. However, imposing this constraint has some practical advantages. For instance, this automatically insures the non-divergence of the energy for infinite ($a_s k_F$).

4.3

SELF-ENERGY RESUMMATION: TEST-PARTICLE TECHNIQUE

From the study made in the previous section, we have two important conclusions:

1. pp ladder diagrams should not be considered alone. To get the quasi-particle properties, pp and hh ladders should be included simultaneously.
2. Naive addition of resummed pp and hh self-energy (GR_{pp+hh}) (i) leads to double counting that should be removed by hand, and (ii) generates divergences of the physical quantities at large ($a_s k_F$).

To solve these problems, we follow the strategy introduced in [240] where a resummed expression of the self-energy was obtained considering simultaneously diagrams composed by multiple pp and hh loops. The goals of the present section is first to recover the analytical/numerical results obtained in [240]; and then to find the quasi-particle properties of a system described by the resummed proper self-energy: chemical potential, effective mass, etc...

This section is organized as follows. We first discuss the methodology employed in [240], namely the test-particle insertion method, and make the connection with the work presented in the last section on the naive resummation of the self-energy.

4.3.A Test-particle insertion technique

SINGLE-PARTICLE POTENTIAL AS DERIVATIVE FUNCTIONAL OF THE ENERGY

In this section, we follow the technique used in [240] where a test particle is added to the Fermi sea. Then the self-energy is obtained from the difference of energy of the systems with and without the test particle. This technique has clear practical advantages that are illustrated below. We first discuss the effect of the addition of a test particle with momentum \mathbf{k} (creation of a hole excitation if $k < k_F$ and of a particle excitation if $k > k_F$) on the occupation number n_i . The density of the system is decreased for a hole excitation (sign $-$) and increased for a particle excitation (sign $+$), i.e. :

$$\rho = g \int_{k_i} n_i \longmapsto \rho \pm \delta\rho(\mathbf{k}) = g \int_{k_i} n_i + \delta n_i(\mathbf{k}). \quad (4.29)$$

Making the inverse Fourier transform of (4.29), we obtain:

$$\pm(2\pi)^3 \delta(\mathbf{k}_i - \mathbf{k}) = g \delta n_i(\mathbf{k}). \quad (4.30)$$

It is convenient to introduce⁹ $\eta = \pm 1$ ($-$ for $k < k_F$ and $+$ for $k > k_F$). Finally, adding a test particle with momentum \mathbf{k} in the system induces an infinitesimal change in the occupation number in (2.36) given by:

$$n_i \mapsto n_i(\eta) = n_i + \frac{\eta}{g}(2\pi)^3 \delta(\mathbf{k}_i - \mathbf{k}) = n_i + \frac{\eta}{g} \bar{\delta}(\mathbf{k}_i - \mathbf{k}). \quad (4.31)$$

We recall that the notation $\bar{\delta}$ is the Dirac distribution adapted to the convention of the Fourier transform adopted in the text, i.e. including the 2π factors such that $\int_x \bar{\delta}(x) = 1$. The total energy density changes, to first order in the infinitesimal parameter $\eta \propto 1/V$, as:

$$\begin{aligned} E[\rho] \mapsto E[\rho + \delta\rho(\mathbf{k})] &= E[\rho] + \int_{\mathbf{k}'} \frac{\delta E}{\delta\rho(\mathbf{k}')} \delta\rho(\mathbf{k}) \\ &\equiv E[\rho] + \eta \Sigma^*(\mathbf{k}), \end{aligned} \quad (4.32)$$

where $\Sigma^*(\mathbf{k}) = U(\mathbf{k}) + iW(\mathbf{k})$ denotes the on-shell complex-valued single-particle potential (equivalent to the on-shell proper self-energy of the system). Therefore, we see that the addition of a particle or hole using (4.31) gives access to the proper self-energy through (4.32).

This approach will be referred below as the test-particle approach. In particular, at $k = k_F$, this expression is also consistent with the definition of the chemical potential [$\mu = \mu_{FG} + \Sigma^*(k_F)$] since, adding a particle at the Fermi surface leads to a change of energy $E \rightarrow E \pm \mu$. Below, we illustrate this method for the free Fermi gas single-particle energy as well as for the first and second order of the self-energy obtained previously in MBPT context.

FREE FERMI GAS

First, we estimate the change in energy by adding/removing a test particle in the free Fermi gas. Starting from (2.10) and applying the methodology in which we make the replacement $n_i \rightarrow n_i(\eta)$, we obtain the perturbed energy:

$$\begin{aligned} E_{FG}(\eta, \mathbf{k}) &= g \int_{k_1} e_1 n_1(\eta) = g \int_{k_1} e_1 n_1 + g \int_{k_1} e_1 \delta n_1, \\ &= E_{FG} + \eta \int_{k_1} e_1 \bar{\delta}(\mathbf{k}_1 - \mathbf{k}) = E_{FG} + \eta e(\mathbf{k}), \end{aligned} \quad (4.33)$$

where $E_{FG} = E_{FG}(\eta = 0)$. We remark that, as expected, the change in energy by adding or removing a free particle in the non-interacting Fermi system is directly given by the single-particle energy $e(\mathbf{k}) = \mathbf{k}^2/2m$.

FIRST ORDER

Now, we estimate the change in the first-order energy using the test-particle technique. The energy of the system with an additional test particle can be obtained from (2.12) with the substitution $n_1 \rightarrow n_1(\eta)$ and retaining the linear order in η :

$$\begin{aligned} E_{(1)}(\eta, \mathbf{k}) &= \frac{g}{2}(g-1)C_0 \left[\int_{k_1} n_1(\eta) \right]^2 = \frac{g}{2}(g-1)C_0 \left[\int_{k_1} n_1 + \delta n_1(\mathbf{k}) \right]^2 \\ &= E_{(1)} + \eta \Sigma_{(1)}^*(\mathbf{k}) + \mathcal{O}(\eta^2), \end{aligned} \quad (4.34)$$

⁹ In fact, $|\eta|$ is the inverse of the unit volume and should be considered as an infinitesimal parameter.

where we have introduced the generic notation $E_{(n)} \equiv E_{(n)}(\eta = 0)$ for the n^{th} order contribution in $(a_s k_F)^n$ to the ground-state energy. Note that, according to the Landau Fermi liquid theory [135,224], we verify [see (4.29) and (4.32)] automatically:

$$\eta \Sigma_{(1)}^*(\mathbf{k}) = \frac{\delta E_{(1)}}{\delta n_1(\mathbf{k})}. \quad (4.35)$$

SECOND ORDER

In perturbation theory, the ground-state energy at second order can be written as [see (2.18)]:

$$E_{(2)} = \frac{g}{2}(g-1)C_0^2 \int_{k_1, k_2} \int_{k_3, k_4}^{\bar{\delta}} \frac{n_1 n_2 (1-n_3)(1-n_4)}{e_1 + e_2 - e_3 - e_4}. \quad (4.36)$$

Now, using the prescription (4.31):

$$n_1 n_2 (1-n_3)(1-n_4) \mapsto n_1 n_2 (1-n_3)(1-n_4) + \begin{bmatrix} + \delta n_1 n_2 (1-n_3)(1-n_4) \\ + n_1 \delta n_2 (1-n_3)(1-n_4) \\ - n_1 n_2 \delta n_3 (1-n_4) \\ - n_1 n_2 (1-n_3) \delta n_4 \end{bmatrix},$$

where δn_i is given by (4.30). This gives the difference of energy to linear order in η :

$$\begin{aligned} E_{(2)}(\eta, \mathbf{k}) - E_{(2)} &= \frac{\eta}{2}(g-1)C_0^2 \int_{k_1, k_2} \int_{k_3, k_4}^{\bar{\delta}} \bar{\delta}(\mathbf{k}_1 - \mathbf{k}) \frac{n_2(1-n_3)(1-n_4)}{e_1 + e_2 - e_3 - e_4} \\ &+ \frac{\eta}{2}(g-1)C_0^2 \int_{k_1, k_2} \int_{k_3, k_4}^{\bar{\delta}} \bar{\delta}(\mathbf{k}_2 - \mathbf{k}) \frac{n_1(1-n_3)(1-n_4)}{e_1 + e_2 - e_3 - e_4} \\ &- \frac{\eta}{2}(g-1)C_0^2 \int_{k_1, k_2} \int_{k_3, k_4}^{\bar{\delta}} \bar{\delta}(\mathbf{k}_3 - \mathbf{k}) \frac{n_1 n_2 (1-n_4)}{e_1 + e_2 - e_3 - e_4} \\ &- \frac{\eta}{2}(g-1)C_0^2 \int_{k_1, k_2} \int_{k_3, k_4}^{\bar{\delta}} \bar{\delta}(\mathbf{k}_4 - \mathbf{k}) \frac{n_1 n_2 (1-n_3)}{e_1 + e_2 - e_3 - e_4}. \end{aligned} \quad (4.37)$$

With a simple change of variable, we obtain:

$$\begin{aligned} E_{(2)}(\eta, \mathbf{k}_1) - E_{(2)} &= \eta(g-1)C_0 \int_{k_2} [n_2 B_{pp}(s, t) + (1-n_2)B_{hh}(s, t)] \\ &= \sum_{ij} \int_{\mathbf{k}} \frac{\delta E_{(2)}}{\delta n_j(\mathbf{k})} \delta n_i(\mathbf{k}_1) = \eta \Sigma_{(2)}^*(\mathbf{k}_1), \end{aligned} \quad (4.38)$$

where, using the definition of the effective pp and hh interaction B_{pp} and B_{hh} given in appendix C [and the dimensionless variables given by (2.19)] we recover the second-order self-energy (4.3). The functional derivative of the energy can also be recovered after a change of variables¹⁰ from (4.36) using the property:

$$\frac{\delta N_i(\mathbf{k})}{\delta N_j(\mathbf{k}')} = \bar{\delta}(\mathbf{k} - \mathbf{k}') \delta_{ij}. \quad (4.39)$$

¹⁰ Note that we have to divide by the degeneracy g due to the reasoning made in (4.29).

In [224], this relation has been first obtained directly using functional derivative. After that, the authors have made direct link with the Landau theory of Fermi liquids [128] to deduce the effective mass, the sound velocity and the chemical potential up to second order in $(a_s k_F)$. These examples show that the self-energy can be obtained at a given order in perturbation theory starting directly from the expression of the ground-state energy in terms of the unperturbed occupation numbers n_i . The test-particle technique is therefore a practical method to obtain the self-energy, and by extension the quasi-particle properties, associated to a n^{th} order energy contribution. In particular, this method allows one to obtain the resummed self-energy coherently with the resummed ground-state energy obtained in chapter 2 from the resummation of ladder diagrams as illustrated below.

4.3.B Resummed self-energy using the test-particle approach

In chapter 2, we have seen that the resummed ground-state energy obtained from ladder resummation of diagrams can be written as:

$$E = E_{FG} + \frac{g}{2}(g-1) \int_{k_1, k_2} n_1 n_2 \Gamma(s, t), \quad (4.40)$$

where Γ is given by (2.52) in terms of the bubble functions B_0, B_1, B_2 . If we restrict the calculation to the particle-particle channel, Γ is replaced by Γ_{pp} given by (2.31) in terms of the effective interaction B_{pp} .

We can now apply the test-particle method starting from (4.40). We remark two contributions when we add a test particle in the systems characterized by the ground-state energy (4.40):

1. an external contribution due to the change $n_1 \rightarrow n_1 + \delta n_1(\mathbf{k})$ and $n_2 \rightarrow n_2 + \delta n_2(\mathbf{k})$;
2. an internal contribution due to the fact that the resummed effective interaction Γ depends on the unperturbed occupation number n_i ($i \neq 1, 2$) through the bubble functions $B_{l=0,1,2,pp}$ (see appendix C where this function is given explicitly in terms of the occupation numbers).

Accounting for these two contributions, we can define the perturbed energy (with respect to to the ground state of the systems) due to the addition of a test particle in the system as:

$$\begin{aligned} E(\eta, \mathbf{k}) &= E_{FG}(\eta, \mathbf{k}) + \frac{g}{2}(g-1) \int_{k_1, k_2} n_1(\eta) n_2(\eta) \Gamma(\eta), \\ &= E + \eta [e(\mathbf{k}) + \Sigma^*(\mathbf{k})] + \mathcal{O}(\eta^2). \end{aligned} \quad (4.41)$$

The resummed self-energy is then given by:

$$\eta \Sigma^*(\mathbf{k}) = \frac{g}{2}(g-1) \int_{k_1, k_2} [\delta n_1(\mathbf{k}) n_2 + n_1 \delta n_2(\mathbf{k})] \Gamma + n_1 n_2 \delta \Gamma(\mathbf{k}), \quad (4.42)$$

where δn_i are given by (4.30). The obtention of the explicit form of $\Sigma^*(\mathbf{k})$ is rather technical. We only give below a guideline and most technical details and expressions are given in appendix C. $\delta \Gamma(\mathbf{k})$ appearing in the internal contribution is obtained in practice as follows:

1. we first estimate, up to linear order in η , the bubble functions B_0, B_1, B_2 and B_{pp} . To do this, we first write the B_l ($l = 0, 1, 2, pp$) in terms of the unperturbed occupation numbers n_i and then we proceed with the test-particle insertion (4.31). Truncated at first order in η , this procedure leads to:

$$B_l \longmapsto B_l(\eta, \mathbf{k}) = B_l + \delta B_l(\mathbf{k}) + \mathcal{O}(\eta^2).$$

2. As usually done, a simplified expression of the perturbed bubble function can be obtained by performing the angle average on \mathbf{k} of the functions δB_l . This angle average function is denoted by $\widehat{\delta B}_l$ in the following (see appendix C for more details), i.e. :

$$B_l \longmapsto B_l(\eta, \mathbf{k}) = B_l + \widehat{\delta B}_l(k) + \mathcal{O}(\eta^2).$$

These functions, B_l and $\widehat{\delta B}_l$ [linear in η and depending only on the norm of \mathbf{k}], are explicitly calculated and properly regularized in appendix C.

3. This linear change in η of the bubble functions $\{B_l(\eta)\}$ induces also a change of the unperturbed effective interaction Γ , denoted by $\delta\Gamma$ and defined as:

$$\Gamma[\{B_l + \widehat{\delta B}_l(k)\}] - \Gamma[\{B_l\}] = \delta\Gamma[\{B_l\}, \{\widehat{\delta B}_l(k)\}] + \mathcal{O}(\eta^2).$$

In practice, we have to distinguish two cases according to the dimensionless variable (s, t) to estimate this function: (i) $s^2 + t^2 < 1$ and (ii) $s^2 + t^2 > 1$. These technical details are discussed and the two cases are explicitly calculated in appendix C.

It remains finally to calculate the external contribution, i.e. the first term of (4.42). This is also done in appendix C.

Finally, collecting the different contributions calculated explicitly in appendix C, the resummed self-energy (4.42) associated with the ladder resummation of the ground-state energy recasts as:

$$\begin{aligned} \frac{\Sigma^*(k)}{(g-1)\varepsilon_F} &= \Theta(k_F - k) \int_0^1 s^2 ds \int_0^{\sqrt{1-s^2}} t dt \mathcal{S}(s, t, p; a_s k_F) \\ &+ \Theta(k - k_F) \int_0^{(1+p)/2} s^2 ds \int_0^{(1+p)/2} t dt \mathcal{S}'(s, t, p; a_s k_F). \end{aligned} \quad (4.43)$$

The dimensionless functions \mathcal{S} and \mathcal{S}' depend on the dimensionless variables $p = k/k_F$ and (s, t) defined by (2.19) as well as on $(a_s k_F)$. We remark that this form is very similar to the expression that we have obtained for the resummed ground-state energy (2.55).

Consistently with the notations of chapter 2, we note respectively $\Sigma^*(k) = U(k) + iW(k)$ for the self-energy obtained from the resummation of combined pp and hh ladder diagrams. This self-energy is called AEI self-energy hereafter. We denote by $\Sigma_{pp}^*(k) = U_{pp}(k) + iW_{pp}(k)$ the self-energy associated with the resummation of pp

ladder diagrams only. This self-energy is called GEI self-energy. In the two cases, we decompose \mathcal{S} and \mathcal{S}' in terms of their real and imaginary parts as:

$$\begin{aligned}\mathcal{S}^{(l)} &= \mathcal{U}^{(l)} + i\mathcal{W}^{(l)} \quad \text{for combined } pp \text{ and } hh \text{ ladder diagrams (AEI),} \\ \mathcal{S}_{pp}^{(l)} &= \mathcal{U}_{pp}^{(l)} + i\mathcal{W}_{pp}^{(l)} \quad \text{for } pp \text{ ladder diagrams only (GEI).}\end{aligned}$$

All functions are given in appendix C [see (C.48) and (C.49)]. These results were first obtained in [240] with another convention for the sign of the scattering length (i.e. $a_s \rightleftharpoons -a_s$).

The test-particle method offers an alternative to the naive method discussed previously to obtain a resummed self-energy. Besides, both AEI and GEI self-energies have the following properties:

- (i) Both reproduce also the low-density limit up to second order in $(a_s k_F)$;
- (ii) They converge to a finite value when $|a_s k_F| \rightarrow \infty$. This is illustrated in figure 4.8 where the results of direct integration¹¹ of (4.43) are shown as a function of k at unitarity.
- (iii) They are consistent with the Hugenholtz-van-Hove (HvH) theorem in the sense that the GEI (respectively AEI) self-energy leads to the GEI (respectively AEI) ground state energy (2.55).

In the next section we discuss and compare the results obtained from the two resummation schemes discussed in section 4.2 (GR_{pp} and GR_{pp+hh} self-energy) and 4.3 (AEI and GEI self-energy).

(I) QUASI-PARTICLE PROPERTIES AT LOW DENSITY

At low density, we have seen that the GR_{pp} self-energy does not reproduce the second-order contribution in $(a_s k_F)$. We have lost this property because we did not consider the external contribution of the resummation of the hole-hole ladder self-energy diagrams. However, the method employed in section 4.3 shows that the second order of the self-energy can be recovered from the resummation of particle-particle ladder energy diagrams within the test-particle method leading to the GEI self-energy. This method automatically includes the internal contribution, contrary to the naive GR_{pp} resummation. In other words, in the limit $|a_s k_F| \ll 1$, the Taylor expansion up to second order of the GEI self-energy matches the analytical results obtained by Galitskii [225,240]. This property is explicitly discussed and detailed in the following chapter. As expected, the AEI self-energy also reproduces the second order at low density.

(II) QUASI-PARTICLE PROPERTIES CLOSE TO UNITARITY

In figure 4.8 we show the real and imaginary parts of the AEI, GEI and GR_{pp} self-energies at strict unitarity. Note that the GR_{pp+hh} self-energy is not shown since it diverges. We see again strong differences according to the scheme used and the class of diagrams retained for the resummation. More precisely, the properties of the real part of the self-energy around the Fermi sea ($k = k_F$) give information on the chemical potential μ [value at $k = k_F$, see (4.6a)] and the effective mass m^* [derivative at $k = k_F$, see (4.6e)] of the quasi-particles. Different resummed self-energies, when non-divergent, lead to very different values of μ and m^* at strict unitarity as summarized in table 4.2.

¹¹ Note that for the multidimensional numerical integration of the equations, we used the Vegas method implemented in the Cuba library [242].

| | | GR_{pp} | GR_{pp+hh} | GEI | AEI |
|--|--|------------------------|------------------------|------------------------|--------------|
| Equation | | (4.14) | (4.24) | (4.43) | |
| Hugenholtz-van-Hove theorem (†) | | \times | \checkmark (‡) | \checkmark | \checkmark |
| Low density | $\Sigma_{(1)}^*$ (4.1) | \checkmark | \checkmark | \checkmark | \checkmark |
| | $\Sigma_{(2)}^*$ (4.4) | \times | \checkmark | \checkmark | \checkmark |
| | $E_{(2)}$ (2.24) | \checkmark | \checkmark | \checkmark | \checkmark |
| Unitary limit | $\xi_0 \simeq 0.376$ | 0.24 | – | 0.24 | 0.51 |
| | $\mu = \xi_0$ (†) | 0 | – | 0.24 | 0.51 |
| | $m^* \simeq 1.0 - 1.2$ | 0.98 | – | 1.2 | 2.1 |

Table 4.2: Summary of the properties of different self-energies obtained by resummation. A check-mark means that the property is verified though a cross means the opposite. The first row gives the equations where the specific form of the self-energy are given. The fulfillment of the Hugenholtz-van-Hove (HvH) theorem [\(4.6c\)](#) here should be understood as follows. For the GR_{pp+hh} case, the HvH theorem is fulfilled up to second order in $(a_s k_F)$ and the GR_{pp} case, it is not fulfilled. For the GEI/AEI cases, the HvH theorem is fulfilled in the sense that applying the HvH theorem we obtain the GEI/AEI ground state energy given by [\(2.55\)](#). The second row corresponds to the low density properties of the self-energy. The third row gives the numerical values of the Bertsch parameter ξ_0 , chemical potential μ (in unit of the Fermi energy) and effective mass m^* (in unit of the bare mass) at strict unitarity. The “–” for the GR_{pp+hh} means that the resummation leads to a divergence at unitarity.

(†) The Hugenholtz-van-Hove theorem insures the relation: $\mu = \xi_0 \mu_{FG}$ at strict unitarity.

(‡) In that case, the HvH theorem is fulfilled up to second order in $(a_s k_F)$.

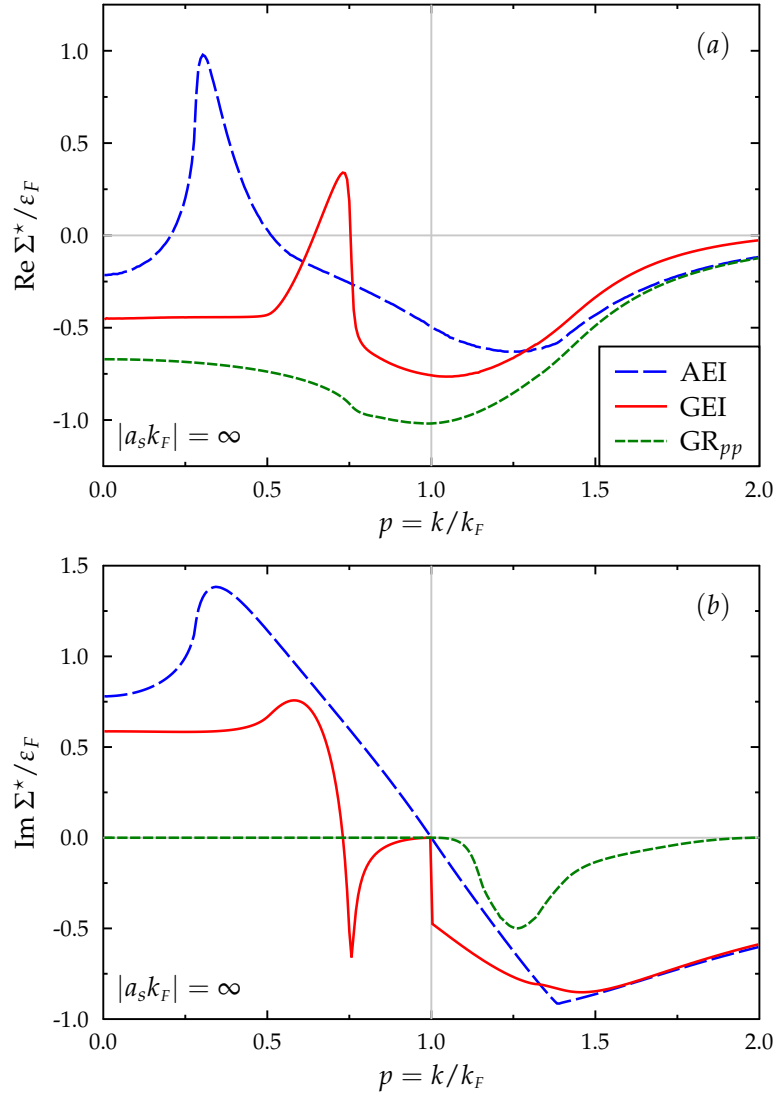


Figure 4.8: (a) real and (b) imaginary parts of the resummed on-shell self-energy at unitarity as a function of the dimensionless momentum $p = k/k_F$. The red solid line is the result obtained with the combined particle-particle and hole-hole ladder diagrams (AEI self-energy), the blue long-dashed line corresponds to the restriction of particle-particle ladder diagrams (GEI self-energy) and the green short-dashed line is the result obtained with the particle-particle resummation of the self-energy under a geometric series form (GR_{pp} self-energy).

(III) GROUND STATE ENERGY AND HUGENHOLTZ-VAN-HOVE THEOREM

It is important to recall that the ground-state energy obtained from the two resummation schemes are not equivalent. The difference comes from the validity of the Hugenholtz-van-Hove theorem which can be expressed at equilibrium by (4.6c). The GR_{pp} (considering only the pp contribution) does not verify the theorem since the second order of the chemical potential is not given by (4.6b) although the energy is correct at second order in $(a_s k_F)$. We have explored here the possibility to add the hh contribution. This solves the problem at low density but leads to divergences at unitarity. The AEI and GEI self-energies verify automatically this theorem in the sense that applying the HvH theorem to the GEI/AEI self-energy leads to the GEI/AEI given by (2.55). They have the advantage to have finite limit at unitarity as shown explicitly in [240] (see also the following chapter). In both cases, the unitarity limit is not well reproduced and in the next chapter we use these two resummations as a starting point to explore and propose a generalization of the functional introduced in chapter 3 including the possibility to describe quasi-particle properties.

4.4

SUMMARY AND DISCUSSIONS

In the present chapter, we have explored the possibility to obtain a resummed expression for the self-energy in the same way as we have discussed in chapter 2 for the energy. We illustrated here that the situation is slightly more complicated compared to the case of the energy due to the fact that both pp and hh contributions should be consistently taken into account. A naive independent resummation of pp and hh diagrams can be made at low and intermediate densities but diverges at unitarity. Following [240], we used the test-particle method to obtain two expressions for the resummed self-energy that are consistent with the AEI and GEI ground-state energies obtained in chapter 2. These resummed self-energies have interesting features: (i) correct low-density limit, (ii) finite limits at unitarity, (iii) fulfillment of the HvH theorem. However, similarly to the AEI and GEI ground-state energy, they lack predictive power at unitarity. They are also rather complex to estimate numerically. For instance, we had difficulties to obtain numerical estimates from the AEI and GEI self-energies away from unitarity. In the next chapter, similarly to what we did in chapter 3 for the energy, we explore the possibility to use the AEI and GEI self-energy as a guidance to obtain simpler expressions for the self-energies with improved predictive power.

5

APPROXIMATE SELF-ENERGY INSPIRED FROM EFT RESUMMATION

*Voici les photos de nos routes
Prises d'avion par nuit de brouillard
Dans ce vieux catalogue des doutes
Aux pages moisies par le hasard
A toujours vouloir être ailleurs
Pyromanes de nos têtes brûlées
On confond les battements du coeur
Avec nos diesels encrassés*

*A toujours voir la paille plantée
Dans la narine de son voisin
On oublie la poutre embusquée
Qui va nous tomber sur les reins
Et l'on pousse à fond les moteurs
A s'en faire péter les turbines
C'est tellement classe d'être loser
Surtout les matins où ça winne*

*Bourlinguer, errer, Errer humanum est
Toujours plus loin à fond la caisse
Et toujours toujours plus d'ivresse
Oh yes, always, on the road again man*

Hubert Félix THIEFAINE – *Errer Humanum Est*

CONTENTS

| | | |
|-------|--|-----|
| 5.1 | Partial phase-space approximation for the resummed self-energy . | 140 |
| 5.1.A | Partial phase-space approximation with Hugenholtz-van-Hove constraint | 140 |
| 5.1.B | Approximate GPS self-energy | 142 |
| 5.1.C | Approximate self-energy consistent with the APS functional | 149 |
| 5.2 | Approximate expressions for the self-energy | 152 |
| 5.2.A | Polynomial form of single-particle potential in power of k^{2n} | 153 |
| 5.2.B | Summary and discussions | 156 |
| 5.3 | Link with the empirical Skyrme functionals | 160 |
| 5.3.A | From non-empirical DFT to density-dependent parameters | 160 |
| 5.3.B | Effective Skyrme potential from quasi-particle properties | 161 |
| 5.3.C | Toward finite systems | 163 |
| 5.4 | Conclusion and critical discussions | 165 |

In this chapter, guided by the resummation on the energy with approximation schemes discussed in chapter 3, we explore the possibility to obtain a compact approximate form of the self-energy from the resummation explained in chapter 4. This leads to simpler self-energies to describe quasi-particle properties of a Fermi gas in the low density and large scattering length limit. The present work is motivated by the fact that: (i) the MBPT technique is rather involved at high order in perturbation and becomes hardly applicable to physical systems (e.g. saturation density of nuclear system), (ii) resummed expression found in chapter 4 are complex to implement in finite systems because of the integral on the phase-space, and (iii) the DFTs based on energy do not contain information about the quasi-particle properties, except the chemical potential of the systems given by a general thermodynamical relationship. For instance, it gives no guidance for the effective mass which is crucial to describe the response to an external field or collective modes of such systems as seen in chapter 3.

In chapter 4, we have obtained resummed self-energies applicable to systems with large scattering length and compatible with the Hugenholtz-van-Hove theorem by summing up all orders of the combined particle-particle and hole-hole ladder diagrams or particle-particle ladder diagrams only (see section 4.4). The real part of these self-energies as well as quasi-particle energies obtained at strict unitarity (below the Fermi surface only) are shown in figure 5.1 and compared with:

- The experimental data of [296] obtained using photoemission spectroscopy. Note that such data correspond to a temperature $T = (0.9 \pm 0.1)T_c$ below the critical temperature $T_c \simeq 0.16T_F$ of the superfluid state transition [67] where $k_B T_F = \varepsilon_{FG}$ defines the Fermi temperature with the Boltzmann constant k_B ;
- The Brueckner Hartree-Fock (BHF) calculation of [84] without pairing effect at temperature $T = 0.2T_F$.

These two results from [296] and [84] will be used as a guidance to design approximate expressions for the self-energy at zero-temperature for non-superfluid systems (see below). The reason why we focus on non-superfluid systems is mostly practical. At present, it is unclear whether resummed analytical expressions can be obtained for the superfluid case in the same way as done in chapter 4.

In figure 5.1, we see that the results obtained in section 4.3 differ significantly from the reference results. Actually, the resummed self-energies present a large peak at $p \simeq 0.35$ for the combined pp and hh ladder diagrams (AEI self-energy) and at $p \simeq 0.7$ for the pp ladder diagrams only (GEI self-energy). Except for these unphysical regions, the resummed self-energies have amplitudes and behaviors compatible with the experimental data and BHF calculations. The peaks however highlight the breakdown of the resummation technique employed in chapter 4 for systems close to the unitary limit leading to unrealistic results. We note that both results from [296] and [84] including or not superfluidity lead to a smooth dependence of the single-particle potential contrary to the AEI and GEI cases.

The goal of this chapter is to obtain a realistic and practical resummed expression of the self-energy (i) with different approximations for the energy given in chapter 2 and (ii) that is inspired from the resummed self-energy discussed in chapter 4. Below, we discuss in more details the strategy we will use.

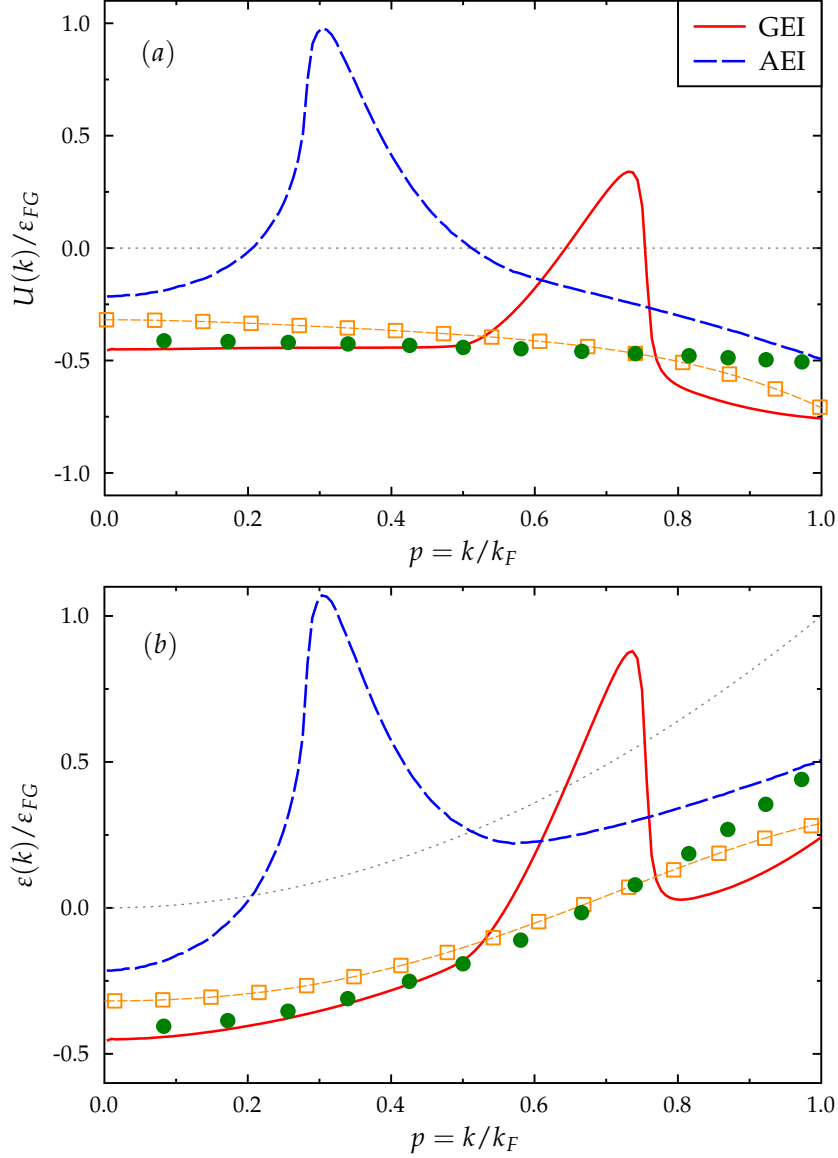


Figure 5.1: (a) Momentum dependence of the real part of the on-shell self-energy $U(k)$ and (b) associated single-particle energy $\epsilon(k)$ at strict unitarity below the Fermi surface ($p = k/k_F \leq 1$). The red solid line (respectively blue long-dashed line) corresponds to the result obtained with the GEI (respectively AEI) self-energy. For comparison, green dots are the Brueckner Hartree-Fock calculations obtained without pairing effect [84] and the orange open squares to the best fit of the experimental results of [296], both obtained at a temperature near the critical temperature of the superfluid state transition $T \simeq T_c$. As a reference, the gray dotted line corresponds to the free Fermi gas limit.

GENERAL STRATEGY

The study of MBPT and the resummation of energy diagrams in chapter 2 have underlined that the ground-state energy can be written as an integral on the accessible phase-space [see (3.4)]:

$$\frac{E}{E_{\text{FG}}} = 1 + (g - 1) \langle\langle \mathcal{E} \rangle\rangle, \quad (5.1)$$

where we used the notation introduced in (3.7). Here, \mathcal{E} is given by (2.55) in the AEI and GEI cases. In chapter 3, we have made some approximations to simplify the form of \mathcal{E} obtained from ladder diagrams resummation to get rid of the integral on the accessible phase-space. This has led to a variety of compact forms of the energy, namely the APS/GPS, ALD/GLD or AUL/GUL functionals (see table 3.1). In this chapter, we explore the possibility to make the same type of approximations for the self-energy while being consistent with the result obtained for the energy.

In chapter 4, we have seen that the self-energy $\Sigma^*(k)$ can also be written as an integral on the accessible phase-space (we recall that $p = k/k_F$ below). Introducing the notation $\langle X \rangle_p^{\lessgtr}$ defined as:

$$\langle X \rangle_p^< \equiv \int_0^1 s^2 ds \int_0^{\sqrt{1-s^2}} t dt X(s, t, p), \quad (5.2a)$$

$$\langle X \rangle_p^> \equiv \int_0^{(1+p)/2} s^2 ds \int_0^{(1+p)/2} t dt X(s, t, p), \quad (5.2b)$$

the resummed AEI/GEI self-energy (5.3) can be rewritten simply as:

$$\frac{\Sigma^*(k)}{(g-1)\varepsilon_F} = \Theta(k_F - k) \langle \mathcal{S} \rangle_p^< + \Theta(k - k_F) \langle \mathcal{S}' \rangle_p^>, \quad (5.3)$$

where \mathcal{S} and \mathcal{S}' are given by (C.48) and (C.49) in appendix C for both AEI and GEI cases¹. Below, we consider a spin degenerate system ($g = 2$) such that the factor $(g - 1)$ will not be explicitly written.

The resummed self-energies (AEI and GEI self-energy) have a number of interesting properties similarly to the GEI/AEI ground-state energy obtained in chapter 2. First, in the low-density regime, the first and second order self-energies given by the Galitskii formula (4.4) are properly recovered by construction taking the Taylor expansion of (5.3) up to second order in $(a_s k_F)$. Another interesting feature of the expression given in appendix C, is that the self-energies also converge to a finite result as $|a_s k_F| \rightarrow +\infty$ for all k . This is illustrated in figure 5.1 where the results of direct integration of (5.3) are shown as a function of k at unitarity. The single-particle energies defined as:

$$\varepsilon(k) = e(k) + U(k) = \frac{k^2}{2m} + U(k) \quad (5.4)$$

¹ We recall also the notations introduced in previous chapter to decompose the self-energy in real and imaginary parts:

$$\begin{aligned} [\text{AEI self-energy}] &\mapsto \Sigma^* = U + iW, \mathcal{S} = \mathcal{U} + i\mathcal{W} \text{ and } \mathcal{S}' = \mathcal{U}' + i\mathcal{W}' \\ [\text{GEI self-energy}] &\mapsto \Sigma_{pp}^* = \mathcal{U}_{pp} + i\mathcal{W}_{pp}, \mathcal{S}_{pp} = \mathcal{U}_{pp} + i\mathcal{W}_{pp} \text{ and } \mathcal{S}'_{pp} = \mathcal{U}'_{pp} + i\mathcal{W}'_{pp} \end{aligned}$$

and obtained in figure 5.1.b coincide with those reported in [240] with marked bumps. These bumps seem unphysical not only because they significantly differ from the BHF calculations of [84] but also due to the presence of single-particle energies above the Fermi energy $\varepsilon(k_F)$ for $k < k_F$. We would like to mention that there is no reason that the deduced self-energy is predictive at large scattering length due to the neglected diagrams.

HUGENHOLTZ-VAN-HOVE THEOREM

An important remark for the discussion below is that the expression of the resummed AEI and GEI self-energies respectively obtained either from pp ladders or combined pp and hh ladders resummations are *consistent* respectively with the GEI and AEI approximations for the ground-state energy given by (2.55). *Consistent* means here that they respect the Hugenholtz-van-Hove (HvH) theorem [290]. This theorem (at zero temperature) states that the single-particle energy given by (5.4) and evaluated at the Fermi surface ($k = k_F$) is equal to the chemical potential of the systems. Using the thermodynamical relation between the chemical potential and the ground state energy, $\mu = \partial E / \partial N|_V$, where V is the unit volume, the HvH theorem leads to (see table 3.3):

$$\frac{\mu}{\mu_{FG}} = \frac{E}{E_{FG}} + \frac{k_F}{5} \frac{\partial E / E_{FG}}{\partial k_F} = 1 + \frac{U(k_F)}{\varepsilon_{FG}} = \frac{\varepsilon(k_F)}{\varepsilon_{FG}}. \quad (5.5)$$

This equation gives a strong constraint between the energy and single-particle potential at $k = k_F$ that will be useful in the following.

As a side but important remark, we have shown in chapter 3 several functionals that reproduce quite well the energy of Fermi gases at unitarity. We would like to mention that the value $\zeta_0 = 0.37$ is the admitted value of superfluid unitary gas. It might then be surprising to reproduce this value with a functional originally motivated by the diagrammatic expansions of [238,240] (see chapters 2 and 4) where superfluidity is not treated. It is however important to keep in mind that whatever is the motivation/strategy to produce a DFT, the only final criterium is the ability of the functional to accurately describe the ground-state energy of the system at various densities. This is actually the only purpose of a DFT constructed in the spirit of the original work of Hohenberg and Kohn who have shown the existence of a functional able to reproduce the exact energy consistently with the exact local one-body density [113].

In the following, however, we would like to consider directly the self-energy that is a priori clearly beyond the scope of a DFT approach. In this case, the discussion made above for the energy is not valid anymore and superfluidity should be explicitly introduced to describe superfluid systems. Such a treatment is beyond the scope of the present work and will be discussed at the end of this chapter. For this reason, below, we will focus our discussion on non-superfluid systems and compare with the reference result without superfluidity [84].

QUASI-PARTICLE PROPERTIES

One of the main goals of the present work is to make a Landau liquid Fermi Theory (LFT) for strongly interacting systems. Direct connection with LFT can be made by developing U around $p = k/k_F = 1$ as:

$$\begin{aligned}\frac{U(k)}{\varepsilon_{FG}} &= \frac{U(k_F)}{\varepsilon_{FG}} + (p-1) \left. \frac{\partial U(k)}{\partial p} \right|_{p=1} \frac{1}{\varepsilon_{FG}} + \dots \\ &= \left[\frac{\mu}{\mu_{FG}} - 1 \right] + 2(p-1) \left[\frac{m}{m^*} - 1 \right] + \dots,\end{aligned}\quad (5.6a)$$

where the chemical potential and the effective mass are by definition given by:

$$\frac{\mu}{\mu_{FG}} \equiv 1 + \frac{U(k_F)}{\varepsilon_{FG}} = 1 + \langle \mathcal{U} \rangle_{p=1}^<, \quad (5.6b)$$

$$\frac{m}{m^*} \equiv 1 + \left. \frac{m}{k_F} \frac{\partial U}{\partial k} \right|_{k=k_F} = 1 + \frac{1}{2} \left\langle \frac{\partial \mathcal{U}}{\partial p} \right\rangle_{p=1}^<. \quad (5.6c)$$

Starting from the different expressions (AEI or GEI self-energies), one can therefore deduce from them the quasi-particle properties by a direct numerical integration. We show in figure 5.2 the evolution of μ and m^*/m as a function of $(a_s k_F)$ obtained in the two types of resummation considered here. We see that both AEI and GEI approximations significantly extend the domain of validity compared to the perturbative theory. The corresponding chemical potential extracted from them are rather close to the BHF result up to $|a_s k_F| \simeq 2 - 3$. For the AEI case, it is remarkable to see, especially having in mind the strange behavior of figure 5.1, that the chemical potential extracted from the AEI case perfectly matches the BHF calculation for all regimes of $(a_s k_F)$. We see however (panels (c) and (d) of figure 5.2) that the comparison is in general less favorable for the effective mass. Both approximations overestimate the effective mass compared to the BHF calculation for $|a_s k_F| > 1$, even if the agreement is slightly better than perturbation theory at second or third order. We also observe that the effective mass, as well as the chemical potential, obtained with each other strongly depend on the selected diagrams.

SUMMARY

We have seen here that the resummation of diagrams is only a semi-success to predict quasi-particle properties. More precisely, the effective mass deviates rather rapidly from the expected result as $|a_s k_F|$ increases. Although their predictive power is limited, the AEI and GEI approximations can serve as a guidance to provide simplified expressions of the self-energy that will be useful later on in the DFT context. Starting from these expressions, our goal is to provide for the self-energy a phase-space approximation similar to the one obtained for the energy in chapter 2. Following the strategy we used previously for the ground-state energy, we will impose the approximate form to fulfill specific constraints:

- (i) *Low-density limit:* We will always impose that the self-energy matches the exact self-energy in the low-density limit up to a certain order in $(a_s k_F)$.
- (ii) *Large $(a_s k_F)$ limit:* We also seek expressions that do not diverge in the limit $|a_s k_F| \rightarrow +\infty$.
- (iii) *Consistency with the H_vH theorem:* while it is not a priori absolutely necessary, in the majority of the cases considered in this chapter, we will in addition impose that the self-energy is consistent² with either the GPS or the APS energy.

² Again, consistency means here that the considered self-energy and the energy obtained through phase-space average lead to the same chemical potential using (5.5).

Note that the latter condition is more constraining than the conditions (i) and (ii). In particular, since the energy already has the constraints (i) and (ii), they will be automatically fulfilled when (iii) is explicitly imposed. We discuss below several approaches to obtain a compact expression of the single-particle potential below the Fermi surface ($k < k_F$), and we focus then on the quasi-particle properties obtained.

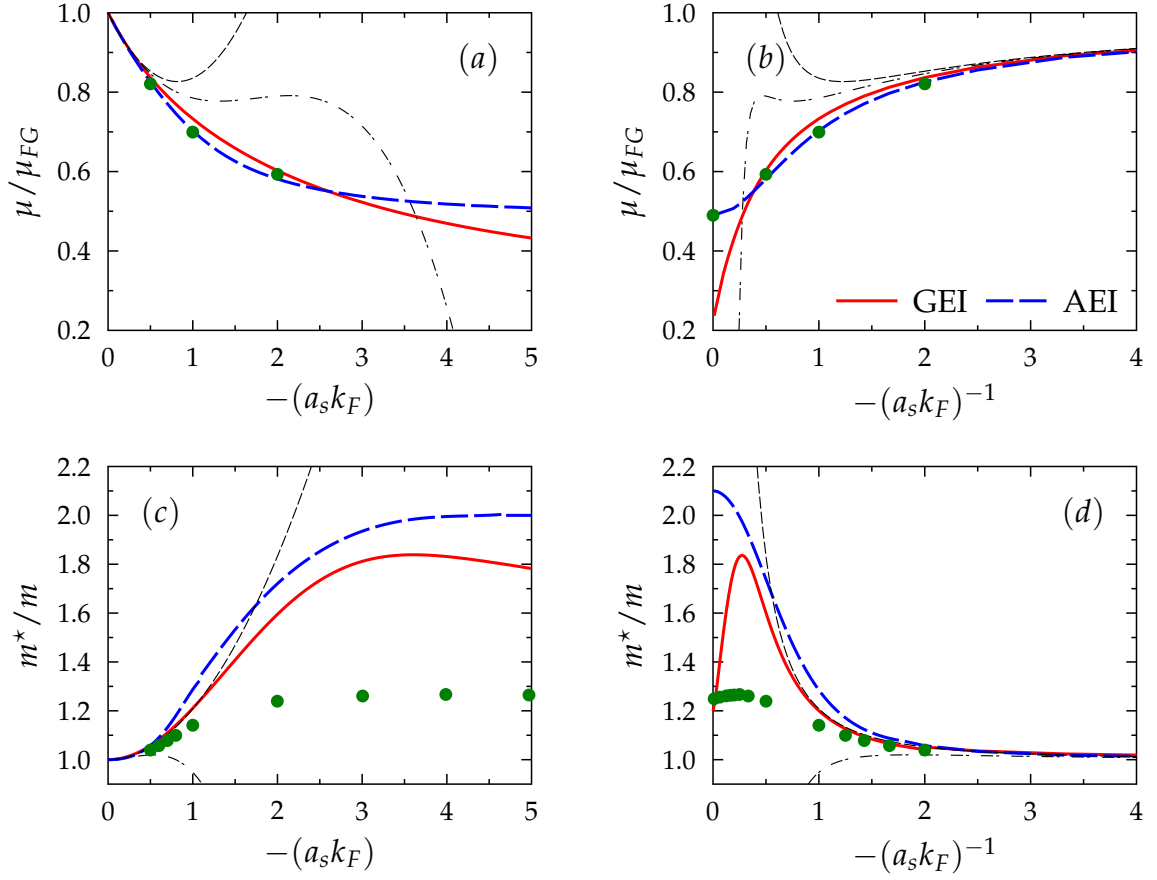


Figure 5.2: Chemical potential and effective mass as a function of $(a_s k_F)$ [panels (a) and (c)] or $-(a_s k_F)^{-1}$ [panels (b) and (d)] obtained with the GEI (red solid line) and AEI (blue dashed line) approximations. Result of the second order (Galitskii formula) and third order expansions [232] in $(a_s k_F)$ are shown with black dashed and dot-dashed thin lines respectively. The green circles correspond to the result of the BHF calculations of [84].

5.1

**PARTIAL PHASE-SPACE AVERAGE APPROXIMATION
FOR THE RESUMMED SELF-ENERGY**

This section is organized as follows: first, we focus on the GEI case obtained by summing up all orders of the pp ladder diagrams. We recall the main results and discuss the constraint imposed by the Hugenholtz-van-Hove (HvH) theorem [290] given by (5.5). Then we explore the possibility to approximate the self-energy consistently with the result obtained with the phase-space approximation of the ground-state energy (APS/GPS functional introduced in chapter 4) according to the constraint imposed by this theorem. Finally we make connection with the Landau Fermi liquid theory (LFT) by evaluating the quasi-particle quantities (as the effective mass) arising from the different approximations of the self-energy.

**5.1.A Partial phase-space approximation
with Hugenholtz-van-Hove constraint**

As a detailed illustration of the strategy used to obtain an approximated self-energy, we start from the real part of the resummed self-energy obtained by summing up all the pp ladder diagrams in chapter 4 (GEI self-energy). Guided by the phase-space approximation of the energy discussed in chapter 3, section 3.1.b, we propose several simplified expressions for the self-energy by replacing the dimensionless functions appearing in the resummed expression for example by their phase-space average. Doing that, we pay attention to the consistency with the GPS functional (3.10) introduced in chapter 3 by phase-space average approximation of the energy that was also obtained by summing up pp ladder energy diagrams.

Let us first recall the useful results obtained in chapter 4. By summing up the pp ladder diagrams, we have shown that the real part of the self-energy can be written as:

$$\frac{U_{pp}(k \leq k_F)}{\varepsilon_{FG}} = \langle \mathcal{U}_{pp} \rangle_p^<, \quad (5.7a)$$

where $p = k/k_F$ and:

$$\mathcal{U}_{pp}(s, t, p; a_s k_F) = \frac{16(a_s k_F) \hat{I}_*(s, t, p)}{\pi - (a_s k_F) F(s, t)} + \frac{16(a_s k_F)^2 \hat{F}(s, t, p) I_*(s, t)}{[\pi - (a_s k_F) F(s, t)]^2}. \quad (5.7b)$$

Below, we concentrate first on the validity of the HvH theorem in this resummation scheme.

VALIDITY OF THE HVH THEOREM FOR THE GEI FUNCTIONAL

As an illustration, we show now that the GEI ground-state energy and the GEI single-particle potential are consistent with the HvH theorem. This was proved first and discussed in details for the AEI case in [240]. We give here a summary of the proof for the sake of completeness. The GEI ground-state energy, using the notation defined by (3.7), can be written as [see (2.55)]:

$$\frac{E}{E_{FG}} = 1 + \frac{80}{\pi} \left\langle\left\langle \frac{(a_s k_F) \pi I_*}{\pi - (a_s k_F) F} \right\rangle\right\rangle. \quad (5.8)$$

From this, we estimate the chemical potential³:

$$\frac{\mu}{\mu_{FG}} = \frac{E}{E_{FG}} + \frac{k_F}{5} \frac{\partial E / E_{FG}}{\partial k_F}, \quad (5.9a)$$

$$= 1 + \left\langle\left\langle \frac{16(a_s k_F)}{\pi - (a_s k_F) F} \times \frac{\partial}{\partial k_F} \{k_F I_*\} + \frac{16(a_s k_F)^2 I_*}{[\pi - (a_s k_F) F]^2} \times \frac{\partial}{\partial k_F} \{k_F F\} \right\rangle\right\rangle, \quad (5.9b)$$

$$= 1 + \langle \mathcal{U}_{pp} \rangle_{p=1}^< = 1 + \frac{U_{pp}(k_F)}{\varepsilon_{FG}}, \quad (5.9c)$$

which proves that the HvH is verified. To establish the equality of the integrand (5.9b) with (5.9c) where \mathcal{U}_{pp} is given by (5.7b), and consequently prove the validity of the HvH theorem using (5.7a), we have used the following identities valid in the region $1 - s^2 - t^2 \geq 0$:

$$\frac{\partial}{\partial k_F} \{k_F I_*(s, t)\} = \frac{1}{s} \Theta(s + t - 1) \equiv \widehat{I}_*(s, t, 1), \quad (5.10a)$$

$$\frac{\partial}{\partial k_F} \{k_F F(s, t)\} = \frac{1}{s} \ln \left| \frac{(s+1)^2 - t^2}{(s-1)^2 - t^2} \right| \equiv \widehat{F}(s, t, 1). \quad (5.10b)$$

This achieves the proof of validity of the HvH theorem for pp ladder diagrams resummation. We now consider the constraint imposed by this theorem when a phase-space average approximation on the energy is made.

CONSTRAINT OF THE PHASE-SPACE AVERAGE APPROXIMATION FROM THE HVH THEOREM

We have seen in chapter 3 that the phase-space approximation using a geometric series for the energy (5.8) [see also (3.10)] is:

$$\frac{E}{E_{FG}} = 1 + \frac{10(a_s k_F)/9}{\pi - (a_s k_F) \|F\|}, \quad (5.11)$$

where we have introduced the notation:

$$\|F\| \equiv \frac{\langle\langle F I_* \rangle\rangle}{\langle\langle I_* \rangle\rangle} = \frac{6}{35} (11 - 2 \ln 2), \quad (5.12)$$

³ Note that the variables (s, t) are dimensionless and they must be understood as $(s, t) = (P/k_F, q/k_F)$. The derivative with respect to k_F is done at fixed P and q . In particular, with $I_*(s, t) \equiv I(s, t) \Theta(1 - s^2 - t^2)$, i.e. in the region $1 - s^2 - t^2 \geq 0$, any function f of k_F verifies:

$$\frac{\partial}{\partial k_F} \langle\langle f I_* \rangle\rangle = \left\langle\left\langle \frac{\partial}{\partial k_F} \{f I_*\} - 5f I_* \right\rangle\right\rangle.$$

which is the phase-space average value of the function $F(s, t)$ (see appendix E). From this, the chemical potential is:

$$\frac{\mu}{\mu_{FG}} = \frac{E}{E_{FG}} + \frac{k_F}{5} \frac{\partial E/E_{FG}}{\partial k_F} = 1 + \frac{4(a_s k_F)/3}{\pi - (a_s k_F) \|F\|} + \frac{2(a_s k_F)^2 \|F\| / 9}{[\pi - (a_s k_F) \|F\|]^2}. \quad (5.13)$$

Comparing (5.13) with (5.7b), we observe that the proper denominator appearing in (5.13) can simply be obtained by replacing $F(s, t)$ by $\|F\|$ in (5.7b). This strongly resembles what was done with the energy in chapter 3, section 3.1.b. Doing so directly in (5.7b), we obtain the approximated expression:

$$\begin{aligned} \frac{U_{pp}(k_F)}{\varepsilon_{FG}} &= \left\langle \frac{16(a_s k_F) \hat{I}_*}{\pi - (a_s k_F) \|F\|} + \frac{16(a_s k_F)^2 I_*}{[\pi - (a_s k_F) \|F\|]^2} \times \frac{\partial}{\partial k_F} \{k_F \|F\|\} \right\rangle_{p=1}^{\leq}, \\ &= \frac{16(a_s k_F) \langle \hat{I}_* \rangle_{p=1}^{\leq}}{\pi - (a_s k_F) \|F\|} + \frac{16(a_s k_F)^2 \langle I_* \rangle_{p=1}^{\leq} \|F\|}{[\pi - (a_s k_F) \|F\|]^2}. \end{aligned} \quad (5.14)$$

Here we have used the property (5.10b) where we have replaced the function $F(s, t)$ by its phase-space average value so that $\|F\|$ appears explicitly in the numerator of the second term. We see that, with these expressions in (5.14), using the value of the partial phase-space value of the functions I_* and \hat{I}_* given in appendix E, the expression (5.13) is obtained. However, this is only valid at $p = k/k_F = 1$. Hereafter, we explore the possibility to obtain a similar expression for $k \neq k_F$.

5.1.B Approximate GPS self-energy

In this section, we discuss the possibility to get a resummed expression of the self-energy consistent with the GPS approximation and fulfilling the HvH theorem. Our starting point is the expansion of the real part of the self-energy in powers of $(a_s k_F)$ as:

$$\frac{U_{pp}(k)}{\varepsilon_{FG}} = \sum_{n=1}^{\infty} (a_s k_F)^n \Phi_n(p), \quad (5.15)$$

where Φ_n is given by the Taylor expansion of (5.7), i.e. :

$$\begin{aligned} \Phi_n(p) &= \frac{16}{\pi^n} \left\langle F^{n-2} \left[\hat{I}_* F + (n-1) \hat{F} I_* \right] \right\rangle_p^{\leq}, \\ &= \underbrace{\frac{16}{\pi^n} \langle \hat{I}_* F^{n-1} \rangle_p^{\leq}}_{\equiv \Phi_n^a(p)} + \underbrace{\frac{16}{\pi^n} (n-1) \langle F^{n-2} \hat{F} I_* \rangle_p^{\leq}}_{\equiv \Phi_n^b(p)}. \end{aligned} \quad (5.16)$$

The term proportional to $\hat{I}_* F$ (respectively $\hat{F} I_*$) noted Φ_n^a (respectively Φ_n^b) comes from the expansion of the first (respectively the second) resummed term of \mathcal{U}_{pp} in (5.7b). The functions Φ_n are shown in figure 5.3 for $n = 1, 2, 3, 4, 5$ as a function of k/k_F . In particular:

$$\Phi_1(p) = \frac{16}{\pi} \langle \hat{I}_* \rangle_p^{\leq} = \frac{4}{3\pi}, \quad \text{and} \quad \Phi_2(p) = \frac{16}{\pi^2} \langle \hat{I}_* F + \hat{F} I_* \rangle_p^{\leq} \quad (5.17a)$$

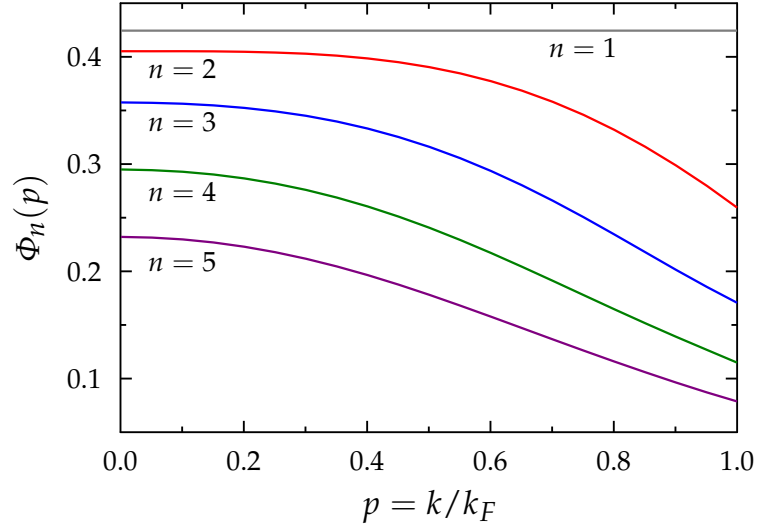


Figure 5.3: Momentum dependence of the perturbative contributions of the real part of the self-energy given by (5.16) for $n = 1, 2, 3, 4, 5$. See also figure 10 of [240].

| p | $\Phi_2(p)$ | $\Phi_2'(p)$ | $\Phi_2''(p)$ |
|----------|----------------------------------|----------------------------------|----------------------------------|
| 1 | $\frac{4}{15\pi^2}(11 - 2\ln 2)$ | $\frac{16}{15\pi^2}(1 - 7\ln 2)$ | $-\frac{16}{15\pi^2}(2 + \ln 2)$ |
| 0 | $\frac{4}{\pi^2}$ | 0 | 0 |
| ∞ | 0 | 0 | 0 |

Table 5.1: Numerical value of $\Phi_2(p)$, its first and second derivative at $p = 0, 1$, and ∞ . Note that at $p = 0$ and 1 , $\Phi_2''(p)$ is not differentiable.

gives the Galitskii formula [225] where the function Φ_2 is given by (B.22a) in appendix B. In table 5.1, we give for reference the asymptotic values of this function as well as its first and second derivatives at $p = 0, 1$, and ∞ . In figure 5.4, the two functions Φ_2^a and Φ_2^b are shown as a function of $p = k/k_F$. We note that Φ_2^a (respectively Φ_2^b) corresponds to the pp contribution (respectively hh contribution) displayed in figure 4.1.c.

NAIVE ATTEMPT OF PHASE-SPACE AVERAGE APPROXIMATION IN RESUMMATION

Guided by the HvH theorem, we see that the denominators of the single-particle potential at $k = k_F$ given by (5.14) contain the resummation of:

$$1 + \frac{a_s k_F}{\pi} \|F\| + \left[\frac{a_s k_F}{\pi} \|F\| \right]^2 + \dots = \left[1 - \frac{a_s k_F}{\pi} \|F\| \right]^{-1},$$

$$1 + 2 \frac{a_s k_F}{\pi} \|F\| + 3 \left[\frac{a_s k_F}{\pi} \|F\| \right]^2 + \dots = \left[1 - \frac{a_s k_F}{\pi} \|F\| \right]^{-2}.$$

Such terms can be obtained assuming for instance:

$$\langle \widehat{I}_* F^{n-1} \rangle_p^< \simeq \|F\|^{n-1} \langle \widehat{I}_* \rangle_p^< \quad \text{and} \quad \langle \widehat{F} F^{n-2} I_* \rangle_p^< \simeq \|F\|^{n-2} \langle \widehat{F} I_* \rangle_p^<, \quad (5.18)$$

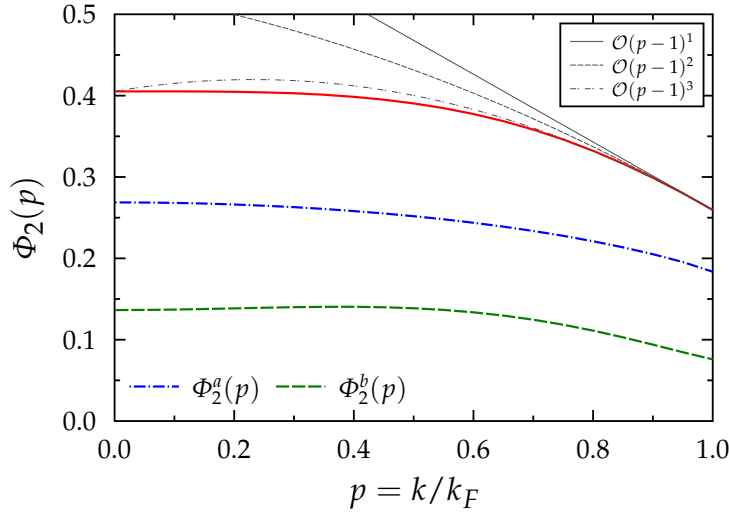


Figure 5.4: Momentum dependence of the two functions Φ_2^a [blue dash-dotted line] and Φ_2^b [green long-dashed line] entering in (5.16) for $n = 2$. The red solid line is the total contribution $\Phi_2 = \Phi_2^a + \Phi_2^b$. For comparison, the gray solid, dashed and dot-dashed thin lines correspond respectively to the expansion up to first, second, and third order in $(p - 1)$ of Φ_2 around the Fermi momentum [see (5.17a)].

in (5.16). Then, summing up all terms using (5.15), we get:

$$\frac{U_{pp}(k)}{\varepsilon_{FG}} = \frac{16a_s k_F \langle \hat{I}_* \rangle_p^<}{\pi - (a_s k_F) \|F\|} + \frac{16(a_s k_F)^2 \langle \hat{F} I_* \rangle_p^<}{[\pi - (a_s k_F) \|F\|]^2}. \quad (5.19)$$

This expression is rather simple. In particular, the same denominator appears in U_{pp} and in the GPS energy. However, at $p = k/k_F = 1$:

$$\langle \hat{F} I_* \rangle_{p=1}^< = \frac{1}{120}(7 - 2 \ln 2) \neq \|F\| \langle I_* \rangle_{p=1}^< = \frac{1}{420}(11 - 2 \ln 2), \quad (5.20)$$

and this expression fails to reproduce (5.14). We see therefore that this naive analysis is not consistent with the phase-space average approximation of the energy since it breaks down the HvH theorem. More generally, we have systematically found that any naive assumption where $F(s, t)$ is replaced by its phase-space average $\|F\|$ leads to a breakdown of the HvH theorem. Therefore, more elaborated strategies should be adopted. In the following, we present an approximate self-energy consistent with the HvH theorem by imposing directly the expansion of U_{pp} in $(a_s k_F)$ up to second order.

RESUMMING THE SELF-ENERGY WITH THE HVH CONSTRAINT

To enforce the HvH theorem, we assume the following momentum dependence:

$$\frac{U_{pp}(k)}{\varepsilon_{FG}} = \frac{16(a_s k_F) \langle \hat{I}_* \rangle_p^<}{\pi - (a_s k_F) \|F\| \{1 + \Delta_a(p)\}} + \frac{16(a_s k_F)^2 \langle I_* \rangle_p^< \|F\| \{1 + \Delta_b(p)\}}{[\pi - (a_s k_F) \|F\| \{1 + \Delta_a(p)\}]^2}, \quad (5.21)$$

where we have generalized (5.19) to allow for different p dependences in the denominator and in the numerator such that the replacements:

$$\|F\| \mapsto \|F\| \{1 + \Delta_a(p)\} \quad \text{and} \quad \langle \widehat{I}_* \rangle_p^< \mapsto \|F\| \{1 + \Delta_b(p)\} \langle I_* \rangle_p^<, \quad (5.22)$$

are made. Here $\Delta_{a,b}(p)$ are unknown functions that we will determine below. Comparing with (5.13), we first remark that the condition $\Delta_{a,b}(p=1) = 0$ is sufficient to insure the validity of the HvH theorem. Let us expand (5.21) up to second order in $(a_s k_F)$ and impose that the expansion matches⁴ the one given by (5.17a) for $p = k/k_F \leq 1$. Replacing $\langle \widehat{I}_* \rangle_p^<$ and $\langle I_* \rangle_p^<$ by their respective (p -independent) values given in appendix E, we obtain the condition:

$$\Phi_2(p) = \underbrace{\frac{4}{3\pi^2} \|F\| \times \{1 + \Delta_1(p)\}}_{\equiv \Phi_2(p)X(p)} + \underbrace{\frac{4}{3\pi^2} \|F\| \times \left\{ \frac{1 + \Delta_2(p)}{6} \right\}}_{\equiv \Phi_2(p)[1 - X(p)]}. \quad (5.23)$$

Here, we have introduced a new function $X(p)$ defined through:

$$\frac{X(p)/6}{1 - X(p)} = \frac{1 + \Delta_1(p)}{1 + \Delta_2(p)}$$

With this, the real part of the self-energy given by (5.21), for $p = k/k_F \leq 1$, can be rewritten as:

$$\frac{U_{GPS_X}(k)}{\varepsilon_{FG}} = \frac{4}{3\pi} \frac{(a_s k_F)}{1 - (3\pi/4)\Phi_2(p)X(p)(a_s k_F)} + \frac{\Phi_2(p)[1 - X(p)](a_s k_F)^2}{[1 - (3\pi/4)\Phi_2(p)X(p)(a_s k_F)]^2}. \quad (5.24)$$

This approximate self-energy, called GPS_X hereafter, has the following properties:

1. Under the condition $X(1) = 6/7$ [see (5.13)], the HvH theorem is verified. Note that only the value of $X(p)$ at $p = k/k_F = 1$ is constrained by the HvH theorem and we have no constraint on its momentum dependence. The case where the function $X(p)$ is assumed constant and equal to $6/7$ will be called GPS single-particle potential in the following. In this case, we recover (5.14) and for $k \neq k_F$ we have:

$$\frac{U_{GPS}(k)}{\varepsilon_{FG}} = \frac{4}{3\pi} \frac{(a_s k_F)}{1 - (9\pi/14)\Phi_2(p)(a_s k_F)} + \frac{(1/7)\Phi_2(p)(a_s k_F)^2}{[1 - (9\pi/14)\Phi_2(p)(a_s k_F)]^2}. \quad (5.25)$$

2. With this condition, both GPS and GPS_X are consistent with the phase-space average approximation of the energy obtained from pp ladder resummation, namely the GPS functional (3.10).
3. Both have the correct limit at low density up to $(a_s k_F)^2$.
4. And both have a finite limit at unitarity.

In figure 5.5, we show finally the full momentum dependence of the approximate self-energy (5.25) obtained at unitarity assuming $X(p) = 6/7$ independent on p

⁴ Note that the first order is automatically obtained since: $\Phi_1(p) = 16/\pi \times \langle \widehat{I}_* \rangle_p = 4/3\pi$ [see (5.16)].

[panel (a)]. In the following, unless it is specified, we will simply assume that $X(p) = 6/7$. We compare it with the full self-energy resummation result obtained from (5.7a), with the BHF calculation obtained in [84], and with experimental data from [296]. The result obtained by (5.7a) at strict unitarity presents a large [non divergent] peak around $p \sim 0.7$ in contradiction with realistic calculation. This peak is absent in the phase-space average approximation. The amplitude of the approximated self-energy (5.25) is similar to the BHF results and to the experimental data. The phase-space approximation proposed here for the self-energy leads to a much better agreement compared to the AEI/GEI self-energy with realistic results. In this figure [panel (b)], we also give for reference the single-particle energy defined by (5.4).

SIMPLE PARTIAL PHASE-SPACE AVERAGE APPROXIMATION FOR THE SELF-ENERGY

Before discussing the partial phase-space approximation of the AEI self-energy and the associated quasi-particle properties of both the GPS and APS cases, we illustrate here a simpler strategy to impose the low-density limit up to second order in $(a_s k_F)$ and the convergence to a finite limit at unitarity avoiding complicated integrals. Let us assume that we seek an approximate form of the self-energy that matches the expansion (5.15) up to second order in $(a_s k_F)$ while being non-divergent at large value of a_s . Guided by the approximation made for the energy, one might simply use a Padé[1/1] approximate form:

$$\frac{U(k)}{\varepsilon_{FG}} \simeq \frac{4}{3\pi} \frac{(a_s k_F)}{1 - (3\pi/4)\Phi_2(p)(a_s k_F)}. \quad (5.26)$$

From this expression and using the expansion of $\Phi_2(p)$ given by (4.5a), we immediately see that the low-density limit of the chemical potential and effective mass given by (4.6) are recovered. In addition starting from the expression of the chemical potential, the corresponding form of the ground-state energy in infinite systems can be obtained⁵ simply using the relationship (4.6c).

We compare in figure 5.6 the dependences of the chemical potential and effective mass on $-(a_s k_F)$ and $-(a_s k_F)^{-1}$ when we used the Padé[1/1] approximate form (5.26) for the single-particle potential. By construction, contrary to an approximation where the self-energy is truncated at a given order in $(a_s k_F)$, the Padé[1/1] approximate form (5.26) and the GEI self-energy leads both to a smooth and converging behavior of these quantities up to infinite values of a_s . These approximate self-energies also reproduce correctly the low density limit. We see in particular that the chemical potential obtained with (5.26) follows closely the one of the original GEI result. We note also that the effective mass is more affected by the Padé approximation. It turns out to be slightly lower compared to the GEI case and closer qualitatively to the BHF results up to $-(a_s k_F) \simeq 3$. As expected from the original result obtained by direct integration, the large $|a_s k_F|$ limit is not correctly accounted for. One difference we have observed is that the dependence of the single-particle potential given by (5.26) close to unitarity remains also very smooth and does not present the bumps seen in figures 5.1.

⁵ Starting from (5.26) and using (4.6c) we can obtain:

$$\frac{E}{E_{FG}} = 1 + \frac{5}{9(a_s k_F)^5 C^6} \left[-12(a_s k_F)^5 C^5 - 75\pi(a_s k_F)^4 C^4 - 500\pi^2(a_s k_F)^3 C^3 - 3750\pi^3(a_s k_F)^2 C^2 - 37500\pi^4(a_s k_F) C - 187500\pi^5 \ln \left(1 - (a_s k_F) \frac{C}{5\pi} \right) \right]$$

where we have defined $C = (11 - 2\ln 2)$. This expression leads at strict unitarity to $\xi_0 \simeq 0.30$, and its expansion up to second order matches the Lee-Yang formula.

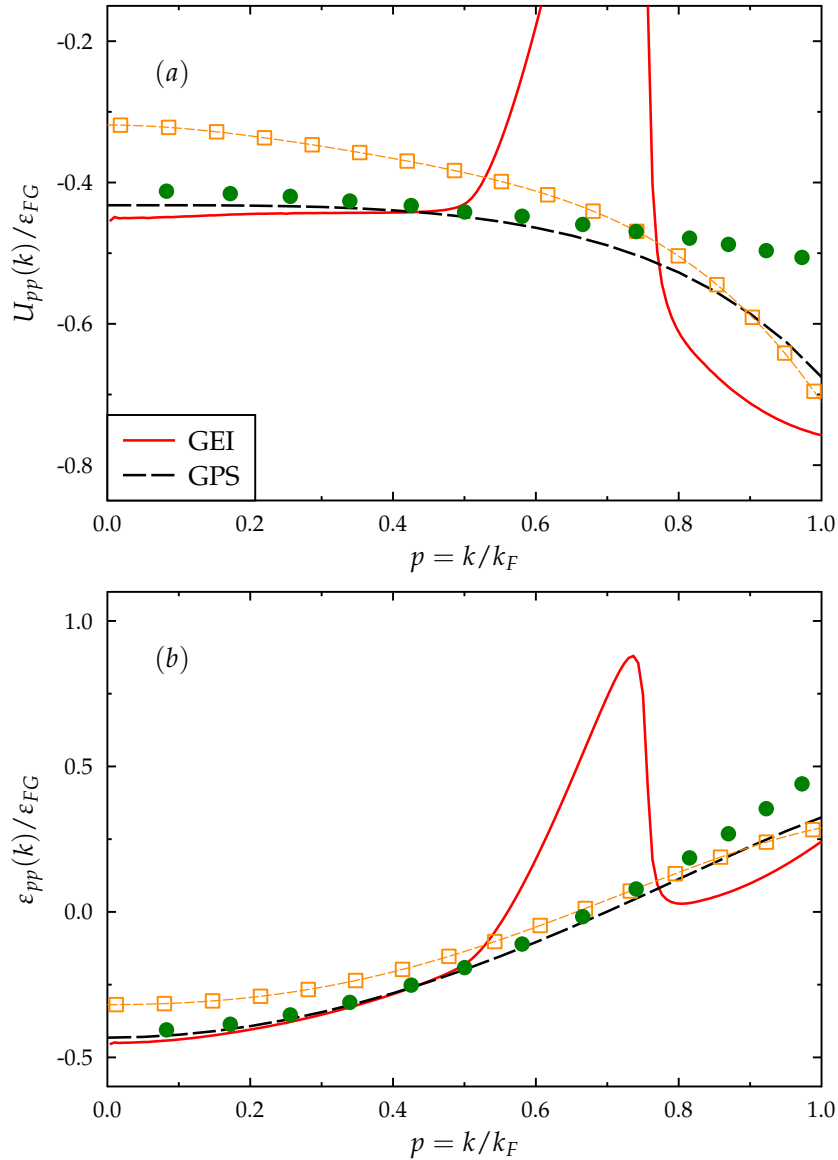


Figure 5.5: (a) Real part of the resummed self-energy and (b) associated single-particle energy (5.4) at strict unitarity below the Fermi surface. The black dashed line corresponds to the GPS results (5.25) with $X(p) = 6/7$, the red solid line to the exact integration of (5.7a). For comparison, the green dots are the Brueckner Hartree-Fock calculations obtained without pairing effect [84] and the orange open squares is the best fit of experimental results of [296], both obtained at temperature near the critical temperature of the superfluid state transition $T \simeq T_c$.

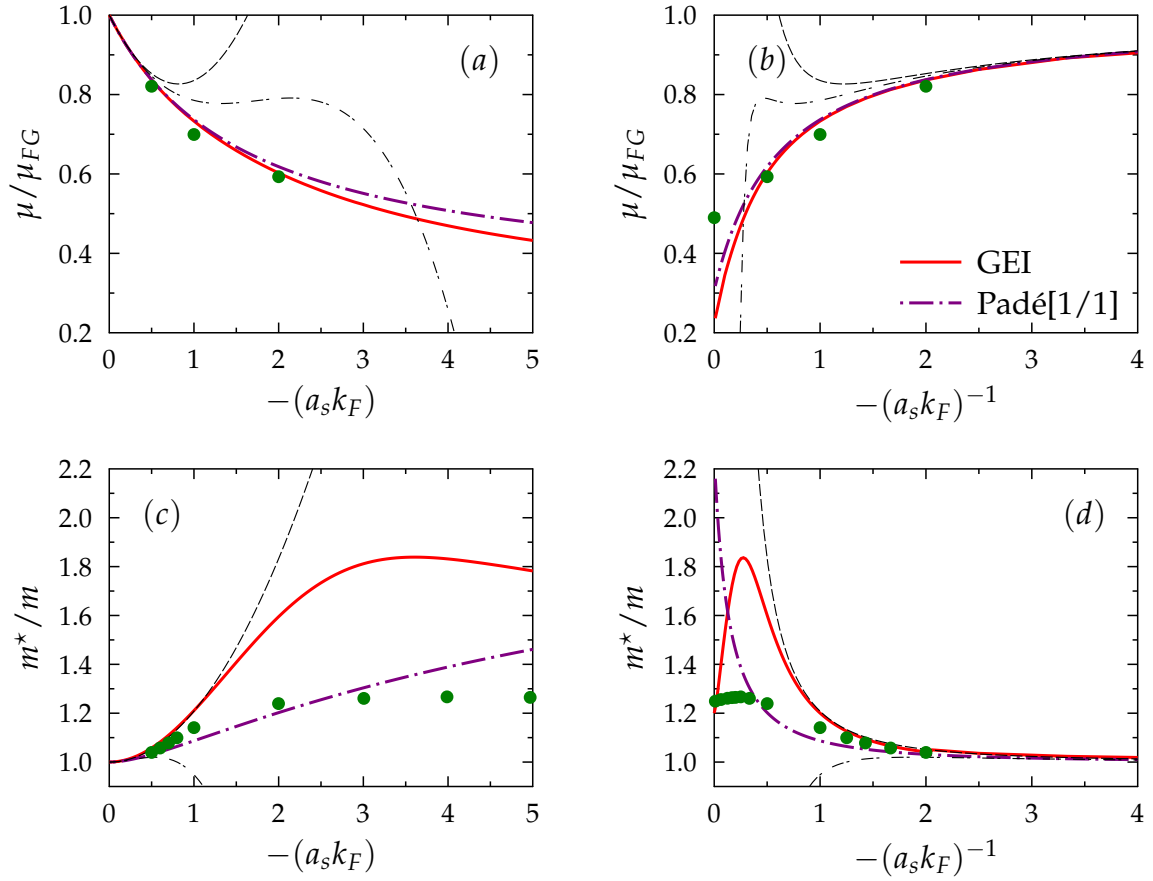


Figure 5.6: Comparison of the chemical potential [panels (a) and (c)] and effective mass [panels (b) and (d)] obtained with the Padé[1/1] approximation given by (5.26) (purple dot-long dashed line) and the original GEI result (red solid line). For comparison, the BHF results [84] are also shown (green circles).

5.1.c Approximate self-energy consistent with the APS functional

In the previous section, starting from a given resummation scheme of the self-energy (particle-particle ladder diagrams resummation in that case), we have presented a general methodology to obtain a simplified form of the self-energy consistent with the HvH theorem. Below we summarize the general methodology applicable for any self-energy and valid up to second order in $(a_s k_F)$.

GENERAL METHODOLOGY

- (a) *Hugenholtz-van-Hove (HvH) theorem constraint.* For a given expression of the self-energy $U(k)$ and knowing the ground-state energy per particle E/N , we first:
- calculate the chemical potential given by the thermodynamical relation $\mu = \partial E / \partial N|_V$.
 - enforce the HvH theorem by imposing that the chemical potential is equal to the single-particle potential estimated at the Fermi surface: $\mu = \mu_{FG} + U(k_F) = \varepsilon(k_F)$.
 - finally impose that the energy expansion up to second order in $(a_s k_F)$ is equal to the Lee-Yang formula. This implies that the single-particle potential at $k = k_F$ can be written as a function of $(6/35)(11 - 2 \ln 2) = (9\pi^2/14)\Phi_2(1)$ [see (2.24) and (4.5a)].
- (b) *Second order in $(a_s k_F)$ for the momentum dependence.* In a second step, the self-energy at $k \neq k_F$ is obtained from $U(k_F) \equiv U(k_F; \Phi_2(1))$ simply by replacing $\Phi_2(1)$ by $\Phi_2(k/k_F)$.

Note that this general methodology is exact in many-body perturbation theory at low density up to second order in $(a_s k_F)$, i.e. starting from Lee-Yang expression of the energy, we automatically find the Galitskii formula given by (4.4).

As a further illustration, we apply below this methodology starting from the resummed self-energy obtained in chapter 4, section 4.3, where now the combined particle-particle and hole-hole ladder diagrams are included.

(a) HVH THEOREM CONSTRAINT WITH THE APS FUNCTIONAL

- We first use the HvH theorem (5.5) to identify the chemical potential given by the APS functional (3.14) to the single-particle energy at the Fermi surface:

$$\frac{\mu}{\mu_{FG}} = \frac{E}{E_{FG}} + \frac{k_F}{5} \frac{\partial E / E_{FG}}{\partial k_F} = 1 + \frac{16\pi(a_s k_F) \langle I_* \rangle_{p=1}^<}{[\pi - (a_s k_F) \|R\|]^2 + [\pi \|I_*\| (a_s k_F)]^2} + \frac{16}{3\pi} \arctan \frac{\pi \|I_*\| (a_s k_F)}{\pi - (a_s k_F) \|R\|}. \quad (5.27)$$

Here $\|\dots\|$ denotes the phase-space values of the functions that are given in appendix E:

$$\|R\| = \frac{\langle\langle RI_* \rangle\rangle}{\langle\langle I_* \rangle\rangle} = \frac{6}{35}(11 - 2 \ln 2) \quad \text{and} \quad \|I_*\| = \frac{\langle\langle I_* \rangle\rangle}{\langle\langle 1 \rangle\rangle} = \frac{5}{24}. \quad (5.28)$$

- We then impose that the HvH theorem is fulfilled to properly obtain the APS functional.
- Then, we identify the phase-space average values of the function $R(s, t)$ appearing in $U(k_F)$ with $\|R\| = (9\pi^2/14)\Phi_2(1)$. This ultimately gives:

$$\frac{U(k_F)}{\varepsilon_{FG}} = 1 + \frac{2}{9\pi} \frac{(a_s k_F)}{[1 - (9\pi/14)\Phi_2(1)(a_s k_F)]^2 + [5(a_s k_F)/24]^2} + \frac{16}{3\pi} \arctan\left(\frac{5(a_s k_F)/24}{1 - (9\pi/14)\Phi_2(1)(a_s k_F)}\right). \quad (5.29)$$

The methodology proposed here is of practical interest in the APS case⁶ since it requires only the resummed ground-state energy to be known.

(b) MOMENTUM DEPENDENCE OF THE APS SELF-ENERGY

We then obtain the momentum dependence of $U(k)$ by making the replacement $\Phi_2(1) \mapsto \Phi_2(p)$ in (5.29) leading to:

$$\frac{U_{APS}(k)}{\varepsilon_{FG}} = \frac{(2/9\pi)(a_s k_F)}{[1 - (9\pi/14)\Phi_2(p)(a_s k_F)]^2 + [5(a_s k_F)/24]^2} + \frac{16}{3\pi} \arctan\left(\frac{5(a_s k_F)/24}{1 - (9\pi/14)\Phi_2(p)(a_s k_F)}\right). \quad (5.30)$$

Similarly to what was done in the GPS_X case, we can eventually introduce a generalization of this single-particle potential called APS_X and defined by:

$$\frac{U_{APS_X}(k)}{\varepsilon_{FG}} = \frac{(2/9\pi)(a_s k_F)}{[1 - (9\pi/4)\Phi_2(p)X(p)(a_s k_F)]^2 + [(5/24)(a_s k_F)]^2} + \frac{16}{3\pi} \arctan\left(\frac{(5/24)(a_s k_F)}{1 - (9\pi/10)\Phi_2(p)[1 - X(p)](a_s k_F)}\right). \quad (5.31)$$

The only constraint on the function $X(p)$ is now $X(p=1) = 2/7$. Assuming that this function is constant for all p leads to the APS approximation of the single-particle potential (5.30). Again, the low-density limit up to second order in $(a_s k_F)$ as well as the consistency with the APS functional are respected, and whatever the explicit form of $X(p)$, in the infinite scattering length limit, we obtain the APS value for the Bertsch parameter.

The chemical potential and the effective mass dependence on $(a_s k_F)$ obtained with the consistent GPS and APS schemes are displayed in figure 5.7 respectively as a function of $-(a_s k_F)$ or $-(a_s k_F)^{-1}$. The conclusion is similar as for the simple GPS case presented previously, i.e. the low-density limit (respectively Lee-Yang and Galitskii formula) is properly reproduced by construction. The BHF results are reproduced qualitatively up to $-(a_s k_F) \simeq 3$ while the perturbative expansion breaks down around $-(a_s k_F) = 0.5$. We note however that the result of the consistent APS approximation is slightly worse compared to the original AEI as far as the chemical potential is concerned.

⁶ Note that, the direct identification term by term with the resummed AEI self-energy, as done before in the GEI case, is more difficult because of the appearance of the Dirac delta function in the integral on the accessible phase-space (see appendix C).

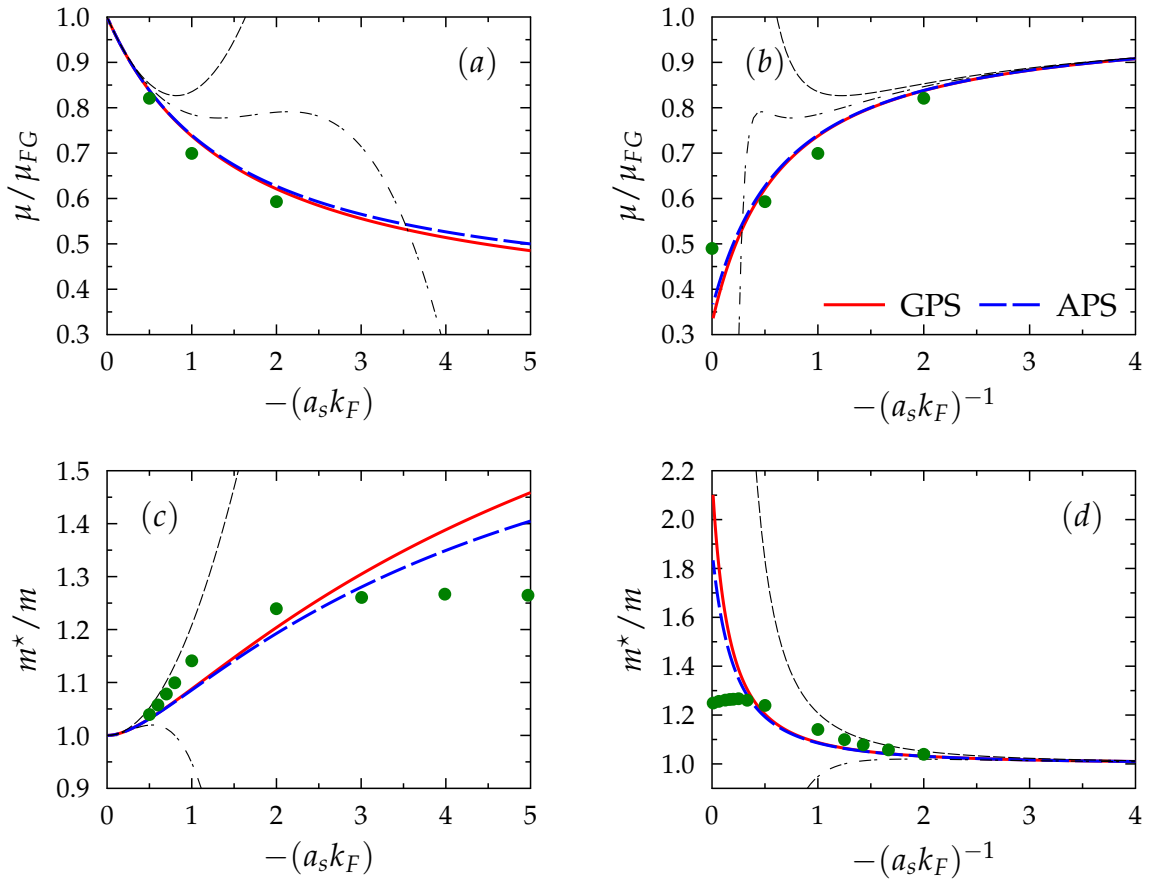


Figure 5.7: Chemical potential and effective mass as a function of $(a_s k_F)$ [panels (a) and (c)] or $-(a_s k_F)^{-1}$ [panels (b) and (d)] obtained with the GPS (red solid line) and APS (blue dashed line) approximations. In panels (a) and (c), results of the second order (Galitskii formula) and third order expansions [232] in $(a_s k_F)$ are shown with black dashed and dot-dashed thin lines respectively. The green circles correspond to the result of the BHF calculations of [84].

5.2

APPROXIMATE EXPRESSIONS FOR THE SELF-ENERGY

The targeted goal of this thesis is to provide a DFT inspired by the many-body resummation techniques presented above. The clear advantage to start from the self-energy level instead of the energy itself is that direct connections can be made between the self-energy and the Fermi Liquid theory. This was illustrated previously with the chemical potential and the effective mass. Such quantities are also standardly obtained with Energy Density Functionals for instance used in the nuclear physics context, like Skyrme or Gogny EDFs [101]. Empirical functionals, especially the functionals derived using Skyrme like contact interactions lead to very simple single-particle potentials (see discussion below) with polynomial dependence in k . For instance, the original parameterization proposed in [110] leads simply to quadratic dependence of the single-particle potential in infinite matter (see section 1.3). Novel generations of Skyrme EDF have been proposed leading to quartic or higher-order dependence in the momentum [151,171,298]. The justification why such simple approximations can contain important physical aspects can be found in [192]. The different single-particle potentials obtained in the previous section presents rather complex density and momentum dependence.

As an illustration of possible simplification of the APS/GPS single-particle potentials, we can first consider several approximate treatments of the function Φ_2 expanding it in powers of $(p - 1)$, i.e. around $k = k_F$. After that, these approximations can be used directly in (5.25), (5.24), (5.30) or (5.31). We have tried this technique and obtained reasonable results for the self-energy, especially around the Fermi momentum ($k = k_F$). However, the simple replacement of the function Φ_2 appearing in the GPS/APS self-energies by an approximate form leads to rather complex expressions in terms on the momentum k . The appearance of a momentum dependence in the denominator of the resummed self-energy could be a source of difficulty for practical applications of the resulting DFT. Having in mind that our ultimate goal will be to obtain a DFT from the self-energy applicable to finite systems, we now consider simpler strategies leading only to a k dependence in the numerator.

The goal here is ultimately to obtain a DFT and, from that point of view, (5.25) or (5.30) are still too complex and it might be useful later to get a simplified expression. In this section, we explore the possibility to simplify further the self-energy obtained by phase-space averaging. Doing so removes the rather complex function $\Phi_2(p)$ appearing in the resummed APS/GPS self-energy. We explore below several ways to obtain a simplified expression of the self-energy while keeping several important properties.

For instance, starting from the partial phase-space average approximation presented in the last section, one might obtain a systematic polynomial expansion to a given order in k . For this, we will explore the possibility to further simplify the functional by approximating the single-particle potential obtained by a polynomial form. We introduce the following expansion:

$$\frac{U(k)}{\varepsilon_F} \simeq U_0(a_s k_F) + U_2(a_s k_F) \left(\frac{k}{k_F}\right)^2 + U_4(a_s k_F) \left(\frac{k}{k_F}\right)^4 + \dots \quad (5.32)$$

This polynomial expansion, truncated at an appropriate order will not only be useful to make contact with empirical density functional theory but will also enable to obtain practical DFT for finite systems based on the present approach.

5.2.A Polynomial form of single-particle potential in power of k^{2n}

The aim here is to approximate the one-body potential as in (5.32) while preserving the quasi-particle properties close to the Fermi energy such as the chemical potential and the effective mass given by the resummed APS/GPS self-energy. This gives strong constraints on the U_{2n} coefficient that must be chosen to reproduce the correct expansion up to a given order in $(k - k_F)$. More precisely, if both μ and m^* are constrained, this means that the expansion (5.32) at first order in $(k - k_F)$ should match the original single-particle potential. In the following, two cases are considered: a quadratic and a fourth order polynomial form of U in powers of k .

- *Quadratic polynomial form.*

We first assume a simple quadratic dependence of the the APS/GPS single-particle potentials given by (5.32). U_0 and U_2 are chosen to reproduce the Taylor expansion of the APS/GPS single-particle potentials around the Fermi surface up to first order in $(k - k_F)$ given by (5.6a). This gives the constraints:

$$\begin{cases} U_0(a_s k_F) = \left[\frac{\mu}{\mu_{FG}} - \frac{m}{m^*} \right], \\ U_2(a_s k_F) = \frac{m}{m^*} - 1, \end{cases} \quad (5.33)$$

where μ and m^* are those obtained either using the APS or the GPS approach. Their expressions are given in appendix F.

- *Fourth-order polynomial form.*

We also considered the possibility to add one order in k^2 , i.e. assuming a fourth-order polynomial form of the single-particle potential given by (5.32). U_0, U_2 and U_4 are now chosen to reproduce the quadratic Taylor expansion around the Fermi surface. This gives now the set of equations:

$$\begin{cases} U_0(a_s k_F) = \left[\frac{\mu}{\mu_{FG}} - 1 \right] - \frac{5}{4} \left[\frac{m}{m^*} - 1 \right] + \frac{D_2}{8}, \\ U_2(a_s k_F) = \frac{3}{2} \left[\frac{m}{m^*} - 1 \right] - \frac{D_2}{4}, \\ U_4(a_s k_F) = \frac{D_2}{8} - \frac{1}{4} \left[\frac{m}{m^*} - 1 \right], \end{cases} \quad (5.34)$$

where D_2 denotes the second derivative according to p of $U(k)/\varepsilon_F$ at $p = 1$. Again, we took for μ , m^* , and D_2 the values obtained respectively from the APS or GPS single-particle potential.

In figures 5.8 and 5.9 for the GPS and APS cases respectively, we show for various density regimes the approximate single-particle potential obtained by replacing the GPS [respectively APS] single-particle potential (5.25) [respectively (5.30)] by

its polynomial form. We see that the polynomial approximations reproduce rather well the amplitudes and shapes of the resummed APS/GPS self-energies at low density. At unitarity, although the quasi-particle properties (μ and m^*) are the same according to the GPS/APS single-particle potentials cases, the quadratic/quartic approximations do not reproduce the amplitude in the small k region where much higher values of $U(k)$ are observed compared to the reference GPS/APS single-particle potentials. That is actually not surprising since the polynomial form is solely constrained around $k = k_F$.

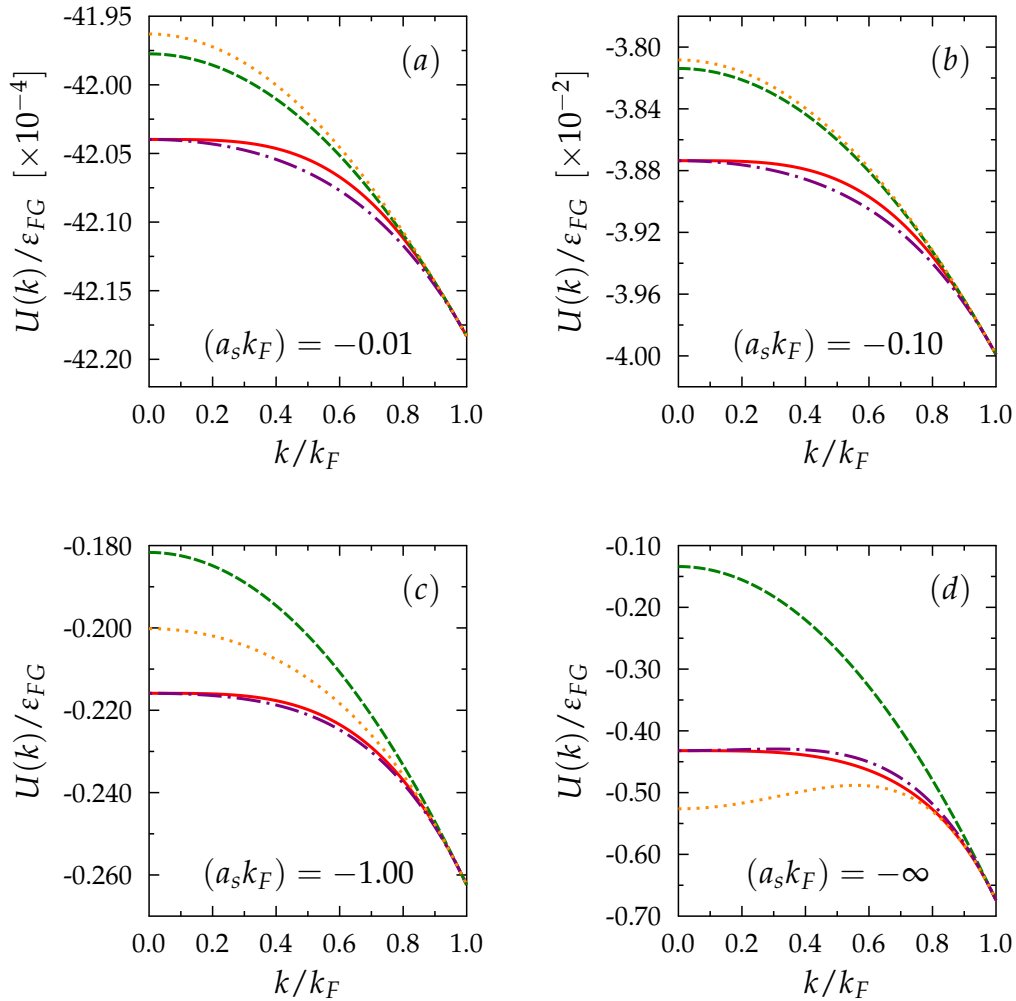


Figure 5.8: Momentum dependence of the polynomial approximation for the self-energy for $-(a_s k_F) = 0.01$ (a), 0.1 (b), 1 (c) and ∞ (d) obtained with the GPS approximation (red solid line). In each panel, the corresponding quadratic or quartic approximations (without constraint at $k = 0$) are shown respectively by the green dashed and orange dotted lines. The purple long-short dashed line correspond to the quartic approximations with constraint at $k = 0$.

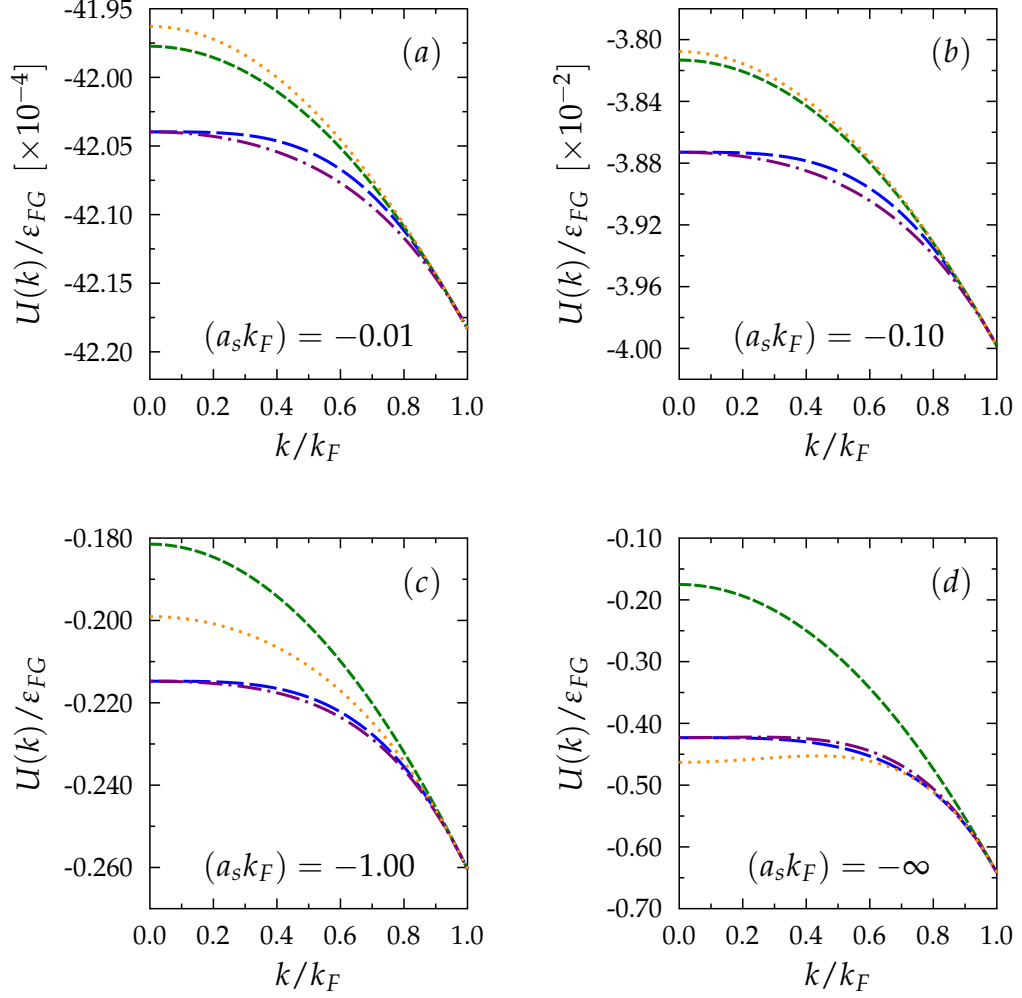


Figure 5.9: Same as figure 5.8 for the APS approximation. The reference APS curve is now shown in blue long-dashed line.

ADDING A CONSTRAINT ON $k = 0$ FOR THE QUARTIC APPROXIMATION

To improve the reproduction of the reference APS/GPS single-particle-potentials, in particular a low momentum k , one possibility is to (i) constrain the value at $k = 0$ of the approximate polynomial form [$U(0) = U_0$] on the low momentum of the APS/GPS self-energies and (ii) maintain the expansion of the APS/GPS single-particle potential up to first order in $(k - k_F)$.

Starting from the single-particle potential given by (5.32) truncated at fourth order in k , the constants U_0, U_2 and U_4 are now chosen to reproduce the Taylor expansion around the Fermi surface of the APS/GPS single-particle potentials up to first order in $(k - k_F)$ as well as the APS/GPS single-particle potentials at $k = 0$. This gives:

$$\begin{cases} U_0(a_s k_F) = \left[\frac{v}{\mu_{FG}} - 1 \right] \\ U_2(a_s k_F) = 2 \times \left[\frac{\mu}{\mu_{FG}} - \frac{v}{\mu_{FG}} \right] - \left[\frac{m}{m^*} - 1 \right] \\ U_4(a_s k_F) = \left[\frac{m}{m^*} - 1 \right] - \left[\frac{\mu}{\mu_{FG}} - \frac{v}{\mu_{FG}} \right] \end{cases} \quad (5.35)$$

where $\nu = \mu_{FG} + U(0)$ is defined using the original single-particle potential at $k = 0$.

The results are shown for various $(a_s k_F)$ in figures 5.8 and 5.9 for the GPS and APS cases respectively. We see that this approximation reproduces rather well the momentum dependence of the reference APS/GPS single-particle potentials for all $(a_s k_F)$ including the unitary limit.

5.2.B Summary and discussions

In conclusion, anticipating eventual future applications of the functionals, we have shown that the APS/GPS functionals can be eventually replaced by a quadratic or quartic polynomial form in k^2 . These polynomial forms have a number of interesting properties:

1. For all polynomial forms discussed above, the coefficients U_{2n} are explicit non-divergent functions of $(a_s k_F)$ [see appendix F for explicit parametrization in term of $(a_s k_F)$];
2. The quasi-particle properties (the chemical potential and the effective mass) of the reference APS/GPS self-energy are reproduced for all $(a_s k_F)$. For instance, in the quadratic case, the single-particle potential can be written as:

$$\frac{U(k)}{\varepsilon_{FG}} = \left[\frac{\mu}{\mu_{FG}} - \frac{m}{m^*} \right] + \left[\frac{m}{m^*} - 1 \right] \left(\frac{k}{k_F} \right)^2. \quad (5.36)$$

where μ and m^* are provided by one of the approximations (APS or GPS) presented previously.

3. Eventually, considering the fourth-order polynomial form with the low-momentum constraint, the full momentum dependence (from $k = 0$ to $k = k_F$) is well approximated by:

$$\begin{aligned} \frac{U(k)}{\varepsilon_{FG}} = & \left[\frac{\nu}{\mu_{FG}} - 1 \right] + \left\{ 2 \times \left[\frac{\mu}{\mu_{FG}} - \frac{\nu}{\mu_{FG}} \right] - \left[\frac{m}{m^*} - 1 \right] \right\} \left(\frac{k}{k_F} \right)^2 \\ & - \left\{ \left[\frac{\mu}{\mu_{FG}} - \frac{\nu}{\mu_{FG}} \right] - \left[\frac{m}{m^*} - 1 \right] \right\} \left(\frac{k}{k_F} \right)^4. \end{aligned} \quad (5.37)$$

It is important to mention that the self-energy shift ν is not related to the Landau theory of Fermi liquid (FLT). Actually, FLT describes the low-energy excitation, i.e. close to the Fermi surface. This constraint turns out to be required however to reproduce the full momentum dependence of the self-energy by a fourth-order polynomial in k . In principle, for a Fermi liquid, only the quasi-particle properties are relevant to describe phenomena, e.g. low-energy particle or hole excitations, linear response, collective modes, etc. [128]. The quadratic form (5.36) is simpler for practical purpose. However, we have seen that the quartic form (5.37) might be sometimes more realistic. For these reasons, we will discuss both cases in the following.

Note that, without loss of generality, the same strategy can be followed starting from a more general momentum dependence of the reference single-particle potential, as the $\text{APS}_X/\text{GPS}_X$, including the function $X(p)$. An explicit parametrization of this case can be found in appendix F.

SINGLE-PARTICLE POTENTIAL OF DILUTE FERMI GAS

We illustrate here the properties of dilute Fermi gases. More precisely, we discuss their quasi-particle properties and the low-momentum limit of the corresponding single-particle energies obtained with the quadratic/quartic approximate form of the APS/GPS single-particle potentials. Starting from (5.36) and (5.37) where μ , m^* and ν are given in appendix F for the GPS and APS single-particle potentials, we show in figure 5.10 the momentum dependence of the quadratic and quartic form of the GPS and APS single-particle energy $\varepsilon(k)$ defined by (5.4). Note that, in the case presented in this figure, the APS and GPS forms give sensibly the same result and cannot be distinguished. The difference is only due to the approximate form chosen, namely the quadratic (5.36) or the quartic form (5.37). These properties stem from the fact that both APS and GPS are built to properly reproduce the correct limit at second order in $(a_s k_F)$. The results are compared with the exact calculation of [232] for dilute Fermi gases up to third order in $(a_s k_F)$. Both quadratic and quartic forms are in good agreement with the second-order result at very low density [panel (a)] where the third-order contribution is negligible. When we increase the density in panel (b), the third-order contribution starts to be significant especially at low momentum. We see that the quartic form is in better agreement with the third order compared to the quadratic approximate forms. It should however be noted that both are largely dominated by the kinetic contribution of the non-interacting Fermi gas $e(k) = k^2/2m$.

At larger values of $(a_s k_F)$ [panel (c)], the perturbative approach breaks down since the difference between two consecutive orders of the result of [232] becomes large compared to the free Fermi gas energy $e(k)$. The resummed forms of the single-particle energy have a more realistic behavior when $(a_s k_F)$ increase. In particular they remain bounded in the non-perturbative regime.

SINGLE-PARTICLE ENERGY AT ZERO MOMENTUM OF DILUTE FERMI GAS

We now consider the properties at low momentum k of the single-particle energy. As mentioned previously, the quadratic single-particle potential at zero-momentum $U(0)$ can be constrained to reproduce the results given by (5.25) for the GPS single-particle potential and by (5.30) for the APS single-particle potential at $k = 0$. To reproduce the $k = 0$ limit, we have to consider a quartic form of the single-particle potential [see (5.37)]. Doing so, we have seen that the quartic form reproduces rather well the global momentum dependence of the single-particle potentials (5.25) or (5.30) in contrast with a quadratic approximate form where $U(0)$ cannot be constrained simultaneously with the chemical potential and effective mass.

In figure 5.11, we compare the single-particle energy at $k = 0$ obtained with the quadratic and quartic approximate form of the GPS and APS single-particle potential. Both quadratic and quartic GPS and the APS results are quite close and follow similar dependences in $(a_s k_F)$ in the low density regime. The results of the GPS and APS cannot be distinguished. Here we only represent the quadratic and quartic results which are valid qualitatively at the same time for the GPS and the APS parametrization of the single-particle potentials.

For reference, we show the exact calculation of [232] for a dilute Fermi gas up to third order in $(a_s k_F)$. Both quadratic and quartic forms are in good agreement with the second-order result. However, only the quartic form has the correct expansion up to $(a_s k_F)^2$ imposed by the constraint given by (5.37). The fact that the quadratic approximation reproduces the correct expansion up to second order seems to be accidental: there is a priori no reason that the second order of $U(0)/\varepsilon_{FG} = \mu/\mu_{FG} - (m/m^*)$ of the quadratic form (5.36) is equal to the second order of $U(0)/\varepsilon_{FG} = \nu/\mu_{FG} - 1$ of the quartic form (5.37). Although, as we have

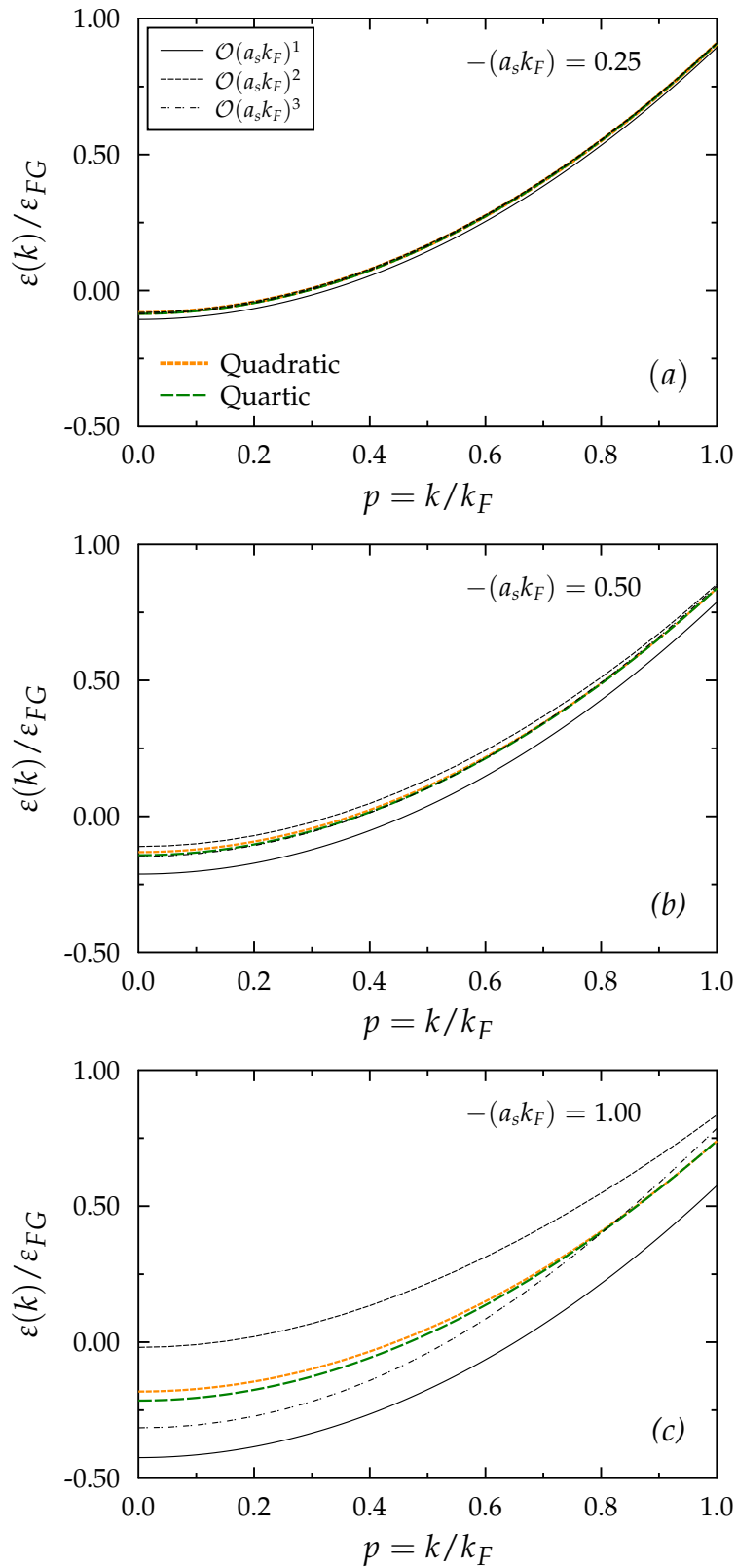


Figure 5.10: Momentum dependence of the single-particle energy divided by μ_{FG} obtained from the quadratic [orange short-dashed line] and quartic [green long-dashed line] approximate forms of the GPS/APS single-particle potentials at $(a_s k_F) = -0.25$ (a), -0.5 (b), and -1 (c). Note that in these cases, the GPS and APS results are indistinguishable and are represented by the same quadratic or quartic lines. For comparison, we show the exact first [black solid thin line], second [black dashed thin line] and third order [black dash-dotted thin line] expansion in $(a_s k_F)$ of the dilute Fermi gas given in [232].

seen for the quasi-particle properties in figure 5.7, the quartic form for which the second-order expansion is valid, is in better agreement with the third-order result of [232] compared to the quadratic form.

We can make the same remark as done for the quasi-particle properties by noting that the perturbative expansion is valid only at very low density and diverges at higher density. On the other hand, the resummed single-particle energy obtained converges smoothly to a finite limit at unitarity. Consequently this approach has an extended domain of validity compared to the standard MBPT for dilute Fermi systems.

To summarize, we have found in this section approximate polynomial form of the GPS/APS single-particle potentials preserving the quasi-particle properties (chemical potential and effective mass). Eventually, adding a constraint on the limit $k = 0$ in the quartic approximate form, we have shown that the full momentum dependence reproduces rather well the original GPS/APS single-particle potentials. These polynomial approximations present an interest towards the exportation of this work to finite systems as we will discuss in the next section.

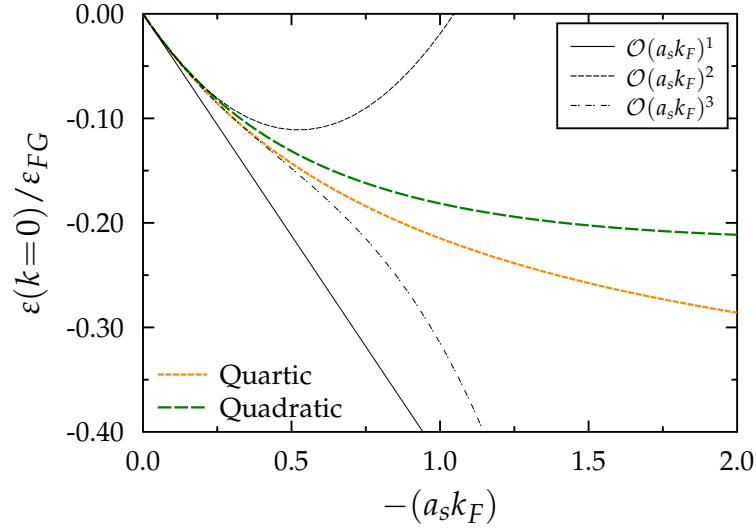


Figure 5.11: The single-particle energy at zero-momentum ($k = 0$) obtained from the GPS and APS single-particle potentials as a function of $-(a_s k_F)$. The green long-dashed line corresponds to the result obtained by assuming a quadratic form of the single-particle potential (5.36) and the orange short-dashed line to a quartic form (5.37). For comparison, we show the first [black solid thin line], second [black dashed thin line] and third order [black dash-dotted thin line] expansion in $(a_s k_F)$ of the dilute Fermi gas given in [232].

5.3

LINK WITH THE EMPIRICAL SKYRME FUNCTIONALS

In this section, we would like to finally discuss how the present work can be helpful to make connection with more empirical nuclear DFTs. More precisely, we discuss one of the question motivating this work: *How can we understand from microscopic calculations the values taken from the empirical Skyrme parameters?* The effective Skyrme interaction (1.13) [considering only the central (t_0, x_0) and (t_1, x_1, t_2, x_2) non-local terms] looks like the $\not\pi$ EFT interaction (1.6) where the coupling constants differ from the physical coupling constants as illustrated in figure 1.18. Intuitively, Skyrme parameters are expected to be linked to effective coupling constants that are strongly renormalized by non-trivial medium effects. The aim of the present discussion is to see if the development made in this thesis could be useful to understand empirical functionals and more precisely the Skyrme functionals. To do so, we will first rewrite the functionals developed here in the form of Skyrme-type EDFs with parameters that will now depend on the density.

We start our investigation by linking directly the density-dependent Skyrme parameters to the EDF introduced in chapter 3. We will show that the functional inspired by the resummation leads to a qualitative understanding of the value taken by the (t_0, x_0) Skyrme parameters generally retained in the empirical EDF. Then, we extend the discussion using the non-empirical DFT introduced in the present work.

5.3.A From non-empirical DFT to density-dependent parameters

Before bridging the DFT introduced in chapter 3 and the empirical Skyrme functional, we recall below some results that will be useful for the discussion.

As a preliminary remark, we note that the Hartree-Fock contribution to the ground-state energy of a dilute Fermi gas at leading order in $(a_s k_F)$ reads:

$$\frac{E_{low}}{E_{FG}} = 1 + \frac{10}{9\pi}(a_s k_F) + \dots \quad (5.38)$$

This expression is identical to the Hartree-Fock result using a Skyrme interaction with only a (t_0, x_0) term. Indeed, we have in this case:

$$\frac{E_{Sk}}{E_{FG}} = 1 + \frac{10}{9\pi}(\tilde{a}_s k_F), \quad (5.39)$$

where $\tilde{a}_s = mt_0(1 - x_0)/4\pi$ [see (1.14)]. For standard parameter sets, the value of the coupling constant \tilde{a}_s has nothing to do with the physical value of the s -wave scattering length (see discussion in section 1.3).

To make contact with the Skyrme functional and the work of the present thesis, we first start from the functionals introduced in chapter 3 (GPS/APS/GUL/AUL, see table 3.2). More precisely, we introduce a density-dependent coupling constant $\tilde{a}_s(k_F)$ such that we can recast the functionals to:

$$\frac{E}{E_{FG}} = 1 + \frac{10}{9\pi}k_F\tilde{a}_s(k_F). \quad (5.40a)$$

Starting from the functional listed in table 3.1, we immediately obtain for $\tilde{a}_s(k_F)$:

$$\tilde{a}_s(k_F) = \begin{cases} \frac{1}{k_F} \frac{(a_s k_F)}{1 - (a_s k_F)C} & \text{for GPS/AUL} \\ \frac{24}{5k_F} \arctan \frac{5(a_s k_F)/24}{1 - (a_s k_F)C} & \text{for APS/AUL} \end{cases}. \quad (5.40b)$$

To shorten the equations, we have introduced the constant C (respectively \mathcal{C}) for the GPS/GUL (respectively APS/AUL) functionals defined in chapter 3 (see table 3.1). These parameters are linked to the Bertsch parameter through:

$$C = \frac{10}{9\pi}(1 - \zeta)^{-1} \quad \text{and} \quad \mathcal{C} = \frac{5}{24} \tan^{-1} \left[\frac{3\pi}{16}(1 - \zeta) \right],$$

where the values of ζ are given in table 3.2 for different functionals.

The obtained evolutions of $\tilde{a}_s(k_F)$ for different functionals are illustrated in the panel (a) of figure 5.12. We can draw several interesting conclusions.

First, the $\tilde{a}_s(k_F)$ obtained from all the functionals (GPS/APS/GUL/AUL) cannot be distinguished. We observe two regimes for the evolution of the coupling constant $\tilde{a}_s(k_F)$. At low density ($k_F \lesssim 0.5 \text{ fm}^{-1}$), $\tilde{a}_s(k_F)$ evolves from the bare coupling constant a_s to much smaller absolute values. These values turn out to be compatible with the empirical values of \tilde{a}_s generally obtained by direct fit of the Skyrme functionals. Indeed, in practice $-\tilde{a}_s \simeq 1 - 5 \text{ fm}$ [see (1.14)]. Then, they present a smoother asymptotic behavior.

The smooth, almost flat, behavior of $\tilde{a}_s(k_F)$ is actually also consistent with the fact that the Skyrme functional uses a density independent parameter and can be seen as an indirect justification of the simplicity of the functional and of the value of the (t_0, x_0) term. For large k_F ($k_F > 0.5$), the value of $\tilde{a}_s(k_F)$ becomes very close to its asymptotic behavior:

$$\tilde{a}_s(k_F) \underset{k_F \rightarrow \infty}{\sim} -\frac{9\pi}{10k_F}(1 - \zeta). \quad (5.41)$$

We see from this relation that $\tilde{a}_s(k_F)$ cannot anymore be connected to the physical value of a_s . This also gives an explanation why the memory of the physical low-energy constant is lost in empirical DFTs.

Note that, in [130], we have generalized this method by including an effective-range effect. In that case, guided by (5.38) and including the leading order in $(r_s k_F)$, we have introduced a second density-dependent coupling constant $\tilde{r}_s(k_F)$ related to the (t_1, x_1) term. We show in panel (b) of figure 5.12 a typical evolution of $\tilde{r}_s(k_F)$ as a function of k_F . The conclusion is quite similar to the renormalization of the coupling constant \tilde{a}_s discussed just above (see [130] for more details) and again we recover typical values of the (t_1, x_1) parameters retained empirically.

5.3.B Effective Skyrme potential from quasi-particle properties

In the discussion presented above, starting from the energy, we have introduced several density-dependent coupling constants. In this section, we generalize the approach starting now from the quasi-particle properties.

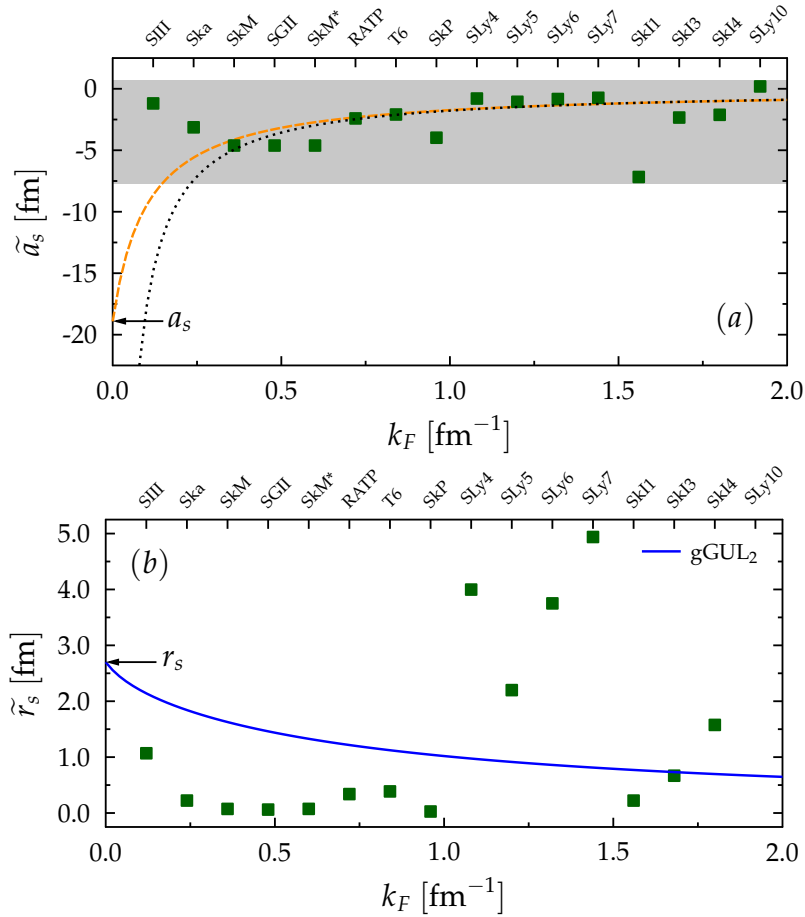


Figure 5.12: Panel (a): Density dependent coupling constant $\tilde{a}_s(k_F)$ as a function of k_F . The orange short-dashed line corresponds to the result (5.40b) obtained for the GPS/AP-S/GUL/AUL functionals (see table 3.2). Note that, the different functionals cannot be distinguished and are represented by the unique orange short-dashed line. The black dotted line corresponds to the approximate asymptotic form (5.41). Panel (b): Density dependent coupling constant $\tilde{r}_s(k_F)$ as a function of k_F obtained using the gGUL₂ functional given by (3.34a) (see [130] for more details). For reference, the green squares in panel (a) [respectively in panel (b)] represent values of the \tilde{a}_s [respectively \tilde{r}_s] parameters for different parameter sets of Skyrme functionals. The physical s -wave scattering length $a_s = -18.9$ fm [effective range $r_s = 2.7$ fm] is indicated by the black arrow on panel (a).

Let us consider the Skyrme effective interaction (1.13) with only the s -wave channel [(t_0, x_0) and (t_1, x_1) terms]. For neutron matter, the single-particle potential reads⁷ [131,171]:

$$\frac{U_{Sk}(k)}{\varepsilon_{FG}} = \frac{ms_0 k_F}{3\pi^2} + \frac{ms_1 k_F^3}{20\pi^2} + \frac{ms_1 k_F^3}{12\pi^2} \left(\frac{k}{k_F}\right)^2, \quad (5.42)$$

where we have defined $s_0 = t_0(1 - x_0)$ and $s_1 = t_1(1 - x_1)$. We remark that the single-particle potential is automatically quadratic. This justifies *a posteriori* the importance for the present discussion to have introduced the quadratic approximation of the GPS/AP-S single-particle potentials (see section 5.2.a).

⁷ Here, we do not consider the (t_2, x_2) term of the Skyrme effective interaction (1.13) for the following reasons: if we include this term, the one-to-one correspondence between s_0, s_1 and the quasi-particle properties μ_{Sk}, m_{Sk}^* is still possible with the substitution $s_1 \rightarrow s_{12} = [t_1(1 - x_0) + 3t_2(1 + x_2)]$ (see [131,171] for instance).

FROM NON-EMPIRICAL SINGLE PARTICLE POTENTIAL TO DENSITY-DEPENDENT PARAMETERS

As done in section 5.3.a at the total energy level, we now start from the quadratic approximation of the single-particle potential introduced in (5.36) for the GPS/APS single-particle potentials. To recover an expression similar to (5.42), we introduce the density-dependent terms $\tilde{s}_0(k_F)$ and $\tilde{s}_1(k_F)$ so that:

$$\frac{U(k)}{\varepsilon_{FG}} = \frac{m\tilde{s}_0(k_F)k_F}{3\pi^2} + \frac{m\tilde{s}_1(k_F)k_F^3}{20\pi^2} + \frac{m\tilde{s}_1(k_F)k_F^3}{12\pi^2} \left(\frac{k}{k_F}\right)^2. \quad (5.43a)$$

$\tilde{s}_0(k_F)$ and $\tilde{s}_1(k_F)$ are then given by:

$$\tilde{s}_0(k_F) = \frac{3\pi^2}{mk_F} \left\{ \left[\frac{\mu}{\mu_{FG}} - 1 \right] - \frac{8}{5} \left[\frac{m}{m^*} - 1 \right] \right\}, \quad (5.43b)$$

$$\tilde{s}_1(k_F) = \frac{12\pi^2}{mk_F^3} \left[\frac{m}{m^*} - 1 \right]. \quad (5.43c)$$

Here, the chemical potential and the effective mass are given by the GPS/APS single-particle potential derived in this chapter and given in appendix F. Note that, up to second order in $(a_s k_F)$, we recover the quadratic approximation of the Galitskii formula⁸.

Therefore, we see that a connection with the density-dependent Skyrme potential can also be made starting from the single-particle potential. However, in the AP-S/GPS single-particle potential presented in this chapter, the effective range effects are neglected. For this reason, the value of \tilde{s}_1 deduced from $U(k)$ does not match the typical values used in the Skyrme functionals. This is a further motivation to include effective range effects in future developments. The possibility to make a connection between the present thesis to the widely used Skyrme functionals and explain partially from first principle the values of the Skyrme parameters opens new ways towards non-empirical functionals. In addition, the possibility to rewrite a functional in a Skyrme-like form will also be useful to apply the non-empirical functionals to finite systems. As a proof of principle, in [208] for instance, this strategy was used to describe the structure properties of neutron drops. Below we give a more general and precise discussion on the possibility to make a DFT description of finite systems using the developments of the present thesis allowing to go beyond the so-called Local Density Approximation.

5.3.c Toward finite systems

Guided by some phenomenological arguments commonly used for nuclei and also by the success of simple empirical functionals like the Skyrme DFT in nuclear systems, the single-particle potential was here further simplified by assuming that the

⁸ Note that the quadratic approximation in power of k^2 [see (5.33)] of the Galitskii formula (4.4) can be written as:

$$\begin{aligned} \frac{U_{low}(k)}{\varepsilon_{FG}} &= \frac{4}{3\pi} (a_s k_F) + \frac{4}{15\pi^2} (11 - 2 \ln 2) (a_s k_F)^2 + \frac{8}{15\pi^2} (7 \ln 2 - 1) (a_s k_F)^2 \\ &\quad - \frac{8}{15\pi^2} (7 \ln 2 - 1) (a_s k_F)^2 \left(\frac{k}{k_F}\right)^2. \end{aligned}$$

single-particle potential can be approximated by a quadratic or quartic polynomial form in k . This second approximation is made in such a way that quasi-particle properties are preserved for all ($a_s k_F$). Again, our methodology has the advantage that the low-density limit of the chemical potential or the effective mass identifies automatically respectively with the Lee-Yang and Galitskii expressions. We finally briefly discuss how the possibility to have analytical density-dependent expressions of these quasi-particle properties can serve to design new DFTs. More generally, in view of the recent scientific emulation that followed the use of resummed formula for the energy [76,148,197,198], the approximate expressions obtained in the present work can also be a strong guidance to obtain semi-empirical or non-empirical functionals constrained at low density and/or at unitary.

An important development that we are now pursuing is the possibility to apply the functionals to finite Fermi systems. Let us assume that we start from one of the GPS/APS energy density functionals. Once the energy is written in terms of powers of k_F , this energy can directly be interpreted as a functional of the local density ρ . For infinite systems, the local density is just a constant. A standard technique to export a DFT from infinite to finite systems is to use a Local Density Approximation (LDA) where the ground-state energy is first transformed into an integral over space of the energy density functional $E = \int d^3r \mathcal{E}(\mathbf{r})$ [see (1.9)]. Here, $\mathcal{E}(\mathbf{r})$ contains the kinetic and the potential energy contributions that are both written in terms of the local density $\rho(\mathbf{r})$, itself linked to a local Fermi momentum $k_F^3(\mathbf{r}) = 6\pi^2\rho(\mathbf{r})/g$. This approach, that has some connections with the Thomas-Fermi approximation [127,182], leads to functionals of the local density consistently with the Hohenberg-Kohn theorem [113]. Such a direct mapping has initiated several novel ways to obtain DFT in the nuclear physics context [197,198,208] (for a review see [148]). A similar strategy is now used in a different context in order to incorporate quantum corrections that might stabilize quantum droplets [209,210]. It is however well known that the simple LDA approach should be generalized by including properly the kinetic term as well as eventual gradient corrections. This is standardly done for instance in empirical nuclear DFT [101] and this was also one of the main motivations to extend our previous work from the energy to the self-energy.

To illustrate how a DFT beyond the LDA can be obtained from the present work, we assume that our starting points are the expressions of $\mu(k_F)$ and $m^*(k_F)$ provided by one of the GPS/APS single-particle potential. We then introduce the quantity:

$$W(\rho) \equiv \frac{E}{N} - \frac{3}{5} \frac{k_F^2}{2m^*(\rho)}. \quad (5.44)$$

Note that the knowledge of $\mu(k_F)$ is sufficient to obtain the energy through the relation (4.6c), thanks to the consistency requirement with the Hugenholtz-van-Hove theorem.

Following [127], we can show that this energy can be obtained from an energy density functional valid in both finite and infinite systems [see (1.9)] of the form:

$$E[\rho, \tau] = \int \left\{ \frac{\tau(\mathbf{r})}{2m^*(\rho)} + \rho(\mathbf{r})W(\rho(\mathbf{r})) \right\} d^3r, \quad (5.45)$$

where the local density ρ and kinetic density τ entering in this equation are given by:

$$\rho(\mathbf{r}) = \sum_{i=1}^N |\varphi_i(\mathbf{r})|^2, \quad \tau(\mathbf{r}) = \sum_{i=1}^N |\nabla \varphi_i(\mathbf{r})|^2. \quad (5.46)$$

The states $\{\varphi_i\}$ play the role of the Kohn-Sham orbitals. The Schrödinger equation they fulfilled are obtained by minimizing the action $\mathcal{S} = E[\rho, \tau] - \sum_i \varepsilon_i |\nabla \varphi_i(\mathbf{r})|^2$ where ε_i are Lagrange multipliers that insure that single particles are properly normalized to 1. Performing the variation of the action with respect to $\varphi_i^*(\mathbf{r})$ gives the set of self-consistent Kohn-Sham equations:

$$\left\{ -\vec{\nabla} \frac{1}{2m^*(\rho)} \cdot \vec{\nabla} + U(\rho, \tau) \right\} \varphi_i(\mathbf{r}) = \varepsilon_i \varphi_i(\mathbf{r}), \quad (5.47)$$

where

$$U(\rho, \tau) = \frac{\tau}{2} \frac{\partial}{\partial \rho} \frac{1}{m^*(\rho)} + \frac{\partial}{\partial \rho} \{\rho W(\rho)\}. \quad (5.48)$$

This approach gives a definite strategy to go beyond the LDA using the functionals proposed in the present work.

5.4

CONCLUSION AND CRITICAL DISCUSSIONS

In this chapter, we have explored the possibility to start from a well-defined many-body approach based on the diagrammatic resummation technique and obtain approximate expressions both for the energy and the self-energy. While the present chapter is mainly focused on this topic, the ultimate goal is to use these approximate expressions as a guidance for proposing new DFTs for Fermi systems beyond the perturbative regime. At the self-energy level, two simplifications are considered that might help in the DFT context. We first propose to use a partial phase-space approximation leading to a simpler density dependence of the self-energy and ultimately of the associated energy. In the former case, the constraint on the energy is made using the Hugenholtz-van-Hove theorem consistency. If the energy is not used as a constraint, the associated self-energy expression turns out to be simpler. In all cases, the self-energy of low-density Fermi gases is properly recovered while a non-diverging limit is reached when $|a_s k_F| \rightarrow +\infty$ contrary to truncated perturbative many-body framework. It is found in general that the combination of a resummation technique with the phase-space average approximation can be used in a wider range of densities compared to the many-body perturbation theory. We note however that without any adjustment, the functionals are not predictive in the unitary regime.

Besides the simplification introduced by the phase-space averages, we note in general that the resulting energy and/or self-energy present both smoother behaviors compared to a direct use of the resummation approach without phase-space average approximation. It turns out to be qualitatively closer to the behavior calculated through Brueckner Hartree-Fock approach for non superfluid systems.

Finally, we have briefly discussed how to relate the work presented in the present thesis to the study of finite systems. We have shown that the novel functionals can be useful to understand some of the parameters entering in more empirical functionals both starting directly from the ground-state energy given in chapter 3 or from the single-particle potentials discussed in the present chapter. A key aspect is the introduction of density-dependent low-energy constants. These results explain qualitatively the values taken by the empirical Skyrme parameters adjusted on nuclear properties. In particular, this study has highlighted the strong renormalization of the low-energy constants starting from the bare s -wave scattering length to an asymptotic behavior in $1/k_F$. Finally, we have also shown how this work can be exported to finite systems beyond the local density approximation.

To conclude, the use of a diagrammatic resummation leads to rather complex expressions in general. For this reason, we concentrated here the discussion on a rather simple case of a non-superfluid system with only one low-energy constant, the s -wave scattering length, and focused on the on-shell self-energy. In addition, an extension to include off-shell effects would be a priori desirable especially to describe the E -mass [291,304]. Another natural extension of the present work is to include also the s -wave effective range r_s and/or p -wave scattering volume. The functional proposed in [76] and further discussed in [130,199] (see chapter 3 for more details) already incorporates the effect of the effective range on the energy density functional. At leading order, one could simply add the present functional, however a proper treatment of the possible interference effects as well as effects beyond the leading order is needed if for instance $(r_s k_F)$ becomes large. This case occurs for instance in nuclear systems at or close to the saturation density. We did not consider here the treatment of the effective range together with a large scattering length, however we mention that the work of [239,305] can be used as a starting point.

CONCLUSION

Vous avez l'air ému, mon fils, comme si vous étiez rempli d'effroi. Soyez tranquille. Maintenant voilà nos divertissements finis ; nos acteurs, comme je vous l'ai dit d'avance, étaient tous des esprits ; ils se sont fondus en air, en air subtil ; et, pareils à l'édifice sans base de cette vision, se dissoudront aussi les tours qui se perdent dans les nues, les palais somptueux, les temples solennels, notre vaste globe, oui, notre globe lui-même, et tout ce qu'il reçoit de la succession des temps ; et comme s'est évanoui cet appareil mensonger, ils se dissoudront, sans même laisser derrière eux la trace que laisse le nuage emporté par le vent. Nous sommes faits de la vaine substance dont se forment les songes, et notre chétive vie est environnée d'un sommeil. – Seigneur, j'éprouve quelque chagrin : supportez ma faiblesse ; ma vieille tête est troublée ; ne vous tourmentez point de mon infirmité. Veuillez rentrer dans ma caverne et vous y reposer. Je vais faire un tour ou deux pour calmer mon esprit agité.

William SHAKESPEARE – *La tempête*

The pivotal period of nuclear physics as we know it today suggests new opportunities for the understanding of strongly correlated fermions like neutronic systems. The nuclear *ab initio* methods, although knowing important progress, in particular with the recent developments of the chiral effective field theory, are extremely complex compared to the density functional theory (DFT) approach. The latter remains even today the only microscopic approach able to treat in a unified framework a large variety of phenomena occurring in nuclear systems. In this context, the goal of this thesis was to explore the possibility to connect the nuclear DFT to the bare nuclear interaction directly and render it less empirical.

I summarize below the main progress made in this thesis. In chapter 1, an overview of current problems and recent advances in nuclear physics is made with specific highlights on *ab initio* methods. Three important concepts around which the present thesis is articulated are discussed: (i) the nuclear interaction and the recent advances of effective field theory (simplifying the many-body calculations), (ii) the many-body *ab initio* theories themselves, and (iii) the empirical density functional theories standardly used in nuclear physics. The actual limitations of different approaches are discussed. Recent attempts to combine the *ab initio* methods and the DFT approaches are summarized. This analysis revealed the possibility to obtain, in some cases (low density, unitarity) relatively simple and explicit expressions for the energy that could be used from the perturbative to the non-perturbative regime.

These examples also were a guidance for the present work to define a specific strategy to render nuclear DFT less empirical. The strategy we employed is depicted schematically in figure A. It starts from a well-defined and well-controlled many-body approach, here the many-body perturbation theory (MBPT) with eventual resummation of some classes of diagrams. More precisely, we start from an EFT framework for dilute Fermi systems using a contact interaction. This approach is justified in chapter 2. In that case, the link with the low-energy constants of the interaction is clear and has similarities with the pionless EFT describing the nuclear interaction. Starting from this interaction, we focus on the case of an infinite

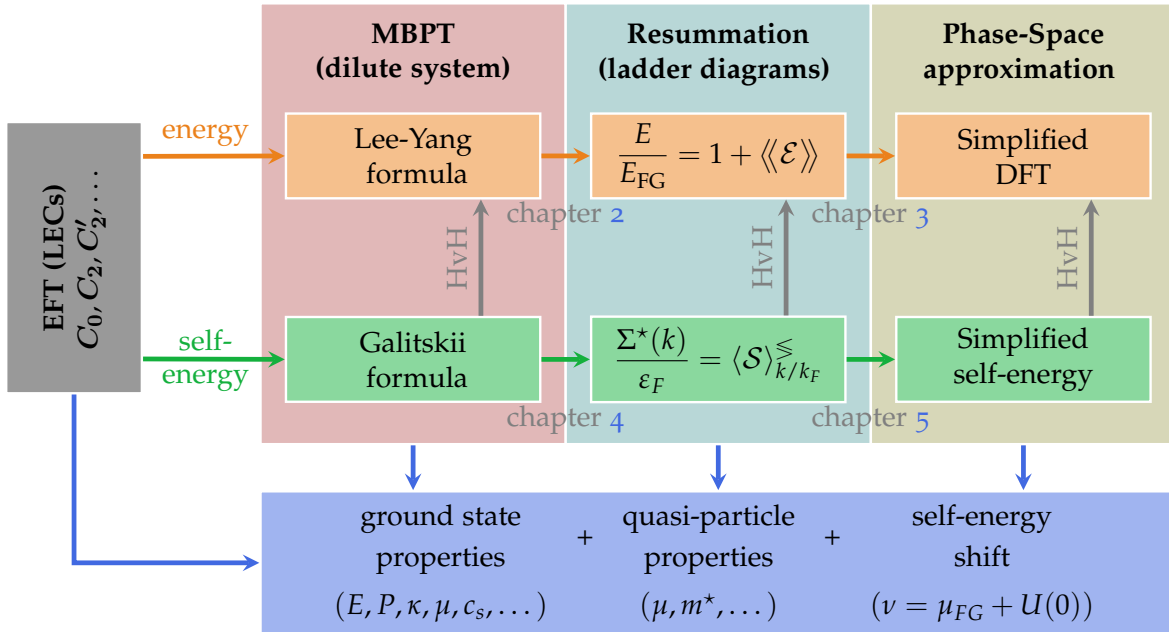


Figure A: Schematic representation of the strategy used in the present thesis to obtain, from an EFT, the phase-space approximation of the ground state and quasi-particle properties guided first by MBPT and then by ladder resummation of the energy and/or self-energy.

spin degenerate Fermi system using the leading order of this contact interaction. This model case is of interest both for atomic systems and neutron systems. Then, we have used the standard (MBPT) and illustrated the calculation of the ground state energy of the systems as a perturbative series in terms of the density (related to the Fermi momentum k_F) and the low-energy constants (the s -wave scattering length a_s). This systematic study highlighted that, under some conditions (consisting in keeping only the contribution of a certain class of correlations related to the ladder diagrams), all the contributions in the ground state energy can be recast in a compact expression which is an explicit function of $(a_s k_F)$ integrated on the accessible phase-space. Ultimately, we obtained the explicit expression of the energy as a function of the low-energy constants. Although it is an interesting step towards a *non-empirical* functional for interacting systems beyond the perturbative approaches, the results (i) strongly depends on the class of diagrams retained, (ii) does not reproduce qualitatively the observations, and (iii) presents a rather complicated density dependence that most probably will prevent from exporting the functionals to finite systems.

An extensive exploratory study is made in chapter 3 starting from the resummed ground state energy to obtain systematic and well defined approximations to simplify the functionals obtained by resummation. Using what is called here the phase-space average approximation leads to much simpler DFT. Some of these non-empirical DFT reproduce very well the thermodynamical properties, e.g. ground-state energy, pressure or compressibility, of the studied systems from the low-density to the unitarity regime. Then, functionals generalized to include effective-range effects have been introduced. The particular case of a large s -wave scattering length and non-negligible effective range is motivated by nuclear physics. It was shown that not only atomic systems are well accounted for with $r_s = 0$ but also these generalizations to $r_s \neq 0$ reproduce properly the low-density of neutron matter equation of state, much beyond the standard MBPT. The proposed functional

was applied to the determination of the linear response of low-density neutron matter. The static response reproduces qualitatively well the *ab initio* calculations and in general much better than the standard empirical DFT. This study also revealed the necessity to improve our knowledge about quasi-particle properties like the effective mass in strongly interacting Fermi systems.

For this reason, following the ideas used for the energy, the resummation technique is directly developed at the self-energy level in chapter 4. Several resummations are discussed with varying success in describing systems with large *s*-wave scattering length. Ultimately, it is shown that direct application of the resummation technique lacks predictive power at or close to the unitary regime. A second drawback is that resulting expressions turns out to be rather complicated which prevents their use in finite systems.

For this reason, in chapter 5, we propose general methodologies, guided by the low-density limit and eventually by the constraint given by the Hugenholtz-van Hove theorem, to extend the phase-space average approximation to the self-energy. When the Hugenholtz-van Hove theorem is imposed, we show in particular that the phase-space approximation introduced in chapter 5 is fully consistent with the one introduced at the energy level in chapter 3. Focusing on the single-particle potential of non-superfluid systems and on the effective mass, we obtained simple and explicit expressions of them in terms of $(a_s k_F)$. In particular, our results are valid much beyond the standard MBPT approach for dilute Fermi systems.

In the present thesis, we have discussed some possible ways towards *ab initio* density functional theory by obtaining DFT directly connected to the low-energy constants of the interaction. This helped to understand medium effects and particularly how in-medium effects strongly renormalize the low-energy constants. This point was clearly highlighted at the end of chapter 5. More precisely, we have shown that the renormalization of the coupling constants at density close to saturation induces a loss of memory of the bare low-energy constants. Indeed as the density increases, we observed a direct link with the unitary limit and the renormalized *s*-wave scattering length. We found that our approach is compatible with the values of some *empirical* parameters appearing in the Skyrme functionals. This observation also emerges from recent works driven by the effective field theory to design new hybrid functionals [76,130,197,198,208] or for instance in [306] where the form of the renormalized coupling constants are driven by Brueckner Hartree-Fock calculations.

As a critical issue, I would like to mention that direct applications of functionals based on resummation techniques is an extremely challenging project in practice in nuclear systems. The main difficulty that is arising in semi-analytical resummation techniques comes from the fact that these approaches towards *ab initio* DFT become extremely complex when the interaction becomes more realistic (effective range effect, *p*-wave contribution, etc...) [238–240,305]. This certainly restricts the domain of application to many-body systems interacting through rather simpler interactions compared to the nuclear interaction. Another difficulty is related to the extension to the symmetric matter where dimmers and more generally multimimers appear due to the existence of bound states.

One of the conclusion of the present thesis is that the design of *ab initio* DFT requires well controlled exact calculations giving access to important pseudo-data to inspire and test new ideas: For instance exact many-body calculations where the equation of state of neutron matter is obtained by branching, step by step, the contributions to the interaction in the chiral EFT. I would like to mention that this thesis has initiated some interesting discussions with the *ab initio* community to get precise *ab initio* calculations for the effective mass of strongly interacting Fermi

systems. This resulted indirectly in the first AFDMC calculation for the effective mass in neutron systems [289]. This specific example illustrates the positive cross-fertilization between the *ab initio* and DFT scientists that could be very productive for future developments.

Despite the restriction to rather simple interactions, the work presented in this thesis also illustrates the connection between atomic and nuclear systems. The functional introduced in the present thesis, extending the MBPT for dilute systems, opens the possibility to describe quantum droplets in which beyond mean field corrections are known to stabilize such systems [209,210].

Another important extension of the present work in the cold atom context would be to include the effect of pairing correlations. A prerequisite for this extension is the possibility to obtain a compact expression of the energy after summing up selected diagrams to all orders in perturbations. By itself, developing a perturbative approach on top of a quasi-particle vacuum is possible (see for instance [307,308]). However, even at second order, by replacing the $2p - 2h$ energy by the 4 quasi-particles, the complexity of the integrals to tackle increases significantly. As far as we know, such problem has not been solved yet analytically. An alternative to the analytical approach using a DFT guided by the work presented in this thesis would be to add a posteriori a pairing energy to the DFT. This procedure is standardly used for nuclei and would at least allow to extend to the so-called Superfluid Local Density Approximation (SLDA) approach of [75] away from unitarity. It could provide new opportunities in infinite [309] as well as in finite systems [310,311].

A

REGULARIZATION OF THE LOOP INTEGRALS

CONTENTS

| | | |
|-----|--|----|
| A.1 | Generalities on the scattering theory: scattering amplitude and S -matrix | A2 |
| A.2 | General features of regularized loop integrals | A3 |
| A.3 | Renormalization of the Low Energy Constants | A5 |

The direct application of the second order (or higher order) many-body perturbation theory of dilute Fermi systems to calculate physical quantities, as the ground state energy or the proper self-energy, from a contact interaction leads to UV divergences [40,44]. One standard way to overcome divergences while guaranteeing the physical properties is to use a renormalization procedure developed in [41,42]: the Power Divergence Subtraction (PDS) scheme. In various places in the main document, chapter 2 and chapter 4 of this thesis, the quantities of interest are given after these divergences have been properly removed. In this appendix, we present the important steps and equations of this method and summarize the useful results of the PDS that are used in the thesis. Note that it is possible to use alternative methods such as the dimensional regularization [39,312,313], the subtraction of divergence (Minimal Subtraction scheme) or the cut-off regularization [44].

A.1

GENERALITIES ON THE SCATTERING THEORY:
SCATTERING AMPLITUDE AND S -MATRIX

We start with the most general non-relativistic local Lagrangian for a fermion field ψ (with mass m), invariant under Galilean, parity and time-reversal transformation:

$$\begin{aligned} \mathcal{L} = \psi^\dagger \left[i\hbar\partial_t + \frac{\overleftrightarrow{\nabla}^2}{2m} \right] \psi - \frac{C_0}{2} (\psi^\dagger\psi)^2 + \frac{C_2}{16} [(\psi\psi)^\dagger (\psi\overleftrightarrow{\nabla}^2\psi) + \text{h.c.}] \\ + \frac{C'_2}{8} (\psi\overleftrightarrow{\nabla}\psi)^\dagger \cdot (\psi\overleftrightarrow{\nabla}\psi) + \dots \end{aligned} \quad (\text{A.1})$$

where $\overleftrightarrow{\nabla} = \overleftarrow{\nabla} - \overrightarrow{\nabla}$ is the Galilean invariant derivative and h.c. denotes the hermitian conjugate. The terms in C_0 and C_2 are the coupling constants related to the s -wave scattering and the term in C'_2 corresponds to the p -wave scattering. The dots represent terms with more derivatives and/or more fields, for example the leading 3-body contact interaction equals to: $-D_0(\psi^\dagger\psi)^3/6$. The corresponding Hamiltonian interaction is given by (1.6).

To connect the coupling constants to the standard low energy constants (LECs) of the interaction, we introduce the (on-shell) S -matrix for the s -wave scattering, the associated (on-shell) T -matrix, and the phase shift δ :

$$S(k) = 1 + i\frac{mk}{2\pi}T(k) = e^{2i\delta(k)} \quad \longmapsto \quad T(k) = \frac{4\pi}{m} \frac{1}{-k \cot \delta(k) + ik}. \quad (\text{A.2})$$

We also consider the low-momentum effective s -wave interaction given by:

$$V(\mathbf{k}, \mathbf{k}') = \langle \mathbf{k}' | \widehat{V} | \mathbf{k} \rangle = C_0 + \frac{C_2}{2} [k^2 + k'^2] + \dots \quad (\text{A.3})$$

coming from the Lagrangian given by (A.1) (considering only the coupling constants related to the s -scattering wave).

- *Low-momentum expansion*

The low-momentum expansion of the phase shift is given by:

$$k \cot \delta(k) = -\frac{1}{a_s} + \frac{1}{2}r_s k^2 + \dots \quad (\text{A.4a})$$

that defines the s -wave scattering length a_s and the s -wave effective range r_s and connects them to the constants C_0 and C_2 of the Lagrangian (A.1). Using (A.3) in the definition of the T -matrix leads to the low-momentum expansion:

$$\begin{aligned} T(k) \equiv T(\mathbf{k}, \mathbf{k}) &= \frac{4\pi a_s}{m} \left[1 + ia_s k - (r_s a_s / 2 - a_s^2) k^2 + \dots \right]^{-1}, \\ &\sim \frac{4\pi a_s}{m} \left[1 - ia_s k + (r_s a_s / 2 - a_s^2) k^2 + \dots \right]. \end{aligned} \quad (\text{A.4b})$$

- *All orders in momentum space*

Considering all orders in momentum, the T -matrix verifies the (on-shell) Lippmann-Schwinger equation:

$$T(\mathbf{k}, \mathbf{k}') = V(\mathbf{k}, \mathbf{k}') + m \int \frac{d^3q}{(2\pi)^3} \frac{V(\mathbf{k}', \mathbf{q})T(\mathbf{q}, \mathbf{k})}{k^2 - q^2 + i\tau}, \quad (\text{A.5a})$$

leading, at low momentum, to (Born series approximation):

$$T(k) = C_0 + C_2 k^2 - \left(\frac{m}{4\pi}\right)^2 C_0^3 k^2 + m C_0^2 L_0(k) + \dots \quad (\text{A.5b})$$

where we have defined the divergent loop integrals:

$$L_0(k) = \int \frac{d^3q}{(2\pi)^3} \frac{1}{k^2 - q^2 + i\tau}. \quad (\text{A.5c})$$

In (A.5b), the dots mean higher orders in C_0, C_2 or C_2^2 . Matching this equation with (A.4b), we deduce:

$$C_0 = \frac{4\pi a_s}{m} \quad \text{and} \quad C_2 = \frac{4\pi a_s^2 r_s}{m}. \quad (\text{A.5d})$$

The next section is devoted to the regularization of this integral illustrated in the framework of the Minimal Subtraction (MS) and Power Divergence Subtraction (PDS) schemes.

A.2

GENERAL FEATURES OF REGULARIZED LOOP INTEGRALS

The loop integral $L_0(k)$ defined by (A.5c) as an integral of the off-shell momentum q needs to be regularized. A standard method is to insert a cutoff momentum Λ on q and a regulator function $f(q/\Lambda)$ such that the integral converges. This regulator satisfies:

$$f(\infty) = 0 \quad \text{and} \quad f(0) = 1. \quad (\text{A.6a})$$

This defines the momentum dependent loop integral:

$$L_0(k) \longmapsto L_0^\Lambda(k) = \int \frac{d^3q}{(2\pi)^3} \frac{f(q/\Lambda)}{k^2 - q^2 + i\tau}. \quad (\text{A.6b})$$

This regularized loop integral can be expanded as a convergent power series in k/Λ :

$$L_0^\Lambda(k) = -\frac{ik}{4\pi} + b_{-1}\Lambda + \frac{k^2}{\Lambda} \sum_{l=0}^{\infty} b_{2l+1} \left(\frac{k}{\Lambda}\right)^{2l}, \quad (\text{A.6c})$$

where the coefficients b_l depend on the function $f(q/\Lambda)$ used. Let us make few remark.

- Using a sharp-cutoff prescription, i.e. $f(q/\Lambda) = \Theta(\Lambda - k)$, we obtain the coefficients

$$b_l = \frac{1}{2\pi^2 l}$$

and, in this case, the loop integral still diverge with Λ due to the b_{-1} term.

- The dimensional regularization using the Minimal Subtraction (MS) scheme consists in putting

$$b_{-1} = b_l = 0$$

and consequently, the T -matrix identifies with:

$$T(k) = C_0 - ik \frac{m}{4\pi} C_0^2 = \frac{4\pi a_s}{m} (1 - ia_s k), \quad (\text{A.7})$$

which is exactly the physical result at lowest order in a_s if $r_s = 0$ given by (A.4b).

- The dimensional regularization using the Power Divergence Subtraction (PDS) scheme simultaneously with the MS scheme consists in choosing

$$b_{-1} = -\frac{1}{4\pi} \quad \text{and} \quad b_{2l+1} = 0.$$

In the literature, the cutoff Λ is often noted μ and called flow parameter or subtraction point of the renormalization group [41]. The PDS + MS scheme leads to the μ -dependent T -matrix:

$$T_\mu(k) = \frac{\sum_n C_{2n} k^{2n}}{1 + \frac{m}{4\pi} (\mu + ik) \sum_n C_{2n} k^{2n}}. \quad (\text{A.8a})$$

Ultimately, the T -amplitude should be cutoff independent and it is necessary to renormalize simultaneously the coupling constants that become μ -dependent to compensate the μ -dependence of the loop integral, i.e.:

$$T(k) = \frac{\sum_n C_{2n}(\mu) k^{2n}}{1 + \frac{m}{4\pi} (\mu + ik) \sum_n C_{2n}(\mu) k^{2n}}. \quad (\text{A.8b})$$

We have introduced the μ -dependent coupling constants $C_{2n}(\mu)$ related to the physical one $C_{2n}(\mu = 0) \equiv C_{2n}$. Note that for $\mu = \Lambda = 0$, we obtain the same result than using the MS scheme. The renormalization of the coupling constants in PDS + MS scheme is discussed in the next section.

A.3

RENORMALIZATION OF THE LOW ENERGY CONSTANTS

The PDS scheme is related to the Renormalization Group (RG) for which we show that the coefficients $C_{2n}(\mu)$ obey to the flow equations derived directly from the fact that the T -amplitude defined by (A.8b) should be μ -independent. This leads to:

$$T(k) : \mu\text{-independent} \quad \longmapsto \quad \mu \frac{dC_{2n}}{d\mu} = \beta_{2n} \equiv \frac{m\mu}{4\pi} \sum_{m=0}^n C_{2m} C_{2(n-m)}. \quad (\text{A.9})$$

Proof: We introduce the notations $C(\mu) \equiv \sum_n C_{2n}(\mu) k^{2n}$ and ∂_μ the derivative with respect to μ . The constraint that the T -amplitude is μ -independent is equivalent to $\partial_\mu T = 0$. Using the definition of T given by (A.8b), it is straightforward to obtain the relation:

$$\begin{aligned} \partial_\mu T(k) = 0 &\Leftrightarrow \partial_\mu C(\mu) = \frac{m}{4\pi} C(\mu)^2 \\ &\Leftrightarrow \sum_n \partial_\mu C_{2n}(\mu) k^{2n} = \frac{m}{4\pi} \left(\sum_n C_{2n}(\mu) k^{2n} \right)^2. \end{aligned}$$

The equation must be verified at all order¹ in k which gives the set of flow equations (A.9).

In particular, we have:

$$\beta_0 = \frac{m\mu}{4\pi} C_0^2 \quad \text{and} \quad \beta_2 = \frac{m\mu}{2\pi} C_0 C_2. \quad (\text{A.10})$$

Using the physical values of the coupling constants at $\mu = 0$, this leads to:

$$C_0(\mu) = \frac{4\pi}{m} \left(\frac{1}{-\mu + 1/a_s} \right) \quad \text{and} \quad C_2(\mu) = \frac{4\pi}{m} \left(\frac{1}{-\mu + 1/a_s} \right)^2 \frac{r_s}{2}. \quad (\text{A.11})$$

To go further: It is possible to solve the complete (coupled) RG equation:

$$\mu \frac{dC_{2n}}{d\mu} = \beta_{2n} \equiv \frac{m\mu}{4\pi} \sum_{m=0}^n C_{2m} C_{2(n-m)}, \quad (\text{A.12a})$$

leading to the solutions:

$$C_{2n}(\mu) = \frac{4\pi}{m(-\mu + 1/a_s)} \left(\frac{r_s/2}{-\mu + 1/a_s} \right)^n + O(\mu^{-n}). \quad (\text{A.12b})$$

Remark: By definition, the Minimal Subtraction (MS) scheme consists in introducing a cut-off momentum Λ and in adding a counter term to avoid the linear divergence in Λ . The MS scheme is equivalent to the PDS scheme taking $\mu = \Lambda \rightarrow 0$ at the end of the calculation. This point is explained in ref. [41].

¹ Here, the right hand side is the Cauchy product between two power series, *i.e.*:

$$\left(\sum_{n=0}^{\infty} C_{2n}(\mu) k^{2n} \right)^2 = \sum_{n=0}^{\infty} \left[\sum_{m=0}^n C_{2m}(\mu) C_{2(n-m)}(\mu) \right] k^{2n}.$$

B | EXPLICIT CALCULATIONS OF THE SECOND ORDER CONTRIBUTION

CONTENTS

| | | |
|-------|---|------------|
| B.1 | MBPT nuclear matter integrals | B2 |
| B.1.A | Preliminary: overlap between two Fermi spheres | B2 |
| B.1.B | Calculation of the integral (B.1a) | B3 |
| B.1.C | Calculation of the integral (B.1b) | B4 |
| B.1.D | Calculation of the integral (B.1e) | B4 |
| B.2 | Calculation of the loop functions | B5 |
| B.2.A | Particle-particle loops function on the accessible phase-space | B6 |
| B.2.B | Hole-hole loops function on the accessible phase-space . . | B8 |
| B.2.C | Remarks | B9 |
| B.3 | Calculation of the Lee-Yang coefficient | B9 |
| B.3.A | Energy contribution from the effective particle-particle interaction | B9 |
| B.3.B | Energy contribution from the effective hole-hole interaction | B10 |
| B.4 | Calculation of the Galitskii formula | B10 |

In this appendix, we give the explicit steps to calculate some integrals on the phase-space (s, t) appearing several times in this thesis, for instance to estimate the Hartree-Fock and Lee-Yang contributions to the ground state energy given by the MBPT for dilute Fermi gas.

B.1

MBPT NUCLEAR MATTER INTEGRALS

Using the notations defined in chapter 2, we define:

$$\mathcal{I}[v] \equiv \int_{s,t} \theta_s^-(\mathbf{t}) v(\mathbf{s}, \mathbf{t}), \quad (\text{B.1a})$$

$$\mathcal{J}[w](\mathbf{s}, \mathbf{t}) \equiv \int_u \theta_s^+(\mathbf{u}) w(\mathbf{s}, \mathbf{t}, \mathbf{u}), \quad (\text{B.1b})$$

where v and w are written in term of matrix elements of the two-body interaction as:

$$v(\mathbf{s}, \mathbf{t}) = \langle k_F(\mathbf{s} \pm \mathbf{t}) | V | k_F(\mathbf{s} \mp \mathbf{t}) \rangle, \quad (\text{B.1c})$$

$$w(\mathbf{s}, \mathbf{t}, \mathbf{u}) = \langle k_F(\mathbf{s} \pm \mathbf{t}) | V | k_F(\mathbf{s} \mp \mathbf{u}) \rangle \frac{1}{t^2 - u^2} \langle k_F(\mathbf{s} \mp \mathbf{u}) | V | k_F(\mathbf{s} \pm \mathbf{t}) \rangle. \quad (\text{B.1d})$$

For a C_0 -contact interaction $V = C_0$, we have $v = C_0$ and $w \propto C_0^2$. These integrals appear in the calculation of the first and second orders of the ground state energy in perturbation [see (2.12) and (2.20)]. This particular case is explicitly treated in the following sections of this appendix.

We first concentrate on a Galilean invariant interaction like (1.6), and therefore v and w do not depend on the center of mass \mathbf{s} and only depend on the norm of the relative momenta \mathbf{t} , i.e. we assume in the following:

$$v(\mathbf{s}, \mathbf{t}) \rightarrow v(t) \quad \text{and} \quad w(\mathbf{s}, \mathbf{t}, \mathbf{u}) \rightarrow w(t, u).$$

The factor $\theta_s^-(\mathbf{t}) \equiv \Theta(k_F - k_F|\mathbf{s} - \mathbf{t}|)\Theta(k_F - k_F|\mathbf{s} + \mathbf{t}|)$ corresponds to the overlap between two Fermi spheres and $\theta_s^+(\mathbf{t}) \equiv \Theta(k_F|\mathbf{s} - \mathbf{t}| - k_F)\Theta(k_F|\mathbf{s} + \mathbf{t}| - k_F)$ to the exterior of the two Fermi spheres. The integration of $\mathcal{J}[w](\mathbf{s}, \mathbf{t})$ on the phase-space leads to the second order contribution to the ground state energy in perturbation [see (2.20)]:

$$\mathcal{K}[w] = \int_{s,t} \theta_s^-(\mathbf{t}) \mathcal{J}[w](\mathbf{s}, \mathbf{t}) = \int_{s,t} \theta_s^-(\mathbf{t}) \int_u \theta_s^+(\mathbf{u}) w(\mathbf{s}, \mathbf{t}, \mathbf{u}). \quad (\text{B.1e})$$

B.1.A Preliminary: overlap between two Fermi spheres

Here, we estimate some integrals that will be useful and that correspond to the volume of the overlap between two Fermi spheres. We define the volume Ω such that:

$$\int d^3s \theta_s^-(\mathbf{t}) = \frac{4\pi}{3} \underbrace{\left(1 - \frac{3}{2}t + \frac{1}{2}t^3\right)}_{\equiv \Omega(t)} \Theta(1-t). \quad (\text{B.2a})$$

Note that the Θ function gives a zero-contribution when the two spheres are too far from each other to overlap. Then, we introduce the coefficients I_{2n} defined by:

$$4\pi I_{2n} = \frac{3}{4\pi} \int d^3s \int d^3t t^{2n} \theta_s^-(t). \quad (\text{B.2b})$$

These coefficients are given analytically by:

$$I_{2n} = \int dt t^{2+2n} \Omega(t) \Theta(1-t) = \frac{1}{3+2n} - \frac{3/2}{4+2n} + \frac{1/2}{6+2n}, \quad (\text{B.2c})$$

and in particular: $I_0 = \frac{1}{24}$, $I_2 = \frac{1}{80}$, $I_4 = \frac{3}{560}$, $I_6 = \frac{1}{360}$, \dots

B.1.B Calculation of the integral (B.1a)

To calculate $\mathcal{I}[v]$, we use the spherical coordinates: $|\mathbf{s} \pm \mathbf{t}| = s^2 + t^2 \pm 2st \cos(\phi_{st} = \phi_s - \phi_t)$ and $d^2\sigma_r = \sin(\phi_r) d\phi_r d\psi_r$. The integral (B.1a) can then be written, for a Galilean invariant interaction, as:

$$\begin{aligned} \mathcal{I}[v] &= \frac{1}{(2\pi)^6} \int s^2 ds \int d^2\sigma_s \int t^2 dt \int d^2\sigma_t v(t), \\ &\quad \times \Theta(1 - \sqrt{s^2 + t^2 - 2st \cos \phi_{st}}) \Theta(1 - \sqrt{s^2 + t^2 + 2st \cos \phi_{st}}). \end{aligned} \quad (\text{B.3a})$$

The integrations on the azimuthal angles ψ_s and ψ_t give a factor $2\pi \times 2\pi$ and we have¹, including explicitly the integration on the polar angles:

$$\begin{aligned} \mathcal{I}[v] &= \frac{8\pi^2}{(2\pi)^6} \int_0^\infty s^2 ds \int_0^\infty t^2 dt \int_0^1 dx v(t), \\ &\quad \times \Theta(1 - \sqrt{s^2 + t^2 - 2stx}) \Theta(1 - \sqrt{s^2 + t^2 + 2stx}), \end{aligned} \quad (\text{B.3b})$$

where we used the change of variable $\cos \phi_{st} = x$. We also used the Heaviside distribution to enforce the domains of integration for s and t ; we choose the domain of the t integration between 0 and 1 (this is guided by the fact that $s, t > 0$), thus the integration on s is constrained by x and t . To find this domain, we use the definition of the Heaviside distribution:

$$\Theta(1 - \sqrt{s^2 + t^2 \pm 2stx}) = 1 \quad \Leftrightarrow \quad s^2 + t^2 \pm 2stx \leq 1. \quad (\text{B.4})$$

Taking into account that s is positive (s is a norm), we denote by $z_\pm(t, x) = \pm tx + \sqrt{1 - t^2(1 - x^2)}$ the solution of $s^2 + t^2 \pm 2stx = 1$. Due to the product of the two

¹ To make the integration on ϕ_{st} we have used the property of the δ -distribution valid for an arbitrary function $f(\cos(\theta_1 - \theta_2))$:

$$\begin{aligned} \int d\cos\theta_1 \int d\cos\theta_2 f(\cos(\theta_1 - \theta_2)) &= \int d\cos\theta f(\cos\theta) \int d\cos\theta_1 \int d\cos\theta_2 \delta(\cos\theta - \cos(\theta_1 - \theta_2)), \\ &= 2 \int d\cos\theta f(\cos\theta). \end{aligned}$$

Heaviside step functions, the upper bound of the integration on s is given by the lowest solution $z_-(t, x)$. This gives² for the integral (B.3b):

$$\mathcal{I}[v] = \frac{8\pi^2}{(2\pi)^6} \int_0^1 t^2 dt v(t) \int_0^1 dx \int_0^{z_-(t,x)} s^2 ds. \quad (\text{B.5})$$

Then, the integration on s and x gives [see (B.2a)]:

$$\int_0^1 dx \int_0^{z_-(t,x)} s^2 ds = \frac{1}{3} \left(1 - \frac{3}{2}t + \frac{1}{2}t^2 \right) \equiv \frac{\Omega(t)}{3}, \quad (\text{B.6})$$

and finally:

$$\mathcal{I}[v] = \frac{2}{3} \times \frac{1}{(2\pi)^4} \int_0^1 t^2 dt v(t) \Omega(t). \quad (\text{B.7})$$

B.1.C Calculation of the integral (B.1b)

Similarly, for (B.1b) we obtain:

$$\mathcal{J}[w](s, t) = \frac{4\pi}{(2\pi)^3} \int_0^1 dy \int_{z_+(t,y)}^\infty u^2 du w(t, u). \quad (\text{B.8})$$

Here, we used the fact that the matrix elements of the interaction do not depend of the angle between t and u .

B.1.D Calculation of the integral (B.1e)

Putting all together, the integral (B.1e) can be written as:

$$\begin{aligned} \mathcal{K}[w] &= \frac{4 \times (2\pi)^3}{(2\pi)^9} \int_0^1 s^2 ds \int_0^1 dx \int_0^{z_-(s,x)} t^2 dt \int_0^1 dy \int_{z_+(s,y)}^\infty u^2 du w(t, u), \\ &= \mathcal{K}_\infty[w] - \mathcal{K}_0[w], \end{aligned} \quad (\text{B.9a})$$

where we have defined:

$$\mathcal{K}_\infty[w] = \frac{4 \times (2\pi)^3}{(2\pi)^9} \int_0^1 s^2 ds \int_0^1 dx \int_0^{z_-(t,x)} t^2 dt \int_0^\infty u^2 du w(t, u), \quad (\text{B.9b})$$

$$\mathcal{K}_0[w] = \frac{4 \times (2\pi)^3}{(2\pi)^9} \int_0^1 s^2 ds \int_0^1 dx \int_0^{z_-(s,x)} t^2 dt \int_0^1 dy \int_{z_+(s,y)}^\infty u^2 du w(t, u). \quad (\text{B.9c})$$

² In fact, $s^2 + t^2 \pm 2stx \leq 1$ is symmetric by the inversion of s and t . Since we have assumed v independent of s , we can take the solution $z_\pm(t, x)$ to find the upper bound of integration on s . But, in the calculation of $\mathcal{K}[w]$, the effective potential $\mathcal{J}[w]$ depends explicitly of s . Thus, in this case, we take the solution $z_-(s, x)$ according to t :

$$\mathcal{I}[v] = \frac{8\pi^2}{(2\pi)^6} \int_0^1 s^2 ds \int_0^1 dx \int_0^{z_-(s,x)} t^2 dt v(t).$$

The contribution $\mathcal{K}_\infty[w]$ is the divergent part of the integral associated to the vacuum energy which is renormalized by the method as discussed in appendix A.

In the following, we consider a C_0 -contact interaction to estimate the integrals and obtain the Lee-Yang formula as well as the Galitskii function.

B.2

CALCULATION OF THE LOOP FUNCTIONS

In the following, we will use these notations:

$$F(s, t) \equiv 1 + s + t \ln \left| \frac{1 + s - t}{1 + s + t} \right| + \frac{1 - s^2 - t^2}{2s} \ln \left| \frac{(1 + s)^2 - t^2}{1 - s^2 - t^2} \right|, \quad (\text{B.10a})$$

$$R(s, t) \equiv 2 + t \ln \left| \frac{(t - 1)^2 - s^2}{(t + 1)^2 - s^2} \right| + \frac{1 - s^2 - t^2}{2s} \ln \left| \frac{(s + 1)^2 - t^2}{(s - 1)^2 - t^2} \right|, \quad (\text{B.10b})$$

$$I_1(s, t) \equiv \frac{\pi}{2s} [1 - s^2 - t^2], \quad (\text{B.10c})$$

$$I_2(s, t) \equiv \frac{\pi}{2s} [1 - (s - t)^2]. \quad (\text{B.10d})$$

Note that the functions F and R are also introduced in appendix C and that we have the identity $I_1(s, t) = I_2(s, t) - \pi t$. In addition, it is useful to introduce new functions that restrict the integration domain:

$$D_{pp}(p_1, s, t) = \Theta \left(s^2 + t^2 - \frac{p_1^2}{2} \right) \Theta \left(\frac{p_1^2 + 1}{2} - s^2 - t^2 \right), \quad (\text{B.11a})$$

$$D_{hh}(p_1, s, t) = \Theta \left(s^2 + t^2 - \frac{p_1^2 + 1}{2} \right). \quad (\text{B.11b})$$

Then, we recall some notations introduced in the previous section and/or in the main text related to the limits of integration:

- $z^\pm(s, y) = \pm sy + \sqrt{1 - s^2(1 - y^2)}$;
- $z(s) = \sqrt{1 - 1/s^2}$;
- $\theta_s^-(\mathbf{u}) = \Theta(1 - |\mathbf{s} + \mathbf{u}|)\Theta(1 - |\mathbf{s} - \mathbf{u}|)$;
- $\theta_s^+(\mathbf{u}) = \Theta(|\mathbf{s} + \mathbf{u}| - 1)\Theta(|\mathbf{s} - \mathbf{u}| - 1)$.

The $z^\pm(s, y)$ functions come from $\theta_s^\pm(\mathbf{u})$ and constrain the domain of integration on u . Noting $y = \cos \theta_{s \cdot \mathbf{u}} \in [-1, 1]$, we have explicitly:

(a) For $s \leq 1$,

$$\begin{aligned} \theta_s^-(\mathbf{u}) &= \Theta(1 - \sqrt{s^2 + u^2 + 2suy})\Theta(1 - \sqrt{s^2 + u^2 - 2suy}) \\ &\Leftrightarrow u \leq z^\mp(s, \pm y > 0) \end{aligned}$$

$$\begin{aligned} \theta_s^+(\mathbf{u}) &= \Theta(\sqrt{s^2 + u^2 + 2suy} - 1)\Theta(\sqrt{s^2 + u^2 - 2suy} - 1) \\ &\Leftrightarrow u \geq z^\pm(s, \pm y > 0). \end{aligned}$$

(b) For $s > 1$, z^\pm is only defined for $|y| \geq \sqrt{1 - 1/s^2} \equiv z(s)$ and we have:

$$\theta_s^-(\mathbf{u}) = \Theta(1 - \sqrt{s^2 + u^2 + 2suy})\Theta(1 - \sqrt{s^2 + u^2 - 2suy}) = 0$$

$$\theta_s^+(\mathbf{u}) = \Theta(\sqrt{s^2 + u^2 + 2suy} - 1)\Theta(\sqrt{s^2 + u^2 - 2suy} - 1)$$

$$\Leftrightarrow u \in [-z^\mp(s, \pm y > 0), z^\pm(s, \pm y > 0)].$$

B.2.A Particle-particle loops function on the accessible phase-space

We have to calculate the following integral defined by (2.21):

$$\Pi_{pp}(s, t) \equiv \int_u \frac{\theta_s^+(\mathbf{u})}{t^2 - u^2 + i\tau}. \quad (\text{B.12})$$

The estimate of Π_{pp} should account for the fact that it is restricted to specific values of $p_2 = k_2/k_F$. Since Π_{pp} appears solely with $\Theta(1 - p_2)$ in (2.18) for the ground state energy and in (4.3) for the proper self-energy, it has to be defined only when $0 \leq p_2 < 1$. Then, we have the restriction for (s, t) :

$$\frac{p_1^2}{2} \leq s^2 + t^2 \equiv \frac{p_1^2 + p_2^2}{2} \leq \frac{p_1^2 + 1}{2}. \quad (\text{B.13})$$

To translate formally this inequalities, we introduce the functions $D_{pp}(p_1, s, t)$ defined by (B.11a). The analytical expression of Π_{pp} is given below.

(a) For $s \leq 1$, we define^{3,4}:

$$\begin{aligned} \Pi_{pp}(s, t) &= L_0(s, t) - \underbrace{\frac{1}{(2\pi)^2} 2 \int_0^1 dy \int_0^{z^+(s,y)} \frac{u^2 du}{t^2 - u^2 + i\tau'}}_{-F_{pp}(s \leq 1, t)} \\ &\equiv L_0(s, t) + \frac{1}{(2\pi)^2} F_{pp}(s \leq 1, t), \end{aligned} \quad (\text{B.14a})$$

where L_0 is the divergent part of the one-loop integral (regularized using minimal subtraction for instance, see (A.6c) in appendix A):

$$L_0(s, t) = \int \frac{d^3u}{(2\pi)^3} \frac{1}{t^2 - u^2 + i\tau} \quad \mapsto \quad -\frac{it}{4\pi}. \quad (\text{B.14b})$$

The general strategy to treat the divergences of an integral is to decompose it into a divergent and a non-divergent part using (at zero temperature) the

³ The factor 2 appearing in the integral definition of Π_{pp} comes from the symmetry under the angle integration:

$$\int \theta_s^+(\mathbf{u}) d^3u = \int_0^1 dy \int_{z^+(s,y)}^\infty u^2 du + \int_{-1}^0 dy \int_{z^-(s,y)}^\infty u^2 du = 2 \int_0^1 dy \int_{z^+(s,y)}^\infty u^2 du$$

⁴ The case $k_1 > k_F$ is possible but do not contribute to the energy, see (2.18).

property on the occupation number: $\Theta(k - k_F) = 1 - \Theta(k_F - k)$. The divergent integral should be regularized with standard methods as MS or PDS schemes introducing a cut-off (see appendix A for an explicit regularization of $L_0(s, t)$) and the convergent part could be calculated. Analytically (using Wolfram Mathematica software), we have obtained for the non-divergent integral:

$$\text{Re}[F_{pp}(s \leq 1, t)] \times D_{pp}(p_1, s, t) = F(s, t), \quad (\text{B.14c})$$

$$\text{Im}[F_{pp}(s \leq 1, t)] \times D_{pp}(p_1, s, t) = \begin{cases} \pi t & 0 \leq t < \sqrt{1 - s^2}, \\ I_2(s, t) & \sqrt{1 - s^2} \leq t < 1 + s, \\ 0 & 1 + s \leq t, \end{cases} \quad (\text{B.14d})$$

leading to, taking into account the one-loop particle-particle integral L_0 :

$$\text{Re}[\Pi_{pp}(s \leq 1, t)] \times D_{pp}(p_1, s, t) = F(s, t), \quad (\text{B.14e})$$

$$\text{Im}[\Pi_{pp}(s \leq 1, t)] \times D_{pp}(p_1, s, t) = \begin{cases} 0 & 0 \leq t < \sqrt{1 - s^2}, \\ I_1(s, t) & \sqrt{1 - s^2} \leq t < 1 + s, \\ -\pi t & 1 + s \leq t. \end{cases} \quad (\text{B.14f})$$

The imaginary part can also be written in a compact form as:

$$\begin{aligned} \text{Im}[F_{pp}(s \leq 1, t)] \times D_{pp}(p_1, s, t) \\ = \left[\pi t \Theta(1 - s^2 - t^2) + I_2(s, t) \Theta(s^2 + t^2 - 1) \right] \Theta(1 + s - t). \end{aligned} \quad (\text{B.14g})$$

(b) For $s > 1$, we obtain similarly:

$$\begin{aligned} \Pi_{pp}(s, t) &= L_0(s, t) - \frac{1}{(2\pi)^2} \underbrace{2 \int_{z(s)}^1 dy \int_{-z^-(s, y)}^{z^+(s, y)} \frac{u^2 du}{t^2 - u^2 + i\eta'}}_{\equiv -F_{pp}(s > 1, t)} \\ &\equiv L_0(s, t) + \frac{1}{(2\pi)^2} F_{pp}(s > 1, t). \end{aligned} \quad (\text{B.15a})$$

Analytically, we have obtained:

$$\text{Re}[F_{pp}(s > 1, t)] \times D_{pp}(p_1, s, t) = R(s, t), \quad (\text{B.15b})$$

$$\text{Im}[F_{pp}(s > 1, t)] \times D_{pp}(p_1, s, t) = \begin{cases} 0 & 0 \leq t < s - 1, \\ I_2(s, t) & s - 1 \leq t < s + 1, \\ \pi t & s + 1 \leq t, \end{cases} \quad (\text{B.15c})$$

leading to, taking into account the one-loop particle-particle integral L_0 :

$$\text{Re}[\Pi_{pp}(s > 1, t)] \times D_{pp}(p_1, s, t) = R(s, t), \quad (\text{B.15d})$$

$$\text{Im}[\Pi_{pp}(s > 1, t)] \times D_{pp}(p_1, s, t) = \begin{cases} -\pi t & 0 \leq t < s - 1, \\ I_1(s, t) & s - 1 \leq t < s + 1, \\ 0 & s + 1 \leq t. \end{cases} \quad (\text{B.15e})$$

The imaginary part can be written as:

$$\begin{aligned} \text{Im}[F_{pp}(s > 1, t)] \times D_{pp}(p_1, s, t) \\ = \left[\pi t \Theta(t - s - 1) + I_2(s, t) \Theta(1 - s + t) \right] \Theta(s - t - 1). \end{aligned} \quad (\text{B.15f})$$

B.2.B Hole-hole loops function on the accessible phase-space

We now have to calculate the following integral:

$$\Pi_{hh}(s, t) \equiv \int \frac{d^3 u}{(2\pi)^3} \frac{\theta_s^-(\mathbf{u})}{t^2 - u^2 - i\tau}. \quad (\text{B.16a})$$

We remark that, with the change of the angle variable in the definition of Π_{hh} , $y \rightarrow -y$, we have $z^-(s, y) \rightarrow z^+(s, y)$ [and $z(s) \rightarrow z(s)$] and we obtain⁵ for $s \leq 1$ and $s > 1$:

$$\text{Re}[\Pi_{hh}(s, t)] = -\text{Re}[\Pi_{pp}(-s, t)]. \quad (\text{B.16b})$$

The integral Π_{hh} is only defined when $p_2 = k_2/k_F \geq 1$ and we can deduce the following inequality:

$$s^2 + t^2 \equiv \frac{p_1^2 + p_2^2}{2} \geq \frac{p_1^2 + 1}{2}. \quad (\text{B.17})$$

We introduce the functions $D_{hh}(p_1, s, t)$ that cut the integration domain defined by (B.11b). The analytical expression of Π_{hh} is given below and obtained in the same way as Π_{pp} .

(a) For $s \leq 1$, we have obtained:

$$\text{Re}[\Pi_{hh}(s \leq 1, t)] \times D_{hh}(p_1, s, t) = -F(-s, t) \quad (\text{B.18a})$$

$$\text{Im}[\Pi_{hh}(s \leq 1, t)] \times D_{hh}(p_1, s, t) = \begin{cases} \pi t & 0 \leq t < 1 - s \\ I_1(s, t) & 1 - s \leq t < \sqrt{1 - s^2} \\ 0 & \sqrt{1 - s^2} \leq t \end{cases} \quad (\text{B.18b})$$

The imaginary part can then be written:

$$\begin{aligned} \text{Im}[\Pi_{hh}(s \leq 1, t)] \times D_{hh}(p_1, s, t) \\ = \left[\pi t \Theta(s - t - 1) + I_1(s, t) \Theta(t - s + 1) \right] \Theta(1 - s^2 - t^2). \end{aligned} \quad (\text{B.18c})$$

(b) For $s > 1$, we have simply:

$$\Pi_{hh}(s > 1, t) \times D_{hh}(p_1, s, t) = 0. \quad (\text{B.19})$$

⁵ We can use also the identity, where \mathcal{P} denotes the principal value:

$$\frac{1}{X \pm i\eta} = \mathcal{P} \frac{1}{X} \mp i\pi\delta(X).$$

B.2.c Remarks

Before we give the second order contribution to the ground state energy given by these two integrals, we would like to make two remarks:

1. We can understand the domain of the t -variable according to s as follow: this domains are delimited by the change of sign in the logarithm appearing in the function F . The complex phase comes from $\ln z = \ln |z| + i\text{Arg}(z)$. It should be also related to different configurations of the three Fermi spheres.
2. We verified the fact that the imaginary part of Π_{pp} is negative for $k_1 > k_F$. This is coherent with the fact that particle states outside the Fermi sphere have a finite life-time.

B.3

CALCULATION OF THE LEE-YANG COEFFICIENT

B.3.A Energy contribution from the effective particle-particle interaction

We estimate now the Lee-Yang contribution to the ground state energy at second order in MBPT, we have to calculate the following integral [see (2.22)]:

$$H_{pp} = \int_{s,t} \theta_s^-(t) \Pi_{pp}(s,t). \quad (\text{B.20a})$$

We have seen that the domain of integration D_{pp} (and the condition $p_1 \leq 1$) enforces:

$$s^2 \leq s^2 + t^2 \leq \frac{p_1^2 + 1}{2} \leq 1, \quad (\text{B.20b})$$

and therefore $s \leq 1$. Formally, as described above, the functions $\theta_s^\pm(t)$ constrain the domains of integration. Noting $x \equiv \cos \theta_{s,t} \in [-1, 1]$, we have to integrate first, for $s \leq 1$, on the variable t from 0 to $z^-(s,x)$ for $x > 0$ and from 0 to $z^+(s,x)$ for $x < 0$. Putting everything together, we obtain:

$$H_{pp} = \frac{4}{(2\pi)^4} \int_0^1 s^2 ds \int_0^1 dx \int_0^{z^-(s,x)} t^2 dt \Pi_{pp}(s,t), \quad (\text{B.20c})$$

and the numerical value:

$$H_{pp} = \frac{1}{(2\pi)^6} \frac{11 - 2 \ln 2}{105}. \quad (\text{B.20d})$$

Note that the imaginary part is identically zero on the domain of integration $1 - s^2 - t^2 \leq 0$.

B.3.B Energy contribution from the effective hole-hole interaction

We can also calculate the integral:

$$H_{hh} = \int_{s,t} \theta_s^+(t) \Pi_{hh}(s,t), \quad (\text{B.21a})$$

and similarly to the calculation of H_{pp} , we have explicitly:

$$H_{hh} = \frac{4}{(2\pi)^4} \int_0^1 s^2 ds \int_0^1 dx \int_{z^+(s,x)}^\infty t^2 dt \Pi_{hh}(s,t). \quad (\text{B.21b})$$

The integral (B.21b) on the variable t is divergent. Thus, as for the renormalization of the particle-particle part, we decompose:

$$H_{hh} = \overline{L}_0 - \frac{4}{(2\pi)^4} \int_0^1 s^2 ds \int_0^1 dx \int_0^{z^+(s,x)} t^2 dt \Pi_{hh}(s,t). \quad (\text{B.21c})$$

\overline{L}_0 is the divergent part of the integral removed using the minimal subtraction scheme⁶:

$$\overline{L}_0 = \frac{4}{(2\pi)^4} \int_0^1 s^2 ds \int_0^\infty t^2 dt \Pi_{hh}(s,t) \longmapsto 0. \quad (\text{B.21d})$$

Finally, taking care of the divergent term, we obtain:

$$H_{hh} = H_{pp} = \frac{1}{(2\pi)^6} \frac{11 - 2 \ln 2}{105}, \quad (\text{B.21e})$$

which is coherent with the symmetry argument. Note that the imaginary part cancels out after integration: we have seen that the domain of integration D_{hh} (and the condition $1 \leq p_1$) enforces $s^2 + t^2 \geq 1$ and, comparing to (B.18c), the imaginary part cannot contribute.

B.4

CALCULATION OF THE GALITSKII FORMULA

Similarly to the estimation of the Lee-Yang formula and treating properly the divergences, we obtain the second order contribution to the self-energy (4.3):

⁶ We have:

$$\overline{L}_0(\Lambda) \equiv \frac{4}{(2\pi)^4} \int_0^1 s^2 ds \int_0^\Lambda t^2 dt \Pi_{hh}(s,t) \underset{\Lambda \rightarrow \infty}{\sim} \frac{1}{(2\pi)^6} \frac{\Lambda}{9} + O(1/\Lambda).$$

$$\begin{aligned}
\Phi_2(p) = & \frac{4}{15\pi^2} \frac{1}{p} \left\{ 11p + 2p^5 \ln \left| \frac{p^2}{p^2 - 1} \right| - 10(p^2 - 1) \ln \left| \frac{p + 1}{p - 1} \right| \right\} \\
& - \frac{8}{15\pi^2} \frac{|2 - p^2|^{5/2}}{p} \left\{ \Theta(2 - p^2) \ln \left| \frac{1 + p\sqrt{2 - p^2}}{1 - p\sqrt{2 - p^2}} \right| \right. \\
& \left. + \Theta(p^2 - 2) \cot^{-1} \sqrt{p^2 - 2} \right\}, \tag{B.22a}
\end{aligned}$$

$$\begin{aligned}
\Omega_2(p) = & \Theta(1 - p) \frac{(1 - p^2)^2}{2\pi} \\
& - \Theta(p - 1) \frac{2}{15\pi^2} \frac{1}{p} \left\{ 5p^2 - 7 + 2(2 - p^2)^{5/2} \Theta(\sqrt{2} - p) \right\}, \tag{B.22b}
\end{aligned}$$

where the Galitskii functions Φ_2 and Ω_2 are defined by (4.4) and have been first obtained in [225].

C

EXPLICIT CALCULATIONS OF THE IN-MEDIUM LOOPS

CONTENTS

| | | |
|-------|--|-----|
| c.1 | Expression in term of the occupation numbers | C2 |
| c.1.A | Bubbles using vacuum-medium Green's functions | C2 |
| c.1.B | On-shell bubble functions | C3 |
| c.1.C | Link between the in-medium loops and the particle-particle loop | C5 |
| c.1.D | Definition of useful notations | C6 |
| c.2 | Calculation of the unperturbed in-medium loops | C7 |
| c.3 | Calculation of the leading order of the perturbed in-medium loops | C8 |
| c.4 | Energy resummation | C10 |
| c.4.A | Full ladder resummation | C11 |
| c.4.B | Restricted particle-particle ladder resummation | C11 |
| c.5 | Self-energy resummation | C12 |
| c.5.A | Full ladder resummation | C12 |
| c.5.B | Restricted particle-particle ladder resummation | C17 |

In this appendix, we calculate explicitly the in-medium loop functions B_0 , B_1 , B_2 , and B_{pp} appearing in chapter 2 and 4. These bubble functions are the key elements to obtain resummed form of the energy and self-energy from resummation of many-body ladder diagrams. At the ground state energy (respectively self-energy) level, these functions depend explicitly on the unperturbed (respectively perturbed) occupation numbers of the infinite Fermi systems. Here, we give, step by step, including discussion on the technical subtleties, the calculations of these key quantities necessary to understand the ladder diagram resummation of [238,240].

C.1

EXPRESSION IN TERM OF THE OCCUPATION NUMBERS

c.1.A Bubbles using vacuum-medium Green's functions

PARTICLE-HOLE FORMALISM

We start by evaluating in term of the particle-hole Green's functions (2.3) the Feynman diagram:

$$= L(\mathbf{k}_1, \omega_1; \mathbf{k}_2, \omega_2). \quad (\text{C.1})$$

As commonly done, despite the fact that the loop diagrams are composed by two vertices of interaction (black dot), they are defined for convenience in the resummation by considering none of them, i.e. the loop L is given by:

$$\begin{aligned} L &= \int_{3,4}^{\bar{\delta}} G_3 G_4 = \int_3 G_{1-3} G_{2+3} = \int_3 \left\{ G_{1-3}^+ + G_{1-3}^- \right\} \times \left\{ G_{2+3}^+ + G_{2+3}^- \right\} \\ &= \underbrace{\int_3 G_{1-3}^- G_{2+3}^-}_{\equiv L_{pp}} + \underbrace{\int_3 G_{1-3}^+ G_{2+3}^+}_{\equiv L_{hh}} + \underbrace{\int_3 G_{1-3}^- G_{2+3}^+}_{\equiv L_{ph}} + \underbrace{\int_3 G_{1-3}^+ G_{2+3}^-}_{\equiv L_{hp}} \end{aligned}$$

where four contributions are labeled by the combination of particle and hole part of the propagator. By contour integration on ω_3 , we have for each of them:

$$\begin{aligned} L_{pp} &= \int_3 G_{1-3}^- G_{2+3}^- = \int_{k_3} \int_{\omega_3} \frac{1 - n_{1-3}}{\omega_{1-3} - e_{1-3} + i\tau} \times \frac{1 - n_{2+3}}{\omega_{2+3} - e_{2+3} + i\tau} \\ &= - \int_{k_3} \frac{[1 - n_{1-3}][1 - n_{2+3}]}{\omega_{1+2} - e_{1-3} - e_{2+3} + i\tau'} \end{aligned} \quad (\text{C.2a})$$

$$\begin{aligned} L_{hh} &= \int_3 G_{1-3}^+ G_{2+3}^+ = \int_{k_3} \int_{\omega_3} \frac{n_{1-3}}{\omega_{1-3} - e_{1-3} - i\tau} \times \frac{n_{2+3}}{\omega_{2+3} - e_{2+3} - i\tau} \\ &= \int_{k_3} \frac{n_{1-3} n_{2+3}}{\omega_{1+2} - e_{1-3} - e_{2+3} - i\tau'} \end{aligned} \quad (\text{C.2b})$$

$$L_{ph} = \int_3 G_{1-3}^- G_{2+3}^+ = \int_{k_3} \int_{\omega_3} \frac{1 - n_{1-3}}{\omega_{1-3} - e_{1-3} + i\tau} \times \frac{n_{2+3}}{\omega_{2+3} - e_{2+3} - i\tau} = 0, \quad (\text{C.2c})$$

$$L_{hp} = \int_3 G_{1-3}^+ G_{2+3}^- = \int_{k_3} \int_{\omega_3} \frac{n_{1-3}}{\omega_{1-3} - e_{1-3} - i\tau} \times \frac{1 - n_{2+3}}{\omega_{2+3} - e_{2+3} + i\tau} = 0. \quad (\text{C.2d})$$

The particle-hole and hole-particle parts (L_{ph} and L_{hp}) vanish automatically after the contour integration. The contour integration yields automatically the sum of the particle-particle and hole-hole contributions (L_{pp} and L_{hh}) considering that the propagation of the particles labeled by 3 and 4 are described by the full particle-hole Green's functions (2.3). This is in agreement with the direction of the arrows labeled by 3 and 4 that are the same.

VACUUM-MEDIUM FORMALISM

We now want to estimate the loop functions in a slightly different way using the vacuum-medium decomposition of the Green's functions (2.36). This leads to the loop function L written as:

$$\begin{aligned}
 L &= \int_{3,4}^{\bar{\delta}} G_3 G_4 = \int_3 G_{1-3} G_{2+3} = \int_3 \left\{ \bar{G}_{1-3} + H_{1-3} \right\} \times \left\{ \bar{G}_{2+3} + H_{2+3} \right\} \\
 &= \int_3 \left\{ \bar{G}_{1-3} \bar{G}_{2+3} + H_{1-3} \bar{G}_{2+3} + \bar{G}_{1-3} H_{2+3} + H_{1-3} H_{2+3} \right\} \\
 &= \underbrace{\int_3 \bar{G}_{1-3} \bar{G}_{2+3}}_{\equiv L_0} + \underbrace{\int_3 \left\{ H_{1-3} \bar{G}_{2+3} + \bar{G}_{1-3} H_{2+3} \right\}}_{\equiv L_1} + \underbrace{\int_3 H_{1-3} H_{2+3}}_{\equiv L_2}
 \end{aligned}$$

where we have used the compact notations introduced in chapter 2. The vacuum-medium decomposition gives three contributions, L_0 , L_1 and L_2 , represented in figure 2.5 and that correspond respectively to 0, 1, and 2 medium insertion as seen from the above equation counting how much times H appears. Below, we estimate these loops after contour integration defining the functions B_0 , B_1 , B_2 and B_{pp} used in this thesis.

c.1.B On-shell bubble functions

ZERO IN-MEDIUM INSERTION LOOPS

The L_0 loop is given by:

$$\begin{aligned}
 L_0 &= \int_3 \bar{G}_{1-3} \bar{G}_{2+3} = \int_{k_3} \int_{\omega_3} \frac{1}{\omega_{1-3} - e_{1-3} + i\tau} \times \frac{1}{\omega_{2+3} - e_{2+3} + i\tau} \\
 &= - \int_{k_3} \frac{1}{\omega_{1+2} - e_{1-3} - e_{2+3} + i\tau}.
 \end{aligned} \tag{C.3a}$$

Evaluating it on-shell by replacing $\omega_1 \rightarrow e_1$ and $\omega_2 \rightarrow e_2$ leads to:

$$B_0 = -C_0 L_0(\mathbf{k}_1, e_1; \mathbf{k}_2, e_2) = C_0 \int_{k_3} \frac{1}{e_1 + e_2 - e_{1-3} - e_{2+3} + i\tau}. \tag{C.3b}$$

Introducing the dimensionless change of variables (2.19) and using the definition of the single-particle energy $e_i = \mathbf{k}_i^2/2m$, the denominator is given by:

$$\begin{aligned}
 \frac{2m}{k_F^2} (e_1 + e_2 - e_{1-3} - e_{2+3}) &= (s + t)^2 + (s - t)^2 - (s + u)^2 - (s - u)^2 \\
 &= 2(t^2 - u^2),
 \end{aligned}$$

leading to:

$$B_0 = mC_0k_F \int_u \frac{1}{t^2 - u^2 + i\tau}. \quad (\text{C.3c})$$

We observe that the bubble function B_0 is independent of the occupation numbers and corresponds to the vacuum scattering function regularized in appendix A. Using the minimal subtraction scheme to evaluate this integral, decomposed in real and imaginary part using the identity (2.37), we obtain:

$$\text{Re} \left[\frac{B_0}{mC_0k_F} \right] = \mathcal{P} \int_u \frac{1}{t^2 - u^2}, \quad (\text{C.3d})$$

$$\text{Im} \left[\frac{B_0}{mC_0k_F} \right] = -\pi \int_u \delta(t^2 - u^2). \quad (\text{C.3e})$$

ONE IN-MEDIUM INSERTION LOOPS

For the one in-medium insertion loop, we have:

$$\begin{aligned} L_1 &= \int_3 \left\{ H_{1-3} \bar{G}_{2+3} + \bar{G}_{1-3} H_{2+3} \right\} \\ &= \int_{k_3} \int_{\omega_3} \left\{ \frac{\bar{\delta}(\omega_{1-3} - e_{1-3})n_{1-3}}{\omega_{2+3} - e_{2+3} + i\tau} + \frac{\bar{\delta}(\omega_{2+3} - e_{2+3})n_{2+3}}{\omega_{1-3} - e_{1-3} + i\tau} \right\} \\ &= \int_{k_3} \frac{n_{1-3} + n_{2+3}}{\omega_{1+2} - e_{1-3} - e_{2+3} + i\tau}. \end{aligned} \quad (\text{C.4a})$$

Then evaluating it on-shell leads to:

$$B_1 = -C_0 L_1(\mathbf{k}_1, e_1; \mathbf{k}_2, e_2) = -mC_0k_F \int_u \frac{n_{1-3} + n_{2+3}}{t^2 - u^2 + i\tau}, \quad (\text{C.4b})$$

and using the identity (2.37), we obtain:

$$\text{Re} \left[\frac{B_1}{mC_0k_F} \right] = -\mathcal{P} \int_u \frac{n_{1-3} + n_{2+3}}{t^2 - u^2}, \quad (\text{C.4c})$$

$$\text{Im} \left[\frac{B_1}{mC_0k_F} \right] = \pi \int_u \delta(t^2 - u^2) \times (n_{1-3} + n_{2+3}). \quad (\text{C.4d})$$

TWO IN-MEDIUM INSERTIONS LOOPS

Finally, for L_2 , we have:

$$\begin{aligned} L_2 &= \int_3 H_{1-3} H_{2+3} = \int_{k_3} \int_{\omega_3} 2i\pi\delta(\omega_{1-3} - e_{1-3})n_{1-3} \times 2i\pi\delta(\omega_{2+3} - e_{2+3})n_{2+3} \\ &= \int_{k_3} 2i\pi\delta(\omega_{1+2} - e_{1-3} - e_{2+3})n_{1-3}n_{2+3}. \end{aligned} \quad (\text{C.5a})$$

Again evaluating on-shell:

$$B_2 = -C_0 L_2(\mathbf{k}_1, e_1; \mathbf{k}_2, e_2) = -mC_0k_F \int_u 2i\pi\delta(t^2 - u^2)n_{1-3}n_{2+3}, \quad (\text{C.5b})$$

or equivalently to:

$$\operatorname{Re} \left[\frac{B_2}{mC_0k_F} \right] = 0, \quad (\text{C.5c})$$

$$\operatorname{Im} \left[\frac{B_2}{mC_0k_F} \right] = -2\pi \int_u \delta(\mathbf{t}^2 - \mathbf{u}^2) n_{1-3} n_{2+3}. \quad (\text{C.5d})$$

USEFUL RELATIONSHIP BETWEEN THE LOOPS

Putting altogether, we remark that:

$$\operatorname{Re} \left[\frac{B_0 + B_1 + B_2}{mC_0k_F} \right] = \operatorname{Re} \left[\frac{B_1}{mC_0k_F} \right] = -\mathcal{P} \int_u \frac{n_{1-3} + n_{2+3}}{\mathbf{t}^2 - \mathbf{u}^2}, \quad (\text{C.6a})$$

$$\begin{aligned} \operatorname{Im} \left[\frac{B_0 + B_1 + B_2}{mC_0k_F} \right] &= -\pi \int_u \delta(\mathbf{t}^2 - \mathbf{u}^2) \left\{ 1 - n_{1-3} - n_{2+3} + 2n_{1-3}n_{2+3} \right\} \\ &= -\pi \int_u \delta(\mathbf{t}^2 - \mathbf{u}^2) \left\{ n_{1-3}n_{2+3} + [1 - n_{1-3}][1 - n_{2+3}] \right\}. \end{aligned} \quad (\text{C.6b})$$

c.1.c Link between the in-medium loops and the particle-particle loop

Some relationships exist between the in-medium loops and the loops L_{pp} and L_{hh} . We illustrate this here for the L_{pp} loop.

$$\begin{aligned} L_{pp} &= \int_3 G_{1-3}^- G_{2+3}^- = \int_{k_3} \int_{\omega_3} \frac{1 - n_{1-3}}{\omega_{1-3} - e_{1-3} + i\tau} \times \frac{1 - n_{2+3}}{\omega_{2+3} - e_{2+3} + i\tau} \\ &= - \int_{k_3} \frac{[1 - n_{1-3}][1 - n_{2+3}]}{\omega_{1+2} - e_{1-3} - e_{2+3} + i\tau}. \end{aligned} \quad (\text{C.7a})$$

Then evaluating on-shell leads to:

$$B_{pp} = -C_0 L_{pp}(\mathbf{k}_1, e_1; \mathbf{k}_2, e_2) = mC_0k_F \int_u \frac{[1 - n_{1-3}][1 - n_{2+3}]}{\mathbf{t}^2 - \mathbf{u}^2 + i\tau}, \quad (\text{C.7b})$$

or equivalently to:

$$\operatorname{Re} \left[\frac{B_{pp}}{mC_0k_F} \right] = \mathcal{P} \int_u \frac{[1 - n_{1-3}][1 - n_{2+3}]}{\mathbf{t}^2 - \mathbf{u}^2}, \quad (\text{C.7c})$$

$$\operatorname{Im} \left[\frac{B_{pp}}{mC_0k_F} \right] = -\pi \int_u \delta(\mathbf{t}^2 - \mathbf{u}^2) [1 - n_{1-3}][1 - n_{2+3}]. \quad (\text{C.7d})$$

Comparing (C.6) and the above equations, we see immediately that:

$$B_{pp} = B_0 + B_1 + \int_u \frac{n_{1-3}n_{2+3}}{\mathbf{t}^2 - \mathbf{u}^2 + i\tau}. \quad (\text{C.8})$$

c.1.d Definition of useful notations

According to the test-particle insertion method described in chapter 4 used to obtain the on-shell self-energy, the occupation numbers appearing in the bubble functions B_j ($j = 0, 1, 2, pp$) are given by (4.31) and depend both on the infinitesimal parameter η and on the momentum \mathbf{k} of the test-particle.

For practical reasons, we introduce the following notations that will be used below:

- The dimensionless infinitesimal parameter defined as: $gk_F^3\tilde{\eta} = 2\pi^2\eta$;
- The dimensionless momentum of the test-particle defined as: $\mathbf{p} = \mathbf{k}/k_F$;
- The dimensionless loop functions defined as $B_j(\eta) = mC_0k_F b_j(\eta)$;
- To linear order in η we define: $b_j(\eta) = \beta_j + \tilde{\eta}\delta\beta_j$;
- For an arbitrary function $f(\mathbf{p})$, we define its angle averaged function as:

$$\hat{f}(p) = \frac{1}{4\pi} \int f(\mathbf{p}) d\Omega_p, \quad (\text{C.9})$$

where Ω_p is the solid angle of \mathbf{p} .

- It is also useful to define
 - $\beta = \beta_0 + \beta_1 + \beta_2, \beta' = \beta_0 + \beta_1$;
 - $\delta\beta = \delta\beta_0 + \delta\beta_1 + \delta\beta_2, \delta\beta' = \delta\beta_0 + \delta\beta_1$;
 - $\widehat{\delta\beta} = \widehat{\delta\beta_0} + \widehat{\delta\beta_1} + \widehat{\delta\beta_2}, \widehat{\delta\beta'} = \widehat{\delta\beta_0} + \widehat{\delta\beta_1}$.

Using these notations and considering that the occupation numbers appearing in the loops B_j above are given by (4.31), we have:

$$\beta_0 = + \int_u \frac{1}{t^2 - \mathbf{u}^2 + i\tau}, \quad (\text{C.10a})$$

$$\beta_1 = - \int_u \frac{\Theta(1 - |\mathbf{s} + \mathbf{u}|) + \Theta(1 - |\mathbf{s} - \mathbf{u}|)}{t^2 - \mathbf{u}^2 + i\tau}, \quad (\text{C.10b})$$

$$\beta_2 = - \int_u 2i\pi\delta(t^2 - \mathbf{u}^2)\Theta(1 - |\mathbf{s} + \mathbf{u}|)\Theta(1 - |\mathbf{s} - \mathbf{u}|), \quad (\text{C.10c})$$

$$\begin{aligned} \beta_{pp} &= + \int_u \frac{\Theta(|\mathbf{s} - \mathbf{u}| - 1)\Theta(|\mathbf{s} - \mathbf{u}| - 1)}{t^2 - \mathbf{u}^2 + i\tau} \\ &= \beta_0 - \int_u \frac{\Theta(1 - |\mathbf{s} - \mathbf{u}| - 1)\Theta(|\mathbf{s} - \mathbf{u}| - 1)}{t^2 - \mathbf{u}^2 + i\tau}, \end{aligned} \quad (\text{C.10d})$$

$$\delta\beta_0 = 0, \quad (\text{C.11a})$$

$$\delta\beta_1 = - \frac{1}{2\pi^2} \int_u \frac{\bar{\delta}(\mathbf{s} + \mathbf{u} - \mathbf{p}) + \bar{\delta}(\mathbf{s} - \mathbf{u} - \mathbf{p})}{t^2 - \mathbf{u}^2 + i\tau} = - \frac{1}{\pi^2} \frac{1}{t^2 - (\mathbf{s} - \mathbf{p})^2 + i\tau}, \quad (\text{C.11b})$$

$$\begin{aligned}
 \delta\beta_2 &= \frac{1}{i\pi} \int_u \bar{\delta}(t^2 - \mathbf{u}^2) \bar{\delta}(\mathbf{s} - \mathbf{u} - \mathbf{p}) \Theta(1 - |\mathbf{s} + \mathbf{u}|) \\
 &\quad + \frac{1}{i\pi} \int_u \bar{\delta}(t^2 - \mathbf{u}^2) \bar{\delta}(\mathbf{s} + \mathbf{u} - \mathbf{p}) \Theta(1 - |\mathbf{s} - \mathbf{u}|) \\
 &= \frac{2}{i\pi} \bar{\delta}(t^2 - (\mathbf{s} - \mathbf{p})^2) \Theta(1 - |2\mathbf{s} - \mathbf{p}|), \tag{C.11c}
 \end{aligned}$$

$$\delta\beta_{pp} = \frac{1}{\pi^2} \frac{1 - \Theta(1 - |2\mathbf{s} - \mathbf{p}|)}{t^2 - (\mathbf{s} - \mathbf{p})^2 + i\tau}, \tag{C.11d}$$

where we used the definition of the unperturbed occupation numbers in term of the Heaviside step function given by (2.4).

C.2

CALCULATION OF THE UNPERTURBED IN-MEDIUM LOOPS

In this section, we concentrate on the calculation of β_j which are the key quantities entering in the ladder resummation of the ground state energy.

COMBINED PARTICLE-PARTICLE AND HOLE-HOLE LOOPS

We observe that the bubble function β_0 corresponds to the vacuum scattering function regularized in appendix A. Using the minimal subtraction scheme to evaluate this integral, decomposed in real and imaginary part using the identity (2.37), we obtain:

$$\text{Re}\beta_0 = \mathcal{P} \int_u \frac{1}{t^2 - \mathbf{u}^2} = 0, \tag{C.12}$$

$$\text{Im}\beta_0 = -\pi \int_u \delta(t^2 - \mathbf{u}^2) = -\frac{it}{4\pi}. \tag{C.13}$$

We see in (2.52) that we only need the two contributions $\beta_0 + \beta_1 + \beta_2$ and $\beta_0 + \beta_1$ for the ladder resummation and β_{pp} in the case where we restrict the calculation to the particle-particle channel.

Using (C.6), we have:

$$\text{Re}[\beta_0 + \beta_1 + \beta_2] = \text{Re}\beta_1 = \frac{R(s, t)}{4\pi^2}, \tag{C.14a}$$

$$\text{Im}[\beta_0 + \beta_1 + \beta_2] = -\frac{I(s, t)}{4\pi}, \tag{C.14b}$$

and, estimating β_2 only, we obtain:

$$\begin{aligned}
 \frac{\beta_2}{2i} &= -\text{Im}[\beta_0 + \beta_1 + \beta_2] \Theta(1 - s^2 - t^2), \\
 &= \frac{I(s, t)}{4\pi} \Theta(1 - s^2 - t^2) = \frac{I_*(s, t)}{4\pi}, \tag{C.14c}
 \end{aligned}$$

where we have defined:

$$R(s, t) \equiv 2 + t \ln \left| \frac{(t-1)^2 - s^2}{(t+1)^2 - s^2} \right| + \frac{1 - s^2 - t^2}{2s} \ln \left| \frac{(s+1)^2 - t^2}{(s-1)^2 - t^2} \right|, \quad (\text{C.14d})$$

$$\begin{aligned} I(s, t) &\equiv \left[t \Theta(1 - s - t) + I'(s, t) \Theta(s + t - 1) \right] \Theta(1 - s^2 - t^2) \\ &\quad + \left[t \Theta(t - s - 1) + I'(s, t) \Theta(s^2 + t^2 - 1) \right] \Theta(1 - s) \\ &\quad + \left[t \Theta(s - 1 - t) + t \Theta(1 + s - t) + I'(s, t) \Theta(t^2 - (s - 1)^2) \right] \Theta(s - 1) \\ &= \min \{t; I'(s, t)\}, \end{aligned} \quad (\text{C.14e})$$

with

$$I'(s, t) = \left| \frac{1 - s^2 - t^2}{2s} \right|.$$

Finally, putting all together, we have:

$$\beta_0 + \beta_1 + \beta_2 = \frac{1}{4\pi^2} \{R(s, t) - i\pi I(s, t)\}, \quad (\text{C.14f})$$

$$\beta_0 + \beta_1 = \frac{1}{4\pi^2} \left\{ R(s, t) - i\pi I(s, t) [1 - 2\Theta(1 - s^2 - t^2)] \right\}. \quad (\text{C.14g})$$

PARTICLE-PARTICLE LOOP

In the case we restrict to the particle-particle channel, we have:

$$\text{Re } \beta_{pp} = \frac{1}{4\pi^2} \{F(s, t) + \Theta(s - 1)F(-s, t)\}, \quad (\text{C.15a})$$

$$\text{Im } \beta_{pp} = \frac{1}{4\pi} I(s, t) [\Theta(1 - s^2 - t^2) - 1], \quad (\text{C.15b})$$

where we have defined:

$$F(s, t) \equiv 1 + s + t \ln \left| \frac{1 + s - t}{1 + s + t} \right| + \frac{1 - s^2 - t^2}{2s} \ln \left| \frac{(1 + s)^2 - t^2}{1 - s^2 - t^2} \right|. \quad (\text{C.15c})$$

Note the relationships $R(s, t) = F(s, t) + F(-s, t)$.

C.3

CALCULATION OF THE LEADING ORDER OF THE PERTURBED IN-MEDIUM LOOPS

In this section, we concentrate on the calculation of the angle average, defined by (C.9), of the functions $\delta\beta_j$ that are given by (C.11). The practical interest to introduce formally the angle average are that (i) it simplifies the expression of the resummed form of the self-energy, and (ii) it allows to write the resummed self-energy as an integral on the phase-space similar to the one appearing in the resummed ground state energy.

Again, we see in (2.52) that we only need the contribution $\delta\beta_0 + \delta\beta_1 + \delta\beta_2$, $\delta\beta_0 + \delta\beta_1$, and $\delta\beta_2$ for the ladder resummation and $\delta\beta_{pp}$ if we restrict the calculation to the particle-particle channel.

COMBINED PARTICLE-PARTICLE AND HOLE-HOLE LOOPS

Using (C.6), the angle average defined by (C.9) of the functions (C.11) are:

$$\text{Re} \left[\widehat{\delta\beta_0} + \widehat{\delta\beta_1} + \widehat{\delta\beta_2} \right] = \text{Re} \widehat{\delta\beta_1} = \frac{\widehat{R}(s, t, p)}{4\pi^2}, \quad (\text{C.16a})$$

$$\text{Im} \left[\widehat{\delta\beta_0} + \widehat{\delta\beta_1} + \widehat{\delta\beta_2} \right] = -\frac{\widehat{I}(s, t, p)}{4\pi}, \quad (\text{C.16b})$$

and, estimating β_2 only, we obtain:

$$\begin{aligned} \frac{\widehat{\delta\beta_2}}{2i} &= -\text{Im} \left[\widehat{\delta\beta} \right] \Theta \left(\frac{1+p^2}{2} - s^2 - t^2 \right) = \frac{\widehat{I}_*(s, t, p)}{4\pi}, \\ &= \frac{1}{sx} \Theta(s+t-p) \Theta(p-|s-t|) \Theta \left(\frac{1+p^2}{2} - s^2 - t^2 \right), \end{aligned} \quad (\text{C.16c})$$

where we have defined:

$$\widehat{R}(s, t, p) \equiv \frac{1}{sp} \ln \left| \frac{t^2 - (s+p)^2}{t^2 - (s-p)^2} \right|, \quad (\text{C.16d})$$

$$\widehat{I}(s, t, p) \equiv \frac{1}{sx} \Theta(s+t-p) \Theta(p-|s-t|) \text{sign} \left(\frac{1+p^2}{2} - s^2 - t^2 \right). \quad (\text{C.16e})$$

Finally, putting all together, we have:

$$\widehat{\delta\beta_0} + \widehat{\delta\beta_1} + \widehat{\delta\beta_2} = \frac{1}{4\pi^2} \left\{ \widehat{R}(s, t, p) - i\pi \widehat{I}(s, t, p) \right\}, \quad (\text{C.16f})$$

$$\widehat{\delta\beta_0} + \widehat{\delta\beta_1} = \frac{1}{4\pi^2} \left\{ \widehat{R}(s, t, p) - i\pi \widehat{I}(s, t, p) \left[1 - 2\Theta \left(\frac{1+p^2}{2} - s^2 - t^2 \right) \right] \right\}. \quad (\text{C.16g})$$

PARTICLE-PARTICLE LOOP

For the restriction to the particle-particle channel, we have similarly:

$$\text{Re} \widehat{\delta\beta_{pp}} = \frac{\widehat{F}(s, t, p)}{4\pi^2}, \quad (\text{C.17a})$$

$$\text{Im} \widehat{\delta\beta_{pp}} = \frac{1}{4\pi} \left[\widehat{I}_*(s, t, p) - \widehat{I}(s, t, p) \right], \quad (\text{C.17b})$$

where we have defined:

$$\begin{aligned} \widehat{F}(s, t, p) &= \frac{\Theta(1-p)}{sp} \left\{ \Theta(2s-1) \Theta(2s-1-p) \ln \left| \frac{(s+p)^2 - t^2}{(s-p)^2 - t^2} \right| \right. \\ &\quad \left. + \Theta(p-|2s-1|) \ln \left| \frac{(s+p)^2 - t^2}{(1+p^2)/2 - s^2 - t^2} \right| \right\} \\ &\quad + \frac{\Theta(p-1)}{sp} \left\{ \Theta(p-2s-1) \ln \left| \frac{(s+p)^2 - t^2}{(s-p)^2 - t^2} \right| \right. \\ &\quad \left. + \Theta(2s+1-p) \ln \left| \frac{(s+p)^2 - t^2}{(1+p^2)/2 - s^2 - t^2} \right| \right\}. \end{aligned} \quad (\text{C.17c})$$

USEFUL RELATIONSHIPS BETWEEN THE LOOP FUNCTIONS

Below we list analytical relations between the functions appearing above that will be useful.

$$\widehat{R}(s, t, p = 0) = \frac{4}{s^2 - t^2}, \quad (\text{C.18a})$$

$$\widehat{F}(s, t, p = 0) = \frac{4}{s^2 - t^2} \Theta(2s - 1), \quad (\text{C.18b})$$

$$\widehat{I}(s, t, p = 0) = \frac{2}{s} \delta(s - t) \text{sgn}(1 - 2s), \quad (\text{C.18c})$$

$$\widehat{I}_*(s, t, p = 0) = \frac{2}{s} \delta(s - t) \Theta(1 - 2s), \quad (\text{C.18d})$$

$$\int_0^1 p^2 dp \widehat{R}(s, t, p) = R(s, t), \quad (\text{C.19a})$$

$$\int_0^1 p^2 dp \widehat{F}(s, t, p) = F(s, t) - F(-s, t), \quad (\text{C.19b})$$

$$\int_0^1 p^2 dp \widehat{I}_*(s, t, p) = 2\widehat{I}_*(s, t), \quad (\text{C.19c})$$

$$\frac{\partial}{\partial k_F} \{k_F R(s, t)\} = \frac{1}{s} \ln \left| \frac{(s+1)^2 - t^2}{(s-1)^2 - t^2} \right| = \widehat{R}(s, t, 1), \quad (\text{C.20a})$$

$$\frac{\partial}{\partial k_F} \{k_F F(s, t)\} = \frac{1}{s} \ln \left| \frac{(s+1)^2 - t^2}{1 - s^2 - t^2} \right| = \widehat{F}(s, t, 1), \quad (\text{C.20b})$$

$$\frac{\partial}{\partial k_F} \{k_F I(s, t)\} = \frac{1}{s} \Theta(s + t - 1) = \widehat{I}_*(s, t, 1). \quad (\text{C.20c})$$

C.4

ENERGY RESUMMATION

Starting from the resummed energy (2.53) [respectively (2.30)] where the resummed effective interaction Γ is given by (2.52) [respectively (2.31)] in term of the β_j calculated in section C.2, we see that the integration on the accessible phase-space (s, t) is restricted to the domain $1 - s^2 - t^2 \geq 0$ due to the appearance of $\theta_s^-(t) = n_1 n_2$. Actually, using the definition of the unperturbed occupation numbers (2.4) in term of the Heaviside step function and the definition of the dimensionless variables defined by (2.19), the conditions $k_1 \leq k_F$ and $k_2 \leq k_F$ lead to:

$$\frac{k_1^2 + k_2^2}{2} \leq k_F^2 \quad \longmapsto \quad \frac{1}{2}(s+t)^2 + \frac{1}{2}(s-t)^2 = s^2 + t^2 \leq 1. \quad (\text{C.21})$$

Then, we can simplify the expressions of the loop functions calculated above as:

$$\beta_0 + \beta_1 + \beta_2 = \frac{1}{4\pi^2} \{R(s, t) - i\pi I_*(s, t)\}, \quad (\text{C.22})$$

$$\beta_0 + \beta_1 = \frac{1}{4\pi^2} \{R(s, t) + i\pi I_*(s, t)\}, \quad (\text{C.23})$$

and

$$\operatorname{Re} \beta_{pp} = \frac{F(s, t)}{4\pi^2}, \quad (\text{C.24})$$

$$\operatorname{Im} \beta_{pp} = 0. \quad (\text{C.25})$$

c.4.A Full ladder resummation

Finally, putting all together, the resummed ground state energy coming from the full ladder resummation (2.53) is given by:

$$E = E_{FG} + 4g(g-1) \frac{k_F^6}{4\pi^4} \int_0^1 s^2 ds \int_0^{\sqrt{1-s^2}} t dt I_*(s, t) C_0 B_2^{-1} \operatorname{Ln} \left[\frac{1 - B_0 - B_1 - B_2}{1 - B_0 - B_1} \right] \quad (\text{C.26})$$

$$= E_{FG} + E_{FG}(g-1) \frac{80}{\pi} \int_0^1 s^2 ds \int_0^{\sqrt{1-s^2}} t dt \frac{1}{2i} \operatorname{Ln} \left[\frac{1 - (a_s k_F / \pi)(R - i\pi I_*)}{1 - (a_s k_F / \pi)(R + i\pi I_*)} \right], \quad (\text{C.27})$$

where we used the relationships (2.32) and (C.14c), the definition of the coupling constant C_0 in terms of the s -wave scattering length (1.7), and the definition of the Free Fermi gas energy (2.10). Then, using the relationship between the complex logarithm and the arctangent functions for an arbitrary complex number z :

$$\arctan z = \frac{1}{2i} \operatorname{Ln} \left[\frac{1 + iz}{1 - iz} \right], \quad (\text{C.28})$$

we obtain¹:

$$\frac{E}{E_{FG}} = 1 + (g-1) \frac{80}{\pi} \int_0^1 s^2 ds \int_0^{\sqrt{1-s^2}} t dt \arctan \frac{(a_s k_F) \pi I_*(s, t)}{\pi - (a_s k_F) R(s, t)}. \quad (\text{C.29})$$

c.4.B Restricted particle-particle ladder resummation

Similarly, the resummed ground state energy coming from the restricted particle-particle ladder resummation (2.30), is given by:

$$\frac{E}{E_{FG}} = 1 + (g-1) \frac{80}{\pi} \int_0^1 s^2 ds \int_0^{\sqrt{1-s^2}} t dt \frac{(a_s k_F) \pi I_*(s, t)}{\pi - (a_s k_F) F(s, t)}, \quad (\text{C.30})$$

where we have used the relationship (2.32).

¹ In that case:

$$z = \frac{(a_s k_F) \pi I_*}{\pi - (a_s k_F) R}.$$

C.5

SELF-ENERGY RESUMMATION

We concentrate in this section on the calculation of the resummed self-energy using the test-particle insertion method described in section 4.3 starting from the resummed ground state energy obtained above. Using the definition of the effective interaction Γ given by (2.52) [or (2.31)] in terms of the perturbed occupation numbers given by (4.31), the self-energy is given by (4.42) where an external and an internal contribution appear.

C.5.A Full ladder resummation

We first determine the effective interaction (2.52), where the occupation number are given by (4.31) at linear order in η . Using the notation introduced in subsection C.1.d, we have:

$$\begin{aligned}\Gamma(\eta) &= C_0 B_2^{-1} \text{Ln} \left[\frac{1 - B_0 - B_1 - B_2}{1 - B_0 - B_1} \right] \\ &= \frac{1}{mk_F} (\beta_2 + \tilde{\eta} \delta\beta_2)^{-1} \text{Ln} \left[\frac{\pi - 4\pi^2 (a_s k_F) (\beta + \tilde{\eta} \widehat{\delta\beta})}{\pi - 4\pi^2 (a_s k_F) (\beta' + \tilde{\eta} \widehat{\delta\beta}')} \right].\end{aligned}\quad (\text{C.31})$$

Now, we expand up to second order in $\tilde{\eta}$ the complex logarithm:

$$\text{Ln} \left[\frac{\pi - 4\pi^2 (a_s k_F) (\beta + \tilde{\eta} \widehat{\delta\beta})}{\pi - 4\pi^2 (a_s k_F) (\beta' + \tilde{\eta} \widehat{\delta\beta}')} \right] = \gamma_0 + \tilde{\eta} (\gamma_{-1} + \gamma_1) + \tilde{\eta}^2 \gamma_2 + \mathcal{O}(\tilde{\eta}^3), \quad (\text{C.32a})$$

with:

$$\gamma_{-1} = -i\pi \widehat{R} \delta \left(\frac{\pi}{a_s k_F} - R \right), \quad (\text{C.32b})$$

$$\gamma_0 = \text{Ln} \left[\frac{\pi - 4\pi^2 (a_s k_F) \beta}{\pi - 4\pi^2 (a_s k_F) \beta'} \right], \quad (\text{C.32c})$$

$$\gamma_1 = \frac{4\pi^2 (a_s k_F) \widehat{\delta\beta}'}{\pi - 4\pi^2 (a_s k_F) \beta'} - \frac{4\pi^2 (a_s k_F) \widehat{\delta\beta}}{\pi - 4\pi^2 (a_s k_F) \beta'} \quad (\text{C.32d})$$

$$\gamma_2 = \frac{1}{2} \left\{ \frac{(4\pi^2)^2 (a_s k_F)^2 \widehat{\delta\beta}'^2}{[\pi - 4\pi^2 (a_s k_F) \beta']^2} - \frac{(4\pi^2)^2 (a_s k_F)^2 \widehat{\delta\beta}^2}{[\pi - 4\pi^2 (a_s k_F) \beta]^2} \right\}. \quad (\text{C.32e})$$

Remark: Occurrence of the γ_{-1} term.

In this remark, we make a careful reasoning on the derivative according to $\tilde{\eta}$ of the complex logarithm leading to a subtle δ contribution noted γ_{-1} . This point is also discussed in [240]. Defining a complex number by $z = |z|e^{i\arg z} = re^{i\theta} = x + iy$, the numbers r, θ, x, y are real and $\arg z = \theta$ is the principal value of the argument θ . The complex logarithm is defined as:

$$\text{Ln} z = \ln |z| + i \arg z = \ln r + i\theta = \ln \sqrt{x^2 + y^2} + i \arctan(y, x),$$

and the function $\arctan(y, x)$ as:

$$\arctan(y, x) = \frac{\pi}{2} \text{sign}(y) - \arctan \frac{x}{y}.$$

In the present case, the argument of the complex logarithm (C.32a) can be written as:

$$\text{Ln} \left[\frac{\pi - 4\pi^2(a_s k_F)(\beta + \tilde{\eta} \widehat{\delta\beta})}{\pi - 4\pi^2(a_s k_F)(\beta' + \tilde{\eta} \widehat{\delta\beta}')} \right] = \text{Ln} \left[\frac{1 + iz_1}{1 + iz_2} \right] = \text{Ln} z,$$

where, defining $h_p = 1 - 2\Theta(1 + p^2 - 2s^2 - 2t^2)$ [in particular $h_1 = 1 - 2\Theta(1 - s^2 - t^2)$], z_1 and z_2 are given by:

$$z_1 = \frac{\pi(a_s k_F)[I + \tilde{\eta} \widehat{I}]}{\pi - (a_s k_F)[R + \tilde{\eta} \widehat{R}]} \quad \text{and} \quad z_2 = \frac{\pi(a_s k_F)[Ih_1 + \tilde{\eta} \widehat{I}h_p]}{\pi - (a_s k_F)[R + \tilde{\eta} \widehat{R}]}.$$

Then, the real and imaginary parts of z are respectively:

$$x = \frac{1 + z_1 z_2}{1 + z_2^2} \quad \text{and} \quad y = \frac{z_1 - z_2}{1 + z_2^2}.$$

Explicitly, we have:

$$1 + z_1 z_2 = 1 + \left[\frac{\pi(a_s k_F)}{\pi - (a_s k_F)[R + \tilde{\eta} \widehat{R}]} \right]^2 [I + \tilde{\eta} \widehat{I}] \times [Ih_1 + \tilde{\eta} \widehat{I}h_p],$$

$$z_1 - z_2 = \frac{\pi(a_s k_F)}{\pi - (a_s k_F)[R + \tilde{\eta} \widehat{R}]} [I(1 - h_1) + \tilde{\eta} \widehat{I}(1 - h_p)].$$

Finally, using $\text{sign}(y) = 2\Theta(y) - 1$, we obtain:

$$\text{Ln} z = \ln |z| + i \arctan(y, x) = \ln |z| - i \arctan \frac{x}{y} + \frac{i\pi}{2} [2\Theta(y) - 1],$$

with:

$$\begin{aligned} i\pi\Theta(y) &= i\pi\Theta \left(\frac{\pi(a_s k_F)[I(1 - h_1) + \tilde{\eta} \widehat{I}(1 - h_p)]}{\pi - (a_s k_F)[R + \tilde{\eta} \widehat{R}]} \right) \\ &= i\pi\Theta \left((1 - h_1) \left\{ \frac{\pi}{a_s k_F} - [R + \tilde{\eta} \widehat{R}] \right\} \right) \\ &= i\pi\Theta \left((1 - h_1) \left\{ \frac{\pi}{a_s k_F} - R \right\} \right) + \tilde{\eta} \gamma_1 + \mathcal{O}(\tilde{\eta}^2), \end{aligned}$$

where:

$$\gamma_{-1} = \left. \frac{\partial}{\partial \tilde{\eta}} \{i\pi\Theta(y)\} \right|_{\tilde{\eta}=0} = -2i\pi \widehat{R} \delta \left(\frac{\pi}{a_s k_F} - R \right) \Theta(1 - s^2 - t^2).$$

There is a constraint on this expansion up to second order in $\tilde{\eta}$ due to the fact that $\beta_2 = 0$ in the region $1 - s^2 - t^2 < 0$. To fulfill this constraint, we have to distinguish two cases.

- *Case $1 - s^2 - t^2 \geq 0$:* In that case, the effective interaction at linear order in $\tilde{\eta}$ is:

$$\Gamma(\eta) = \left[\gamma_0 + \tilde{\eta} \left((\gamma_{-1} + \gamma_1) - \frac{\delta\beta_2}{\beta_2} \gamma_0 \right) \right] \frac{\beta_2^{-1}}{mk_F}. \quad (\text{C.33})$$

- *Case 1* $1 - s^2 - t^2 < 0$: In that case, the effective interaction at linear order in $\tilde{\eta}$ is:

$$\Gamma(\eta) = \left[\frac{\gamma_0}{\tilde{\eta}} + (\gamma_{-1} + \gamma_1) + \tilde{\eta}\gamma_2 \right] \frac{\delta\beta_2^{-1}}{mk_F} = [(\gamma_{-1} + \gamma_1) + \tilde{\eta}\gamma_2] \frac{\delta\beta_2^{-1}}{mk_F}. \quad (\text{C.34})$$

We remark that, using (C.14f) and (C.14g), in this region of the phase space, $\beta = \beta'$ and consequently $\gamma_0 = 0$.

Putting all together, at linear order in $\tilde{\eta}$, the effective interaction can be written as:

$$\Gamma(\eta) = \Gamma + \tilde{\eta} \widehat{\delta\Gamma} + \mathcal{O}(\tilde{\eta})^2, \quad (\text{C.35a})$$

where:

$$\Gamma = \Theta(1 - s^2 - t^2) \frac{\gamma_0}{mk_F} \beta_2^{-1} + \Theta(s^2 + t^2 - 1) \frac{(\gamma_{-1} + \gamma_1) \delta\beta_2^{-1}}{mk_F}, \quad (\text{C.35b})$$

$$\widehat{\delta\Gamma} = \Theta(1 - s^2 - t^2) \left((\gamma_{-1} + \gamma_1) - \frac{\delta\beta_2}{\beta_2} \gamma_0 \right) \frac{\beta_2^{-1}}{mk_F} + \Theta(s^2 + t^2 - 1) \frac{\gamma_2 \delta\beta_2^{-1}}{mk_F}. \quad (\text{C.35c})$$

Finally, using (4.42), the definition of the perturbed occupation number (4.31), the resummed self-energy is given by:

$$\Sigma^*(k) = (g - 1) \frac{2k_F^3}{\pi^2} \int s^2 ds \int t dt \left[\widehat{I}_*(s, t, p) \Gamma + I_*(s, t) \widehat{\delta\Gamma} \right], \quad (\text{C.36})$$

where the terms $\widehat{I}_* \Gamma$ and $I_* \widehat{\delta\Gamma}$ correspond respectively to the external and internal contributions. To obtain this result, we have used the following relationships valid for an arbitrary function $f(s, t, p)$:

$$\int_{k_1, k_2} [\delta n_1(\mathbf{k}) n_2 + n_1 \delta n_2(\mathbf{k})] f(s, t, p) = \frac{\eta}{g} \frac{4k_F^3}{\pi^2} \int s^2 ds \int t dt \widehat{I}_*(s, t, p) f(s, t, p), \quad (\text{C.37a})$$

$$\int_{k_1, k_2} n_1 n_2 f(s, t, p) = \frac{2k_F^6}{\pi^4} \int s^2 ds \int t dt I_*(s, t) f(s, t, p). \quad (\text{C.37b})$$

BOUNDARY OF INTEGRAL ON THE ACCESSIBLE PHASE-SPACE

To obtain the correct boundaries of the phase-space integral (C.36) and obtain an explicit result in term of the loop functions introduced in this appendix, we distinguish two cases discriminated by the definition of the following functions:

$$\widehat{I}_*(s, t, p) \propto \Theta \left(\frac{1 + p^2}{2} - s^2 - t^2 \right) \quad \text{and} \quad I_*(s, t) \propto \Theta(1 - s^2 - t^2)$$

- *Case $p \leq 1$* : In that case, the integrals appearing in (C.36) can be reduced to:

$$\int_0^1 s^2 ds \int_0^{\sqrt{1-s^2}} t dt \dots \quad (\text{C.38a})$$

- *Case $p > 1$* : In that case, the integrals appearing in (C.36) can be reduced to:

$$\int_0^{(1+p)/2} s^2 ds \int_0^{(1+p)/2} t dt \dots \quad (\text{C.38b})$$

Note that this is done here for a practical reason, namely to estimate numerically the resummed self-energy at various $(a_s k_F)$, since the conditions:

$$0 \leq s < \frac{1+p}{2} \quad \text{and} \quad 0 \leq t < \frac{1+p}{2},$$

are sufficient to ensure:

$$s^2 + t^2 < \frac{1+p^2}{2} \leq \left(\frac{1+p}{2}\right)^2 + \left(\frac{1+p}{2}\right)^2 = \frac{1+p^2}{2} + p,$$

restricting the integration on the relevant phase-space encoded by $\hat{I}_*(s, t, p)$ in a finite region in the (s, t) plane.

EXPLICIT RESUMMED SELF-ENERGY IN TERM OF THE LOOP FUNCTIONS

We first rewrite explicitly the integrand of (C.36) in terms of the loop function obtained above:

- *Case $1 - s^2 - t^2 \geq 0$* .

$$\begin{aligned} mk_F \left[\hat{I}_* \Gamma + I_* \widehat{\delta \Gamma} \right] &= \hat{I}_* \beta_2^{-1} \gamma_0 + I_* \left((\gamma_{-1} + \gamma_1) - \frac{\delta \beta_2}{\beta_2} \gamma_0 \right) \beta_2^{-1} \\ &= \frac{4\pi \gamma_0 \hat{I}_*}{2i I_*} + \frac{4\pi}{2i} \left((\gamma_{-1} + \gamma_1) - \frac{\hat{I}_*}{I_*} \gamma_0 \right) \\ &= \frac{4\pi}{2i} (\gamma_{-1} + \gamma_1) = -2i\pi (\gamma_{-1} + \gamma_1), \end{aligned} \quad (\text{C.39})$$

where we remark that the two contributions in γ_0 cancel each others.

- *Case $1 - s^2 - t^2 < 0$* .

$$\begin{aligned} mk_F \left[\hat{I}_* \Gamma + I_* \widehat{\delta \Gamma} \right] &= \hat{I}_* (\gamma_{-1} + \gamma_1) \delta \beta_2^{-1} + I_* \gamma_2 \delta \beta_2^{-1} \\ &= \left[\hat{I}_* (\gamma_{-1} + \gamma_1) + I_* \gamma_2 \right] \delta \beta_2^{-1} \\ &= \frac{4\pi}{2i} (\gamma_{-1} + \gamma_1) = -2i\pi (\gamma_{-1} + \gamma_1), \end{aligned} \quad (\text{C.40})$$

where we have used the fact that the function $I_* \propto \Theta(1 - s^2 - t^2)$ vanishes in this region.

We remark that, in the two regions, the integrand of the self-energy (C.36) depends on γ_1 defined in (C.32) which can be rewritten in term of the loop functions as:

$$\begin{aligned}\gamma_1 &= \frac{(a_s k_F)[\widehat{R} - i\pi(\widehat{I} - 2\widehat{I}_*)]}{\pi - (a_s k_F)[R - i\pi(I - 2I_*)]} - \frac{(a_s k_F)[\widehat{R} - i\pi\widehat{I}]}{\pi - (a_s k_F)[R - i\pi I]} \\ &= \frac{(a_s k_F)[\widehat{R} - i\pi(\widehat{I} - 2\widehat{I}_*)][\pi - (a_s k_F)[R + i\pi(I - 2I_*)]]}{[\pi - (a_s k_F)R]^2 + [(a_s k_F)\pi I]^2} \\ &\quad - \frac{(a_s k_F)[\widehat{R} - i\pi\widehat{I}][\pi - (a_s k_F)[R + i\pi I]]}{[\pi - (a_s k_F)R]^2 + [(a_s k_F)\pi I]^2},\end{aligned}\tag{C.41}$$

where we have used the properties $(I - 2I_*)^2 = I^2$ in the two regions of the phase-space $1 - s^2 - t^2 \geq 0$ and $1 - s^2 - t^2 > 0$. Then, we discriminate the real and imaginary contributions of γ_1 :

$$\operatorname{Re} \left[\frac{\gamma_1}{2i\pi} \right] = \frac{(a_s k_F)\widehat{I}_*[\pi - (a_s k_F)R] + (a_s k_F)^2 \widehat{R}I_*}{[\pi - (a_s k_F)R]^2 + [(a_s k_F)\pi I]^2},\tag{C.42a}$$

$$\operatorname{Im} \left[\frac{\gamma_1}{2i\pi} \right] = \frac{\pi(a_s k_F)^2 [2\widehat{I}_*I_* - (\widehat{I}I_* + \widehat{I}_*I)]}{[\pi - (a_s k_F)R]^2 + [(a_s k_F)\pi I]^2}.\tag{C.42b}$$

Note that [see (C.32b)], we have:

$$\frac{\gamma_{-1}}{2i\pi} = \operatorname{Re} \left[\frac{\gamma_{-1}}{2i\pi} \right] = -\widehat{R}\delta \left(\frac{\pi}{a_s k_F} - R \right) \Theta(1 - s^2 - t^2).\tag{C.42c}$$

Finally, we obtain:

$$\begin{aligned}\operatorname{Re} \Sigma^*(k) = U(k) &= (g - 1) \frac{2k_F^3}{\pi^2} \int s^2 ds \int t dt \operatorname{Re} \left[\widehat{I}_*\Gamma + I_*\widehat{\delta}\Gamma \right] \\ &= (g - 1) \frac{2k_F^3}{\pi^2} \frac{(2\pi)^2}{mk_F} \int s^2 ds \int t dt \operatorname{Re} \left[\frac{\gamma_{-1} + \gamma_1}{2i\pi} \right] \\ &= (g - 1) \frac{8k_F^2}{m} \int s^2 ds \int t dt \frac{(a_s k_F)\widehat{I}_*[\pi - (a_s k_F)R] + (a_s k_F)^2 \widehat{R}I_*}{[\pi - (a_s k_F)R]^2 + [(a_s k_F)\pi I]^2} \\ &\quad - (g - 1) \frac{8k_F^2}{m} \int s^2 ds \int t dt \widehat{R}\delta \left(\frac{\pi}{a_s k_F} - R \right) \Theta(1 - s^2 - t^2),\end{aligned}\tag{C.43a}$$

$$\begin{aligned}\operatorname{Im} \Sigma^*(k) = W(k) &= (g - 1) \frac{2k_F^3}{\pi^2} \int s^2 ds \int t dt \operatorname{Im} \left[\widehat{I}_*\Gamma + I_*\widehat{\delta}\Gamma \right] \\ &= (g - 1) \frac{2k_F^3}{\pi^2} \frac{(2\pi)^2}{mk_F} \int s^2 ds \int t dt \operatorname{Im} \left[\frac{\gamma_{-1} + \gamma_1}{2i\pi} \right] \\ &= (g - 1) \frac{8k_F^2}{m} \int s^2 ds \int t dt \frac{\pi(a_s k_F)^2 [2\widehat{I}_*I_* - (\widehat{I}I_* + \widehat{I}_*I)]}{[\pi - (a_s k_F)R]^2 + [(a_s k_F)\pi I]^2}.\end{aligned}\tag{C.43b}$$

We remark that we can simplify the imaginary part considering the two possible cases:

- *Case $p \leq 1$* : In that case, the domain of integration of the phase-space variables (s, t) is given by (C.38), and using the definition of the loop functions we deduce:

$$[2\widehat{I}_* I_* - (\widehat{I} I_* + \widehat{I}_* I)] = [(2\widehat{I}_* - \widehat{I})\Theta(1 - s^2 - t^2) - \widehat{I}_*] I \quad (\text{C.44})$$

$$= [(2\widehat{I}_* - \widehat{I}) - \widehat{I}_*] I = [\widehat{I}_* - \widehat{I}] I. \quad (\text{C.45})$$

- *Case $p > 1$* : Similarly, we deduce:

$$[2\widehat{I}_* I_* - (\widehat{I} I_* + \widehat{I}_* I)] = (\widehat{I}_* - \widehat{I}) I_* - \widehat{I}_* I \Theta(s^2 + t^2 - 1) \quad (\text{C.46})$$

$$= -\widehat{I}_* I \Theta(s^2 + t^2 - 1). \quad (\text{C.47})$$

These expressions were first obtained in [240] with another convention for the sign of the scattering length (i.e. $a_s \rightleftharpoons -a_s$).

COMPACT EXPRESSIONS

Now, using the compact notations introduced in chapter 5 [see (5.2)], we obtain:

$$\begin{aligned} \mathcal{U} = \mathcal{U}' &= \frac{16(a_s k_F) \widehat{I}_* [\pi - (a_s k_F) R] + 16(a_s k_F)^2 \widehat{R} \widehat{I}_*}{[\pi - (a_s k_F) R]^2 + [(a_s k_F) \pi I]^2} \\ &\quad - 16\widehat{R} \delta \left(\frac{\pi}{a_s k_F} - R \right) \Theta(1 - s^2 - t^2), \end{aligned} \quad (\text{C.48a})$$

$$\mathcal{W} = \mathcal{W}' = \frac{16\pi(a_s k_F)^2 [2\widehat{I}_* I_* - (\widehat{I} I_* + \widehat{I}_* I)]}{[\pi - (a_s k_F) R]^2 + [(a_s k_F) \pi I]^2}. \quad (\text{C.48b})$$

c.5.B Restricted particle-particle ladder resummation

Similarly, for the resummation restricted to the particle-particle, we have:

$$\mathcal{U}_{pp} = \frac{16(a_s k_F) \widehat{I}_*}{\pi - (a_s k_F) F} + \frac{16(a_s k_F)^2 \widehat{F} \widehat{I}_*}{[\pi - (a_s k_F) F]^2}, \quad (\text{C.49a})$$

$$\mathcal{W}_{pp} = \frac{16\pi(a_s k_F)^2 [2\widehat{I}_* I_* - (\widehat{I} I_* + \widehat{I}_* I)]}{[\pi - (a_s k_F) F]^2}, \quad (\text{C.49b})$$

$$\begin{aligned} \mathcal{U}'_{pp} &= \frac{16(a_s k_F) \widehat{I}_* \Theta(1 - s^2 - t^2)}{\pi - (a_s k_F) F} + \frac{16(a_s k_F)^2 \widehat{F} \widehat{I}_*}{[\pi - (a_s k_F) F]^2} \\ &\quad + \frac{16(a_s k_F) \widehat{I}_* [\pi - (a_s k_F) F] \Theta(s^2 + t^2 - 1)}{[\pi - (a_s k_F) F]^2 + [(a_s k_F) \pi I]^2}, \end{aligned} \quad (\text{C.49c})$$

$$\mathcal{W}'_{pp} = \frac{16\pi(a_s k_F)^2 [2\widehat{I}_* I_* - (\widehat{I} I_* + \widehat{I}_* I)]}{[\pi - (a_s k_F) F]^2 + [(a_s k_F) \pi I]^2}. \quad (\text{C.49d})$$

D | EXTENSIONS OF THE LADDER RESUMMATION

CONTENTS

| | | |
|-----|---|----|
| D.1 | Ladder resummation of the ground-state energy including effective range | D2 |
| D.2 | Ladder resummation of the p -wave ground-state energy | D2 |

In this appendix, we give the final form of the ground-state energy obtained by summing up the ladder diagrams contribution starting from pionless potential (1.6). In particular:

1. the s -wave interaction $V = C_0 + C_2(\mathbf{k}^2 + \mathbf{k}'^2)$ including effective range which is discussed in section 3.3;
2. the leading-order contribution of the p -wave interaction $V = C'_2 \mathbf{k} \cdot \mathbf{k}'$.

Their detailed derivations can be found in [239] and, in this appendix, we only give the final results in term of $(a_s k_F)$, and $(r_s k_F)$, or $(a_p k_F)$.

D.1

LADDER RESUMMATION OF THE GROUND-STATE ENERGY INCLUDING EFFECTIVE RANGE

FULL LADDER RESUMMATION

The ground state energy for the full ladder resummation is given by:

$$\frac{E_s}{E_{FG}} = (g-1) \frac{80}{\pi} \int_0^1 s^2 ds \int_0^{\sqrt{1-s^2}} t dt \arctan \left[\frac{(a_s k_F) \pi I_*(s, t)}{\pi \phi^{-1} - (a_s k_F) R(s, t)} \right], \quad (\text{D.1a})$$

with:

$$\phi = \left[1 + \frac{a_s^2 r_s}{3\pi} k_F^3 \right]^{-2} \times \left\{ 1 + \frac{a_s r_s}{4} k_F^2 \left[2t^2 + \frac{a_s^2 r_s}{3\pi} k_F^3 \left(t^2 - s^2 - \frac{3}{5} \right) \right] \right\}, \quad (\text{D.1b})$$

and where the functions R and I_* are defined in appendix C by (C.14d) and (C.14e) respectively.

RESTRICTED PARTICLE-PARTICLE LADDER CHANNEL

When the resummation is restricted to the particle-particle ladder channel, we have:

$$\frac{E_s}{E_{FG}} = (g-1) \frac{80}{\pi} \int_0^1 s^2 ds \int_0^{\sqrt{1-s^2}} t dt \frac{(a_s k_F) \pi I_*(s, t)}{\pi \psi^{-1} - (a_s k_F) F(s, t)}, \quad (\text{D.2a})$$

with:

$$\psi = \left[1 + \frac{a_s^2 r_s}{3\pi} k_F^3 \frac{(1+s)^2}{4} (2-s) \right]^{-2} \times \left\{ 1 - \frac{a_s r_s}{4} k_F^2 \left[2t^2 - \frac{a_s^2 r_s}{3\pi} k_F^3 \frac{(1+s)^2}{4} \left((2-s)t^2 + \frac{1+s}{5} (3s-6-s^2) \right) \right] \right\}, \quad (\text{D.2b})$$

and where the function F is defined in appendix C by (C.15c).

D.2

LADDER RESUMMATION OF THE p -WAVE GROUND-STATE ENERGY

We give here the formula for the ground state energy resumming the p -wave effect:

FULL LADDER RESUMMATION

$$\frac{E_p}{E_{FG}} = (g+1) \frac{80}{\pi} \int_0^1 s^2 ds \int_0^{\sqrt{1-s^2}} t dt \left\{ 2 \arctan \frac{(a_p k_F)^3 \pi I_{\perp}}{3\pi - (a_p k_F)^3 R_{\perp}} + \arctan \frac{(a_p k_F)^3 \pi I_{\parallel}}{3\pi - (a_p k_F)^3 R_{\parallel}} \right\}, \quad (\text{D.3a})$$

where:

$$\begin{aligned}
R_{\perp} &= \frac{2}{3} - \frac{s^2}{4} + 2t^2 + \frac{(1-t^2)^2}{4s^2} \\
&+ \frac{[(s+t)^2 - 1]^2}{16s^3} (s^2 + t^2 - 4st - 1) \ln \left| \frac{1+s+t}{1-s-t} \right| \\
&+ \frac{[(s-t)^2 - 1]^2}{16s^3} (s^2 + t^2 + 4st - 1) \ln \left| \frac{1+s-t}{1-s+t} \right|, \tag{D.3b}
\end{aligned}$$

$$\begin{aligned}
R_{\parallel} &= \frac{8}{3} + \frac{s^2}{2} + 2t^2 - \frac{(1-t^2)^2}{2s^2} + \left[\frac{(1-s^2-t^2)^3}{8s^3} - t^3 \right] \ln \left| \frac{1+s+t}{1-s-t} \right| \\
&+ \left[\frac{(1-s^2-t^2)^3}{8s^3} + t^3 \right] \ln \left| \frac{1+s-t}{1-s+t} \right|, \tag{D.3c}
\end{aligned}$$

$$I_{\perp} = t^3 \Theta(1-s-t) + \frac{1-s^2-t^2}{16s^3} \left[12s^2t^2 - (1-s^2-t^2)^2 \right] \Theta(s+t-1), \tag{D.3d}$$

$$I_{\parallel} = t^3 \Theta(1-s-t) + \frac{(1-s^2-t^2)^3}{8s^3} \Theta(s+t-1). \tag{D.3e}$$

RESTRICTED PARTICLE-PARTICLE LADDER CHANNEL

$$\begin{aligned}
\frac{E_p}{E_{FG}} &= (g+1) \frac{80}{\pi} \int_0^1 s^2 ds \int_0^{\sqrt{1-s^2}} t dt \\
&\left\{ \frac{2(a_p k_F)^3 I_{\perp}(s,t)}{3\pi - (a_p k_F)^3 F_{\perp}(s,t)} + \frac{(a_p k_F)^3 \pi I_{\parallel}(s,t)}{3\pi - (a_p k_F)^3 F_{\parallel}(s,t)} \right\}, \tag{D.4a}
\end{aligned}$$

where:

$$\begin{aligned}
F_{\perp} &= \frac{1}{3} + \frac{(1-t^2)^2}{8s^2} + t^2 - \frac{s^2}{8} - \frac{5s^3}{12} + \frac{s}{8}(6+7t^2) - \frac{t^2}{8s}(1-t^2) - t^3 \ln \frac{1+s+t}{1+s-t} \\
&+ \frac{1-s^2-t^2}{16s^3} \left[2s^2(1+5t^2) - s^4 - (1-t^2)^2 \right] \ln \frac{(1+s)^2 - t^2}{1-s^2-t^2}, \tag{D.4b}
\end{aligned}$$

$$\begin{aligned}
F_{\parallel} &= \frac{4}{3} - \frac{(1-t^2)^2}{4s^2} + t^2 + \frac{s^2}{4} - \frac{s^3}{6} + \frac{s}{4}(6+5t^2) + \frac{t^2}{4s}(1-t^2) \\
&- t^3 \ln \frac{1+s+t}{1+s-t} + \frac{(1-s^2-t^2)^3}{8s^3} \ln \frac{(1+s)^2 - t^2}{1-s^2-t^2}. \tag{D.4c}
\end{aligned}$$

E | PHASE-SPACE AVERAGE OF USED FUNCTIONS

CONTENTS

| | | |
|-----|---|--------------------|
| E.1 | Full phase-space average approximation | E1 |
| E.2 | Partial phase-space average approximation | E2 |

In this appendix, we list the useful phase-space and/or the partial phase-space average values of some functions using the notations defined by (3.7) and (5.2).

E.1

FULL PHASE-SPACE AVERAGE APPROXIMATION

We first recall the definition of the full phase-space approximation defined by (3.7) for an arbitrary function X :

$$\langle\langle X \rangle\rangle \equiv \int_0^1 s^2 ds \int_0^{\sqrt{1-s^2}} t dt X(s, t). \quad (\text{E.1})$$

Then, below, we list the full phase-space average value of some functions (defined in appendix B and C) used in the main document:

$$\langle\langle 1 \rangle\rangle = \frac{1}{15}, \quad (\text{E.2a})$$

$$\langle\langle I_* \rangle\rangle = \frac{1}{72}, \quad (\text{E.2b})$$

$$\langle\langle I_* R \rangle\rangle = \frac{1}{72} \times \frac{6}{35} (11 - 2 \ln 2), \quad (\text{E.2c})$$

$$\langle\langle I_* F \rangle\rangle = \frac{1}{72} \times \frac{6}{35} (11 - 2 \ln 2), \quad (\text{E.2d})$$

$$\langle\langle I_* t^2 \rangle\rangle = \frac{1}{72} \times \frac{3}{10}. \quad (\text{E.2e})$$

E.2

PARTIAL PHASE-SPACE AVERAGE APPROXIMATION

We first recall the definition of the partial phase-space approximation defined by (5.2) for an arbitrary function X :

$$\langle X \rangle_p^< \equiv \int_0^1 s^2 ds \int_0^{\sqrt{1-s^2}} t dt X(s, t, p), \quad (\text{E.3a})$$

$$\langle X \rangle_p^> \equiv \int_0^{(1+p)/2} s^2 ds \int_0^{(1+p)/2} t dt X(s, t, p), \quad (\text{E.3b})$$

Then, below, we list the partial phase-space average value of some functions (defined in appendix B and C) used in the main document.

FULL MOMENTUM DEPENDENCE

$$\langle 1 \rangle_p^< = \frac{1}{15}, \quad (\text{E.4a})$$

$$\langle 1 \rangle_p^> = \frac{(p^2 + 1)^{5/2}}{60\sqrt{2}} \xrightarrow{p \rightarrow 1} \frac{1}{15}, \quad (\text{E.4b})$$

$$\langle \hat{I}_* \rangle_p^< = \frac{1}{12}, \quad (\text{E.4c})$$

$$\langle \hat{I}_* \rangle_p^> = \frac{1}{12}, \quad (\text{E.4d})$$

$$\langle \hat{I}_* F + \hat{F} I_* \rangle_p^< = \frac{\pi^2}{16} \Phi_2(p < 1), \quad (\text{E.4e})$$

where Φ_2 is given by (B.22a).

AT FERMI SURFACE

$$\langle 1 \rangle_{p=1}^< = \frac{1}{15}, \quad (\text{E.5a})$$

$$\langle \hat{I}_* \rangle_{p=1}^< = \frac{1}{12}, \quad (\text{E.5b})$$

$$\langle \hat{I}_* F \rangle_{p=1}^< = \frac{1}{120} (15 - 2 \ln 2), \quad (\text{E.5c})$$

$$\langle \hat{F} I_* \rangle_{p=1}^< = \frac{1}{120} (7 - 2 \ln 2), \quad (\text{E.5d})$$

$$\left\langle \frac{\partial \hat{I}_*}{\partial p} \right\rangle_{p=1}^< = 0. \quad (\text{E.5e})$$

F | PARAMETRIZATION OF THE APPROXIMATE SELF-ENERGY

CONTENTS

| | | |
|-----|-------------------------------|----|
| F.1 | GPS parametrization | F2 |
| F.2 | APS parametrization | F3 |

In this appendix we give the explicit parametrization of the GPS/APS and GPS_X/APS_X single-particle potential (noted generically $U(k)$) obtained in chapter 5 and their associated chemical potential μ , effective mass m^* and self-energy shift at zero momentum ν as function of $(a_s k_F)$. We recall:

$$\frac{\mu}{\mu_{FG}} \equiv 1 + \frac{U(k_F)}{\varepsilon_{FG}}, \quad \frac{m}{m^*} \equiv 1 + \frac{m}{k_F} \left. \frac{\partial U}{\partial k} \right|_{k=k_F}, \quad \text{and} \quad \frac{\nu}{\varepsilon_{FG}} \equiv 1 + \frac{U(0)}{\varepsilon_{FG}}.$$

F.1

GPS PARAMETRIZATION

We recall the expression of GPS_X single particle potential given by (5.24):

$$\frac{U_{\text{GPS}_X}(k)}{\varepsilon_{FG}} = \frac{4}{3\pi} \frac{(a_s k_F)}{1 - (3\pi/4)\Phi_2(p)X(p)(a_s k_F)} + \frac{\Phi_2(p) [1 - X(p)] (a_s k_F)^2}{[1 - (3\pi/4)\Phi_2(p)X(p)(a_s k_F)]^2}. \quad (\text{F.1})$$

where Φ_2 is the Galitskii function given by (B.22a) and X an arbitrary function with the constraint $X(1) = 6/7$ imposed by the Hugenholtz-van-Hove theorem. Considering $X(p) = 6/7$ constant, we obtain the GPS single particle potential given by (5.25). The associated quasi-particle properties then read:

$$\frac{\mu}{\mu_{FG}} = 1 + P_\alpha^a(a_s k_F), \quad (\text{F.2a})$$

$$\frac{\nu}{\mu_{FG}} = 1 + P_\gamma^c(a_s k_F), \quad (\text{F.2b})$$

$$\frac{m}{m^*} = 1 + \{\beta Q_\alpha^a(a_s k_F) + b R_\alpha^a(a_s k_F)\}, \quad (\text{F.2c})$$

where we have introduced the notations:

$$P_\delta^d(a_s k_F) = \frac{4}{3\pi} F_\delta^d(a_s k_F)^2 \times \{A_\delta^d + (a_s k_F)^{-1}\}, \quad (\text{F.3a})$$

$$Q_\delta^d(a_s k_F) = \frac{4}{3\pi} \frac{7}{12} F_\delta^d(a_s k_F)^3 \{B_\delta^d + (a_s k_F)^{-1}\}, \quad (\text{F.3b})$$

$$R_\delta^d(a_s k_F) = \frac{4}{3\pi} \frac{7}{6} F_\delta^d(a_s k_F)^3 \times C_\delta^d, \quad (\text{F.3c})$$

$$F_\delta^d(a_s k_F) = \frac{a_s k_F}{1 - (7\delta d/6)a_s k_F}, \quad (\text{F.3d})$$

$$A_\delta^d = \frac{7}{6}\delta [1 - 2d],, \quad B_\delta^d = \frac{7}{6}\delta d [1 - 2d],, \quad \text{and} \quad C_\delta^d = \frac{7}{6}\delta^2(1 - d), \quad (\text{F.3e})$$

for $\delta = \{\alpha, \beta, \gamma\}$, $d = \{a, b, c\}$, with:

$$\alpha = \frac{9\pi}{14} \Phi_2(1) = \frac{6}{35\pi} (11 - 2 \ln 2), \quad (\text{F.4a})$$

$$\beta = \frac{9\pi}{14} \Phi_2'(1) = \frac{24}{35\pi} (1 - 7 \ln 2), \quad (\text{F.4b})$$

$$\gamma = \frac{9\pi}{14} \Phi_2(0) = \frac{18}{7\pi}, \quad (\text{F.4c})$$

$$a = X(1) = 6/7, \quad b = X'(1), \quad \text{and} \quad c = X(0). \quad (\text{F.4d})$$

Note that the quasi-particle properties associated to the GPS single-particle potential take the same form using $c = a = 6/7$ and $b = 0$.

F.2

APS PARAMETRIZATION

Similarly, the APS_X single particle potential given by (5.31) reads:

$$\frac{U_{\text{APS}_X}(k)}{\varepsilon_{FG}} = \frac{(2/9\pi)(a_s k_F)}{[1 - (9\pi/4)\Phi_2(p)X(p)(a_s k_F)]^2 + [(5/24)(a_s k_F)]^2} + \frac{16}{3\pi} \arctan \left(\frac{(5/24)(a_s k_F)}{1 - (9\pi/10)\Phi_2(p)[1 - X(p)](a_s k_F)} \right). \quad (\text{F.5})$$

where the constraint $X(1) = 2/7$ is now imposed by the Hugenholtz-van-Hove theorem and again considering $X(p) = 2/7$ constant, we obtain the APS single particle potential given by (5.30). The associated quasi-particle properties can be written as:

$$\frac{\mu}{\mu_{FG}} = 1 + \mathcal{S}_\alpha^a(a_s k_F) + \mathcal{P}_\alpha^a(a_s k_F), \quad (\text{F.6a})$$

$$\frac{\nu}{\mu_{FG}} = 1 + \mathcal{S}_\gamma^c(a_s k_F) + \mathcal{P}_\gamma^c(a_s k_F), \quad (\text{F.6b})$$

$$\frac{m}{m^*} = 1 + \beta \mathcal{Q}_\alpha^a(a_s k_F) + b \mathcal{R}_\alpha^a(a_s k_F), \quad (\text{F.6c})$$

where we have defined for $\delta = \{\alpha, \beta, \gamma\}$, $d = \{a, b, c\}$:

$$\mathcal{S}_\delta^d(a_s k_F) = \frac{16}{3\pi} \arctan \frac{5a_s k_F / 24}{1 - 7\delta(1-d)a_s k_F / 5}, \quad (\text{F.7a})$$

$$\mathcal{P}_\delta^d(a_s k_F) = \frac{2}{9\pi} (a_s k_F)^{-1} \mathcal{F}_\delta(d; a_s k_F), \quad (\text{F.7b})$$

$$\mathcal{Q}_\delta^d(a_s k_F) = \frac{7}{9\pi} \left[d \mathcal{H}_\delta^d(a_s k_F) + (1-d) \mathcal{G}_\delta^d(a_s k_F) \right], \quad (\text{F.7c})$$

$$\mathcal{R}_\delta^d(a_s k_F) = \frac{7}{9\pi} \left[\delta \mathcal{H}_\delta^d(a_s k_F) - \delta \mathcal{G}_\delta^d(a_s k_F) \right], \quad (\text{F.7d})$$

$$\mathcal{F}_\delta^d(a_s k_F) = \frac{(a_s k_F)^2}{[1 - 7a_s k_F \delta d / 2]^2 + [5a_s k_F / 24]^2}, \quad (\text{F.7e})$$

$$\mathcal{G}_\delta^d(a_s k_F) = \frac{(a_s k_F)^2}{[1 - 7a_s k_F \delta(1-d) / 5]^2 + [5a_s k_F / 24]^2}, \quad (\text{F.7f})$$

$$\mathcal{H}_\delta^d(a_s k_F) = \frac{(a_s k_F)^2 (1 - 7a_s k_F \delta d / 2)}{\left[(1 - 7a_s k_F \delta d / 2)^2 + (5a_s k_F / 24)^2 \right]^2}. \quad (\text{F.7g})$$

Note that the quasi-particle properties associated to the GPS single-particle potential take the same form using $c = a = 2/7$ and $b = 0$.

G

SUMMARY IN FRENCH RESUMÉ EN FRANÇAIS

Dans ce travail de thèse, des théories de type fonctionnelle de la densité sont développées pour des systèmes en interaction forte possédant une longueur de diffusion d'onde s , notée a_s , anormalement grande. Les gaz atomiques ou la matière neutronique sont des exemples physiques de tels systèmes. La théorie des perturbations à N -corps est tout d'abord utilisée pour décrire les systèmes de fermions dilués. Cette approche conduit par exemple à la fonctionnelle de Lee-Yang, qui est valide dans une plage de densité très restreinte, lorsque la longueur de diffusion en onde s devient grande. Pour étendre le domaine de validité de l'approche perturbative, des techniques de resommation associées à l'approximation dite en échelle sont utilisées. Cette approche conduit à des expressions compactes pour l'énergie et/ou la self-énergie on-shell dans des systèmes infinis pouvant être appliquées à des systèmes plus ou moins denses. Cela conduit également à une énergie finie du gaz atomique à la limite unitaire, i.e. lorsque $|a_s k_F| \rightarrow +\infty$. Les fonctionnelles ainsi déduites restent assez complexes et manquent en général de pouvoir prédictif. Pour simplifier ces fonctionnelles, des approximations appelées respectivement approximations de "l'espace des phases" ou de "l'espace des phases partiel" sont proposées pour l'énergie ou la self-énergie. Ces approximations simplifient non seulement la forme des fonctionnelles, mais améliorent également leur pouvoir prédictif tout en reproduisant correctement la limite de basse densité. Guidées par les techniques de resommation non-perturbatives développées dans cette thèse, plusieurs nouvelles fonctionnelles sont proposées ainsi que leurs extensions permettant d'inclure des effets de portée effective. Ces fonctionnelles non-empiriques, qui ne contiennent aucun paramètre libre, sont testées par rapport aux propriétés des systèmes d'atomes froids et/ou de la matière neutronique. Ces fonctionnelles reproduisent très bien les propriétés obtenues dans les calculs *ab-initio* ou observées expérimentalement dans les systèmes d'atomes froids. L'équation d'état de la matière neutronique est également reproduite jusqu'à $\rho = 0.01 \text{ fm}^{-3}$. La réponse statique de la matière neutronique, récemment calculée dans des théories *ab initio*, est également mieux reproduite par rapport aux fonctionnelles empiriques utilisées généralement en physique nucléaire. Cette étude a aussi mis en évidence la nécessité de mieux comprendre les propriétés des quasi-particules, telle que la masse effective. Pour progresser sur ce point, en partant des expressions resommées de la self-énergie et de l'approximation de l'espace des phases partiel, des expressions compactes du potentiel chimique et de la masse effective ont été obtenues ; ces expressions étant compatibles avec les fonctionnelles proposées dans la première partie de cette thèse. Ces expressions devraient élargir considérablement le domaine de validité des fonctionnelles non-empiriques par rapport aux théories perturbatives. Enfin, il est montré que les développements de ce travail sont également utiles pour réconcilier les paramètres généralement utilisés dans les fonctionnelles empiriques de la physique nucléaire avec les propriétés de l'interaction nucléaire forte.

INTRODUCTION

Le problème nucléaire à N -corps de basse énergie présente une richesse incroyable et une rare complexité. La question n'est pas tant de connaître les propriétés individuelles des nucléons, mais bien de comprendre comment ils s'organisent pour former ces systèmes complexes que sont les noyaux atomiques. Bien que les noyaux atomiques puissent être considérés comme un problème à N -corps standard, les spécificités du problème nucléaire les rendent complexes et encore loin d'être bien compris. Les difficultés rencontrées dans la description des systèmes nucléaires sont nombreuses ; et, parmi celles-ci, on peut citer la compréhension de l'interaction nucléaire structurant les noyaux atomiques et les interactions mutuelles entre noyaux, leur propriétés, y compris leur description à partir de la chromodynamique quantique (QCD).

Une autre difficulté provient du fait que les noyaux atomiques sont des systèmes mésoscopiques de fermions fortement corrélés où les effets de taille finie compliquent considérablement les méthodes à N -corps s'appuyant, directement ou non, sur l'interaction nucléaire nue. Malgré la complexité apparente du problème dans un contexte fondamental, des propriétés simples apparaissent dans les noyaux atomiques, de sorte que les propriétés nucléaires varient qualitativement de manière régulière le long de la carte des noyaux. Par exemple, l'énergie de liaison des noyaux peut être paramétrée avec très peu de paramètres (formule de la goutte liquide) pour une large gamme de noyaux ; leur taille présente également un comportement très lisse sous-tendant la propriété incompressible des systèmes nucléaires. Cette coexistence entre complexité et simplicité est illustrée par le fait que les noyaux peuvent être discutés très précisément avec des théories relativement simples dans lesquelles les systèmes ne sont décrits qu'en termes de densité de nucléons. De nos jours en physique nucléaire, la théorie microscopique la plus aboutie et prédictive considère la densité à un corps comme le principal degré de liberté permettant d'obtenir une description correcte des observations. Cette théorie est souvent appelée théorie fonctionnelle de la densité nucléaire (DFT nucléaire), théorie de l'énergie fonctionnelle de la densité nucléaire (EDF nucléaire), ou simplement DFT/EDF. Son pouvoir prédictif illustre le fossé entre la complexité intrinsèque qui organise les systèmes nucléaires et la simplicité avec laquelle des propriétés phénoménologiques peuvent être expliquées. Les questions naturelles qu'il est légitime de poser sont alors :

- (a) *Comment une telle simplicité peut-elle émerger ?*
- (b) *Pouvons-nous relier les DFT qui sont généralement ajustées empiriquement pour reproduire les propriétés globales des noyaux avec l'interaction nucléaire nue sous-jacente ?*

Il est à noter que le fait de répondre à la question (a) pourrait fournir des indications pour répondre à la question (b) et réciproquement.

Nous vivons actuellement une période charnière pour la physique nucléaire avec un renouvellement des idées et des concepts. L'une des raisons de ce renouveau dans ce domaine est le progrès récent des théories effectives des champs (EFT). Ces progrès ont amélioré notre compréhension de l'interaction nucléaire, qui est maintenant directement liés au secteur de basse énergie de la QCD. Une telle nouvelle génération d'interactions nucléaires s'avère simplifier les méthodes à N -corps. C'est pourquoi, parallèlement aux progrès de l'interaction nucléaire elle-même, les méthodes *ab initio* ont tiré parti de ces avancées. Malgré la puissance des méthodes *ab initio* et les améliorations exceptionnelles des techniques à N -corps, ces approches du problème à N -corps nucléaire ne permettent pas de décrire de manière

globale la richesse des phénomènes en jeu dans les systèmes nucléaires. Ils sont actuellement limités à la description des noyaux légers à moyens, en se concentrant principalement sur leurs propriétés statiques.

Même si l'approche DFT basée sur un ajustement empirique semblent avoir atteint ses limites en termes de pouvoir prédictif et d'applicabilité, elles restent les seules approches microscopiques capables de traiter dans un cadre simple et unifié la structure, la dynamique de petites et grandes amplitudes, ainsi que les propriétés thermodynamiques des systèmes nucléaires. Ces approches permettent également d'appréhender d'autres domaines à la frontière de la physique nucléaire et d'établir des liens avec l'astrophysique, la physique atomique, la matière condensée, etc. Récemment, un lien intéressant a été établi entre la physique nucléaire et la physique atomique. Plus spécifiquement, les systèmes atomiques proches de la limite unitaire ont suscité un intérêt particulier et croissant pour la physique nucléaire. En effet, ces systèmes, comme les systèmes neutroniques, présentent une longueur de diffusion en onde s anormalement grande. Ils ont été largement étudiés tant du point de vue théorique qu'expérimental au cours des dernières décennies et en particulier, contrairement aux noyaux, ils peuvent être manipulés en laboratoire avec une interaction ajustable. Cette flexibilité offre la possibilité de tester les idées et les approches dans un cadre simplifié et contrôlable par rapport aux noyaux.

Ces avancées ont suscité un regain d'intérêt pour relier les DFT à l'interaction nue sous-jacente avec le but ultime de répondre à la question (b). Le défi consiste à partir des aspects fondamentaux de l'interaction nucléaire et à les combiner à la polyvalence des approches DFT dans le but de rendre les DFT moins empiriques et d'accroître leur pouvoir prédictif. Dans ce contexte, cette thèse vise à contribuer à cet objectif commun. Ce travail se concentre sur la description de systèmes ayant une longueur de diffusion en onde s anormalement grande, comme c'est le cas dans la matière neutronique et/ou les gaz atomiques proches de l'unitarité. Plus précisément, l'objectif est de développer une DFT pour ces systèmes à partir de l'interaction. Ce problème est particulièrement complexe car il est hautement non-perturbatif. La stratégie utilisée dans cette thèse est de partir des techniques classiques à N -corps, d'abord dans un régime perturbatif, et de les étendre au régime non-perturbatif. Les développements de l'approche perturbative à non-perturbative nous serviront de guide robuste pour obtenir une DFT pour ces systèmes où les paramètres sont directement connectés aux constantes de basse énergie de l'interaction. La flexibilité de la méthodologie ainsi que la possibilité d'obtenir des propriétés importantes telles que la masse effective seront examinées.

La thèse présentée est organisée comme suit. Nous introduisons d'abord le contexte, les développements récents et les principaux concepts autour desquels est articulée cette thèse au chapitre 1. Une attention particulière est portée (i) sur l'interaction nucléaire elle-même et, en particulier, aux théories effectives des champs (EFT) chiraux, (ii) sur les méthodes *ab initio* utilisées en physique nucléaire, et (iii) sur les EDF nucléaires empiriques. A chaque étape, les avantages et les inconvénients sont discutés et quelques avancées sur les DFT *ab initio* sont présentées. La possibilité de rendre les DFT moins empiriques motive en grande partie le travail présenté dans ce manuscrit. Dans le chapitre 2, nous discutons de la possibilité d'utiliser la limite des gaz de Fermi diluée comme guide pour la conception d'une nouvelle génération d'EDF non-empiriques. Nous montrons que, dans ce cas limite, l'interaction fournie par l'EFT simplifie les calculs à N -corps. Ceci est illustré par la théorie de perturbation à plusieurs corps (MBPT) utilisant le formalisme des fonctions de Green. Dans ce chapitre académique, d'importants concepts techniques et physiques utiles à cette thèse sont introduits. Nous montrons que l'énergie de l'état fondamental du système de Fermi dilué peut être écrite comme une fonction

explicite de la densité et directement connectée aux constantes de basse énergie de l'interaction. Ce type de fonctionnelle est un cas limite valable pour des densités très faibles que nous souhaitons développer et qui servira de guide pour le travail présenté. Notre objectif ultime est d'étendre l'approche, qu'elle soit MBPT ou DFT nucléaire, au régime dense ou aux systèmes avec une longueur de diffusion en onde s anormalement grande. Pour cela, nous proposerons et développerons des stratégies spécifiques applicables au régime non-perturbatif.

L'exigence d'approches non-perturbatives pour décrire correctement les systèmes nucléaires impose d'aller au-delà des développements MBPT pour le gaz de Fermi dilué. Une possibilité est d'introduire des techniques de re-sommation permettant de re-sommer toutes les corrélations MBPT conduisant à des formes d'énergie relativement compactes. Cependant, comme nous le verrons, le manque de prédictivité des énergies re-sommées dans le régime non-perturbatif ainsi que la complexité des expressions obtenues en utilisant ces méthodes de re-sommation en termes de densité incitent à explorer d'autres stratégies. Dans le chapitre 3, nous faisons un survol des tentatives récentes pour obtenir des DFT non-empiriques guidées par ces résultats issus des techniques de re-sommation. Une stratégie générale et bien contrôlée appelée approximation de l'espace des phases est introduite et des extensions de ces fonctionnelles, comprenant l'effet de la portée effective en onde s , sont proposées.

Les nouvelles fonctionnelles seront ensuite appliquées à la fois dans les systèmes atomiques et nucléaires et montreront leur puissance prédictive dans le régime non-perturbatif. Dans le chapitre 3, une étude de la réponse linéaire statique des systèmes d'atomes froids et de la matière neutronique ainsi que des modes collectifs de systèmes piégés utilisant certaines des fonctionnelles non-empiriques obtenues est présentée. Cette étude révèle que de tels processus ne pourraient être décrits que si les propriétés des quasi-particules sont correctement prises en compte. Pour cette raison, une étude exploratoire est réalisée pour décrire les propriétés des quasi-particules en utilisant le concept de self-énergie. De la même manière que ce qui a été fait pour l'énergie, nous abordons d'abord la re-sommation des diagrammes directement en termes de self-énergie dans le chapitre 4. Ceci jette les bases de la conception d'une théorie fonctionnelle incluant des propriétés de quasi-particules et reste un guide solide pour les DFT non-empiriques. Puis, dans le chapitre 5, nous proposons une méthodologie générale, guidée par la limite de basse densité et la self-énergie obtenue dans l'approche MBPT, pour étendre l'approximation de l'espace des phases à la self-énergie. Cette approche conduit à une méthode bien contrôlée et à des expressions simplifiées pour l'énergie et plus généralement pour les propriétés de quasi-particules ouvrant la voie à des applications pour les systèmes finis.

CHAPITRE 1 :**ASPECTS IMPORTANTS DES THÉORIES AB INITIO ET FONCTIONNELLE DE LA DENSITÉ**

Le but de ce chapitre a été de présenter les concepts utilisés tout au long de cette thèse, en particulier sur l'interaction nucléon-nucléon. En outre, un aperçu des progrès récents des méthodes *ab initio* et des DFT a été également présenté. En particulier, cet aperçu a aidé à mieux comprendre et mettre en perspective le but de cette thèse ainsi que les questions importantes. Nous avons d'abord présenté l'interaction nucléon-nucléon et ses nouvelles modélisations basées sur les EFT. Nous avons ensuite montré comment ces progrès ont permis une avancée décisive pour les méthodes *ab initio* et pourquoi il apparaît de plus en plus opportun de faire le lien avec la DFT.

CHAPITRE 2 :**RE-SOMMATION DE L'ÉNERGIE**

Le but de ce chapitre a été d'introduire et de résumer les progrès récents réalisés en EFT afin de décrire les systèmes de Fermi en interaction qui seront utiles dans la suite de la thèse. Nous avons introduit de manière didactique/académique l'approche MBPT dans le formalisme des fonctions de Green pour le gaz de Fermi dilué. Par exemple, la formule Lee-Yang (1.28) a été redécrite dans ce cadre de l'EFT. Nous avons utilisé ce travail comme guide pour obtenir des fonctionnelles non-empiriques pour l'énergie de l'état fondamental, en tant que fonctions explicites de la densité et de la longueur de diffusion d'ondes s uniquement. Nous avons ensuite procédé à une re-sommation de certaines classes de corrélations pour aller au-delà du régime perturbatif de faible densité et présenter ce que nous appelons ici l'approximation de l'espace des phases afin de simplifier ces fonctionnelles. Un accent particulier a enfin été mis sur la limite du gaz unitaire où $|a_s k_F| \rightarrow \infty$. Dans ce chapitre, nous avons d'abord présenté des remarques générales sur la théorie des fonctions de Green. L'un des principaux objectifs de ce chapitre a été de présenter différentes formes compactes de l'énergie obtenue par re-sommation.

CHAPITRE 3 :**DFT INSPIRÉE DES TECHNIQUE DE RE-SOMMATION EN EFT**

Dans ce chapitre, nous avons exploré la possibilité de partir des expressions re-sommées de l'énergie obtenue dans le chapitre 2 et d'obtenir une DFT explicite décrivant le gaz de Fermi dans les limites de basse densité et de grande longueur de diffusion. Il a été montré que les différentes re-sommations donnent des indications importantes pour obtenir une DFT simple où l'énergie est écrite directement en fonction de $(a_s k_F)$ sous une forme compacte. Ensuite, interpréter le moment de Fermi k_F comme une fonction de la densité ρ conduit à une DFT. Une telle reformulation des DFT est motivée par le fait que (i) les calculs MBPT deviennent rapidement très compliqués lorsque l'ordre de perturbation augmente et que (ii) les expressions compactes retrouvées dans le chapitre 2 sont difficiles à implémenter dans des systèmes finis en raison des intégrales sur l'espace des phases. Une fois que des fonctions plus simples ont été trouvées, nous avons vu comment cela pourrait servir de guide pour obtenir une DFT pour les systèmes avec une grande longueur de diffusion d'onde s . Nous avons ensuite illustré le pouvoir prédictif de la fonctionnelle que nous avons récemment proposée dans cette voie.

CHAPITRE 4 :**RE-SOMMATION DE LA SELF-ÉNERGIE**

Dans le chapitre 2, nous avons discuté une technique de re-sommation pour l'énergie conduisant à une forme compacte dans laquelle les diagrammes sélectionnés, à savoir les diagrammes en échelle, ont été conservés. Comme nous l'avons vu, la re-sommation des diagrammes en échelle particules-particules conduit à une forme de série géométrique tandis que les diagrammes en échelle combinant les canaux particules-particules et trou-trou mènent à une forme d'arctangente [voir (2.55)]. Le but de ce chapitre a été d'effectuer une re-sommation équivalente directement pour la self-énergie. Cela a fourni des informations microscopiques sur le système, telles que la masse effective et/ou la durée de vie des quasi-particules. Cela a également établi un lien direct avec la théorie de Landau des liquides de Fermi. Nous avons déjà souligné au chapitre 3 l'importance de ces quantités pour décrire des propriétés de non-équilibre telles que la réponse linéaire ou les modes collectifs. Ici, nous avons d'abord illustré le calcul des diagrammes de self-énergie du premier au troisième ordre en $(a_s k_F) \ll 1$ et discuté la relation avec le calcul MBPT pour l'énergie de l'état fondamental présentée en section 2.2.b. Nous avons ensuite expliqué comment obtenir des expressions compactes pour la self-énergie, comme ce fut le cas pour l'énergie, en incluant uniquement les diagrammes en échelle particule-particule ou combinant les canaux particules-particules et trou-trou. Nous avons discuté des avantages et des inconvénients des deux classes de diagrammes sélectionnées.

CHAPITRE 5 :**SELF-ÉNERGIE INSPIRÉE DES TECHNIQUE DE RE-SOMMATION EN EFT**

Dans ce chapitre, guidés par la re-sommation sur l'énergie avec les approximations abordés au chapitre 3, nous avons exploré la possibilité d'obtenir une forme approximative compacte de la self-énergie à partir de la re-sommation présentée au chapitre 4. Cela a conduit à des self-énergies plus simples pour décrire les propriétés de quasi-particules des gaz de Fermi dans la limite de faible densité et de grande longueur de diffusion. Le travail présenté est motivé par le fait que: (i) la technique MBPT est plutôt compliquée au grand ordre en perturbations et devient difficilement applicable aux systèmes physiques (par exemple, pour décrire la densité de saturation des systèmes nucléaires), (ii) les expressions re-sommées trouvées dans le chapitre 4 sont complexes à implémenter dans les systèmes finis en raison de l'intégrale sur l'espace des phases et (iii) les DFT basées sur l'énergie ne contiennent pas d'informations sur les propriétés des quasi-particules, sauf le potentiel chimique des systèmes donné par une relation thermodynamique générale. Par exemple, ce travail ne donne aucune indication sur la masse effective, ce qui est crucial pour décrire la réponse à un champ extérieur ou les modes collectifs de tels systèmes, comme indiqué dans le chapitre 3.

CONCLUSION

La période charnière de la physique nucléaire telle que nous la connaissons aujourd'hui laisse entrevoir de nouvelles possibilités de compréhension des fermions fortement corrélés, tels que les systèmes neutroniques. Les méthodes nucléaires *ab initio*, bien que connaissant des progrès importants, en particulier avec les récents développements des EFT, sont extrêmement complexes comparées à une approche DFT. Cette dernière reste encore aujourd'hui la seule approche microscopique capable de traiter dans un cadre unifié une grande variété de phénomènes se produisant dans les systèmes nucléaires. Dans ce contexte, l'objectif de cette thèse était d'explorer la possibilité de connecter directement les DFT nucléaire à l'interaction nucléaire nue et de les rendre moins empiriques.

Nous pouvons alors résumer ci-dessous les principaux progrès réalisés au cours de cette thèse. Dans le chapitre 1, un aperçu des problèmes actuels et des progrès récents en physique nucléaire est présenté. Trois concepts importants autour desquels la thèse présentée est articulée sont discutés: (i) l'interaction nucléaire et les avancées récentes en EFT (simplification des calculs à N -corps), (ii) les théories à N -corps *ab initio* elles-mêmes, et (iii) les DFT empiriques couramment utilisées en physique nucléaire. Les limites réelles des différentes approches sont discutées et les tentatives récentes pour combiner les méthodes *ab initio* et les approches DFT sont résumées. Cette analyse a révélé la possibilité d'obtenir, dans certains cas (basse densité, unitarité), des expressions relativement simples et explicites de l'énergie pouvant être utilisée du régime perturbatif au régime non-perturbatif.

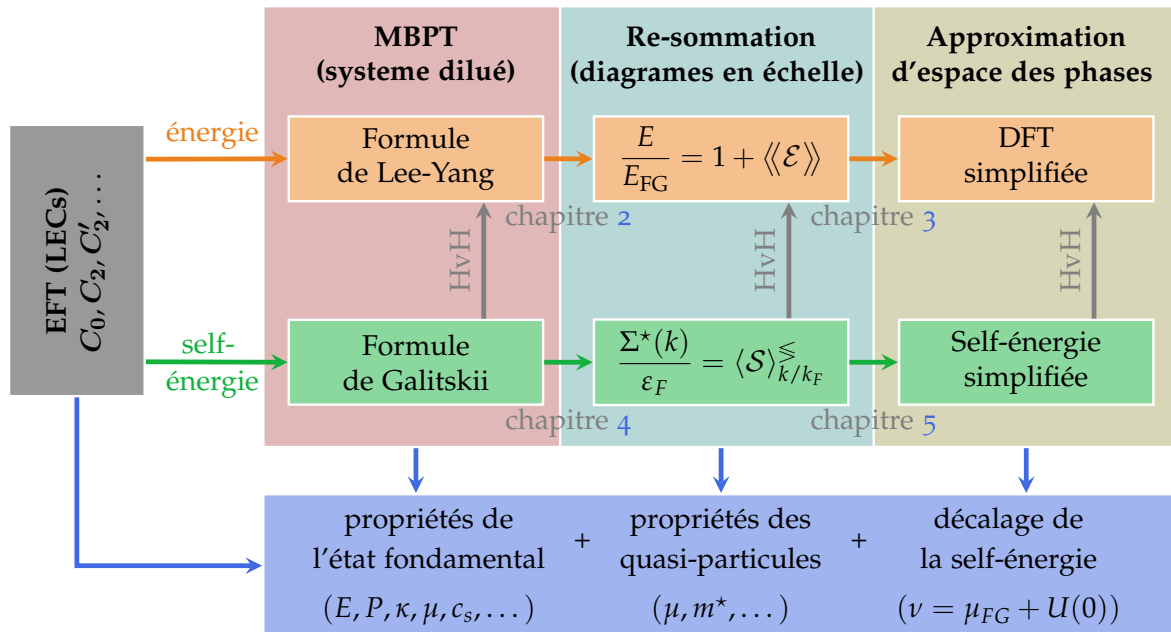


Figure B: Représentation schématique de la stratégie utilisée dans cette thèse pour obtenir, à partir de l'EFT, l'approximation d'espace des phases pour les propriétés de l'état fondamental et de quasi-particules guidées d'abord par l'approche MBPT, puis par une re-sommation des diagrammes en échelle de l'énergie et/ou de la self-énergie.

Ces exemples ont également servi de guide pour le travail présenté afin de définir une stratégie spécifique visant à rendre les DFT nucléaires moins empiriques. La stratégie que nous avons employée est décrite schématiquement dans la figure B. Cela commence par une approche à N -corps bien définie et bien contrôlée, ici l'approche MBPT avec la re-sommation éventuelle de certaines classes de dia-

grammes. Plus précisément, nous partons d'un cadre EFT pour les systèmes de Fermi dilués en utilisant une interaction de contact. Cette approche est justifiée dans le chapitre 2. Dans ce cas, le lien avec les constantes de basse énergie de l'interaction est clair et présente des similitudes avec l'EFT sans pion décrivant l'interaction nucléaire. À partir de cette interaction, nous nous intéressons au cas d'un système infini de Fermi dégénéré en spin utilisant l'ordre principal de cette interaction de contact. Ce cas de modèle présente un intérêt tant pour les systèmes atomiques que pour les systèmes neutroniques. Ensuite, nous avons utilisé l'approche MBPT et illustré le calcul de l'énergie de l'état fondamental des systèmes en tant que série perturbative en termes de densité (liée au moment de Fermi k_F) et de constantes basse énergie (la longueur de diffusion d'onde a_s). Cette étude systématique a mis en évidence que, dans certaines conditions (consistant à ne conserver que la contribution d'une certaine classe de corrélations liées aux diagrammes en échelles), toutes les contributions de l'énergie de l'état fondamental peuvent être écrites avec une expression compacte comme une fonction explicite de $(a_s k_F)$ intégré sur l'espace des phases accessible. Finalement, nous avons obtenu l'expression explicite de l'énergie en fonction des constantes de basse énergie. Bien qu'il s'agisse d'une étape intéressante vers les fonctionnelles non-empirique pour les systèmes en interaction au-delà des approches perturbatives, les résultats (i) dépendent fortement de la classe de diagrammes sélectionnée, (ii) ne reproduisent qualitativement pas les observations, et (iii) présentent une dépendance relativement complexe de la densité qui empêchera très probablement d'exporter ces fonctions vers des systèmes finis.

Une étude exploratoire approfondie est faite au chapitre 3 en partant de l'énergie de l'état fondamental re-sommée pour obtenir des approximations systématiques et bien définies afin de simplifier les fonctionnelles obtenues par re-sommation. En utilisant ce que l'on appelle ici l'approximation de l'espace des phases conduit à des DFT beaucoup plus simples. Certaines de ces DFT non-empiriques reproduisent très bien les propriétés thermodynamiques, par exemple l'énergie de l'état fondamental, la pression ou la compressibilité des systèmes étudiés, du régime de basse densité au régime unitaire. Ensuite, des généralisations de ces fonctionnelles pour inclure les effets de portée effective r_s ont été introduites. Le cas particulier d'une grande longueur de diffusion d'onde s et d'une portée effective non négligeable est motivé par la physique nucléaire. Il a été démontré que non seulement les systèmes atomiques sont bien expliqués avec $r_s = 0$, mais que ces généralisations pour $r_s \neq 0$ reproduisent correctement l'équation d'état à de faibles densités de la matière neutronique, bien au-delà de l'approche MBPT standard. La fonctionnelle proposée a été appliquée à la détermination de la réponse linéaire de la matière neutronique à basse densité. La réponse statique reproduit qualitativement bien les calculs *ab initio* et est en général beaucoup plus prédictive que les DFT empiriques standards. Cette étude a également révélé la nécessité d'améliorer nos connaissances sur les propriétés des quasi-particules, telles que la masse effective dans les systèmes fermionique en interaction forte.

Pour cette raison, suivant les idées utilisées pour l'énergie, la technique de re-sommation est directement développée au niveau de la self-énergie dans le chapitre 4. Plusieurs re-sommations sont discutées avec plus ou moins de succès dans la description de systèmes ayant une grande longueur de diffusion d'onde s . En fin de compte, il est démontré que l'application directe de cette technique de re-sommation manque de pouvoir prédictif au régime unitaire ou proche de celui-ci. Un deuxième inconvénient est que les expressions résultantes s'avèrent plutôt compliquées, ce qui empêche leur utilisation dans des systèmes finis.

Ainsi, au chapitre 5, nous avons proposé des méthodologies générales, guidées par la limite de basse densité et éventuellement par la contrainte donnée par le théorème de Hugenholtz-van Hove, pour étendre l'approximation de l'espace des phases à la self-énergie. Lorsque le théorème de Hugenholtz-van Hove est imposé, nous montrons en particulier que l'approximation d'espace des phases introduite dans le chapitre 5 est pleinement cohérente avec celle introduite au niveau de l'énergie dans le chapitre 3. En nous concentrant sur le potentiel à un corps des systèmes non superfluides et sur la masse effective, nous en avons obtenu des expressions simples et explicites en termes de $(a_s k_F)$. En particulier, nos résultats sont valables bien au-delà de l'approche MBPT standard pour les systèmes de fermions dilués.

Dans la thèse présentée, nous avons discuté des voies possibles vers des DFT *ab initio* en obtenant une DFT directement connectée aux constantes de basse énergie de l'interaction. Cela a permis de comprendre les effets de milieu et en particulier comment les effets de milieu renormalisent fortement les constantes de basse énergie. Ce point a été clairement mis en évidence à la fin du chapitre 5. Plus précisément, nous avons montré que la renormalisation des constantes de couplage à une densité proche de la saturation induit une perte de mémoire des constantes de basse énergie nues. En effet, à mesure que la densité augmente, nous avons observé un lien direct avec la limite unitaire et la longueur de diffusion d'ondes s renormalisée. Nous avons constaté que notre approche est compatible avec les valeurs de certains paramètres empiriques figurant dans les fonctionnelles de Skyrme. Cette observation se dégage également des travaux récents guidés par l'EFT pour concevoir de nouvelles fonctionnelles hybrides [76,130,197,198,208] ou, par exemple, dans [306] où sont déterminées les constantes de couplage renormalisées d'après des calculs Brueckner Hartree-Fock.

En tant que question critique, les applications directes des fonctionnelles basées sur des techniques de re-sommation sont un projet extrêmement difficile en pratique pour les systèmes nucléaires. La principale difficulté des techniques de re-sommation semi-analytiques provient du fait que les DFT deviennent extrêmement complexes lorsque l'interaction devient plus réaliste (effet de la portée effective, contribution de l'onde p , etc.) [238–240,305]. Cela limite certainement le domaine d'application aux systèmes à N -corps qui interagissent par le biais d'interactions plutôt simples comparées à l'interaction nucléaire. Une autre difficulté est liée à l'extension à la matière symétrique où des dimmers et plus généralement des multimers apparaissent en raison de l'existence d'états liés.

Une des conclusions de cette thèse est que la conception de DFT *ab initio* nécessite des calculs exacts et bien contrôlés donnant accès à d'importantes pseudo-données pour inspirer et tester de nouvelles idées comme des calculs exacts à N -corps où l'équation d'état de la matière neutronique est obtenue en ramifiant, étape par étape, les contributions de l'interaction obtenue avec les EFT. Cette thèse a initié des discussions intéressantes avec la communauté *ab initio* afin d'obtenir des calculs *ab initio* précis pour la masse effective de systèmes de Fermi en interaction forte. Ceci a entraîné indirectement le premier calcul AFDMC de la masse effective dans les systèmes neutroniques [289]. Cet exemple spécifique illustre la fertilisation croisée positive entre les scientifiques des communautés *ab initio* et DFT qui pourrait être très productive pour les développements futurs.

Malgré la limitation aux interactions assez simples, le travail présenté dans cette thèse illustre également le lien entre les systèmes atomique et nucléaire. La fonctionnelle introduite dans cette thèse, qui étend l'approche MBPT pour les systèmes dilués, ouvre la possibilité de décrire des gouttelettes quantiques dans lesquelles

des corrections au-delà du champ moyen sont connues pour stabiliser ces systèmes [209,210].

Une autre extension importante des travaux actuels dans le contexte des systèmes d'atomes froids consisterait à inclure l'effet des corrélations d'appariement. Une condition préalable à cette extension est la possibilité d'obtenir une expression compacte de l'énergie après la re-sommation des diagrammes sélectionnés pour tous les ordres en perturbations. En soi, il est possible de développer une approche perturbative au dessus d'un vide quasi-particulaire (voir par exemple [307,308]). Cependant, même au second ordre, en remplaçant l'énergie de $2p - 2h$ par quatre quasi-particules, la complexité des intégrales à traiter augmente considérablement. À notre connaissance, un tel problème n'a pas encore été résolu de manière analytique. Une alternative à l'approche analytique utilisant une DFT guidée par le travail présenté dans cette thèse serait d'ajouter a posteriori une énergie d'appariement à la DFT. Cette procédure est couramment utilisée pour les noyaux et permettrait au moins d'étendre la méthode dite d'approximation de densité locale de superfluides (SLDA) de [75] en dehors de l'unitarité. Il pourrait offrir de nouvelles opportunités pour les systèmes infinis [309] ainsi que pour les systèmes finis [310,311].

BIBLIOGRAPHY

- [1] B. A. Loiseau and Y. Nogami, *Nucl. Phys. B* **2**, 470 (1967).
Three-Nucleon Force
- [2] H. Witala, W. Glöckle, D. Hüber, J. Golak, and H. Kamada, *Phys. Rev. Lett.* **81**, 1183 (1998).
Cross Section Minima in Elastic Nd Scattering: Possible Evidence for Three-Nucleon Force Effects
- [3] E. Epelbaum, A. Nogga, W. Glöckle, H. Kamada, U.-G. Meißner, and H. Witala, *Phys. Rev. C* **66**, 064001 (2002).
Three-nucleon forces from chiral effective field theory
- [4] P. Mermod *et al.*, *Phys. Lett. B* **597**, 243 (2004).
Search for three-body force effects in neutron-deuteron scattering at 95 MeV
- [5] W. Greiner, S. Schramm, and E. Stein, *Quantum chromodynamics* (Springer, 2004).
- [6] M. D. Schwartz, *Quantum Field Theory and the Standard Model* (Cambridge University Press, 2014).
- [7] S. Weinberg, *Physica A* **96**, 327 (1979).
Phenomenological Lagrangians
- [8] H. Leutwyler, *Annals of Physics* **235**, 165 (1994).
On the foundations of chiral perturbation theory
- [9] S. Scherer, *Adv. Nucl. Phys.* **27**, 277 (2003).
Introduction to Chiral Perturbation Theory
- [10] G. Ecker, *Prog. Part. Nucl. Phys.* **35**, 1 (1995).
Chiral perturbation theory
- [11] R. Machleidt and F. Sammarruca, *Phys. Scr.* **91**, 083007 (2016).
Chiral EFT based nuclear forces: achievements and challenges
- [12] P. F. Bedaque and U. van Kolck, *Annu. Rev. Nucl. Part. Sci.* **52**, 339 (2002).
Effective Field Theory for Few-Nucleon Systems
- [13] E. Epelbaum, H.-W. Hammer, and U.-G. Meißner, *Rev. Mod. Phys.* **81**, 1773 (2009).
Modern theory of nuclear forces
- [14] D. R. Entem, R. Machleidt, and Y. Nosyk, *Phys. Rev. C* **96**, 024004 (2017).
High-quality two-nucleon potentials up to fifth order of the chiral expansion
- [15] M. Grasso, D. Lacroix, and U. van Kolck, *Phys. Scr.* **91**, 063005 (2016).
From effective field theories to effective density functionals in and beyond the mean field

- [16] H. Georgi, *Weak interactions and modern particle theory* (Benjamin/Cummings Pub. Co., 1984).
- [17] D. J. Griffiths, *Introduction to Elementary Particles* (Wiley, John & Sons, Inc., 1987).
- [18] H. Yukawa, *Proc. Phys. Math. Soc. Japan* **17**, 48 (1935).
On the Interaction of Elementary Particles
- [19] T. E. O. Ericson and W. Weise, *Pions and nuclei* (Clarendon Press, 1988).
- [20] R. Machleidt and I. Slaus, *J. Phys. G: Nucl. Part. Phys.* **27** R69 (2001).
The nucleon-nucleon interaction
- [21] S. Aoki, T. Hatsuda, and N. Ishii, *Comput. Sci. Disc.* **1**, 015009 (2008).
The nuclear force from Monte Carlo simulations of lattice quantum chromodynamics
- [22] R. B. Wiringa, R. A. Smith, and T. L. Ainsworth, *Phys. Rev. C* **29**, 1207 (1984).
Nucleon-nucleon potentials with and without $\Delta(1232)$ degrees of freedom
- [23] R. Machleidt, K. Holinde, and Ch. Elster, *Phys. Rep.* **149**, 1 (1987).
The bonn meson-exchange model for the nucleon-nucleon interaction
- [24] M. M. Nagels, T. A. Rijken, and J. J. de Swart, *Phys. Rev. D* **17**, 768 (1978).
Low-energy nucleon-nucleon potential from Regge-pole theory
- [25] M. Lacombe, B. Loiseau, J. M. Richard, R. Vinh Mau, J. Côté, P. Pirès, and R. de Tournail, *Phys. Rev. C* **21**, 861 (1980).
Parametrization of the Paris N-N potential
- [26] R. V. Reid, *Ann. Phys.* **50**, 411 (1968).
Local phenomenological nucleon-nucleon potentials
- [27] C. A. Bertulani and P. Danielewicz, *Introduction to Nuclear Reactions* (CRC Press, 1993).
- [28] G. R. Satchler, *Introduction to Nuclear Reactions* (Palgrave, 1990).
- [29] J. R. Taylor, *Scattering Theory: The Quantum Theory of Nonrelativistic Collisions* (Dover Publications, 2006).
- [30] S. K. Bogner, T. T. S. Kuo, and A. Schwenk, *Physics Reports* **386**, 1 (2003).
Model-independent low momentum nucleon interaction from phase shift equivalence
- [31] R. B. Wiringa, *Rev. Mod. Phys.* **65**, 231 (1993).
From deuterons to neutron stars: variations in nuclear many-body theory
- [32] J. Schwinger, *Phys. Rev.* **72**, 742 (1947).
A Variational Principle for Scattering Problems
- [33] J. M. Blatt, *Phys. Rev.* **74**, 92 (1948).
On the Neutron-Proton Force
- [34] H. A. Bethe, *Phys. Rev.* **76**, 38 (1949).
Theory of the Effective Range in Nuclear Scattering
- [35] H.-W. Hammer and R. J. Furnstahl, *Nuclear Physics A* **678**, 277 (2000).
Effective field theory for dilute Fermi systems

- [36] U. van Kolck, *Prog. Part. Nucl. Phys.* **43**, 337 (1999).
Effective field theory of nuclear forces
- [37] M. Pavon Valderrama and E. Ruiz Arriola, [arXiv:nucl-th/0407113](https://arxiv.org/abs/nucl-th/0407113) (2004).
Determination of low energy parameters for NN-scattering at N₄LO in all partial waves with $j \leq 5$
- [38] R. Machleidt and D. R. Entem, *Phys. Rep.* **503**, 1 (2011).
Chiral effective field theory and nuclear forces
- [39] C. G. Bollini and J. J. Giambiagi, *Nuovo Cimento B* **12**, 20 (1972).
Dimensional renormalization : The number of dimensions as a regularizing parameter
- [40] G. P. Lepage, [arXiv:nucl-th/9706029](https://arxiv.org/abs/nucl-th/9706029) (1997).
How to Renormalize the Schrodinger Equation
- [41] D. B. Kaplan, M. J. Savage and M. B. Wise, *Phys. Lett. B* **424**, 390 (1998).
A New Expansion for Nucleon-Nucleon Interactions
- [42] D. B. Kaplan, M. J. Savage and M. B. Wise, *Nucl. Phys. B* **534**, 329 (1998).
Two-nucleon systems from effective field theory
- [43] D. R. Phillips, [arXiv:nucl-th/9804040](https://arxiv.org/abs/nucl-th/9804040) (1998).
Regularization and the potential of effective field theory in nucleon-nucleon scattering
- [44] M. C. Birse, [arXiv:nucl-th/9804028](https://arxiv.org/abs/nucl-th/9804028) (1998).
Renormalising NN scattering: is power counting powerless?
- [45] J. R. Oppenheimer and G. M. Volkoff, *Phys. Rev.* **55**, 374 (1939).
On Massive Neutron Cores
- [46] R. C. Tolman, *Phys. Rev.* **55**, 364 (1939).
Static Solutions of Einstein's Field Equations for Spheres of Fluid
- [47] K. Hebeler, J. D. Holt, J. Menéndez, and A. Schwenk, *Annu. Rev. Nucl. Part. Sci.* **65**, 457 (2015).
Nuclear Forces and Their Impact on Neutron-Rich Nuclei and Neutron-Rich Matter
- [48] P. B. Demorest, T. Pennucci, S. M. Ransom, M. S. E. Roberts, and J. W. T. Hessels, *Nature* **467**, 1081 (2010).
A two-solar-mass neutron star measured using Shapiro delay
- [49] A. Carbone, A. Rios, and A. Polls, *Phys. Rev. C* **90**, 054322 (2014).
Correlated density-dependent chiral forces for infinite-matter calculations within the Green's function approach
- [50] H. F. Arellano and J.-P. Delaroche, *Eur. Phys. J. A* **51**, 7 (2015).
Low-density homogeneous symmetric nuclear matter: Disclosing dinucleons in coexisting phases
- [51] H. F. Arellano, F. Isaule, and A. Rios, *Eur. Phys. J. A* **52**, 299 (2015).
Di-nucleon structures in homogeneous nuclear matter based on two- and three-nucleon interactions

- [52] F. Isaule, H. F. Arellano, and A. Rios, *Phys. Rev. C* **94**, 034004 (2016).
Di-neutrons in neutron matter within a Brueckner-Hartree-Fock approach
- [53] A. Gezerlis and J. Carlson, *Phys. Rev. C* **81**, 025803 (2010).
Low-density neutron matter
- [54] S. Gandolfi, J. Carlson, and S. Reddy, *Phys. Rev. C* **85**, 032801 (2012).
Maximum mass and radius of neutron stars, and the nuclear symmetry energy
- [55] A. Gezerlis, I. Tews, E. Epelbaum, M. Freunek, S. Gandolfi, K. Hebeler, A. Nogga, and A. Schwenk, *Phys. Rev. C* **90**, 054323 (2014).
Local chiral effective field theory interactions and quantum Monte Carlo applications
- [56] K. Hebeler, J. M. Lattimer, C. J. Pethick, and A. Schwenk, *Astrophys. J.* **773**, 11 (2013).
Equation of state and neutron star properties constrained by nuclear physics and observation
- [57] I. Tews, T. Krüger, K. Hebeler, and A. Schwenk, *Phys. Rev. Lett.* **110**, 032504 (2013).
Neutron Matter at Next-to-Next-to-Next-to-Leading Order in Chiral Effective Field Theory
- [58] T. Krüger, I. Tews, K. Hebeler, and A. Schwenk, *Phys. Rev. C* **88**, 025802 (2013).
Neutron matter from chiral effective field theory interactions
- [59] L. Coraggio, J. W. Holt, N. Itaco, R. Machleidt, and F. Sammarruca, *Phys. Rev. C* **87**, 014322 (2013).
Reduced regulator dependence of neutron-matter predictions with perturbative chiral interactions
- [60] C. Wellenhofer, J. W. Holt, and N. Kaiser, *Phys. Rev. C* **92**, 015801 (2015).
Thermodynamics of isospin-asymmetric nuclear matter from chiral effective field theory
- [61] G. Hagen, T. Papenbrock, A. Ekström, K. A. Wendt, G. Baardsen, S. Gandolfi, M. Hjorth-Jensen, and C. J. Horowitz, *Phys. Rev. C* **89**, 014319 (2014).
Coupled-cluster calculations of nucleonic matter
- [62] B. Friedman and V. Pandharipande, *Nucl. Phys. A* **361**, 502 (1981).
Hot and cold, nuclear and neutron matter
- [63] A. Akmal, V. R. Pandharipande, and D. G. Ravenhall, *Phys. Rev. C* **58**, 1804 (1998).
Equation of state of nucleon matter and neutron star structure
- [64] A. Roggero, A. Mukherjee, and F. Pederiva, *Phys. Rev. C* **92**, 054303 (2015).
Constraining the Skyrme energy density functional with quantum Monte Carlo calculations
- [65] K. Hebeler, S. K. Bogner, R. J. Furnstahl, A. Nogga, and A. Schwenk, *Phys. Rev. C* **83**, 031301(R) (2011).
Improved nuclear matter calculations from chiral low-momentum interactions

- [66] J. W. Holt and N. Kaiser, *Phys. Rev. C* **95**, 034326 (2017).
Equation of state of nuclear and neutron matter at third-order in perturbation theory from chiral effective field theory
- [67] W. Zwerger, *The BCS-BEC Crossover and the Unitary Fermi Gas* (Springer-Verlag, Berlin, 2012).
- [68] C. Chin, R. Grimm, P. Julienne, and E. Tiesinga, *Rev. Mod. Phys.* **82**, 1225 (2010).
Feshbach resonances in ultracold gases
- [69] I. Bloch, J. Dalibard, and W. Zwerger, *Rev. Mod. Phys.* **80**, 885 (2008).
Many-body physics with ultracold gases
- [70] N. Navon, S. Nascimbène, F. Chevy, and C. Salomon, *Science* **328**, 729 (2010)
The Equation of State of a Low-Temperature Fermi Gas with Tunable Interactions
- [71] M. J. H. Ku, A. T. Sommer, L. W. Cheuk, and M. W. Zwierlein, *Science* **335**, 563 (2012).
Revealing the superfluid lambda transition in the universal thermodynamics of a unitary Fermi gas
- [72] J. Carlson, S. Gandolfi, and A. Gezerlis, *Prog. Theor. Exp. Phys.* 01A209 (2012).
Quantum Monte Carlo approaches to nuclear and atomic physics
- [73] R. Haussmann, M. Punk, and W. Zwerger, *Phys. Rev. A* **80**, 063612 (2009).
Spectral functions and rf response of ultracold fermionic atoms
- [74] T. Papenbrock, *Phys. Rev. A* **72**, 041603(R) (2005).
Density-functional theory for fermions in the unitary regime
- [75] A. Bulgac, *Phys. Rev. A* **76**, 040502 (2007).
Local-density-functional theory for superfluid fermionic systems: The unitary gas
- [76] D. Lacroix, *Phys. Rev. A* **94**, 043614 (2016).
Density-functional theory for resonantly interacting fermions with effective range and neutron matter
- [77] S. Y. Chang, V. R. Pandharipande, J. Carlson, and K. E. Schmidt, *Phys. Rev. A* **70**, 043602 (2004).
Quantum Monte Carlo studies of superfluid Fermi gases
- [78] A. Bulgac, J. Drut, and P. Magierski, *Phys. Rev. A* **78**, 023625 (2008).
Quantum Monte Carlo simulations of the BCS-BEC crossover at finite temperature
- [79] M. M. Forbes, S. Gandolfi, and A. Gezerlis, *Phys. Rev. Lett.* **106**, 235303 (2011).
Resonantly Interacting Fermions in a Box
- [80] A. Gezerlis and J. Carlson, *Phys. Rev. C* **77**, 032801(R) (2008).
Strongly paired fermions: Cold atoms and neutron matter
- [81] M. M. Forbes, S. Gandolfi, and A. Gezerlis, *Phys. Rev. A* **86**, 053603 (2012).
Effective-range dependence of resonantly interacting fermions

- [82] M. G. Endres, D. B. Kaplan, J.-W. Lee, and A. N. Nicholson, *Phys. Rev. A* **87**, 023615 (2013).
Lattice Monte Carlo calculations for unitary fermions in a finite box
- [83] R. Haussmann, W. Rantner, S. Cerrito, and W. Zwerger, *Phys. Rev. A* **75**, 023610 (2007).
Thermodynamics of the BCS-BEC crossover
- [84] E. V. H. Doggen and J. J. Kinnunen, *Scientific Reports* **5**, 9539 (2015).
Momentum-resolved spectroscopy of a Fermi liquid
- [85] K. van Houcke, F. Werner, E. Kozik, N. Prokof'ev, B. Svistunov, M. J. H. Ku, A. T. Sommer, L. W. Cheuk, A. Schirotzek, and M. W. Zwierlein, *Nature Phys.* **8**, 366 (2012).
Feynman diagrams versus Fermi-gas Feynman emulator
- [86] R. Rossi, T. Ohgoe, E. Kozik, N. Prokof'ev, B. Svistunov, K. Van Houcke, and F. Werner, *Phys. Rev. Lett.* **121**, 130406 (2018).
Contact and Momentum Distribution of the Unitary Fermi Gas
- [87] R. Rossi, T. Ohgoe, K. Van Houcke, and F. Werner, *Phys. Rev. Lett.* **121**, 130405 (2018).
Resummation of Diagrammatic Series with Zero Convergence Radius for Strongly Correlated Fermions
- [88] I. Tews, J. M. Lattimer, A. Ohnishi, and E. E. Kolomeitsev, *ApJ* **848**, 105 (2017).
Symmetry Parameter Constraints From A Lower Bound On The Neutron-Matter Energy
- [89] R. B. Wiringa, *Nucl. Phys. A* **631**, 70 (1998).
Quantum Monte Carlo calculations for light nuclei
- [90] R. B. Wiringa, S. C. Pieper, J. Carlson, and V. R. Pandharipande, *Phys. Rev. C* **62**, 014001 (2000).
Quantum Monte Carlo calculations of $A = 8$ nuclei
- [91] S. Quaglioni and P. Navratil, *Few Body Syst.* **44** 337 (2008).
Ab initio no-core shell model and microscopic reactions: Recent achievements
- [92] P. Navratil, S. Quaglioni, I. Stetcu, and B. R. Barrett, *J. Phys. G: Nucl. Part. Phys.* **36**, 083101 (2009).
Recent developments in no-core shell-model calculations
- [93] H. Hergert, S. K. Bogner, T. D. Morris, A. Schwenk, and K. Tsukiyama, *Phys. Rept.* **621**, 165 (2016).
The In-Medium Similarity Renormalization Group: A Novel Ab Initio Method for Nuclei
- [94] K. Kowalski, D. J. Dean, M. Hjorth-Jensen, T. Papenbrock, and P. Piecuch, *Phys. Rev. Lett.* **92**, 132501 (2004).
Coupled cluster calculations of ground and excited states of nuclei
- [95] W. H. Dickhoff and C. Barbieri, *Prog. Part. Nucl. Phys.* **52**, 377 (2004).
Selfconsistent Green's function method for nuclei and nuclear matter

- [96] M. Musiał, A. Perera, and R. J. Bartlett, *J. Chem. Phys.* **134**, 114108 (2011).
Multireference coupled-cluster theory: The easy way
- [97] V. Somà, T. Duguet, and C. Barbieri, *Phys. Rev. C* **84**, 064317 (2011).
Ab initio self-consistent Gorkov-Green's function calculations of semimagic nuclei: Formalism at second order with a two-nucleon interaction
- [98] V. Somà, C. Barbieri, and T. Duguet, *Phys. Rev. C* **87**, 011303 (2013).
Ab initio Gorkov-Green's function calculations of open-shell nuclei
- [99] V. Somà, A. Cipollone, C. Barbieri, P. Navrátil, and T. Duguet, *Phys. Rev. C* **89**, 061301 (2014).
Chiral two- and three-nucleon forces along medium-mass isotope chains
- [100] A. Signoracci, T. Duguet, G. Hagen, and G. R. Jansen, *Phys. Rev. C* **91**, 064320 (2015).
Ab initio Bogoliubov coupled cluster theory for open-shell nuclei
- [101] M. Bender, P.-H. Heenen, and P.-G. Reinhard, *Rev. Mod. Phys.* **75**, 121 (2003).
Self-consistent mean-field models for nuclear structure
- [102] Y. Qiu, T. M. Henderson, T. Duguet, G. E. Scuseria, *Phys. Rev. C* **99**, 044301 (2019).
Particle-number projected Bogoliubov coupled cluster theory. Application to the pairing Hamiltonian
- [103] T. Duguet, *J. Phys. G: Nucl. Part. Phys.* **42**, 025107 (2015).
Symmetry broken and restored coupled-cluster theory: I. Rotational symmetry and angular momentum
- [104] T. Duguet and A. Signoracci, *J. Phys. G: Nucl. Part. Phys.* **44**, 015103 (2017).
Symmetry broken and restored coupled-cluster theory: II. Global gauge symmetry and particle number
- [105] Y. Qiu, T. M. Henderson, J. Zhao, and G. E. Scuseria, *J. Chem. Phys.* **147**, 064111 (2017).
Projected coupled cluster theory
- [106] A. Ekström, G. R. Jansen, K. A. Wendt, G. Hagen, T. Papenbrock, B. D. Carlsson, C. Forssén, M. Hjorth-Jensen, P. Navrátil, and W. Nazarewicz, *Phys. Rev. C* **91**, 051301(R) (2015).
Accurate nuclear radii and binding energies from a chiral interaction
- [107] P. Navrátil, S. Quaglioni, G. Hupin, C. Romero-Redondo, and A. Calci, *Phys. Scr.* **91**, 053002 (2013).
Unified ab initio approaches to nuclear structure and reactions
- [108] D. Vautherin and D. M. Brink, *Phys. Lett. B* **32**, 149 (1970).
Hartree-Fock calculations with Skyrme's interaction
- [109] J. W. Negele and D. Vautherin, *Phys. Rev. C* **5**, 1472 (1972).
Density-Matrix Expansion for an Effective Nuclear Hamiltonian
- [110] D. Vautherin and D. M. Brink, *Phys. Rev. C* **5**, 626 (1972).
Hartree-Fock Calculations with Skyrme's Interaction. I. Spherical Nuclei

- [111] D. Vautherin, *Phys. Rev. C* **7**, 296 (1973).
Hartree-Fock Calculations with Skyrme's Interaction. II. Axially Deformed Nuclei
- [112] J. Meyer, *Ann. Phys. Fr.* **28**, 3 (2003).
Interactions effectives, théories de champs moyen, masses et rayons nucléaire
- [113] P. Hohenberg and W. Kohn, *Phys. Rev.* **136**, B864 (1964).
Inhomogeneous Electron Gas
- [114] W. Kohn, *Phys. Rev.* **140**, A1133 (1965).
Self-Consistent Equations Including Exchange and Correlation Effects
- [115] W. Kohn, *Rev. Mod. Phys.* **71**, 1253 (1999).
Electronic structure of matter-wave functions and density functionals
- [116] R. M. Dreizler and E. K. U. Gross, *Density functional theory: an approach to the quantum many-body problem* (Springer-Verlag Berlin, 1990).
- [117] C. Fiolhais, F. Nogueira, and M. Marques,
A Primer in Density Functional Theory, Lecture Notes in Physics **620** (Springer, Berlin and Heidelberg, 2003).
- [118] W. Koch and M. C. Holthausen, *A Chemist's Guide to Density Functional Theory* (Wiley-VCH, Weinheim, 2001).
- [119] R. G. Parr and W. Yang, *Density-Functional Theory of Atoms and Molecules* (Clarendon, Oxford, 1989).
- [120] N. H. March, *Electron Density Theory of Atoms and Molecules* (Elsevier Science & Technology Books, 1997).
- [121] J. Engel, *Phys. Rev. C*, **75**, 014306 (2007).
Intrinsic-density functionals
- [122] B. G. Giraud, *Phys. Rev. C* **77**, 014311 (2008).
Density functionals in the laboratory frame
- [123] J. Messud, *Phys. Rev. C* **80**, 054614 (2009).
Time-dependent internal density functional theory formalism and Kohn-Sham scheme for self-bound systems
- [124] P. Fantucci and S. Polezzo, *International Journal of Quantum Chemistry* **52**, 817 (1994).
Direct minimization of the energy in density functional theory
- [125] O. Benhar, [arXiv:0906.3144](https://arxiv.org/abs/0906.3144) [nucl-th] (2009).
How much nuclear physics do we need, to understand the neutrino nucleus cross section?
- [126] J. Dechargé and D. Gogny, *Phys. Rev. C* **21**, 1568 (1980).
Hartree-Fock-Bogolyubov calculations with the D1 effective interaction on spherical nuclei
- [127] E. Lipparini, *Modern Many-Particle Physics: Atomic Gases* (World Scientific, Singapore, 2008).

- [128] G. Baym and C. Pethick, *Landau Fermi-Liquid Theory: Concepts and Applications* (John Wiley & Sons, 2008).
- [129] T. H. R. Skyrme, *Nucl. Phys.* **9**, 615 (1959).
The effective nuclear potential
- [130] D. Lacroix, A. Boulet, M. Grasso, and C.-J. Yang, *Phys. Rev. C* **95**, 054306 (2017).
From bare interactions, low-energy constants, and unitary gas to nuclear density functionals without free parameters: Application to neutron matter
- [131] H. M. M. Mansour, *Acta Physica Polonica B* **21**, 741 (1990).
Neutron Matter and Skyrme Forces
- [132] E. Chabanat, P. Bonche, P. Haensel, J. Meyer, and R. Schaeffer, *Nucl. Phys. A* **627**, 710 (1997).
A Skyrme parametrization from subnuclear to neutron star densities
- [133] E. Chabanat, P. Bonche, P. Haensel, J. Meyer, and R. Schaeffer, *Nucl. Phys. A* **635**, 231 (1998).
A Skyrme parametrization from subnuclear to neutron star densities Part II. Nuclei far from stabilities
- [134] C. F. Weizsäcker, *Zeit. Phys.* **96**, 431 (1935).
Zur Theorie der Kernmassen
- [135] L. D. Landau, *JETP* **3**, 920 (1957).
The theory of a Fermi liquid
- [136] L. D. Landau, *JETP* **3**, 101 (1957).
Oscillations in a Fermi liquid
- [137] L. D. Landau, *JETP* **8**, 70 (1959).
On the theory of the Fermi liquid
- [138] J. Friedrich and P.-G. Reinhard, *Phys. Rev. C* **33**, 335 (1986).
Skyrme-force parametrization: Least-squares fit to nuclear ground-state properties
- [139] S. Krewald, V. Klemt, J. Speth, and A. Faessler, *Nucl. Phys. A* **281**, 166 (1977).
On the use of Skyrme forces in self-consistent RPA calculations
- [140] M. Waroquier, K. Heyde, and G. Wenes, *Nucl. Phys. A* **404**, 269 (1983).
An effective Skyrme-type interaction for nuclear structure calculations: (I). Ground-state properties
- [141] M. Waroquier, G. Wenes, and K. Heyde, *Nucl. Phys. A* **404**, 298 (1983).
An effective Skyrme-type interaction for nuclear structure calculations: (II). Excited-state properties
- [142] N. van Giai and H. Sagawa, *Phys. Lett. B* **106**, 379 (1981).
Spin-isospin and pairing properties of modified Skyrme interactions
- [143] M. Dutra, O. Lourenço, J. S. Sá Martins, A. Delfino, J. R. Stone, and P. D. Stevenson *Phys. Rev. C* **85**, 035201 (2012).
Skyrme interaction and nuclear matter constraints

- [144] C. Golabek and C. Simenel, *Phys. Rev. Lett.* **103**, 042701 (2009).
Collision Dynamics of Two ^{238}U Atomic Nuclei
- [145] D. J. Rowe, *Nucl. Phys.* **80**, 209 (1966).
An interpretation of time-dependent Hartree-Fock theory
- [146] P. A. M. Dirac, *Proc. Cambridge Philos. Soc.* **26**, 376 (1930).
Note on Exchange Phenomena in the Thomas Atom
- [147] R. Balian and M. Vénéroni, *Ann. Phys.* **164**, 334 (1985).
Static and dynamic variational principles for expectation values of observables
- [148] M. Grasso, *Progress in Particle and Nuclear Physics* **106**, 256 (2019).
Effective density functionals beyond mean field
- [149] J. W. Negele and D. Vautherin, *Phys. Rev. C* **11**, 1031 (1975).
Density-matrix expansion for an effective nuclear Hamiltonian. II
- [150] B. G. Carlsson, J. Dobaczewski, and M. Korteleinen, *Phys. Rev. C* **78**, 044326 (2008).
Local nuclear energy density functional at next-to-next-to-next-to-leading order
- [151] F. Raimondi, B. G. Carlsson, and J. Dobaczewski, *Phys. Rev. C* **83**, 054311 (2011).
Effective pseudopotential for energy density functionals with higher-order derivatives
- [152] J. W. Negele, *Density dependent interactions*. In: Barrett B.R. (eds) *Effective Interactions and Operators in Nuclei* (Springer, Berlin, Heidelberg, 1975).
- [153] B. Gebremariam, T. Duguet, and S. K. Bogner, *Phys. Rev. C* **82**, 014305 (2010).
Improved density matrix expansion for spin-unsaturated nuclei
- [154] M. Stoitsov, M. Kortelainen, S. K. Bogner, T. Duguet, R. J. Furnstahl, B. Gebremariam, and N. Schunck, *Phys. Rev. C* **82**, 054307 (2010).
Microscopically based energy density functionals for nuclei using the density matrix expansion: Implementation and pre-optimization
- [155] B. G. Carlsson and J. Dobaczewski, *Phys. Rev. Lett.* **105**, 122501 (2010).
Convergence of Density-Matrix Expansions for Nuclear Interactions
- [156] B. Gebremariam, S. K. Bogner, and T. Duguet, *Nucl. Phys. A* **851**, 17 (2011).
Microscopically-constrained Fock energy density functionals from chiral effective field theory. I. Two-nucleon interactions
- [157] S. K. Bogner, R. J. Furnstahl, H. Hergert, M. Kortelainen, P. Maris, M. Stoitsov, and J. P. Vary, *Phys. Rev. C* **84**, 044306 (2011).
Testing the density matrix expansion against ab initio calculations of trapped neutron drops
- [158] A. Dyhdalo, S. K. Bogner, and R. J. Furnstahl, *Phys. Rev. C* **95**, 054314 (2017).
Applying the density matrix expansion with coordinate-space chiral interactions
- [159] B. G. Carlsson, J. Dobaczewski, J. Toivanen, and P. Vesely, *Comput. Phys. Commun.* **181**, 1641 (2010).
Solution of self-consistent equations for the $N_3\text{LO}$ nuclear energy density functional in spherical symmetry. The program hosphe (v1.02)

- [160] J. Dobaczewski, B. G. Carlsson, and M. Korteleinen, *J. Phys. G: Nucl. Part. Phys.* **37**, 075106 (2010)
The Negele–Vautherin density-matrix expansion applied to the Gogny force
- [161] J. Erler, P. Klüpfel, and P.-G. Reinhard, *Phys. Rev. C* **82**, 044307 (2010).
Exploration of a modified density dependence in the Skyrme functional
- [162] F. Raimondi, B. G. Carlsson, and J. Dobaczewski, *Phys. Rev. C* **83**, 054311 (2011).
Effective pseudopotential for energy density functionals with higher-order derivatives
- [163] R. Navarro Pérez, N. Schunck, A. Dyhdalo, R. J. Furnsthal, and S. K. Bogner, *Phys. Rev. C* **97**, 054304 (2018).
Microscopically based energy density functionals for nuclei using the density matrix expansion. II. Full optimization and validation
- [164] D. Lacroix and K. Bennaceur, *Phys. Rev. C* **91**, 011302(R) (2015).
Semicontact three-body interaction for nuclear density functional theory
- [165] J. Dobaczewski, K. Bennaceur, and F. Raimondi, *J. Phys. G: Nucl. Part. Phys.* **39**, 125103 (2012).
Effective theory for low-energy nuclear energy density functionals
- [166] K. Bennaceur, J. Dobaczewski, and F. Raimondi, *EPJ Web of Conferences* **66**, 02031 (2014).
New density-independent interactions for nuclear structure calculations
- [167] F. Raimondi, K. Bennaceur, and J. Dobaczewski, *J. Phys. G: Nucl. Part. Phys.* **41**, 055112 (2014).
Nonlocal energy density functionals for low-energy nuclear structure
- [168] K. Bennaceur, A. Idini, J. Dobaczewski, P. Dobaczewski, M. Kortelainen, and F. Raimondi, *J. Phys. G: Nucl. Part. Phys.* **44**, 045106 (2017).
Nonlocal energy density functionals for pairing and beyond-mean-field calculations
- [169] D. Davesne, J. Navarro, P. Becker, R. Jodon, J. Meyer, and A. Pastore, *Phys. Rev. C* **91**, 064303 (2015).
Extended Skyrme pseudopotential deduced from infinite nuclear matter properties
- [170] P. Becker, D. Davesne, J. Meyer, A. Pastore, and J. Navarro, *J. Phys. G: Nucl. Part. Phys.* **42**, 034001 (2015).
Tools for incorporating a D-wave contribution in Skyrme energy density functionals
- [171] D. Davesne, J. Navarro, J. Meyer, K. Bennaceur, and A. Pastore *Phys. Rev. C* **97**, 044304 (2018).
Two-body contributions to the effective mass in nuclear effective interactions
- [172] S. A. Fayans, *JETP Lett.* **68**, 169 (1998).
Towards a universal nuclear density functional
- [173] S. A. Fayans, S. V. Tolokonnikov, E. L. Trykov, and D. Zawischa, *Nucl. Phys. A* **676**, 49 (2000).
Nuclear isotope shifts within the local energy-density functional approach
- [174] A. Bulgac, M. M. Forbes, S. Jin, R. N. Pérez, and N. Schunck, *Phys. Rev. C* **97**, 044313 (2018).
Minimal nuclear energy density functional

- [175] M. Baldo, P. Schuck, and X. Viñas, *Phys. Lett. B* **663**, 390 (2008).
Kohn–Sham density functional inspired approach to nuclear binding
- [176] M. Baldo, L. M. Robledo, P. Schuck, and X. Viñas, *Phys. Rev. C* **87**, 064305 (2013).
New Kohn-Sham density functional based on microscopic nuclear and neutron matter equations of state
- [177] M. Baldo, C. Maieron, P. Schuck, and X. Viñas, *Nucl. Phys. A* **736**, 241 (2004).
Low densities in nuclear and neutron matters and in the nuclear surface
- [178] E. Garrido, P. Sarriguren, E. Moya de Guerra, and P. Schuck, *Phys. Rev. C* **60**, 064312 (1999).
Effective density-dependent pairing forces in the $T = 1$ and $T = 0$ channels
- [179] J. L. Egido, and L. M. Robledo, *Extended Density Functionals in Nuclear Structure Physics* (Springer Berlin, 2004)
- [180] M. N. Butler, D. W. L. Sprung, and J. Martorell, *Nucl. Phys. A* **422**, 157 (1984).
An improved approximate treatment of c.m. motion in DDHF calculations
- [181] J. Dobaczewski, *J. Phys. G: Nucl. Part. Phys.* **43**, 04LT01 (2016).
Ab initio derivation of model energy density functionals
- [182] P. Ring and P. Schuck, *The Nuclear Many–Body Problem* (Springer-Verlag New York, 1980).
- [183] D. Lacroix, S. Ayik, and P. Chomaz, *Prog. Part. Nucl. Phys.* **52**, 497 (2004).
Nuclear collective vibrations in extended mean-field theory
- [184] D. Gambacurta, M. Grasso, and F. Catara, *J. Phys.: Conf. Ser.* **267**, 012052 (2011).
Second RPA with Skyrme Interaction
- [185] D. Gambacurta and M. Grasso, *Eur. Phys. J. A* **52**, 198 (2016).
Second RPA calculations with the Skyrme and Gogny interactions
- [186] H. Hansen, G. Chanfray, D. Davesne, and P. Schuck, *Eur. Phys. J. A* **14**, 397 (2002).
Random phase approximation and extensions applied to a bosonic field theory
- [187] A. Rabhi, R. Bennaceur, G. Chanfray, and P. Schuck, *Phys. Rev. C* **66**, 064315 (2002).
Self-consistent quasiparticle random phase approximation for the description of superfluid Fermi systems
- [188] A. P. Severyukhin, C. Stoyanov, V. V. Voronov, and N. Van Giai, *Phys. Rev. C* **66**, 034304 (2002).
Quasiparticle random phase approximation with finite rank approximation for Skyrme interactions
- [189] M. Bender, T. Duguet, and D. Lacroix, *Phys. Rev. C* **79**, 044319 (2009).
Particle-number restoration within the energy density functional formalism

- [190] T. Duguet, M. Bender, K. Bennaceur, D. Lacroix, and T. Lesinski, *Phys. Rev. C* **79**, 044320 (2009).
Particle-number restoration within the energy density functional formalism: Nonviability of terms depending on noninteger powers of the density matrices
- [191] D. Lacroix, T. Duguet, and M. Bender, *Phys. Rev. C* **79**, 044318 (2009).
Configuration mixing within the energy density functional formalism: Removing spurious contributions from nondiagonal energy kernels
- [192] A. L. Fetter and J. D. Walecka, *Quantum Theory of Many-Particle Systems* (McGraw-Hill, New York, 1971).
- [193] J. W. Negele and H. Orland, *Quantum Many-particle Systems* (CRC Press, 2018).
- [194] A. A. Abrikosov, L. P. Gorkov, and I. E. Dzyaloshinski, *Methods of Quantum Field Theory in Statistical Physics* (Courier Corporation, 2012).
- [195] K. Moghrabi, M. Grasso, G. Colò, and N. Van Giai, *Phys. Rev. Lett.* **105**, 262501 (2010).
Beyond Mean-Field Theories with Zero-Range Effective Interactions: A Way to Handle the Ultraviolet Divergence
- [196] C.-J. Yang, M. Grasso, X. Roca-Maza, G. Colò, and K. Moghrabi, *Phys. Rev. C* **94**, 034311 (2016).
Second-order equation of state with the Skyrme interaction: Cutoff and dimensional regularization with the inclusion of rearrangement terms
- [197] C.-J. Yang, M. Grasso, and D. Lacroix, *Phys. Rev. C* **94**, 031301(R) (2016).
From dilute matter to the equilibrium point in the energy-density-functional theory
- [198] M. Grasso, D. Lacroix, and C.-J. Yang, *Phys. Rev. C* **95**, 054327 (2017).
Lee-Yang-inspired functional with a density-dependent neutron-neutron scattering length
- [199] A. Boulet and D. Lacroix, *Phys. Rev. C* **97**, 014301 (2018).
Static response, collective frequencies, and ground-state thermodynamical properties of spin-saturated two-component cold atoms and neutron matter
- [200] A. Boulet and D. Lacroix, *J. Phys. G: Nucl. Part. Phys.* **46**, 105104 (2019).
Approximate self-energy for Fermi systems with large s-wave scattering length: a step towards density functional theory
- [201] C.-J. Yang, M. Grasso, K. Moghrabi, and U. van Kolck, *Phys. Rev. C* **95**, 054325 (2017).
Renormalizability of the nuclear many-body problem with the Skyrme interaction beyond mean field
- [202] C.-J. Yang, M. Grasso, and D. Lacroix, *Phys. Rev. C* **96**, 034318 (2017).
Toward a systematic strategy for defining power counting in the construction of the energy density functional
- [203] B. A. Brown, *Phys. Rev. Lett.* **85**, 5296 (2000).
Neutron Radii in Nuclei and the Neutron Equation of State

- [204] R. J. Furnstahl, *EFT for DFT*
In: Renormalization Group and Effective Field Theory Approaches to Many-Body Systems. **Lecture Notes in Physics 852**. (Springer, Berlin, Heidelberg, 2012).
- [205] K. Huang and C. N. Yang, **Phys. Rev.** **105**, 767 (1957).
Quantum-Mechanical Many-Body Problem with Hard-Sphere Interaction
- [206] K. Huang, C. N. Yang, and J. M. Luttinger, **Phys. Rev.** **105**, 776 (1957).
Imperfect Bose Gas with Hard-Sphere Interaction
- [207] T. D. Lee and C. N. Yang, **Phys. Rev.** **105**, 1119 (1957).
Many-Body Problem in Quantum Mechanics and Quantum Statistical Mechanics
- [208] J. Bonnard, M. Grasso, and D. Lacroix, **Phys. Rev. C** **98**, 034319 (2018).
Energy-density functionals inspired by effective-field theories: Applications to neutron drops
- [209] A. Bulgac, **Phys. Rev. Lett.** **89**, 050402 (2002).
Dilute Quantum Droplets
- [210] I. Ferrier-Barbut, H. Kadau, M. Schmitt, M. Wenzel, and T. Pfau, **Phys. Rev. Lett.** **116**, 215301 (2016).
Observation of Quantum Droplets in a Strongly Dipolar Bose Gas
- [211] R. J. Furnstahl, J. V. Steele, and N. Tiffessa, **Nuclear Physics A** **671**, 396 (2000).
Perturbative effective field theory at finite density
- [212] J. V. Steele and R. J. Furnstahl, **Nuclear Physics A** **663&664**, 999c (2000).
Describing nuclear matter with effective field theories
- [213] A. Mecca, A. Lovato, O. Benhar, and A. Polls, **Phys. Rev. C** **91**, 034325 (2015).
Effective-interaction approach to the Fermi hard-sphere system
- [214] A. Mecca, A. Lovato, O. Benhar, and A. Polls, **Phys. Rev. C** **93**, 035802 (2016).
Transport properties of the Fermi hard-sphere system
- [215] C. Ordonez, L. Ray, and U. van Kolck, **Phys. Rev. Lett.** **72**, 1982 (1994).
Nucleon-nucleon potential from an effective chiral Lagrangian
- [216] C. Ordonez, L. Ray, and U. van Kolck, **Phys. Rev. C** **53**, 2086 (1996).
Two-nucleon potential from chiral Lagrangians
- [217] R. J. Furnstahl, H.-W. Hammer, and S. J. Puglia, **Annals of Physics** **322**, 2703 (2007).
Effective field theory for dilute fermions with pairing
- [218] G. D. Mahan, *Many-Particle Physics* (Springer Science & Business Media, 2013).
- [219] H. Bruus and K. Flensberg, *Many-Body Quantum Theory in Condensed Matter Physics* (OUP Oxford, 2004).
- [220] R. D. Mattuck, *A Guide to Feynman Diagrams in the Many-body Problem* (Courier Corporation, 1992).

- [221] E. K. U. Gross, E. Runge, and O. Heinonen, *Many-Particle Theory* (Taylor & Francis, 1991).
- [222] P. Nozières, *Theory of Interacting Fermi Systems* (Benjamin, 1964).
- [223] W. H. Dickhoff and D. Van Neck, *Many-Body Theory Exposed!* (World Scientific, 2008).
- [224] A. A. Abrikosov and I. M. Khalatnikov, *JETP* **6**, 888 (1958).
Concerning a Model for a Non-Ideal Fermi Gas
- [225] V. M. Galitskii, *JETP* **7**, 104 (1958).
The Energy Spectrum of a Non-ideal Fermi Gas
- [226] S. Wilson and I. Hubac, *Brillouin-Wigner Methods for Many-Body Systems* (Springer Science & Business Media, 2009).
- [227] J. V. Steele, [arXiv:nucl-th/0010066](https://arxiv.org/abs/nucl-th/0010066) (2000).
Effective Field Theory Power Counting at Finite Density
- [228] M. Ya. Amus'ya and V. N. Efimov, *Ann. Phys.* **47**, 377 (1968).
Pair collisions in a low-density fermi gas
- [229] V. N. Efimov and M. Ya. Amus'ya, *JETP* **20**, 388 (1965).
Ground State of a Rarefied Fermi Gas of Rigid Spheres
- [230] G. A. Baker Jr., *Rev. Mod. Phys.* **43**, 479 (1971).
Singularity Structure of the Perturbation Series for the Ground-State Energy of a Many-Fermion System
- [231] R. F. Bishop, *Ann. Phys.* **77**, 106 (1973).
Ground-state energy of a dilute fermi gas
- [232] L. Platter, H.-W. Hammer and U.-G. Meißner, *Nucl. Phys. A* **714**, 250 (2003).
Quasiparticle properties in effective field theory
- [233] C. Wellenhofer, C. Drischler, and A. Schwenk, [arXiv:1812.08444](https://arxiv.org/abs/1812.08444) [nucl-th] (2018).
Dilute Fermi gas at fourth order in effective field theory
- [234] K. A. Brueckner, C. A. Levinson, and H. M. Mahmoud, *Phys. Rev.* **95**, 217 (1954).
Two-Body Forces and Nuclear Saturation. I. Central Forces
- [235] B. D. Day, *Rev. Mod. Phys.* **39**, 719 (1967).
Elements of the Brueckner-Goldstone Theory of Nuclear Matter
- [236] B. D. Day, *Rev. Mod. Phys.* **50**, 495 (1978).
Current state of nuclear matter calculations
- [237] T. Schäfer, C.-W. Kao, and S. R. Cotanch, *Nucl. Phys. A* **762**, 82 (2005).
Many body methods and effective field theory
- [238] N. Kaiser, *Nucl. Phys. A* **860**, 41 (2011).
Resummation of fermionic in-medium ladder diagrams to all orders
- [239] N. Kaiser, *Eur. Phys. J. A* **48**, 148 (2012).
Single-particle potential from resummed ladder diagrams

- [240] N. Kaiser, *Eur. Phys. J. A* **49**, 140 (2013).
Single-particle potential from resummed ladder diagrams
- [241] E. E. Salpeter and H. A. Bethe *Phys. Rev.* **84**, 1232 (1951).
A Relativistic Equation for Bound-State Problems
- [242] T. Hahn, *Comput. Phys. Commun.* **168**, 78 (2005).
Cuba – a library for multidimensional numerical integration
- [243] A. Bulgac and G. F. Bertsch, *Phys. Rev. Lett.* **94**, 070401 (2005).
Collective oscillations of a trapped fermi gas near the unitary limit
- [244] C. Lobo, I. Carusotto, S. Giorgini, A. Recati, and S. Stringari, *Phys. Rev. Lett.* **97**, 100405 (2006).
Pair Correlations of an Expanding Superfluid Fermi Gas
- [245] G. E. Astrakharchik, J. Boronat, J. Casulleras, and S. Giorgini, *Phys. Rev. Lett.* **93**, 200404 (2004).
Equation of State of a Fermi Gas in the BEC-BCS Crossover: A Quantum Monte Carlo Study
- [246] G. A. Baker Jr., *Phys. Rev. C* **60**, 054311 (1999).
Neutron matter model
- [247] H. Heiselberg, *Phys. Rev. A* **63**, 043606 (2001).
Fermi systems with long scattering lengths
- [248] S. K. Adhikari, *Phys. Rev. A* **77**, 045602 (2008).
Nonlinear Schrödinger equation for a superfluid Fermi gas in the BCS-BEC crossover
- [249] W. Weimer, K. Morgener, V. P. Singh, J. Siegl, K. Hueck, N. Luick, L. Mathey, and H. Moritz, *Phys. Rev. Lett.* **114**, 095301 (2015).
Critical Velocity in the BEC-BCS Crossover
- [250] J. Joseph, B. Clancy, L. Luo, J. Kinast, A. Turlapov, and J. E. Thomas, *Phys. Rev. Lett.* **98**, 170401 (2007).
Measurement of Sound Velocity in a Fermi Gas near a Feshbach Resonance
- [251] M. Horikoshi, M. Koashi, H. Tajima, Y. Ohashi, and M. Kuwata-Gonokami, *Phys. Rev. X* **7**, 041004 (2017).
Ground-State Thermodynamic Quantities of Homogeneous Spin-1/2 Fermions from the BCS Region to the Unitarity Limit
- [252] H. Hu, X. Liu and P. Drummond, *Europhys. Lett.* **74**, 574 (2006).
Equation of state of a superfluid Fermi gas in the BCS-BEC crossover
- [253] P. Pieri, L. Pisani and G. C. Strinati, *Phys. Rev. B* **72**, 012506 (2005).
Comparison between a diagrammatic theory for the BCS-BEC crossover and quantum Monte Carlo results
- [254] S. Tan, *Ann. Phys.* **323**, 2952 (2008).
Energetics of a strongly correlated Fermi gas
- [255] S. Tan, *Ann. Phys.* **323**, 2971 (2008).
Large momentum part of a strongly correlated Fermi gas

- [256] S. Tan, *Ann. Phys.* **323**, 2987 (2008).
Generalized virial theorem and pressure relation for a strongly correlated Fermi gas
- [257] F. Werner, L. Tarruell, and Y. Castin, *Eur. Phys. J. B* **68**, 401 (2009).
Number of closed-channel molecules in the BEC-BCS crossover
- [258] J. T. Stewart, J. P. Gaebler, T. E. Drake, and D. S. Jin, *Phys. Rev. Lett.* **104**, 235301 (2010).
Verification of Universal Relations in a Strongly Interacting Fermi Gas
- [259] E. D. Kuhnle, H. Hu, X.-J. Liu, P. Dyke, M. Mark, P. D. Drummond, P. Hannaford, and C. J. Vale, *Phys. Rev. Lett.* **105**, 070402 (2010).
Universal Behavior of Pair Correlations in a Strongly Interacting Fermi Gas
- [260] A. Schwenk and C. J. Pethick, *Phys. Rev. Lett.* **95**, 160401 (2005).
Resonant Fermi Gases with a Large Effective Range
- [261] L. M. Schonenberg and G. J. Conduit, *Phys. Rev. A* **95**, 013633 (2017).
Effective-range dependence of resonant Fermi gases
- [262] M. Buraczynski and A. Gezerlis, *Phys. Rev. Lett.* **116**, 152501 (2016).
Static Response of Neutron Matter
- [263] M. Buraczynski and A. Gezerlis, *Phys. Rev. C* **95**, 044309 (2017).
Ab initio and phenomenological studies of the static response of neutron matter
- [264] D. Pines and P. Nozières, *The Theory of Quantum Liquids* (Benjamin, Reading, 1966)
- [265] C. Kittel, *Introduction to solid state physics* (Wiley, 2005).
- [266] C. García-Recio, J. Navarro, Van Giai Nguyen, and L. L. Salcedo, *Ann. of Phys.* **214**, 293 (1992).
Response functions for infinite fermion systems with velocity dependent interactions
- [267] A. Pastore, D. Davesne, Y. Lallouet, M. Martini, K. Bennaceur, and J. Meyer, *Phys. Rev. C* **85**, 054317 (2012).
Nuclear response for the Skyrme effective interaction with zero-range tensor terms. II. Sum rules and instabilities
- [268] A. Pastore, M. Martini, V. Buridon, D. Davesne, K. Bennaceur, and J. Meyer, *Phys. Rev. C* **86**, 044308 (2012).
Nuclear response for the Skyrme effective interaction with zero-range tensor terms. III. Neutron matter and neutrino propagation
- [269] A. Pastore, K. Bennaceur, D. Davesne, and J. Meyer, *Int. J. Mod. Phys. E* **21**, 1250040 (2012).
Linear response in infinite nuclear matter as a tool to reveal finite size instabilities
- [270] A. Pastore, D. Davesne, and J. Navarro, *Phys. Rep.* **563**, 1 (2015).
Linear response of homogeneous nuclear matter with energy density functionals
- [271] A. Schwenk, B. Friman, and G. E. Brown, *Nucl. Phys. A* **713**, 191 (2003).
Renormalization group approach to neutron matter: quasiparticle interactions, superfluid gaps and the equation of state

- [272] J. Wambach, T. L. Ainsworth, and D. Pines, *Nucl. Phys. A* **555**, 128 (1993).
Quasiparticle interactions in neutron matter for applications in neutron stars
- [273] C. Drischler, V. Somà, and A. Schwenk, *Phys. Rev. C* **89**, 025806 (2014).
Microscopic calculations and energy expansions for neutron-rich matter
- [274] M. M. Forbes and R. Sharma, *Phys. Rev. A* **90**, 043638 (2014).
Validating simple dynamical simulations of the unitary Fermi gas
- [275] P. Magierski, G. Wlazlowski, A. Bulgac, and J. E. Drut, *Phys. Rev. Lett.* **103**, 210403 (2009).
Finite-Temperature Pairing Gap of a Unitary Fermi Gas by Quantum Monte Carlo Calculations
- [276] S. Stringari, *Phys. Rev. Lett.* **77**, 2360 (1996).
Collective Excitations of a Trapped Bose-Condensed Gas
- [277] H. Heiselberg, *Phys. Rev. Lett.* **93**, 040402 (2004).
Collective Modes of Trapped Gases at the BEC-BCS Crossover
- [278] M. Cozzini and S. Stringari, *Phys. Rev. Lett.* **91**, 070401 (2003).
Fermi Gases in Slowly Rotating Traps: Superfluid versus Collisional Hydrodynamics
- [279] M. Bartenstein, A. Altmeyer, S. Riedl, S. Jochim, C. Chin, J. H. Denschlag, and R. Grimm, *Phys. Rev. Lett.* **92**, 203201 (2004).
Collective Excitations of a Degenerate Gas at the BEC-BCS Crossover
- [280] J. Kinast, A. Turlapov, and J. E. Thomas, *Phys. Rev. A* **70**, 051401 (2004).
Breakdown of hydrodynamics in the radial breathing mode of a strongly interacting Fermi gas
- [281] J. Kinast, S. L. Hemmer, M. E. Gehm, A. Turlapov, and J. E. Thomas, *Phys. Rev. Lett.* **92**, 150402 (2004).
Evidence for Superfluidity in a Resonantly Interacting Fermi Gas
- [282] N. Manini and L. Salasnich, *Phys. Rev. A* **71**, 033625 (2005).
Bulk and collective properties of a dilute Fermi gas in the BCS-BEC crossover
- [283] S. Hoinka, M. Lingham, M. Delehay, and C. J. Vale, *Phys. Rev. Lett.* **109**, 050403 (2012).
Dynamic Spin Response of a Strongly Interacting Fermi Gas
- [284] G. E. Astrakharchik, J. Boronat, E. Krotscheck and T. Lichtenegger, *J. Phys. Conf. Ser.* **529**, 012009 (2014).
Dynamic structure function of a cold Fermi gas at unitarity
- [285] M. W. Zwierlein, J. R. Abo-Shaeer, A. Schirotzek, C. H. Schunck, and W. Ketterle, *Nature* **435**, 1047 (2005).
Vortices and superfluidity in a strongly interacting Fermi gas
- [286] P. Zou, F. Dalfovo, R. Sharma, X. J. Liu, and H. Hu, *New J. Phys.* **18**, 113044 (2016).
Dynamic structure factor of a strongly correlated Fermi superfluid within a density functional theory approach

- [287] S. Hoinka, M. Lingham, K. Fenech, H. Hu, C. J. Vale, J. E. Drut, and S. Gandolfi, *Phys. Rev. Lett.* **110**, 055305 (2013).
Precise Determination of the Structure Factor and Contact in a Unitary Fermi Gas
- [288] J. Carlson and S. Gandolfi, *Phys. Rev. A* **90**, 011601 (2014).
Predicting energies of small clusters from the inhomogeneous unitary Fermi gas
- [289] M. Buraczynski, N. Ismail, and A. Gezerlis, *Phys. Rev. Lett.* **122**, 152701 (2019).
Non-perturbative Extraction of the Effective Mass in Neutron Matter
- [290] N. M. Hugenholtz and L. van Hove, *Physica* **24**, 363 (1958).
A theorem on the single particle energy in a Fermi gas with interaction
- [291] C. Mahaux, K. T. R. Davis, and G. R. Satchler, *Phys. Rep.* **224**, 237 (1993).
Retardation and dispersive effects in the nuclear mean field
- [292] R. Sator and C. Mahaux, *Phys. Rev. C* **21**, 1546 (1980).
Self-energy, momentum distribution, and effective masses of a dilute Fermi gas
- [293] R. Sator and C. Mahaux, *Phys. Rev. C* **21**, 2613 (1980).
Single-particle states in nuclear matter and in finite nuclei
- [294] H. Orland and R. Schaeffer, *Nucl. Phys. A* **299**, 442 (1978).
Single particle states in nuclei
- [295] J. W. Holt, N. Kaiser, G. A. Miller, and W. Weise, *Phys. Rev. C* **88**, 0246614 (2013).
Microscopic optical potential from chiral nuclear forces
- [296] J. T. Stewart, J. P. Gaebler, and D. S. Jin, *Nature* **454**, 744 (2008).
Using photoemission spectroscopy to probe a strongly interacting Fermi gas
- [297] S. Nascimbène, N. Navon, K. J. Jiang, F. Chevy, and C. Salomon, *Nature* **463**, 1057 (2011).
Exploring the thermodynamics of a universal Fermi gas
- [298] D. Davesne, A. Pastore, and J. Navarro, *J. Phys. G: Nucl. Part. Phys.* **41**, 065104 (2014).
Fitting N_3LO pseudo-potentials through central plus tensor Landau parameters
- [299] R. Combescot, A. Recati, C. Lobo, and F. Chevy, *Phys. Rev. Lett.* **98**, 180402 (2007).
Normal State of Highly Polarized Fermi Gases: Simple Many-Body Approaches
- [300] Y. Sagi, T. E. Dracke, R. Paudel, R. Chapurin, and D. S. Jin, *Phys. Rev. Lett.* **114**, 075301 (2015).
Breakdown of the Fermi Liquid Description for Strongly Interacting Fermions
- [301] A. Gezerlis and G. F. Bertsch, *Phys. Rev. Lett.* **105**, 212501 (2010).
Effective 3-Body Interaction for Mean-Field and Density-Functional Theory
- [302] A. Gezerlis and G. F. Bertsch, *Phys. Rev. C* **85**, 037303 (2012).
Energy spectrum and effective mass using a nonlocal 3-body interaction
- [303] P. W. Anderson, *Science* **177**, 393 (1972).
More Is Different

- [304] J. P. Jeukenne, A. Lejeune, and C. Mahaux, *Phys. Rep. C* **25**, 83 (1976).
Many-body theory of nuclear matter
- [305] A. Lacour, J. A. Oller, and U.-G. Meißner, *Ann. Phys.* **326**, 241 (2011).
Non-perturbative methods for a chiral effective field theory of finite density nuclear systems
- [306] Y. N. Zhang, S. K. Bogner, and R. J. Furnstahl, *Phys. Rev. C* **98**, 064306 (2018).
Incorporating Brueckner-Hartree-Fock correlations in energy density functionals
- [307] D. Lacroix and D. Gambacurta, *Phys. Rev. C* **86**, 014306 (2012).
Projected quasiparticle perturbation theory
- [308] J. Ripoche, D. Lacroix, D. Gambacurta, J.-P. Ebran, and T. Duguet, *Phys. Rev. C* **95**, 014326 (2017).
Combining symmetry breaking and restoration with configuration interaction: A highly accurate many-body scheme applied to the pairing Hamiltonian
- [309] A. Bulgac and M. M. Forbes, [arXiv:0808.1436](https://arxiv.org/abs/0808.1436) [cond-mat.supr-con] (2008).
The Asymmetric Superfluid Local Density Approximation (ASLDA)
- [310] A. Bulgac, *Superfluid Local Density Approximation: A Density Functional Theory Approach to the Nuclear Pairing Problem*
In: *Fifty Years of Nuclear BCS: Pairing in Finite Systems* (World Scientific, 2013).
- [311] A. Bulgac and M. M. Forbes, *Time-Dependent Superfluid Local-Density Approximation*
In: *Quantum Gases: Finite Temperature and Non-Equilibrium Dynamics* (World Scientific, 2013).
- [312] G. 't Hooft and M. Veltman, *Nucl. Phys. B* **44**, 189 (1972).
Regularization and renormalization of gauge fields
- [313] G. 't Hooft, *Nucl. Phys. B* **61**, 455 (1973).
Dimensional regularization and the renormalization group

Ce livre, le plus pénible de tous à déchiffrer, est aussi le seul que nous ait dicté la réalité, le seul dont « l'impression » ait été faite en nous par la réalité même. De quelque idée laissée en nous par la vie qu'il s'agisse, sa figure matérielle, trace de l'impression qu'elle nous a faite, est encore le gage de sa vérité nécessaire. Les idées formées par l'intelligence pure n'ont qu'une vérité logique, une vérité possible, leur élection est arbitraire. Le livre aux caractères figurés, non tracés par nous, est notre seul livre. Non que les idées que nous formons ne puissent être justes logiquement, mais nous ne savons pas si elles sont vraies. Seule l'impression, si chétive qu'en semble la matière, si invraisemblable la trace, est un critérium de vérité et à cause de cela mérite seule d'être appréhendée par l'esprit, car elle est seule capable, s'il sait en dégager cette vérité, de l'amener à une plus grande perfection et de lui donner une pure joie. L'impression est pour l'écrivain ce qu'est l'expérimentation pour le savant, avec cette différence que chez le savant le travail de l'intelligence précède et chez l'écrivain vient après : Ce que nous n'avons pas eu à déchiffrer, à éclaircir par notre effort personnel, ce qui était clair avant nous, n'est pas à nous. Ne vient de nous-même que ce que nous tirons de l'obscurité qui est en nous et que ne connaissent pas les autres. Et comme l'art recompose exactement la vie, autour de ces vérités qu'on a atteintes en soi-même flotte une atmosphère de poésie, la douceur d'un mystère qui n'est que la pénombre que nous avons traversée.

Marcel PROUST – *À la Recherche du temps perdu*

Density Functional theory for Fermi systems with large s -wave scattering length: application to atomic and nuclear physics

ABSTRACT – In the present work, a density functional theory (DFT) is developed for systems interacting through an anomalously large s -wave scattering length a_s . Examples of such systems are atomic gas or neutron matter. The Many-Body Perturbation Theory (MBPT) is first discussed to describe dilute Fermi systems. This approach leads to the well-known Lee-Yang functional valid in a very narrow range of density when the s -wave scattering length is large. To extend the domain of validity of the perturbative approach, resummation techniques with the ladder approximation is used. This leads to compact expressions for both the energy and/or the on-shell self-energy in infinite spin-degenerated systems that can be applied from diluted to dense systems. It also leads to finite energy in atomic gas at the unitary limit, i.e. when $|a_s k_F| \rightarrow +\infty$. The deduced functionals remain rather complex and lacks of predictive power in general. To simplify the functional, approximations called phase-space or partial phase-space approximations respectively for the energy or for the self-energy, are proposed. These approximations not only simplify the form of the functionals, but also improve their predictive power at various density while properly reproducing the low density limit. Guided by the non-perturbative resummation technique developed in this thesis, several novel

functionals are proposed as well as extensions of them to include effective range effects. These non-empirical functionals, that essentially contain no free parameters, are tested against cold atom and/or neutron matter properties. A very good reproduction of ab initio and experimental observations in cold atom is obtained. The equation of state obtained for neutron matter is also reproduced up to $\rho = 0.01 \text{ fm}^{-3}$. The static response of neutron matter, recently obtained from ab initio theory, is also better reproduced compared to standardly used empirical nuclear DFT. This study has also pointed out the necessity to better understand quasi-particle properties like the effective mass. To further progress, starting from resummed expressions of the self-energy together with partial phase-space approximation, compact expressions of the chemical potential and effective masses are obtained that are eventually compatible with the DFTs proposed in the first part of this thesis. These expressions are anticipated to significantly extend the domain of validity compared to the perturbative approach. We finally show that the developments made in this work are also useful to reconcile the parameters generally used in the empirical nuclear DFT with the properties of the strong nuclear interaction.

KEYWORDS: theoretical physics, nuclear interaction, effective field theory, density functional theory, nuclear matter, ultra-cold atoms

Théorie Fonctionnelle de la Densité pour les systèmes de fermions en interaction forte : application à la physique atomique et à la physique nucléaire

RÉSUMÉ – Dans ce travail de thèse, des théories de type fonctionnelle de la densité sont développées pour des systèmes en interaction forte possédant une longueur de diffusion en onde s , notée a_s , anormalement grande. Les gaz atomiques ou la matière neutronique sont des exemples physiques de tels systèmes. La théorie des perturbations à N -corps est tout d'abord utilisée pour décrire les systèmes de fermions dilués. Cette approche conduit par exemple à la fonctionnelle de Lee-Yang qui est valide dans une plage de densité très restreinte lorsque la longueur de diffusion en onde s devient grande. Pour étendre le domaine de validité de l'approche perturbative, des techniques de resommation associées à l'approximation dite en échelle sont utilisées. Cette approche conduit à des expressions compactes pour l'énergie et/ou la self-énergie on-shell dans des systèmes infinis pouvant être appliquées à des systèmes plus ou moins denses. Cela conduit également à une énergie finie du gaz atomique à la limite unitaire, i.e. lorsque $|a_s k_F| \rightarrow +\infty$. Les fonctionnelles ainsi déduites restent assez complexes et manquent en général de pouvoir prédictif. Pour simplifier ces fonctionnelles, des approximations appelées respectivement approximations de "l'espace des phases" ou de "l'espace des phases partiel" sont proposées pour l'énergie ou la self-énergie. Ces approximations simplifient non seulement la forme des fonctionnelles, mais améliorent également leur pouvoir prédictif tout en reproduisant correctement la limite de basse densité. Guidé par les techniques de resommation non-perturbatives développées dans cette thèse, plusieurs

nouvelles fonctionnelles sont proposées ainsi que leurs extensions permettant d'inclure des effets de portée effective. Ces fonctionnelles non empiriques, qui ne contiennent aucun paramètre libre, sont testées par rapport aux propriétés des systèmes d'atomes froids et/ou de la matière neutronique. Ces fonctionnelles reproduisent très bien les propriétés obtenues dans les calculs ab-initio ou observées expérimentalement dans les systèmes d'atomes froids. L'équation d'état de la matière neutronique est également reproduite jusqu'à $\rho = 0.01 \text{ fm}^{-3}$. La réponse statique de la matière neutronique, récemment calculée dans des théories ab-initio, est également mieux reproduite par rapport aux fonctionnelles empiriques utilisées généralement en physique nucléaire. Cette étude a aussi mis en évidence la nécessité de mieux comprendre les propriétés des quasi-particules telle que la masse effective. Pour progresser sur ce point, en partant des expressions resommées de la self-énergie et de l'approximation de l'espace des phases partiel, des expressions compactes du potentiel chimique et de la masse effective ont été obtenues ; ces expressions étant compatibles avec les fonctionnelles proposées dans la première partie de cette thèse. Ces expressions devraient élargir considérablement le domaine de validité des fonctionnelles non-empiriques par rapport aux théories perturbatives. Enfin, il est montré que les développements de ce travail sont également utiles pour réconcilier les paramètres généralement utilisés dans les fonctionnelles empiriques de la physique nucléaire avec les propriétés de l'interaction nucléaire forte.

MOTS CLÉS : physique théorique, interaction nucléaire, théorie effective des champs, théorie fonctionnelle de la densité, matière nucléaire, atomes ultra-froids